FE-2666-F(Vol.1)
Distribution Category UC-90c

MIXING AND GASIFICATION OF COAL IN ENTRAINED FLOW SYSTEMS

Volume 1, Final Report
for the Period 1 May 1977 to 31 October 1979

L. Douglas Smoot, Paul O. Hedman, and Philip J. Smith

Chemical Engineering Department
Brigham Young University
Provo, Utah 84602

Date Published 31 January 1980

PREPARED FOR THE UNITED STATES

DEPARTMENT OF ENERGY

Under Contract No. EF-77-S-01-2666

FOREWORD

This report (Volume 1) summarizes technical progress accomplished during a thirty month study conducted for the United States Department of Energy (DOE) under contract no. EF-77-S-01-2666. A second volume of this final report is a user's manual for the one-dimensional computer code for coal gasification. The contract period was 1 May 1977 to 31 October 1979. Work was accomplished under the direction of Dr. L. Douglas Smoot, principal investigator, and Drs. Paul O. Hedman and Richard W. Hanks, senior investigators. Dr. Robert C. Wellek was the Program Manager for DOE.

Graduate and undergraduate students who have contributed to the technical progress and to this document were John Baardson, Vearl Beck, Richard Guercio, Stanley Harding, Steven Johnson, Don Leavitt, Wesley Pack, Tracy Price, Dee Rees, Lyle Richins, Jerald Sharp, Douglas Skinner, Philip Smith, Christopher Tice, Keith Wilson and Scott Woodfield. Mr. James Hoen, Supervisor of the Research Machine Shop, provided assistance in design and construction of reactor components. Michael King, Elaine Alger and Kathy Hartman provided technician, typing and drafting services. Subcontract work at the University of Utah on generalized model develoment was conducted under the direction of Dr. David Pratt with contributions from Dr. John Wormeck and Miss Angela Varma.

SUMMARY

This document summarizes research accomplishments of a thirty month, second phase study of mixing and kinetic processes in an entrained coal gasifier. Principal objectives were to measure the extent of particle reaction and dispersion, the extent of gas mixing, the local product composition, and the extent of pollutant formation. Additional objectives included the completion of the one-dimensional computerized model for describing entrained coal gasification systems and the use of that model in analyzing the gasification processes, and extension of the coal reaction model to two-dimensional systems. Non-reactive mixing tests were to be completed to quantify gas and particle mixing rates independent of chemical reaction. Contacts with industrial and governmental organizations were to be continued and reports and papers were to be prepared in order to transfer the research results to the technical community.

The analysis of a series of non-reactive (cold-flow) experiments (Test Series 2) which were performed under the Phase 1 part of this study (ERDA Contract No. E(49-18)-1767) was completed and is reported herein. Test Series 2 was designed to investigate gas and particle mixing in an expanded mixing chamber with parallel injection of both the primary and secondary streams. Sixty tests were completed in two different sized ducts where the effects of mixing chamber diameter, secondary velocity, particle size, solids-loading and the influence of a primary wire screen were investigated.

Three additional cold-flow test series were also performed and analyzed during the contract period (Test Series 3, 4, and 5). In Test Series 3, the effects of nonparallel secondary injection into the expanded mixing chamber were investigated in 57 experiments. Test variables evaluated included the effects of secondary injection angle, particle size, secondary velocity, and mixing duct size. In Test Series 4, coal dust was used in place of the silicon dust of previous tests. A total of 38 experiments were performed in this test series, 17 with non-parallel injection, ten with parallel injection and 11 reproduced tests which duplicated conditions of earlier test series. The final cold flow tests series performed during this contract period (Test Series 5) involved a major facility modification to introduce swirl into the secondary stream. A series of preliminary tests to check-out the modified hardware, and a series of 28 experiments to quantify the effects of secondary swirl on gas and particle mixing rates were completed. Details of these three cold-flow test series (No's 3, 4 and 5) are included herein.

Gasification tests were performed in a laboratory-scale entrained coal gasifier which was equipped with a set of water-quench sample probes. Gas and particle samples were extracted from the gasifier and analyzed to determine the extent of gas mixing, particle dispersion and reaction, and gaseous reaction products including nitrogen and sulfur pollutants. A total of 114 gasifier experiments were performed in three separate test series. Test Series 1 was a set of 88 system evaluation tests. These tests were completed in order to validate igniter operation,

to obtain stable methane/oxygen flames, to check coal feeder calibration, to stabilize coal/oxygen flames, to validate steam boiler flow and control, to develop and validate sample probe and sample collection system operation, to validate the flow stability of the gas delivery system and to test isokinetic sampling. In addition to hardware development, two significant experimental problems were resolved as a part of these system evaluation tests. The first of these problems related to the maximum coal feed rate that could be obtained and still maintain stable reactor operation. The second related to a problem of flame flashback into the primary jet which feeds a mixture of argon, oxygen, and coal dust. The minimum velocity limits to prevent recurring flashback were determined and safe operation was established.

In the second series of gasification experiments, operating limits in terms of oxygen/coal and steam/coal ratios were investigated. Twenty-one tests, including 6 preliminary tests were performed at nominal oxygen/coal ratios of 0.67, 0.83 and 1.00 and steam/coal ratios which ranged from 0.0 up to 0.54. The steam/coal ratio was progressively increased at a set oxygen/coal ratio until the limits of flame stability were reached. Local samples of gas and particles were obtained at a near exit location from within the reactor. This allowed the effects of changing stoichiometry on gaseous products, including nitrogen and sulfur pollutants, and coal reaction to be measured. These results are presented in detail herein.

A third set of 5 gasification experiments (Test Series 3) were performed at an oxygen/coal ratio of 0.83 and a steam/coal ratio of 0.24. These tests provided detailed radial profile measurements of the local gas composition, particle composition and particle mass flux at various axial locations within the reactor. In these tests, argon and helium trace gases were introduced into the primary and secondary streams respectively. The mole fractions of these inert gases were used to determine gas mixing rates within the reactor. As in Test Series 2, local gas and particle samples were removed from within the reactor. These samples were used to determine the local gas and particle compositions which can then be used to deduce chemical reaction rates. Pollutant data on the nitrogen pollutants of NH_3, HCN, and NO and on the sulfur pollutants of H_2S and SO_2 were also taken. These data are also discussed in detail herein.

A fourth series of experiments were conducted to investigate the effects of operating pressure on the gas and particle mixing rates and to obtain some basic gasification data at elevated pressure. This test series was limited to 22 cold flow tests which were used primarily to check out pressurized operation of the reactor (including high pressure controls, coal gasifier, scrubber, and back pressure regulator) of the reactor and the accuracy of the sample collection system. A limited number of these tests were used to obtain cold flow mixing rates in the gasifier. No final data were obtained in Test Series 4 during this contract period.

One and two-dimensional codes were developed to describe pulverized coal gasification. The one-dimensional code was completed, and a user's manual was prepared (Volume II of this final report). Code efficiency was improved and converged solutions were completed. Predictions compared

well with laboratory combustor measurements for both large and small coal particle cases. The code was also applied to selected industrial combustors and gasifiers. The one-dimensional code is available for use in predicting and analyzing pulverized coal gasifiers. While this code can be applied effectively in many situations, it does not provide for detailed local predictions in multi-dimensional furnaces or gasifiers. Thus, development of a two-dimensional code for gaseous, reacting, turbulent systems was also completed during this study. Characteristics of the code were analyzed, and fifty-two converged solutions were obtained. Predictions were compared with laboratory-combustor measurements for the natural gas-air system. Methods for extension of the code to include coal dust were outlined.

In addition to the two volumes of this final report, research results have been documented in nine quarterly progress reports, two doctoral dissertations, four Master of Science theses three technical journal publications and a book. Four technical presentations were also made at combustion meetings. The Industrial Advisory Board was expanded to six members and this group met at Brigham Young University to review the results of this research program. Technical presentation of results was also made at three major boiler manufacturer sites.

TABLE OF CONTENTS - VOLUME 1

LIST OF FIGURES

LIST OF TABLES

NOMENCLATURE

Symbol	Units	Definition
A	$m^3 kg^{-1} s^{-1}$	Pre-exponential factor
C	---	"Universal" constant
D	m	Diameter
E	J $kmol^{-1}$	Activation energy
f	---	Mixture fraction
g	m s^{-2}	Gravitational acceleration
g	---	Mean square fluctuation of f
h	J kg^{-1}	Enthalpy
I	---	Turbulent intensity
k	m^2 s^{-2}	Kinetic energy of turbulence
l	m	Length scale of turbulence
m	kg	Mass
m	---	Mass fraction of species
M	kg	Mass of fluid atoms
M	---	Molecular weight
p	N m^{-2}	Pressure
p	---	Probability density function
q	J $m^{-2} s^{-1}$	Heat flux
r	m	Radial direction
r	kg $m^{-3} s^{-1}$	Reaction rate
R	J $kmol^{-1} K^{-1}$	Universal gas constant
S	arbitrary	Source term
t	s	Time
T	K	Temperature
u	m s^{-1}	Axial velocity component

Symbol	Units	Definition
v	$m\ s^{-1}$	Velocity, radial velocity component
V	m^3	Volume
W	---	Weight fraction
X	---	Mole fraction
y	---	Mole fraction of species
z	m	Axial position
α	---	Intermittency factor
β	arbitrary	Arbitrary property
ϕ	---	Normalized mixing parameter
Γ	arbitrary	Exchange coefficient
δ	---	Normalized dispersion parameter
ε	$m^2\ s^{-3}$	Dissipation rate of turbulence energy
κ	---	Constant
μ	$kg\ m^{-1}s^{-1}$	Dynamic viscosity
ρ	$kg\ m^{-3}$	Density
σ	---	Schmidt or Prandtl Number
τ	$m^2\ s^{-2}$	Shear stress
φ	arbitrary	General variable
Φ	$kg\ m^{-1}s^{-3}$	Dissipation function

Subscripts

A	Argon
ash	Coal or char ash
c	Cell
D	Direction
E	East direction
e	Effective
g	Gas
H	Helium

Subscripts

H	Helium
i	Gas species, summation index
j	Gas species
k	Kinetic energy, element
k	Coal
ℓ	Laminar
N	North direction
p	Primary stream
p	Pollutant
p	P node point
p	Primary jet
r	Reactor
s	Secondary stream
s	Secondary jet
S	South direction
t	Turbulent
w	Water, wall
W	West direction
x	Mixture
ϕ	General ϕ variable
+	Maximum
-	Minimum

Superscripts

$\rightarrow$	Vector
=	Tensor
-	Reynolds mean
$\sim$	Favre mean

I. INTRODUCTION AND SCOPE

A. BACKGROUND

The large energy requirements of our country and the necessity of importing a major fraction of our petroleum fuels have clearly demonstrated the need to develop alternative energy sources. Nuclear, geothermal or solar energy may eventually meet part of this increasing energy need. However, with our present level of technology, we will not be able to supply all of the increasing demands economically from these sources during the present century. As a consequence, it is necessary to continue to convert energy from fossil fuels for a considerable time into the future.

There is significant development work underway to develop new coal gasification, coal liquefaction and coal combustion processes. However, there is very little work of a more fundamental nature directed toward understanding the basic reaction processes in this complex environment. A basic understanding of coal reaction processes is important in successfully developing these advanced conversion systems. In fact, over the years, several developing processes have not been successful, at least in part, because they lacked the fundamental data and techniques needed for optimum design. Several of these coal processes involve, either directly or indirectly, the injection of finely pulverized coal, suspended in a gas stream, into a reactor where the conversion reactions take place, creating a variety of different products. Associated with such particle processes are technical problems involving the entrainment of the coal. The basic principles of this process are not at all well understood and require considerable study before optimum engineering designs are possible. One problem associated with the entrainment of the coal particles is the influence of the turbulent mixing characteristics of a particle-laden gas stream on chemical reactions which take place in the reactor, and on the subsequent yield of products. Questions such as, "How can the reaction vessel best be designed to maximize yields of desirable products and to minimize the undesirable effects of thermal breakdown and decomposition of various unstable products at the extreme operating reaction conditions" cannot be answered until the details of these processes are understood. Such mixing problems have been identified (1)[1] as among the most critical and key problems which need to be solved in order to render the design of entrained pulverized coal reactors practicable.

The Combustion Laboratory of Brigham Young University has been studying the gasification of pulverized coal in an entrained coal gasifier in a two-phase research program. The first phase of the study was supported by the U.S. Energy Research and Development Administration (Contract

---

1( )denotes reference number.

No. E(49-18)-1767) and has been reported previously (2). The second phase of the study was supported by the U.S. Department of Energy (Contract EF-77-S-01-2666) and is reported herein.

During the Phase 1 study, an investigation of the mixing and gasification of coal in an entrained flow reactor was initiated (2). A laboratory-scale, entrained-coal gasifier was designed and constructed to study the effects of turbulent mixing and kinetic processes occurring in entrained coal gasifiers. The reactor, which was designed to operate at up to 2150 kPa (300 psig), was constructed in sections with one section containing several probes for simultaneous gas-particulate sampling. Operation of the gasifier was demonstrated and several preliminary checkout tests were performed. To support these gasification tests, about 180 cold-flow tests were completed to investigate mixing characteristics of particle-laden, confined jets under conditions that simulate the operation of industrial pulverized coal furnaces and gasifiers but without chemical reaction.

A one-dimensional model of coal combustion processes was also developed to account for jet mixing and recirculation, coal pyrolysis, radiation, char oxidation, gas phase reaction, and particle-gas heat transfer. This model was applied to laboratory and industrial pulverized coal furnaces and gasifiers. Development of a second, multi-dimensional coal gasifier model was also initiated. The results of this earlier study were reported in detail in the previous final report (2).

This Phase 2 study, sponsored by the U.S. Department of Energy, is a continuation of the Phase 1 effort. Both the Phase 1 and Phase 2 cold-flow jet mixing tests and analytical modeling efforts have been sponsored jointly by the ERDA/DOE studies and by related studies on pulverized coal combustion which are being sponsored by The Electric Power Research Institute (EPRI) (3,4). The objectives of both the Phase 1 and Phase 2 studies are contained in the following sections.

B. PROGRAM OBJECTIVES

The general objective of this research program was to develop an understanding of physical and chemical rate processes that occur during gasification of entrained, pulverized coal particles. Specific research tasks, which were designed to accomplish the above general objectives, are as follows:

1. Phase 1 Research Tasks

1. Conduct visits to facilities where research and development on entrained coal gasification units are in progress. Identify more specifically the configurations, operating conditions and input properties of reactants and clarify the nature of potential particle/gas mixing problems.

2. Analyze in detail the configurations, reactant systems and operating properties in entrained coal gasifiers and char combustors and select a set of variables for a subsequent experimental test program.

Variables considered included: (1) operating conditions, such as pressure, residence time and flow rates; (2) configurations, such as injection angle and reactor size; (3) reactant stream conditions, such as temperature, gas phase composition, particle size and particle loading level.

3. Design and construct a laboratory-scale facility capable of operation over a range of conditions for study of non-reacting and reacting coal/char/gas systems in different geometries. Include the capability to sample the particle/gas mixtures locally in order to determine the extent of gas mixing, the extent of particle dispersion, the amount of particle reaction and local product composition.

4. Conduct a series of non-reacting tests using the laboratory scale facility to determine the gas dispersion rates for various operating conditions, stream compositions and geometric configurations.

5. Interpret experimental particle/gas dispersion results and analyze for potential impact on configuration and operating conditions in entrained coal-gasification units.

6. Initiate the development of a computerized mathematical model for describing reacting coal gasification and char combustion processes.

2. Phase 2 Research Tasks

1. Maintain contact with industrial and governmental organizations which are conducting entrained gasification development and design work. Present study results at technical meetings. Report periodically on research progress to DOE fossil energy representatives.

2. Complete the non-reactive, atmospheric and high pressure cold-flow tests initiated under Phase 1. Atmospheric tests emphasize recirculation effects in ducts of several different diameters.

3. Conduct a series of reacting experiments using char and coal particles. Measure, locally in the reacting system, the extent of particle dispersion, the extent of gas mixing, the amount of particle reaction, the local product composition, the extent of pollutant formation and the temperature and/or velocity distribution.

4. Complete the development of the macroscopic computerized mathematical model for describing the reacting coal gasification or char combustion processes. Include recirculation effects and also include available theory and measurements on the behavior of char or coal particle reaction and on gas/particle dispersion. Investigate the characteristics of the model and conduct parametric studies to determine relative tradeoffs resulting from variation to controllable parameters. Compare model predictions with measured results and deduce dominant processes that occur during these particle reaction sequences.

5. Analyze all reacting and non-reacting data with model predictions, where appropriate, to determine the impact of results on design of coal gasification units. Make recommendations of possible configuration

and operating conditions for improvement of gasification efficiency, pollutant formation and reactor size.

6. Investigate the effects of coal feed rate and inlet coal/steam/-oxygen mixture ratios on flame stability and extent of coal reaction in the laboratory gasifier. Probes will be located toward the exist of the gasifier. Results will include determination of the regions of flame stability and will be compared with several commercial and pilot-scale entrained gasification systems.

7. Conduct additional detailed gasification tests using the gasifier and probe system to characterize the effects of such variables as pressure, secondary gas temperature, coal particle size and coal type. Emphasis will be on radial profile measurements of gas and solids composition at several axial locations. Data will help to clarify important rate processes inside the gasifier and will provide a basis for evaluation of predictive codes.

8. Document the results in a final report.

A detailed description of work completed during the Phase 2 program follows.

II. TESTS WITHOUT REACTION

A. OBJECTIVES AND APPROACH

Definition of the mixing characteristics of particle-laden confined jets is important in developing a complete understanding of the processes which influence the operation of entrained coal gasifiers. The mixing characteristics of the primary and secondary streams can have important effects upon coal reaction processes. Efficiency of the gasification process and the accompanying production of pollutants are closely linked to this mixing process. Design variables such as stream flow rates and velocities, secondary injection angle, inlet turbulence level and inlet expansion ratio all affect the rates at which the streams mix. Therefore, determination of the mixing rates of confined jets under varying flow conditions and geometries is important in understanding, characterizing and predicting the behavior of systems in which jet mixing is an integral part.

The purpose of this part of the present research study was to investigate the mixing characteristics of particle-laden, confined jets under experimental conditions that would simulate the operation of entrained coal gasifiers and pulverized coal combustors but without chemical reaction. The cold-flow test program complements the gasification tests such that a number of flow variables and reactor geometries can be studied without chemical reaction. This allows the physical effects of mixing and reaction to be separately evaluated. In addition, the cold-flow experiments provide a valuable data base for analytical model evaluation. The non-reactive tests allow the various hydrodynamic mixing models to be separately validated without the complicating effects of chemical reaction.

The approach used in this study was to measure radial profiles of gas composition, particle mass flux and gas velocity in the mixing zone at various axial locations downstream of the jet exit plane. Effects of inlet velocity, gas density, mass flow rate, injection angle, particle loading level, particle size and mixing duct size on the rates of particle and gas mixing were examined. These cold-flow tests have been conducted under joint sponsorship of DOE (2 and this study) and EPRI (3, 4).

Previous cold-flow studies in support of the coal gasification program have included the work of Memmott (5, 6) and, Tice (7, 8). Effects of parallel and nonparallel secondary injection (Test Series 1) into the mixing chamber and the effects of injection into a larger recirculation mixing chamber (Test Series 2) were investigated. Results of Test Series 1 were reported in detail and preliminary results from Test Series 2 were included in a previous ERDA final report (2). Analysis of the results of the 61 tests from Test Series 2 mentioned in that report are detailed herein. Subsequently, three additional cold-flow test series were undertaken. Test Series 3, a study recently completed by Sharp (9), included the effects of angular injection into an expanded recirculation chamber. Test Series 4 included tests with combined angular

injection and recirculation and effects of pulverized coal, and Test Series 5 investigated the effects of secondary swirl. Test Series 4 and 5 are reported in detail by Leavitt (10). Results from Test Series 3, 4 and 5 are summarized in this section.

B. TEST FACILITY

The test facility used in this study had been used previously in other jet mixing studies (5,7,11,and 12) and required only minor modifications for use in Test Series 3,4, and 5. The facility has been described in detail elsewhere (2,3,5-12). A description of the modifications to the facility required for Test Series 3, 4, and 5 is contained in the following two subsections.

1. Recirculation with Angular or Coaxial Injection

In these test series, both parallel and nonparallel secondary injection were investigated. These injection systems are illustrated in Figure 1. The parallel injection system used is similar to that by Hedman and Smoot (11), but with some modifications introduced by Tice (7, 8). The nonparallel system used was originally designed and constructed by Allred (12), who investigated systems with 30^{o}, 60^{o}, and 90^{o} secondary injection. Results showed angular injection to have a significant effect on the mixing rates. The 30^{o} injection system is compatible with existing coal combustion and gasification systems.

In order to simulate the configurations of "sudden-dump" combustors, modifications were made by Tice (7, 8) which allowed use of expanded mixing chambers. Three expanded mixing chambers were fabricated. The chamber diameters were 206 mm (small), 260 mm (medium), and 343 mm (large). The sudden enlargement of the mixing section causes flow separation and extensive recirculation. In the tests performed by Memmott (5, 6), there was no expansion of the basic 130 mm diameter mixing section.

A number of minor modifications were made to the mixing chamber-instrument collar sections for Test Series 3 and 4. Modifications of the nonparallel injection collar were required in order to accommodate the expanded mixing chambers. Also, minor alterations were made on the instrument collar which allowed extension of the expanded mixing chamber downstream of the collar. Previously (7, 8), the instrument collar was always the last section of the mixing chamber. A description of the data acquisition procedures and data reduction methods was reported in the previous ERDA report (2) and will not be repeated here.

2. Swirl Tests

After an extensive investigation into methods of introducing swirl into the secondary air stream, it was decided to design and fabricate a swirl block generator patterned after the design used in the International Flame Foundation furnace (13) at Ijmuiden, Holland. Figure 2 shows a schematic of the stationary and moveable swirl blocks as well

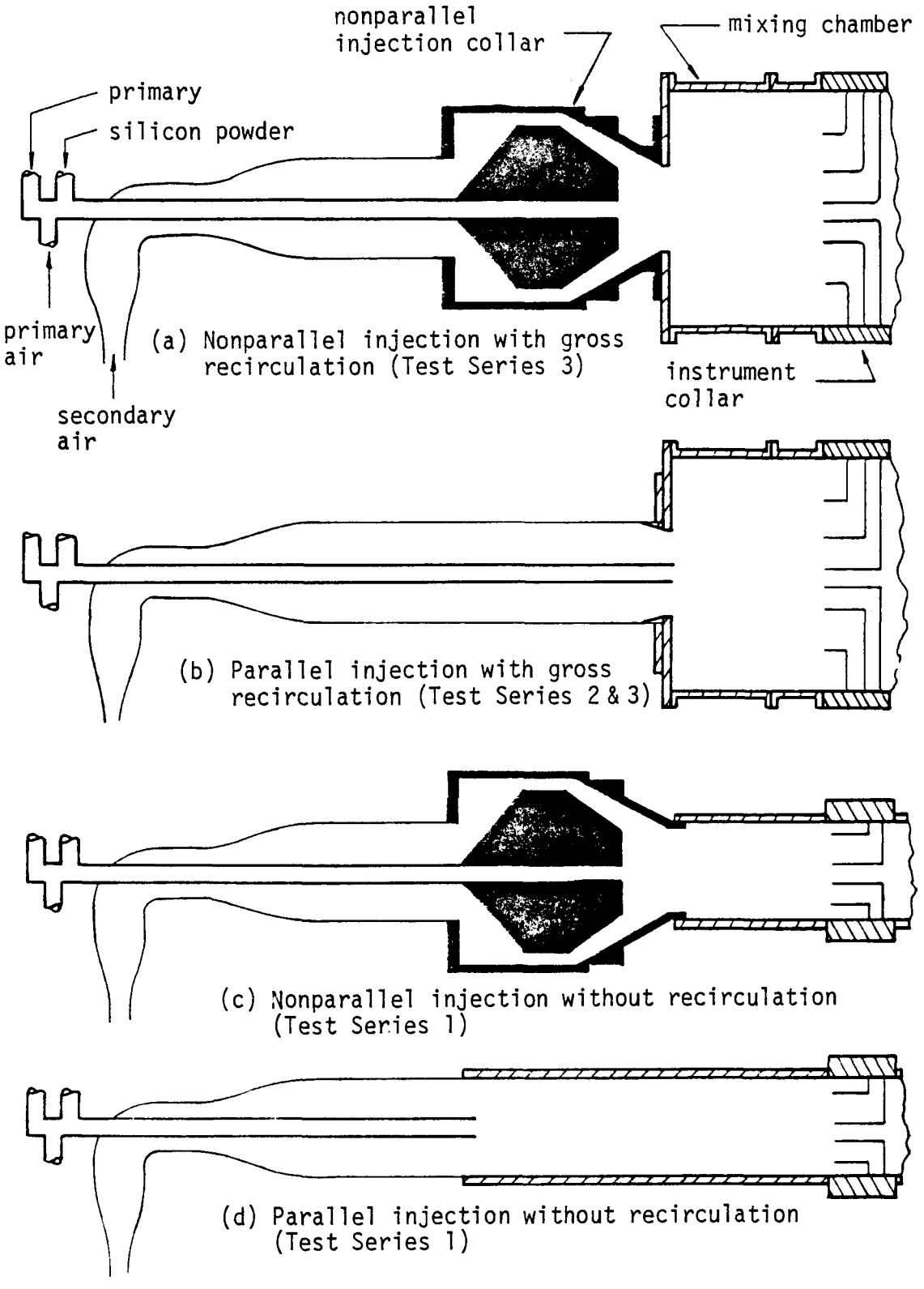

Figure 1. Schematics of flow geometries used in cold-flow test series 1, 2 and 3

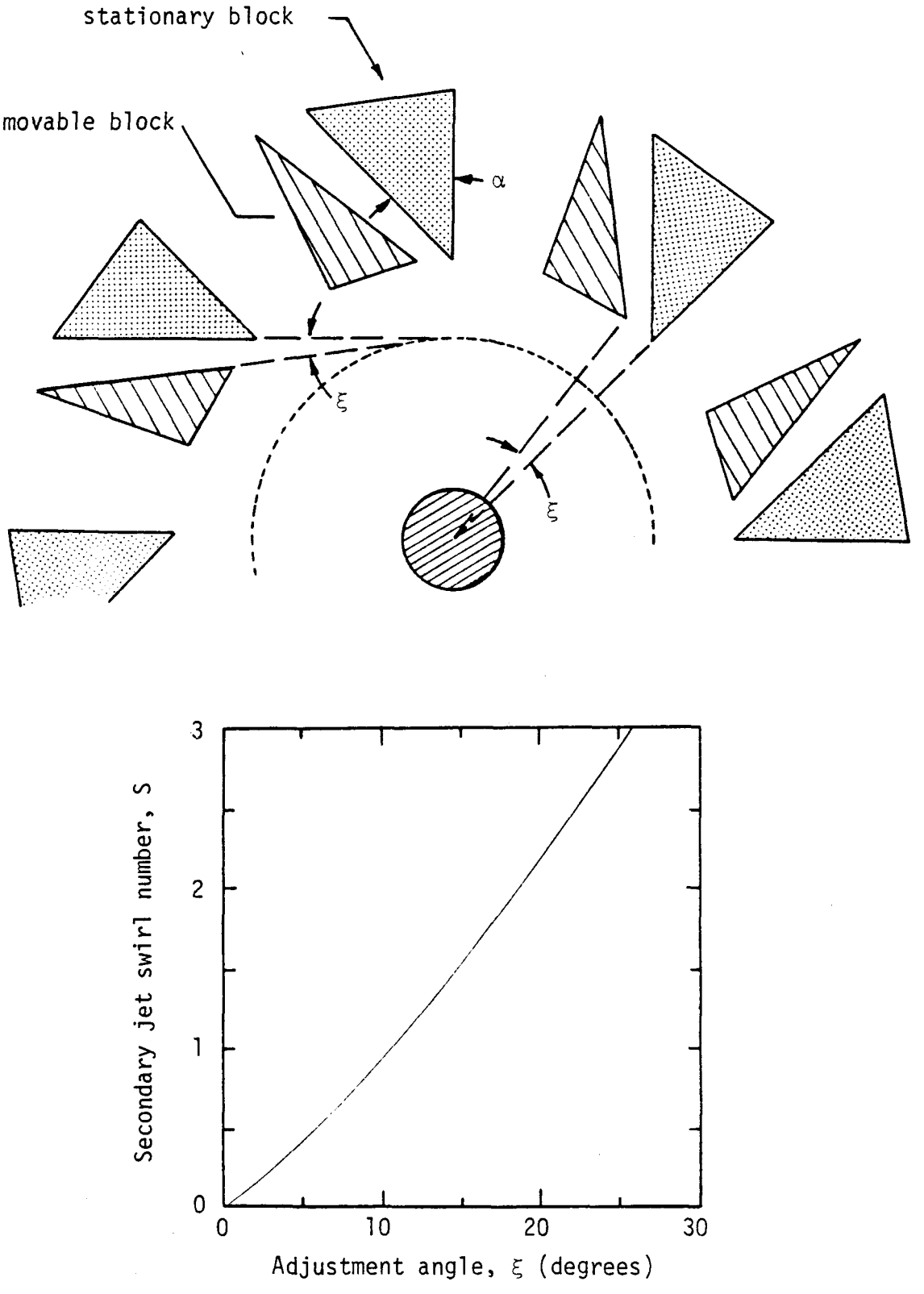

Figure 2. Schematic of swirl blocks and variation of theoretical swirl number with adjustment angle

as the variation in theoretical Swirl Number with swirl-block adjustment angle. A more detailed drawing of the swirl block generator is shown in Figure 3, and photographs of the unit are shown in Figure 4. The swirl block generator has been fabricated, installed on the cold flow facility, and preliminary check-out and 28 final tests were completed.

Sampling of particles and gases in a swirling, turbulent flow presents some interesting challenges. The preliminary swirl data were obtained with the existing fixed sample probes and sample collection system. It was recognized that these probes would not always be aligned to the swirling flow except at far downstream positions. Consequently, a sampling probe was designed and fabricated which could be aligned to the swirling flow, as shown in Figure 5. A photograph showing this probe installed in the probe collar is shown in Figure 6. This single, traversing-rotating probe was designed to replace the rigid multiple-probe bank used in the instrument collar. The new probe rotated about the probe entrance so that it could be aligned to the flow without a positional change in the probe inlet. The probe also included a dusty gas stagnation pressure probe (11) and the associated static pressure probes. Two static pressure probes were incorporated into the design in anticipation of the strong radial pressure gradients expected in swirling flows. The various probe components used in this special probe have been used successfully in all of the previous cold-flow test programs (5-12). Additional features of the new probe design are the symmetrical top and bottom pressure taps near the rear of the probe assembly. These taps, which were patterned after velocity probes used at Ijmuiden (13) were used to align the sample probe to the mean flow direction. This was accomplished by rotating the probe in the flow stream until the pressure difference measured between the top and bottom pressure taps was zero. Not only did this align the probe to the flow, but it also gave an independent measurement of the local flow direction.

C. TEST PROCEDURES AND DATA REDUCTION

The test procedures as well as methods of data reduction and presentation have been presented in detail (5, 7, 9) and were summarized in the previous ERDA report (2). Briefly, a cold flow test proceeded by introducing a particle-laden, primary jet surrounded by a concentric, secondary air jet into a mixing chamber. The primary jet was composed of air, an argon trace gas and a solid particle phase -- silicon or coal dust. Gas and particle samples were obtained in isokinetic sampling probes. The stagnation pressure of the gas was measured in dusty gas stagnation probes (11). Static pressure across the mixing duct was measured with the static taps of conventional pitot tubes. The pressure measurements allowed the gas velocity to be determined if the velocity was not too small.

Samples were collected and analyzed for argon concentration, and particle mass. The argon concentration data allowed the local extent of gas mixing to be determined. A local particle mass flux was deduced from the particle sample. Comparison of the particle mass flux to the particle flux in the primary provides a measure of the rate of particle dispersion.

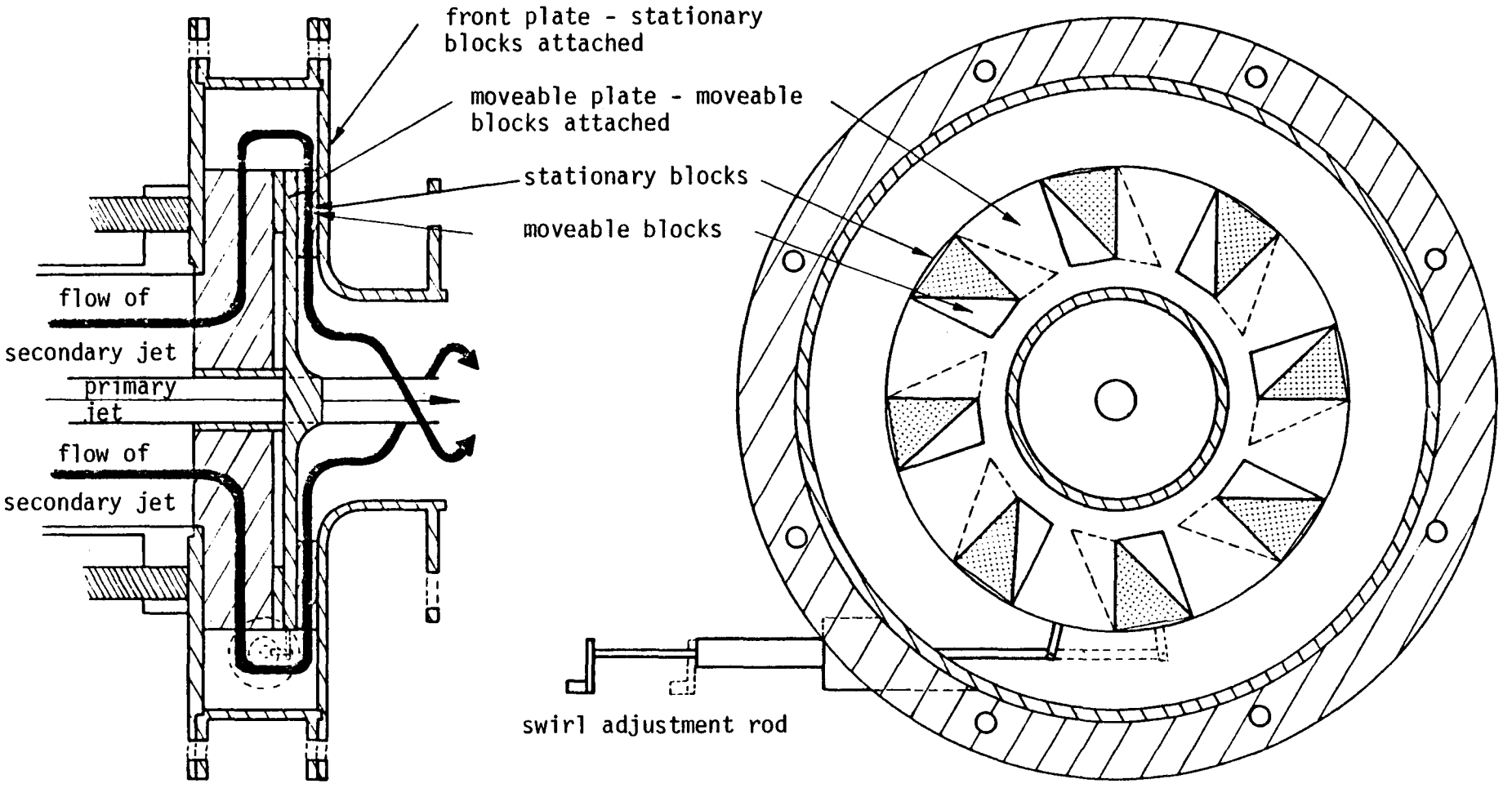

Figure 3. Schematic of cold-flow swirl block generator.

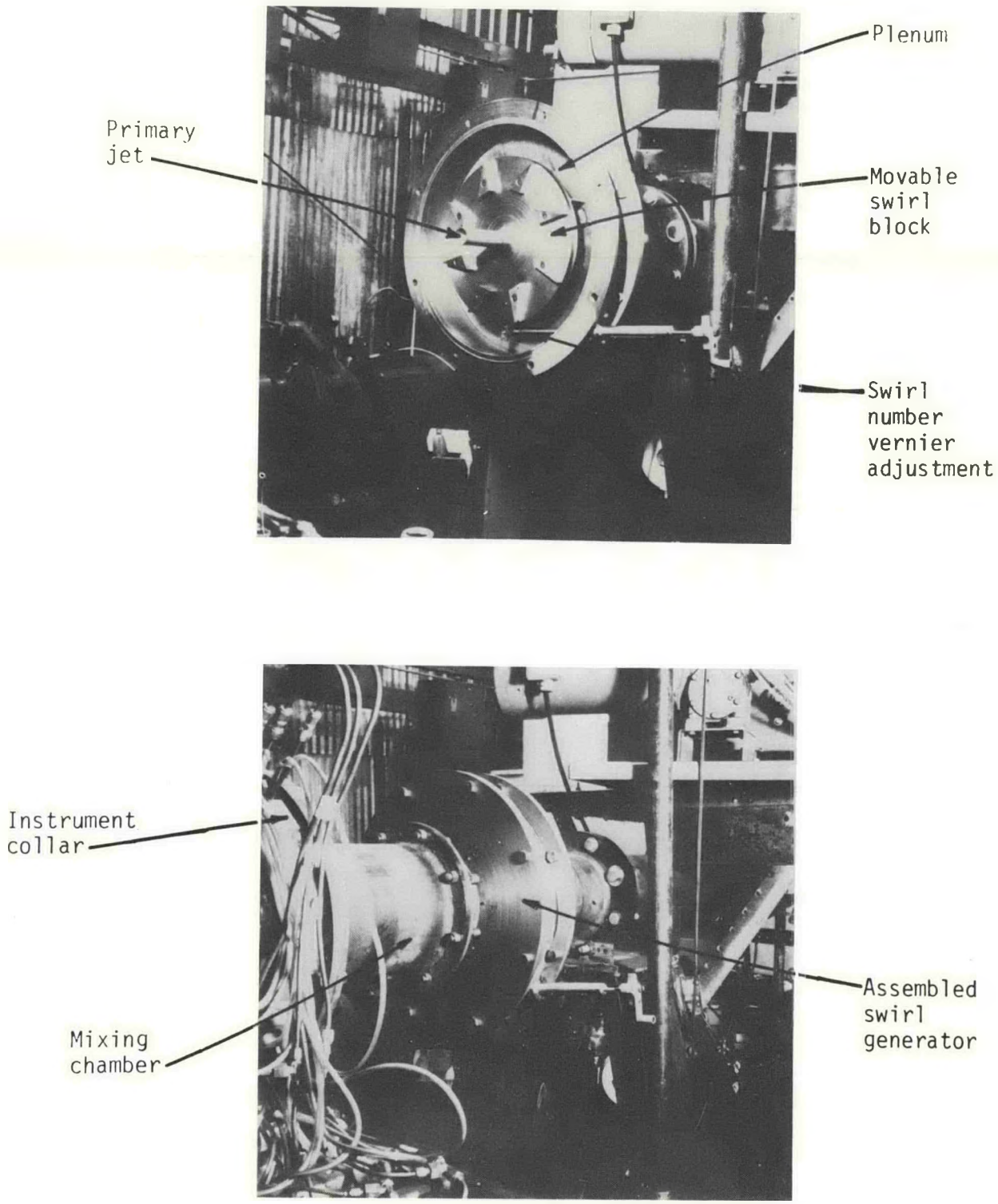

Figure 4. Photographs of cold-flow swirl generator.

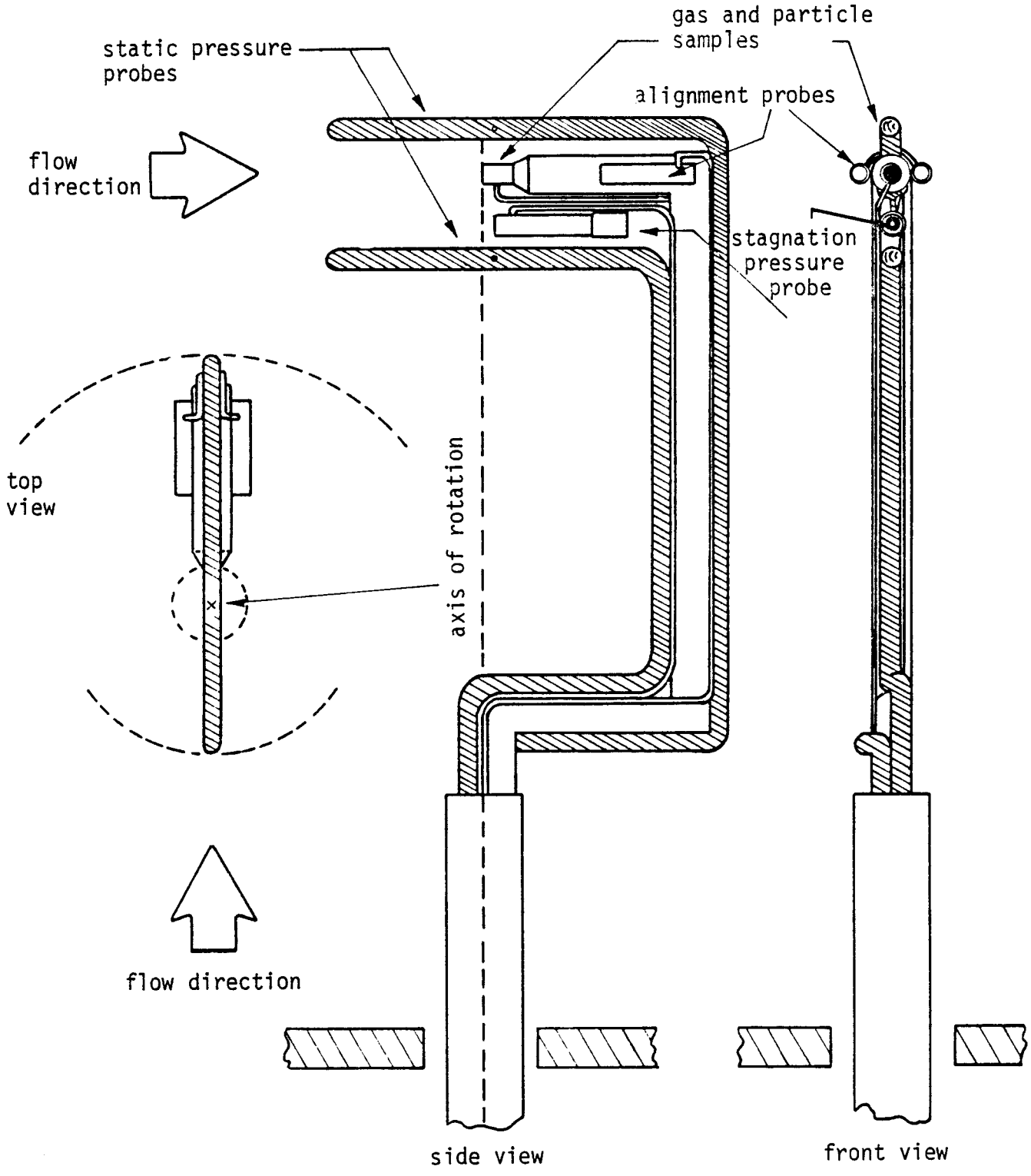

Figure 5. Schematic of rotating, traversing, isokinetic probe for cold-flow swirl tests

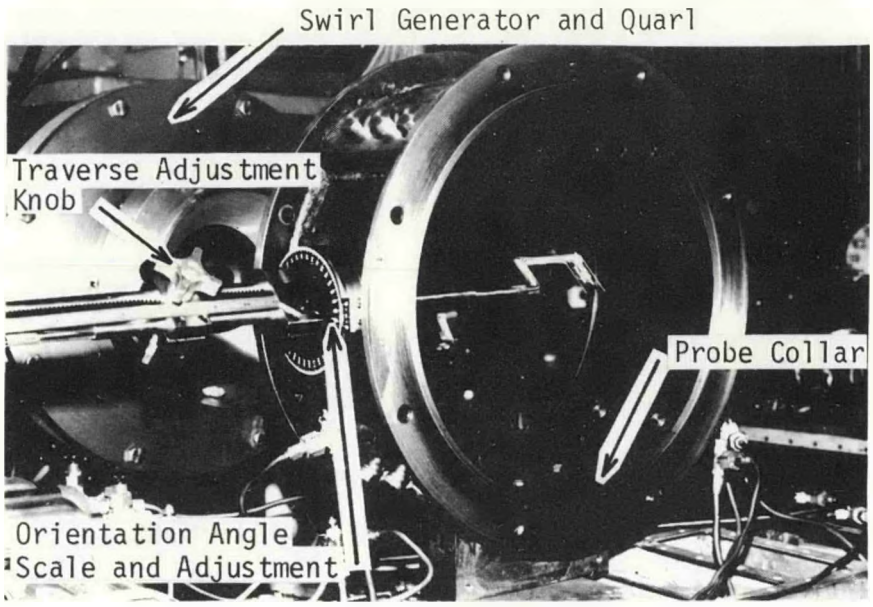

a) Probe installed in probe collar.

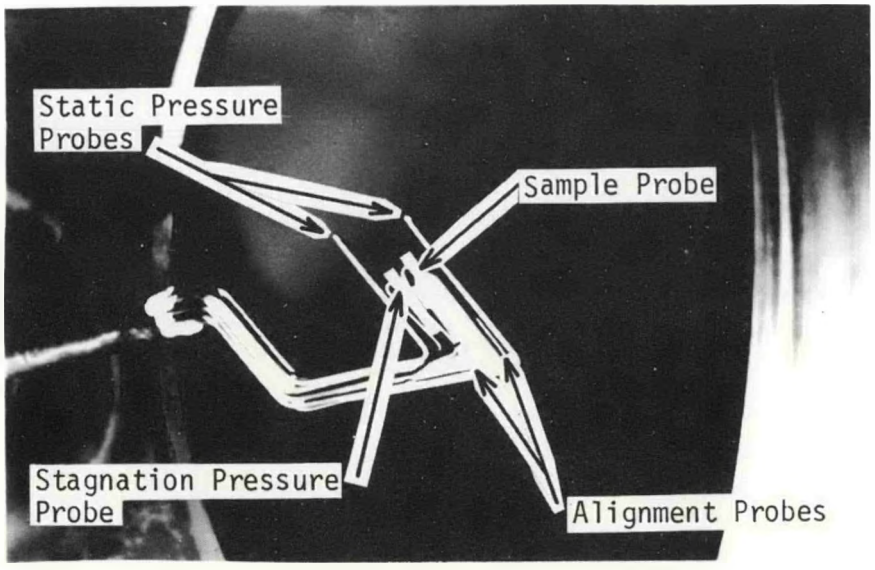

b) Close up view of probe.

Figure 6. Photographs of cold flow rotating traversing probe.

Gas and particle samples were obtained at various radial and axial locations within the mixing chamber. The local radial data were fit with an exponential equation (or a polynomial equation for the swirl tests) in order to smooth the results, and interpolate or extrapolate the radial profiles to the wall or centerline. Axial centerline data allowed a core length and/or a complete mixing length to be determined for both gas and particle phases. A comparison of the reciprocal core lengths provided a quantitative measure of the initial gas and particle mixing rates (5, 7, 9). The reader is referred to the previous ERDA report (2) as well as the Theses of Memmott (5), Tice (7), Sharp (9) and Leavitt (10) for more detail regarding testing procedure and data analysis.

D. TEST RESULTS

1. Tests with Recirculation and Parallel Injection (Test Series 2)

The objectives of the cold-flow tests with recirculation were to measure the rates of mixing of a particle-laden, primary jet with a secondary air jet and particularly to determine the effect of mixing duct diameter on the rates of mixing of the particles and the gas. The cold-flow tests were performed under conditions similar to those of the reacting tests in order to provide useful information for interpretation of the reacting portion of the study and for computer code evaluation. A summary of the flow conditions used in Test Series 2 is given in Table 1. The velocity of the primary jet was constant for all flow conditions at approximately 30.5 m/s (100 fps) while the secondary velocity was approximately 61 m/s (200 fps) for one flow condition and 38 m/s (125 fps) for the remaining flow conditions. The secondary temperature was approximately 283 K (50^{0}F). Silicon powder was used in this test series. The size distribution of the standard silicon powder used in this study compared very closely with that of coal used in typical pulverized coal furnaces. Some of the silicon powder was classified using a vortex cyclone particle classifier to separate the smaller and larger particles. This gave three different size distributions of particles. Two of the flow conditions differed only in the size distribution of particles used. The mass mean diameters of the two size distributions are 38.6 μm, and 54.1 μm.

The cold-flow tests with recirculation were performed in a parallel-flow configuration, with both jets exhausting into a mixing chamber larger in diameter than the secondary jet diameter. This flow configuration was shown in Figure 1(b). The tests performed correspond to flow conditions 1 (reference), 1-GO(reference-gas only), 2 (high solids loading and large silicon dust), 3 (high secondary velocity) and 6 (large silicon dust). Since these conditions were very similar to the parallel and nonparallel cold-flow conditions, the effects of recirculation on mixing rates was readily determined.

The test program was designed to measure effects of the following variables on the rates of mixing: primary and secondary flow rates, particle size, particle-solids loading, and diameter of the mixing section. Also, the use of a primary flow screen was a variable which was introduced

TABLE 1

SUMMARY OF FLOW CONDITIONS FOR COLD-FLOW TEST - SERIES 2

Flow Condition[1]	1 Standard Condition		1-GO Standard Gas-Only		2 High Solids Loading		3 High Velocity Secondary		6 Large Particles	
Parameter	Pri	Sec	Pri	Sec	Pri	Sec	Pri	Sec	Pri	Sec
Velocity, m/s	30.5	38.1	30.5	38.1	30.5	38.1	30.5	61.0	30.5	38.1
Flow Rate, g/s										
Air	5.4	456	5.4	456	5.4	456	5.4	729	5.4	456
Argon	17.4		17.4		17.4		17.4		17.4	
Particles	15.2		Gas-Only		34.2		15.2		15.2	
Temperature, K	283	283	283	283	283	283	283	283	283	283
Particle Size	Std.[2]				Large		Std.		Large	
Wt. % Solids	40		0		60		40		40	
Mole % Argon	70		70		70		70		70	
Sec/Pri Ratios										
Velocity	1.25		1.25		1.25		2.00		1.25	
Gas Density	0.79		0.79		0.79		0.79		0.79	
Total Density	0.47				0.32		0.47		0.47	
Gas Flow	20.0		20.0		20.0		32.0		20.0	
Total Flow	12.0				8.00		19.2		12.0	

[1] Tests are run at ambient conditions unless otherwise noted, i.e., pressure is about 90 kPa (0.88 atm) and temperature is about 283 K.

[2] Silicon powder as received, before classification.

[3] GO ≡ Gas-only

during the execution of the test program to better understand some unusual characteristics of the particle mixing pattern which were observed and will be shown later.

For Test Series 2, 61 tests were completed, of which 59 provided reliable data. Tests were run for the five flow conditions outlined previously. These tests used the large test chamber (343 mm) and small (206 mm) test chamber and were compared with the data from the nonrecirculating tests (5, 6), which used the same flow conditions but with a mixing chamber diameter equal to that of the secondary jet.

The analysis of the data made extensive use of the centerline axial decay plot. The centerline axial decay plots for these tests are shown in Figures 7 through 10. The comparison of the core lengths and decay slopes with other test series showed the effects of each variable on the rates of mixing of particles and gases. Data for all 61 tests are reported in detail by Tice (7, 8).

Gas vs. Particle Mixing Rates. Results from Test Series 2 confirmed that of previous work at this laboratory wherein the gas mixing rate was always faster than the particle mixing rate for all conditions tested. The gas mixing rate was usually about twice as fast as the particle mixing rate, but ranged from factors of 1.3 to 3.6, as illustrated by comparing Figures 7 through 10 and as summarized in Table 2. These results clearly demonstrate that the particles did not follow the motion of the gas, but lagged significantly. Special precautions were taken to insure that the particle and gas velocites were comparable at the primary nozzle exit. Thus, the observed particle lag was induced during the mixing process itself.

The ratio of the gas mixing rate to the particle mixing rate was often somewhat smaller than that observed in Test Series 1. Thus, while the gas mixed more rapidly in the expanded mixing chamber over that for chambers without recirculation, the particle mixing rate often increased even more in these expanded chambers.

Effect of Mixing Chamber Diameter. Most pulverized coal reactors provide for injection of the coal into a large reaction chamber. Thus, determination of mixing rates in such expanded chambers can be useful to the design and performance-evaluation of such systems. Use of the expanded mixing chambers (206 mm and 343 mm) affected the gas and particle mixing rates significantly. The particle mixing rates in the expanded mixing chambers were 1.4 to 1.9 times faster than the corresponding rates of the non-expanded mixing chamber (130 mm diameter) as illustrated in Table 2. The gas mixing rates for the expanded chamber systems were faster than for the non-expanded chamber system by factors of 1.2 to 2.4, also illustrated in Table 2, except for one case. Flow condition 3 (high velocity secondary jet) was the only case where the gas mixing rates of the expanded chambers were not greatly enhanced over those for non-expanded chambers. Thus, it appeared that both the particles and gas were influenced by recirculation in the larger mixing chambers, with attendant increases in residence time and enhancement in gross mixing rate.

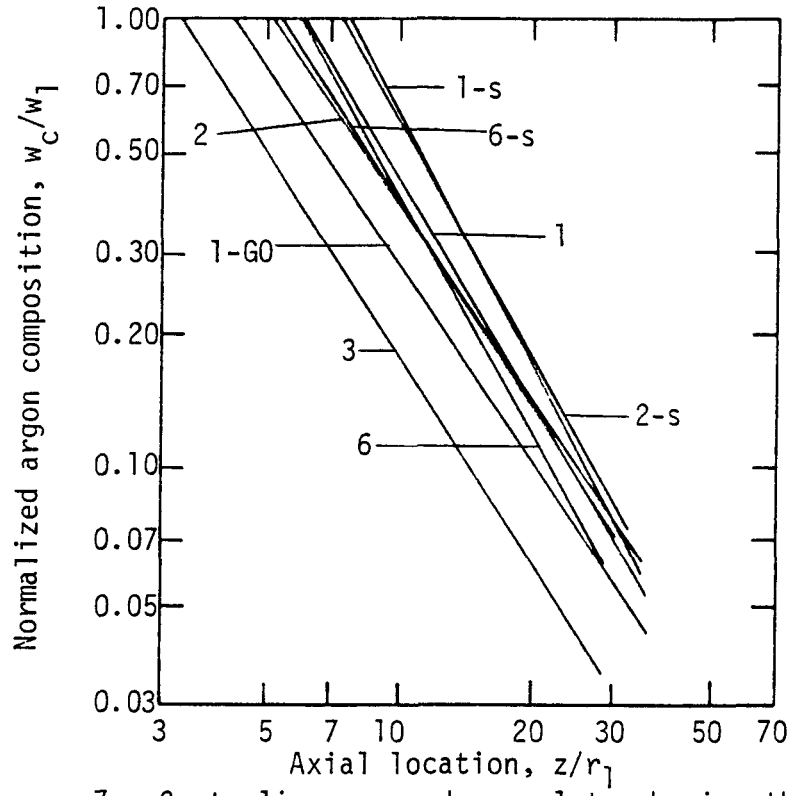

Figure 7. Centerline argon decay plots showing the effect of flow condition for the small (206mm) expanded duct

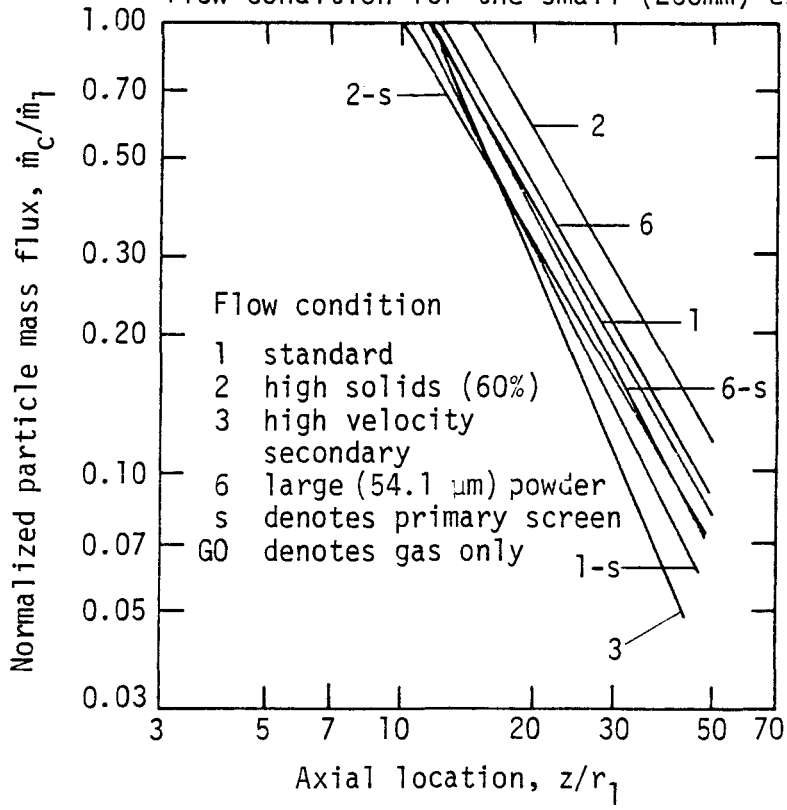

Figure 8. Centerline particle decay plots showing the effect of flow condition for the small (206mm) expanded duct

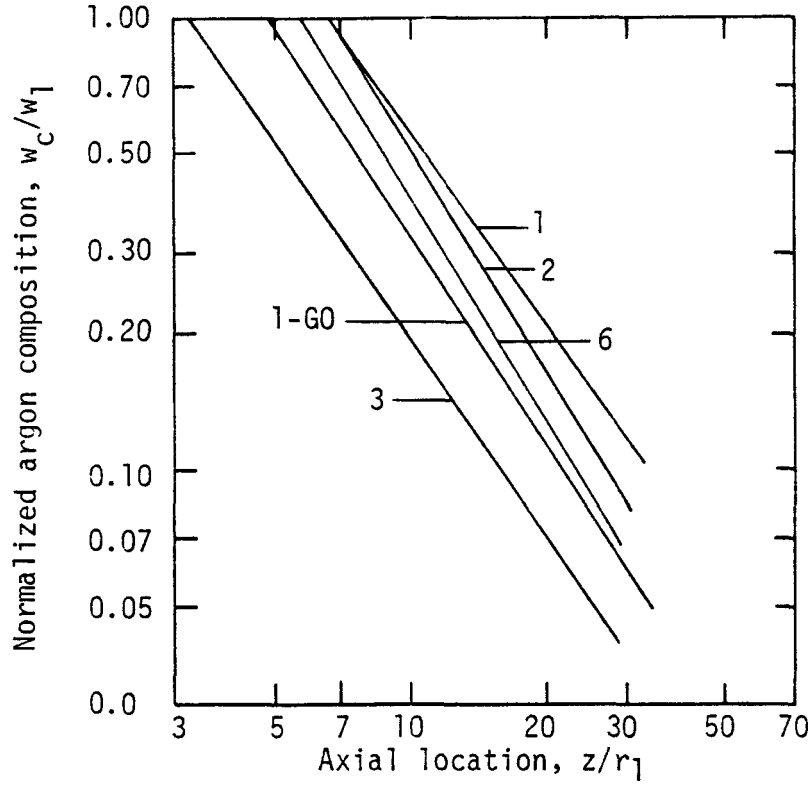

Figure 9. Centerline argon decay plots showing the effect of flow condition for the large (343mm) expanded duct

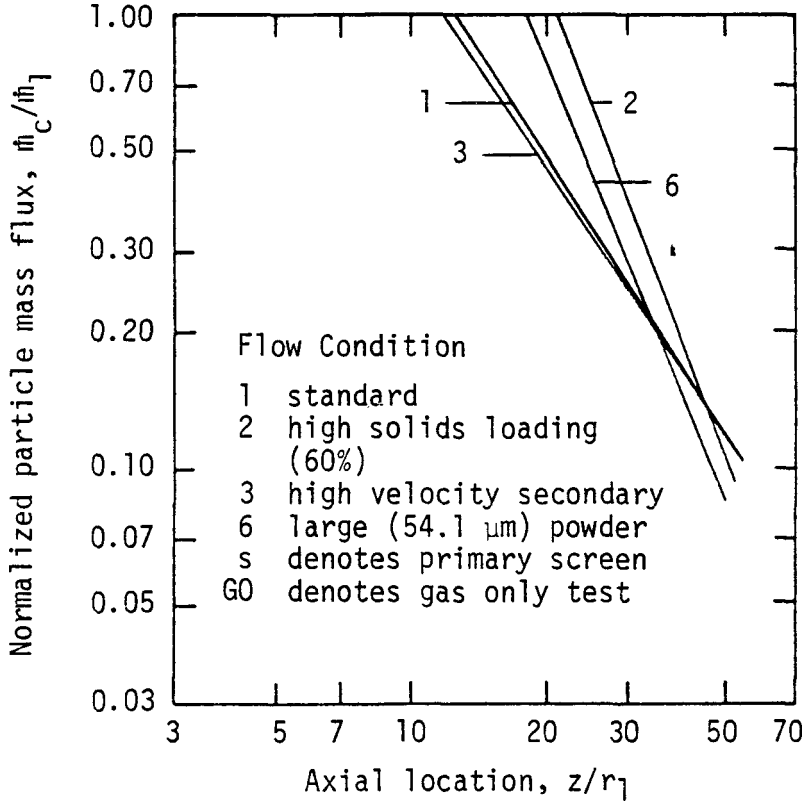

Figure 10. Centerline particle decay plots showing the effect of flow condition for the large (343mm) expanded duct

TABLE 2

SUMMARY OF MIXING RATES FOR RECIRCULATION TESTS (SERIES 2)
(Reciprocal Core Length, m^{-1})

	Parallel Injection (5,6) (130 mm)		Small Chamber (206 mm)		Large Chamber (343 mm)	
Flow Condition	Gas	Particle	Gas	Particle	Gas	Particle
1 -GO(Gas only)	7.5	-	18.5	-	16.5	-
1 (Reference case)	10.6	4.9	12.7	6.8	12.2	6.2
2 (60% Loading, Large, 54.1 μm)	-	-	14.7	5.4	12.1	3.7
3 (High Secondary Velocity)	22.7	3.9	23.6	6.7	24.4	6.6
6 (Large, 54.1 μm)	7.4	3.3	12.9	6.3	13.9	4.3

Rates of mixing of particles and of gases in the two expanded chambers (206 mm and 343 mm, diameter) were very similar. Thus, once a recirculating flow was established, the size of the duct did not have a major effect on mixing rates. However, for tests with large particles, use of the largest mixing chamber did retard particle dispersion, which was approximately 70% of that of the particle mixing rate with the smaller expanded mixing chamber. Apparently, larger particles did not recirculate as readily as the small particles.

Effect of Secondary Velocity. The effect of increasing the secondary jet velocity from 38 m/s to 61 m/s, while maintaining the primary jet at 30.5 m/s, was very similar to the findings in Test Series 1 (5, 6). The gas mixing rates nearly doubled when the secondary velocity was increased but the particle mixing rates remained essentially unchanged, as shown in Figures 7 and 9. Although particles were not affected, the increase in the secondary jet velocity was one of the most important flow parameters for controlling gas mixing, as illustrated in Table 2. Since the values of primary and secondary velocity were initially of comparable magnitude, the increase of secondary velocity by about 60% apparently caused a major increase in turbulent stresses in the gas, which were related to the difference in primary and secondary velocities. However, the particles were apparently not able to respond to the more rapid gas mixing. Many of the pulverized coal combustors and entrained gasifiers use jet velocities in the range examined here. Because of the effects of a change in velocity, this parameter is one that can potentially be used to control the gas mixing processes of such systems, without significantly altering particle mixing rates.

Effect of Particle Size. The standard-sized silicon used in this study had a mass mean diameter of 38.6 μm (flow conditions 1 and 3). A larger size was also used (flow conditions 2 and 6) which had a mass mean diameter of 54.1 μm. Typical pulverized coal has mass mean diameters in the range of 40-60 μm and is therefore similar in size to the silicon powders used in this study. Increasing the particle size at a fixed solids-loading level caused the gas mixing rate to change only slightly as illustrated in Figures 7 and 9 and in Table 2. Further, when the small expanded mixing chamber was used, both particle sizes dispersed at nearly the same rate, with the large particles mixing slightly slower, as shown in Figures 8 and 10 and in Table 2. However, in tests where the large expanded chamber was involved, the smaller particles mixed nearly one and a half times as fast as the larger paticles. This was consistent with the variation of drag forces of the gas upon particles, which vary strongly with particle size.

Effect of Solids-Loading. The particle solids-loading of the primary stream was varied from 0 weight percent (flow condition 1-G0) to 40 weight percent (flow conditions 1, 3 and 6) and to 60 weight percent (condition 2). Typical pulverized coal gasifiers and furnaces use solids-loading levels ranging from 40 to 90 weight percent. Test results in Figures 7 through 10 and summarized in Table 2 show an appreciable decrease in gas mixing rates when going from 0% solids loading to 40% solids loading. A further increase in solids loading from 40% to 60% showed only a slight additional change in gas mixing rate. The particle mixing rate showed a moderate decrease when going from the 40% loading (flow

condition 6) to the 60% loading (flow condition 2). Overall, the parameter of solids-loading level did not seem to be an important variable in control of mixing rates, although at higher solids-loadings in the range of 80 to 90 weight percent, the results may be quite different.

Effect of Primary Screen. For large particle and high solids-loading tests, particle profiles indicated a lack of uniformity, and material balance errors were high. A screen was therefore inserted at the end of the primary tube to smooth the initial particle distribution in the primary gas. The screen did produce a smoother particle profile and generally increased the particle mixing rate slightly. However, the effect of the screen on the gas mixing rates was small. Thus the screen apparently increased particle mixing rates by improving the initial particle distribution in the primary tube and not by increasing turbulence levels in the gas.

2. Tests with Recirculation and Nonparallel Injection (Test Series 3)

Reference 9 has summarized and analyzed the cold-flow tests performed under Test Series 3. The previous cold-flow Test Series (numbers 1 and 2) showed the effects of angular injection of the secondary stream and expansion of the primary and secondary jets into expanded recirculation mixing chambers. In Test Series 3, the effect of angular injection of the secondary into the expanded recirculation mixing chamber was examined. Figure 1(a) showed schematically the geometry used for this test series. Primary and secondary jet velocities were nominally 30.5 and 38.1 m/s (100 and 125 fps) respectively. Clean gas tests, as well as tests with 40% solids loading in the primary jet, were performed. Tests were also performed with a higher 61.0 m/s secondary velocity (200 fps) and with a smaller mean particle size (24 μm versus 46 μm). A summary of the test conditions used for Test Series 3 is contained in Table 3.

Each test was run at a certain flow condition and a specific system geometry. With the four flow conditions and seven geometries chosen for this study, a total of twenty-eight different combinations were possible. Table 4 gives a summary of the number of tests actually performed. In the constant length mixing chamber tests, the overall mixing chamber length was held constant by addition of extra mixing chamber spools behind the instrument collar as needed. In these tests, the mixing chamber length was held constant regardless of the location of the instrument collar.

The relative mixing rates of the particles and gases for Test Series 3 are shown in Figures 11 and 12. Figure 11 also presents data obtained in Test Series 3 with parallel injection into the expanded mixing chambers. This compliments that presented previously (2, 3). The previous parallel data were for the small and large duct. The data in Figure 11 reproduce the same small duct data and add data for injection into the medium size duct. Figure 12 summarizes the data obtained with a 30^{o} secondary injection into the expanded recirculation ducts. Data were collected for the small and large ducts only.

TABLE 3

SUMMARY OF FLOW CONDITIONS USED IN TEST SERIES 3*

FLOW CONDITION:	1		2		3		4	
PARAMETERS:	Pri.	Sec.	Pri.	Sec.	Pri.	Sec.	Pri.	Sec.
Velocity (m/s)	30.5	38.1	30.5	38.1	30.5	38.1	30.5	61.0
Particle	Gas Only		Std. Silicon (46.1 μm)		Small Silicon (24.2 μm)		Std. Silicon (46.1 μm)	
Wt. % Solids	0.		40.		40.		40.	
Mole % Argon	70.		70.		70.		70.	
Flow Rates (gm/s)								
Air	5.3	520.	5.3	520.	5.3	520.	5.3	835.
Argon	17.0		17.0		17.0		17.0	
Particle	0.0		14.9		14.9		14.9	
Ratios of Sec/Pri								
Velocity	1.25		1.25		1.25		2.00	
Gas Density	0.79		0.79		0.79		0.79	
Total Density	0.79		0.47		0.47		0.47	
Gas Flow	23.3		23.3		23.3		37.4	
Total Flow	23.3		14.0		14.0		22.4	

*Pressure is about 0.88 atm and temperature is about 283 K.

TABLE 4

SUMMARY OF TESTS IN TEST SERIES 3

FLOW CONDITION:	1	2	3	4
FLOW CONFIGURATION (Mixing Chamber Diameter and Injection Angle)	(Reference, Gas Only)	(Reference)	(Small Silicon)	(High Velocity Secondary)
Small Diameter (206mm), Parallel	-	5	4	-
Small Diameter (206mm), 30 Degree	4	4	-	5
Medium Diameter (260mm), Parallel	4	4	-	-
Medium Diameter (260mm), Parallel (Constant Length Mixing Chamber)	-	8	-	-
Medium Diameter (260mm), 30 Degree	-	-	-	-
Large Diameter (343mm), Parallel	-	-	-	-
Large Diameter (343mm), 30 Degree	7	8	-	4

NOTE: Numbers listed denote number of tests completed. Total number of tests run: 57.

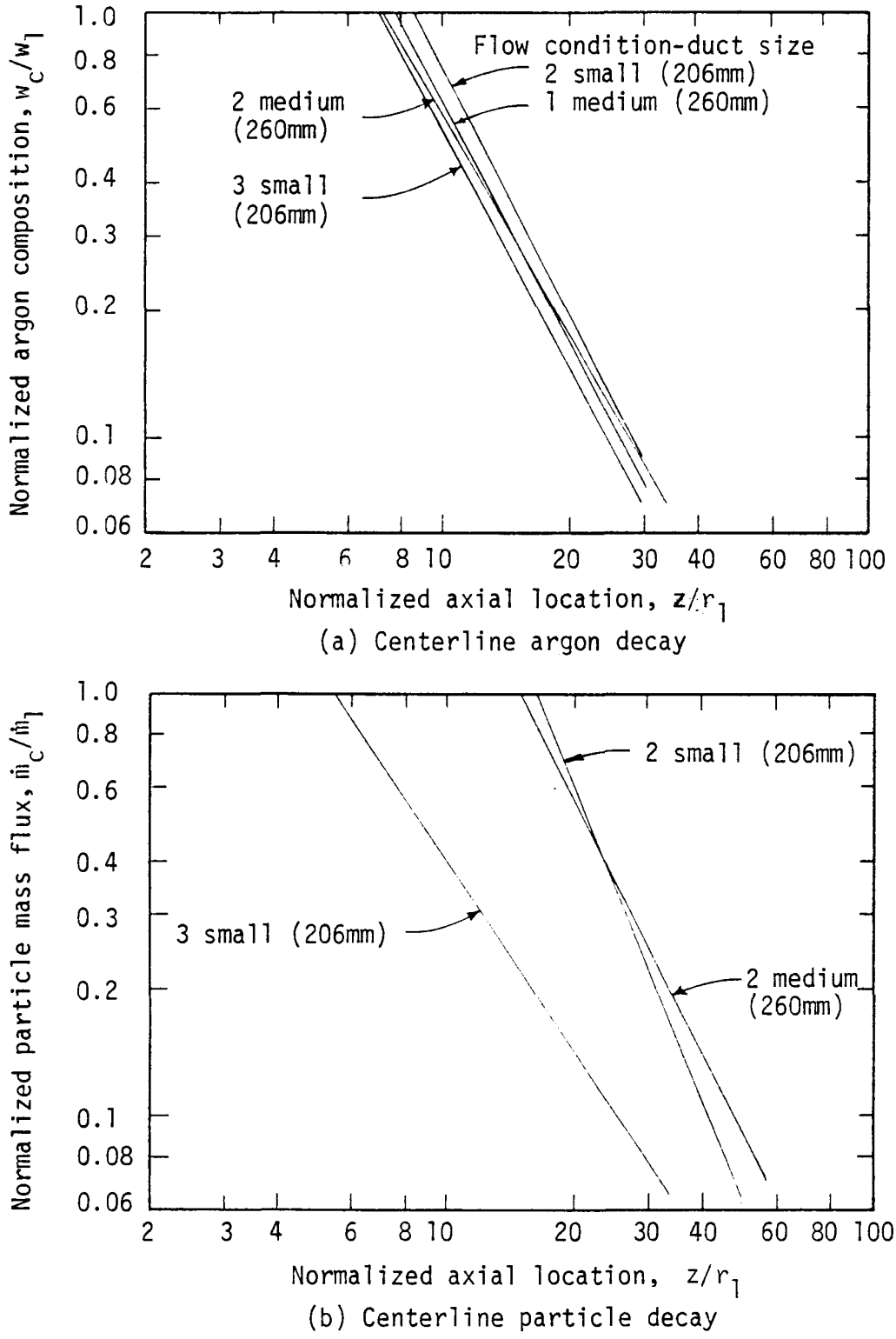

Figure 11. Centerline gas and particle mixing for parallel secondary injection (9).

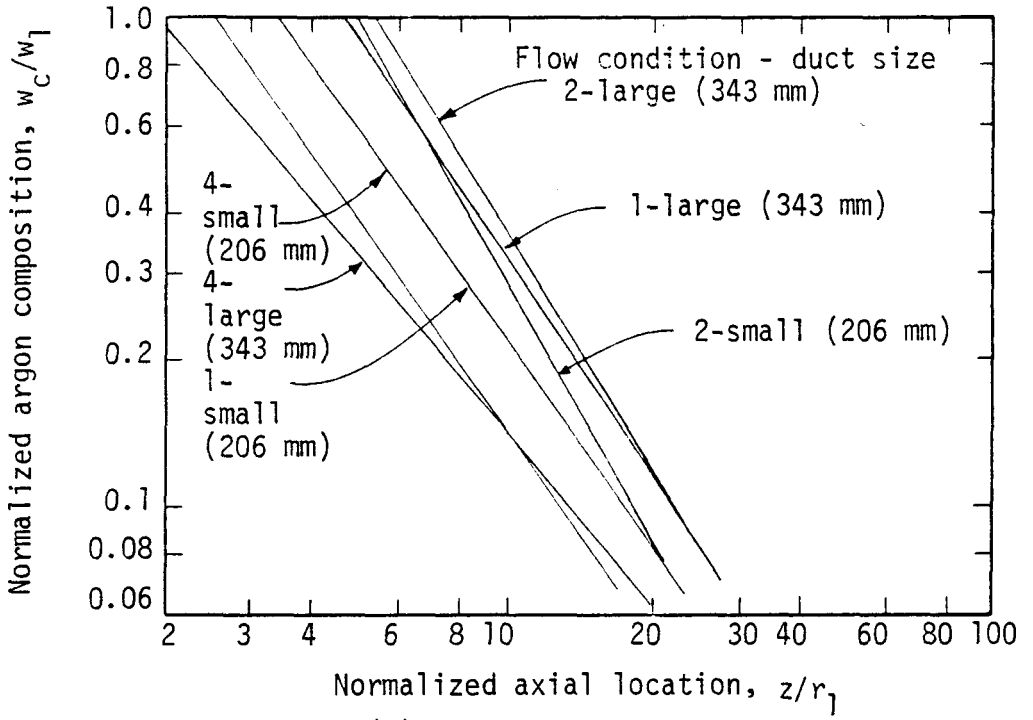

(a) Centerline argon decay

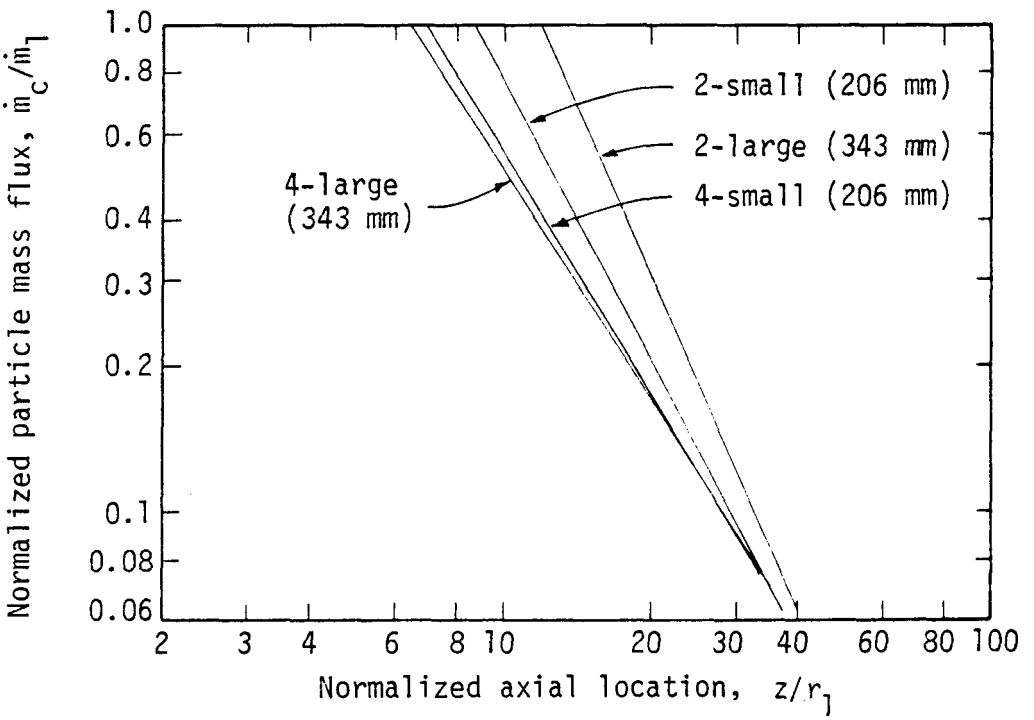

(b) Centerline particle decay

Figure 12. Centerline gas and particle mixing for 30° secondary injection angle (9).

Gas and Particle Mixing Rates. In the 30° secondary injection data, as in all of the previous data (5-8), the gases dispersed at a more rapid rate then did the particles. Introduction of particles caused the gas mixing rate to be slightly less than the gas in absence of particles. This can be seen by comparing flow condition 1 data (gas only) on Figure 12(a) with flow condition 2 data for both small and large ducts. The gas mixing rates for gas only and with particles were more rapid in the small duct. The higher secondary velocity, as seen previously, caused considerable increase in the gas mixing rates.

Figure 12(b) shows a faster particle mixing rate for the reference flow condition (flow condition 2) in the small duct. The particle mixing rates for the high secondary velocity were about the same, irrespective of the duct size.

Effect of Secondary Injection Angle Comparison of the core length data from Figure 12 with that reported above allowed the effect of secondary injection angle into the recirculation duct to be determined. Table 5 summarizes the previous data (7,8) and the mixing rates deduced from Figure 12. In general, both the particle and gas mixing rates were enhanced by the angular secondary injection for the small chamber. These increases ranged from 21% to 63%. However, the gas and particle mixing rates were nearly the same for either parallel or 30° injection into the large chamber. The exception was flow condition 4 (high secondary velocity) where the particle mixing rate with 30° injection was about 70% higher than for the parallel injection case.

Effect of Particle Size The effect of reducing particle size was determined for the small chamber with parallel injection, as shown in Figure 11. The gas mixing rate for the 24 μm diameter silicon tests was slightly faster than that for the standard 46 μm powder. The mixing rate of the 24 μm powder however was much more rapid than for the standard 46 μm powder. Results for larger 54.1 μm powder were reported previously (2, 3). These previous mixing data as well as the recent particle size data are summarized in Table 6.

Effect of Secondary Velocity Comparison of the flow condition 4 results with the flow condition 2 results on Figure 12 allowed the effect of increased secondary velocity for 30° secondary injection into both the large and small recirculation ducts to be determined. The mixing rates deduced from the core lengths were also summarized in Table 5. The higher secondary velocity caused average increases of 92% and 25% in the mixing rates for the gas and particles respectively in the small chamber over those for the reference velocity. In the large chamber, these increases were 85% and 74% respectively. As found in the earlier work (5-8), the secondary velocity had a very major effect on both gas and particle mixing rates.

A correlation of the mixing rates of this research work and the previous work (5-8) is shown in Figure 13. This figure correlates the reciprocal core length (which is related to a mixing rate) as a function of secondary to primary velocity ratio. The dramatic increase in gas mixing rate with increasing velocity ratio is apparent. The particle mixing rate also increased but the increase was not as great.

TABLE 5

SUMMARY OF MIXING RATES FOR RECIRCULATION TESTS
WITH AND WITHOUT 30° ANGULAR SECONDARY INJECTION
(RECIPROCAL CORE LENGTH, m^{-1})

Test Condition	Small (206mm) Chamber		Large (343mm) Chamber	
	Gas	Particles	Gas	Particles
Parallel Injection (Ref. 7, 8)				
1 (Gas only)	18.2	-	16.5	-
2 (Reference)	12.7	6.8	12.2	6.2
4 (High sec. velocity)	23.6	6.7	24.4	6.6
30° Angular Injection (Ref. 9)				
1 (Gas only)	22.1	-	16.3	-
2 (Reference)	15.5	8.7	12.2	6.5
4 (High sec. velocity)	29.7	10.9	22.6	11.3

TABLE 6

EFFECT OF PARTICLE SIZE ON GAS AND PARTICLE MIXING RATE FOR PARALLEL INJECTION INTO THE SMALL (206mm) MIXING CHAMBER* (RECIPROCAL CORE LENGTH, m^{-1})

	Particle Size,** μm		
	24.2	46.1	54.1
Gas	11.0	9.2(12.7)‡	(12.9)‡
Particle	12.9	4.7(6.8)‡	(6.3)‡

*Reference flow condition (No. 2).

‡Taken from reference 3.

**Mass mean particle diameter.

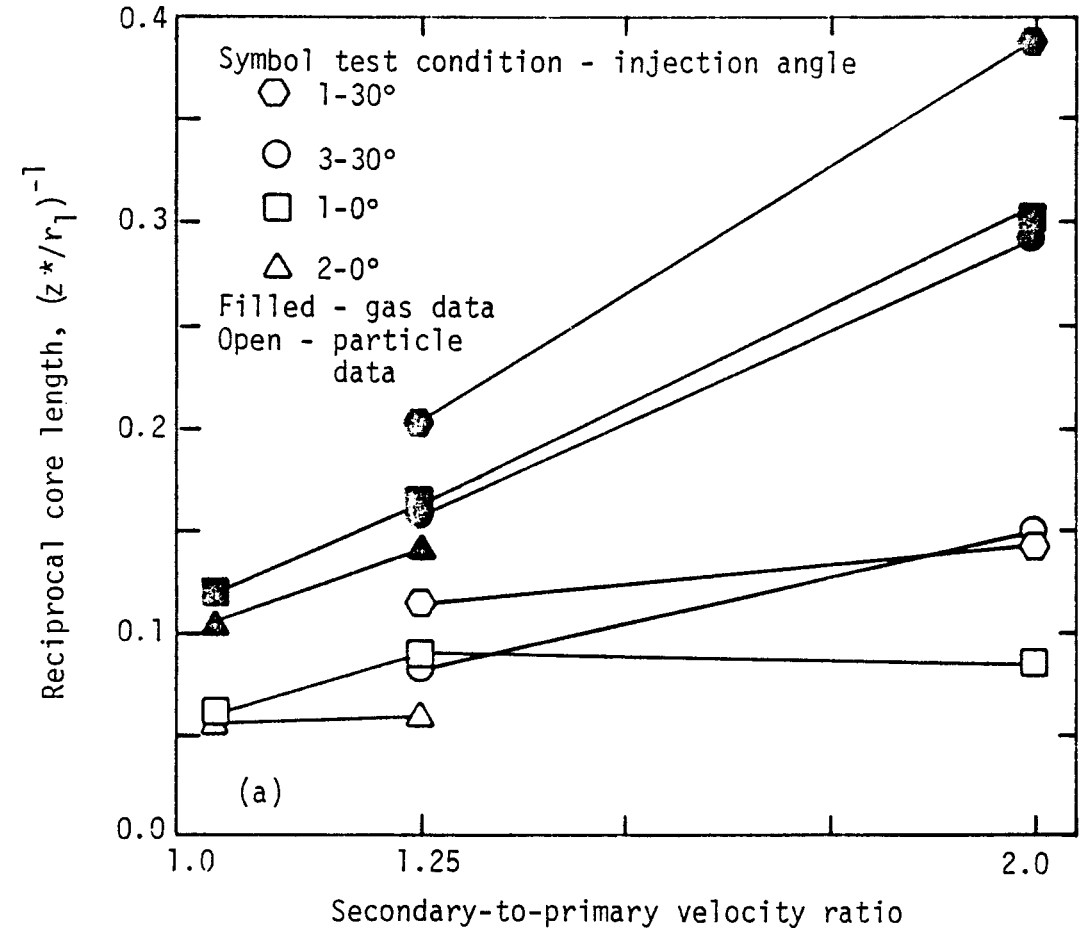

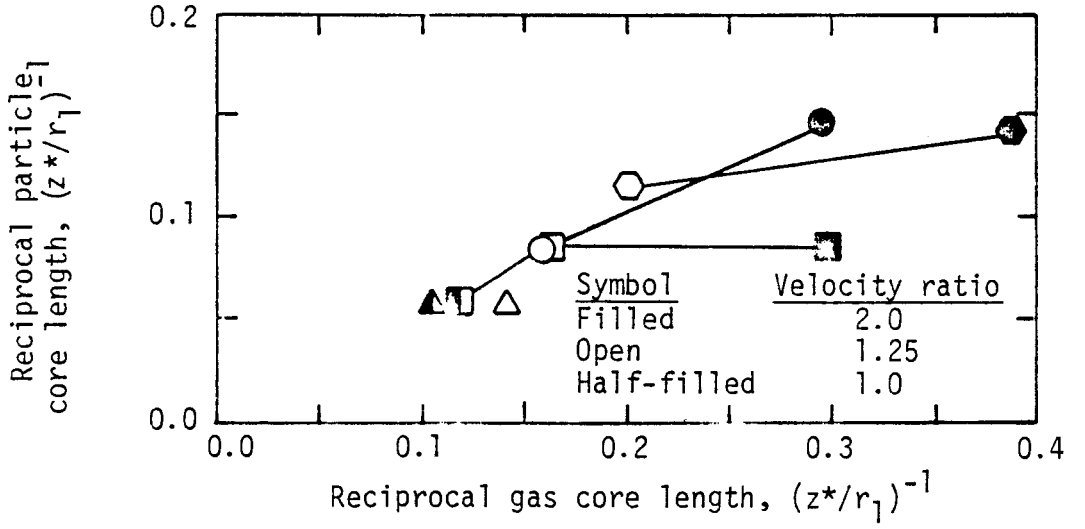

Figure 13. Comparison of core length data showing the effects of velocity ratio (V.R.)

Effect of Mixing Duct Size The gas and particle mixing data collected in this test series and those previously reported (2) have allowed the effect of duct size to be determined for different jet inlet configuratons and flow conditions. Figure 14(a) and (b) present the mixing rate, both gas and particle, as a function of mixing duct size for different flow conditions at secondary injection angles of 0^{o} and 30^{o} respectively. These data show that the effect of mixing duct size on gas and particle mixing rates is very dependent on flow conditions, and inlet geometry. There was no appreciable effect on mixing duct size on either gas or particle dispersion for 0^{o} secondary injection and the reference test conditions, as seen in Figure 14(a). A significant increase (up to a factor of 2.3) was observed for all other flow conditions at 0^{o} secondary injection with the exception of the effect of high secondary velocity on gas mixing. With high secondary velocity, the effect was reversed i.e., in increase in mixing duct size caused a reduction in gas mixing rate.

It was generally observed at the 0^{o} injection angle that the major change occured in going from the straight mixing section (130 mm) to the next larger mixing chamber (206 mm). Further size increases had litle additional effect and frequently resulted in a reduced mixing rate.

The mixing data for 30^{o} secondary injection are shown in Figure 14(b). The data were not as extensive for this inlet configuration; nevertheless, the effect on gas and particle mixing is shown for the reference flow condition, gas only condition, and the high secondary velocity flow condition. These data show an initial increase in mixing rate with increasing duct size for the gas only case and for the particle mixing rate with the reference flow conditions. The particle mixing rate for the high secondary velocity flow condition was higher but independent of mixing duct size. The gas mixing rate for both the reference flow condition and the high secondary velocity flow condition decreased with increased mixing duct size.

3. Coal Dust Tests (Test Series 4)

Cold-flow mixing tests performed in Series 1, 2, and 3 were all conducted using silicon dust as the particulate phase of the primary jet. A total of 38 cold-flow mixing tests were conducted in Test Series 4, including 27 coal-dust tests, 6 silicon-dust tests, and 5 dust-free (gas-only) tests. The coal-dust tests included 17 tests with non-parallel (30^{o}) secondary jet injection and 10 tests with parallel injection. The purpose of the 11 silicon-dust and dust-free tests was for reproduction of tests performed by previous investigators. All 38 tests were run with the standard flow conditions and are summarized in Table 7.

Reproduction of Previous Tests. In order to compare the results obtained from the cold-flow coal-dust tests performed in this study with the results from previous silicon-dust tests, several silicon-dust and dust-free tests were conducted. Six silicon-dust tests were conducted with non-parallel injection and large diameter (343 mm) mixing chamber. All six tests showed good reproducibility with earlier tests of the particle mixing data. Difficulties were encountered in reproducing gas mixing data due to plugging in the gas sample collection lines.

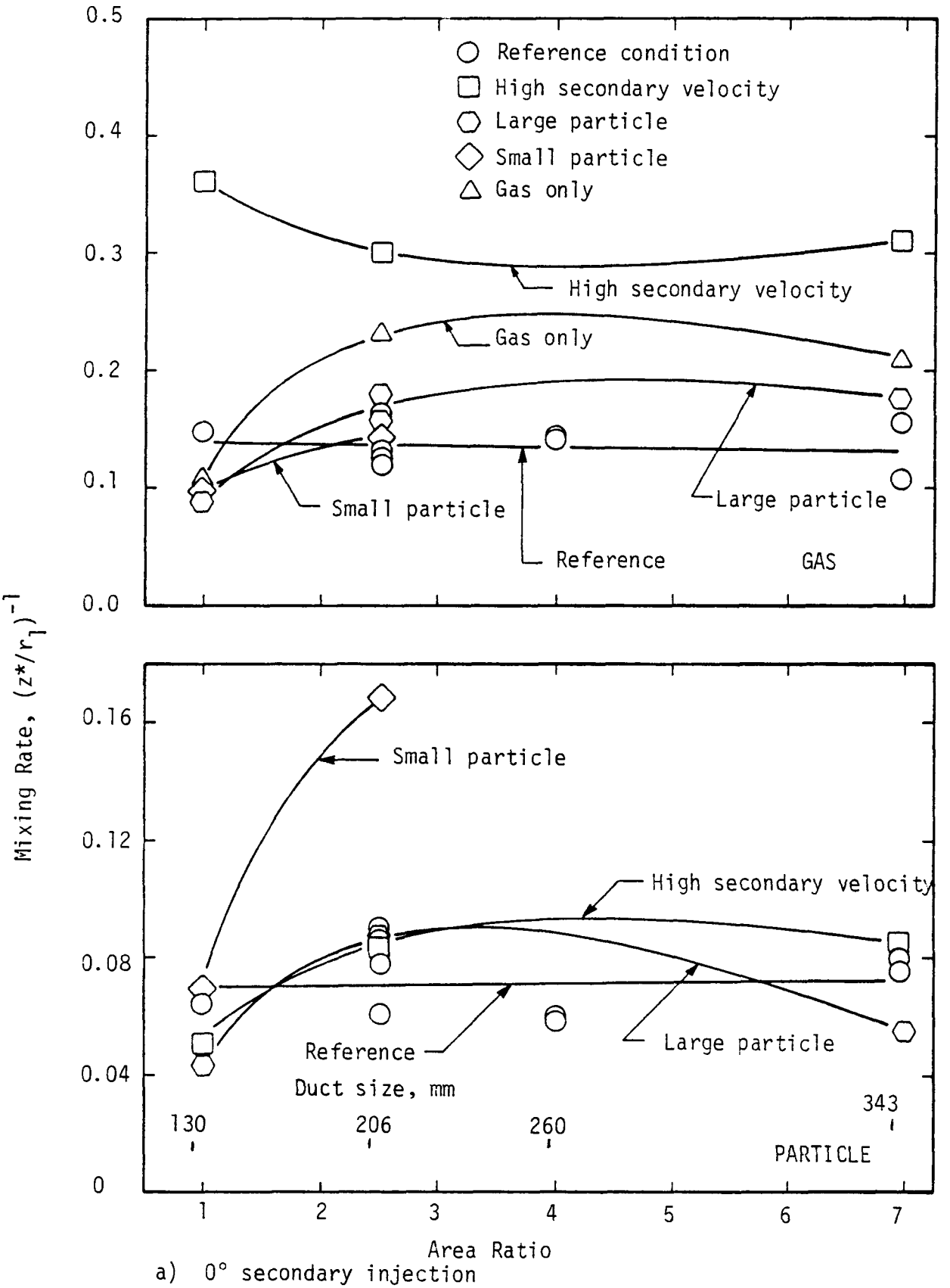

a) 0° secondary injection

Figure 14. Comparison of core length data showing the effects of mixing chamber diameter.

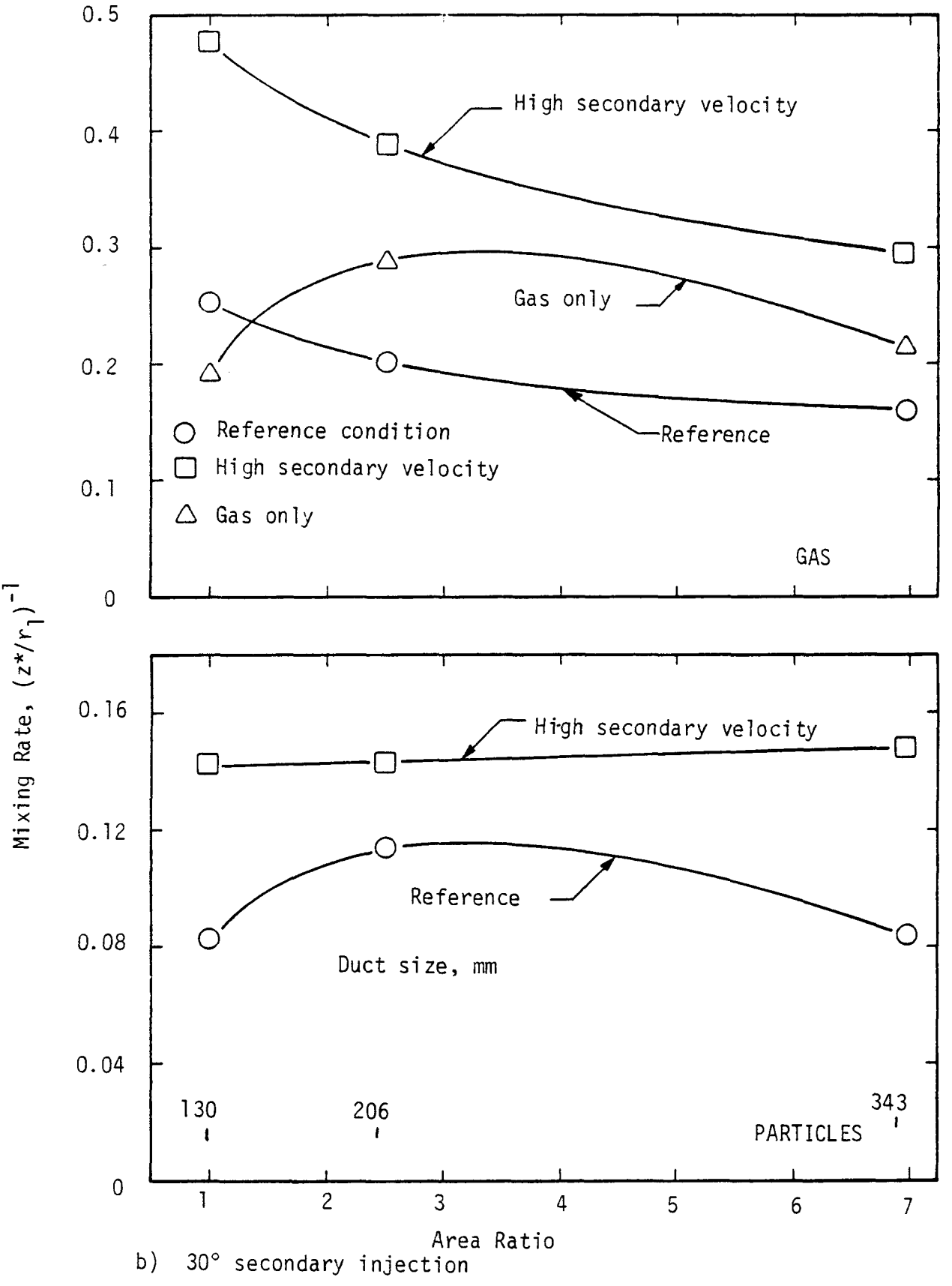

b) 30° secondary injection

Figure 14. (Cont.)

TABLE 7

SUMMARY OF COLD-FLOW COAL-DUST AND RELATED TESTS
(Test Series 4)

Configuration	30° Injection	30° Injection	Parallel Injection Constant Total Length	Parallel Injection Constant Total Length
Mixing Chamber Diameter	Small (206mm)	Large (343mm)	Small (206mm)	Large (343mm)
Velocity, m/s				
Secondary	38.1	38.1	38.1	38.1
Primary	30.5	30.5	30.5	30.5
Flow Rates, 10^{-3} kg/s				
Secondary Air	540	540	540	540
Primary Air	5.5	5.5	5.5	5.5
Primary Argon	16.5	16.5	16.5	16.5
Mole % Argon	75	75	75	75
Particle Type: (% Loading in Primary)		Number of Tests		
Coal (40%)	9	8	5	5
Silicon (40%)	-	6	-	-
Gas Only (0%)	-	1	-	4

However, this problem was corrected and the desired reproducibilty was achieved. Figure 15 shows the radial profile curve fit comparison of mixing data from a previous test (9) with reproduced tests from this test series. Four of the dust-free tests were conducted with parallel injection and large mixing chamber. The fifth was conducted with non-parallel injection in conjunction with the silicon dusts tests. Figure 16 compares the axial decay plot obtained from the data of these tests with that obtained from previous tests (7, 8) and shows good agreement.

Test Results. Axial decay data and plots from the 27 coal-dust tests were used to analyze coal-dust and gas mixing rates. The data from the 27 tests are summarized in Table 8 along with data from corresponding silicon dust tests. This information is also shown graphically in Figures 17 to 19. The presence of coal dust generally resulted in somewhat faster mixing rates, when compared to silicon tests. Particle density was used to correlate the mixing rates as illustrated in Figure 20. This figure shows much more rapid gas mixing for the coal particles with nonparallel injection than for the silicon particles. The particle-phase mixing was less strongly affected. Table 9 summarizes mixing rates of coal and silicon dust tests. The decrease in particle density increased overall gas mixing by about 50%, but increased overall particle mixing rates by only about 15%, which may not be significant.

In addition to determining the effect of coal dust on gas and particle mixing rates, the coal-dust tests themselves produced results which compare with those obtained by previous investigators in this study. Table 10 and summarizes these results. Nonparallel injection increased overall mixing rates by 1.8 times over parallel injection. Decreasing the mixing-duct-to-secondary-area ratio produced little change in mixing rates. Gas mixing rates were about twice that of the particles and an increasing injection angle also doubled the gas and particle mixing rates.

4. Swirl Tests (Test Series 5)

The primary objective of this part of the cold-flow test program was to determine how particle and gas mixing rates are affected by swirl in the secondary jet in comparison to non-swirl situations. The type of secondary jet swirl generator used for this study was a moveable-block system patterned after the system developed at the International Flame Foundation Laboratory in Ijmuiden, Holland (13). Figures 2 to 6 illustrated the facility configuration used for the swirl tests in relation to that used for parallel secondary injection with recirculation.

System Evaluation Tests. A set of preliminary cold-flow tests was conducted to check out the operation of the swirl generator and to evaluate potential testing problems. Figure 21 shows approximate radial velocity profiles obtained from these preliminary tests for various low Swirl Numbers. The velocities shown are approximate axial velocity components only, since the fixed probe bank was used. There is a considerable change in the nature of the flow with change in the secondary Swirl Number from 0 to 0.34. These tests were run with the probe collar at a normalized axial distance of 25.1 and no quarl was used. Velocities

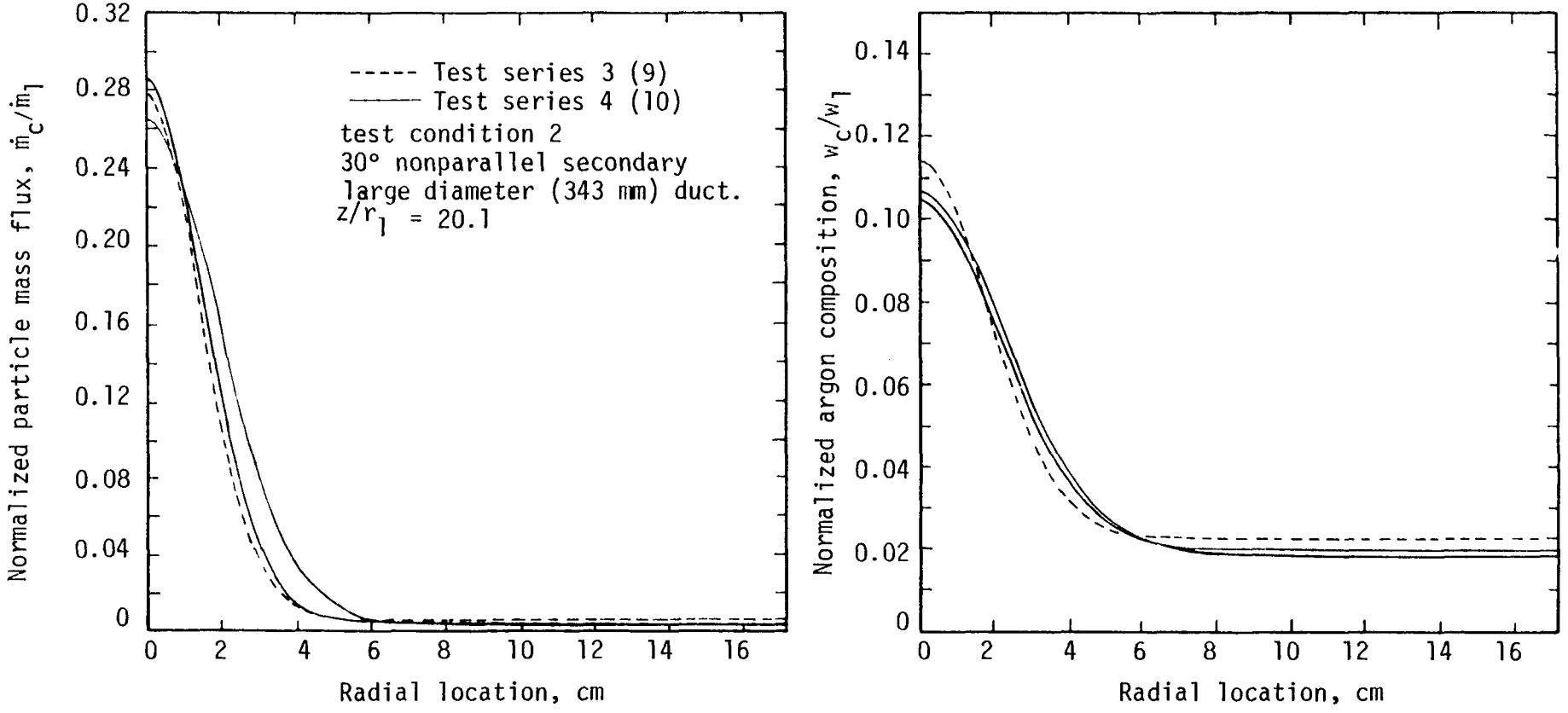

Figure 15. Reproducibility of gas and particle radial mixing profiles for cold-flow silicon dust tests

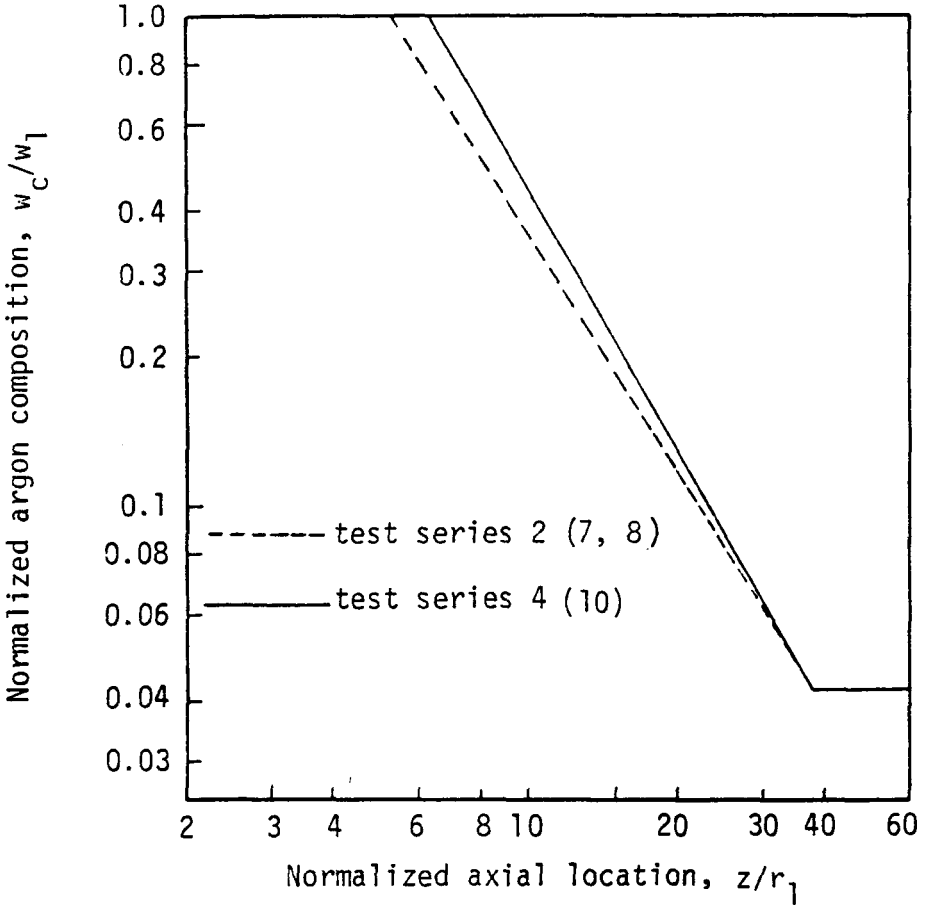

Figure 16. Reproducibility of gas mixing axial decay profile for cold-flow silicon dust tests.

TABLE 8

SUMMARY OF CENTERLINE MIXING DATA FOR
COAL-DUST TESTS AND CORRESPONDING SILICON-DUST TESTS*

Test Condition	Injection Angle	Core Length	Core Length Interval	Slope	Slope Variance
A. Gas Data					
2-Coal (206mm)	0°	6.69	6.21- 7.18	-1.83	0.055
2-Coal (343mm)	0°	7.82	7.98- 7.66	-1.96	0.037
2-Coal (206mm)	30°	3.93	3.55- 4.31	-1.46	0.082
2-Coal (343mm)	30°	2.84	2.65- 3.03	-1.21	0.040
2-Silicon (206mm)	0°	7.98	7.04- 8.85	-1.84	0.194
2-Silicon (343mm)#	0°	9.22	-	-1.80	-
2-Silicon (206mm)	30°	4.95	4.78- 5.11	-1.76	0.041
2-Silicon (343mm)	30°	6.25	5.17- 7.28	-1.82	0.207
B. Particle Data					
2-Coal (206mm)	0°	12.20	10.32-13.75	-2.34	0.460
2-Coal (343mm)	0°	12.29	10.14-14.01	-1.96	0.447
2-Coal (206mm)	30°	9.68	9.32-10.02	-2.11	0.080
2-Coal (343mm)	30°	7.88	7.19- 8.53	-1.66	0.130
2-Silicon (206mm)	0°	13.03	12.41-13.61	-1.90	0.113
2-Silicon (343mm)	0°	13.28	11.25-14.97	-1.62	0.330
2-Silicon (206mm)	30°	8.76	7.89- 9.56	-1.90	0.182
2-Silicon (343mm)	30°	11.86	11.39-12.32	-2.28	0.090

*Silicon dust data from theses by Tice and Sharp. (7-9).

#Only two points used to determine axial decay data.

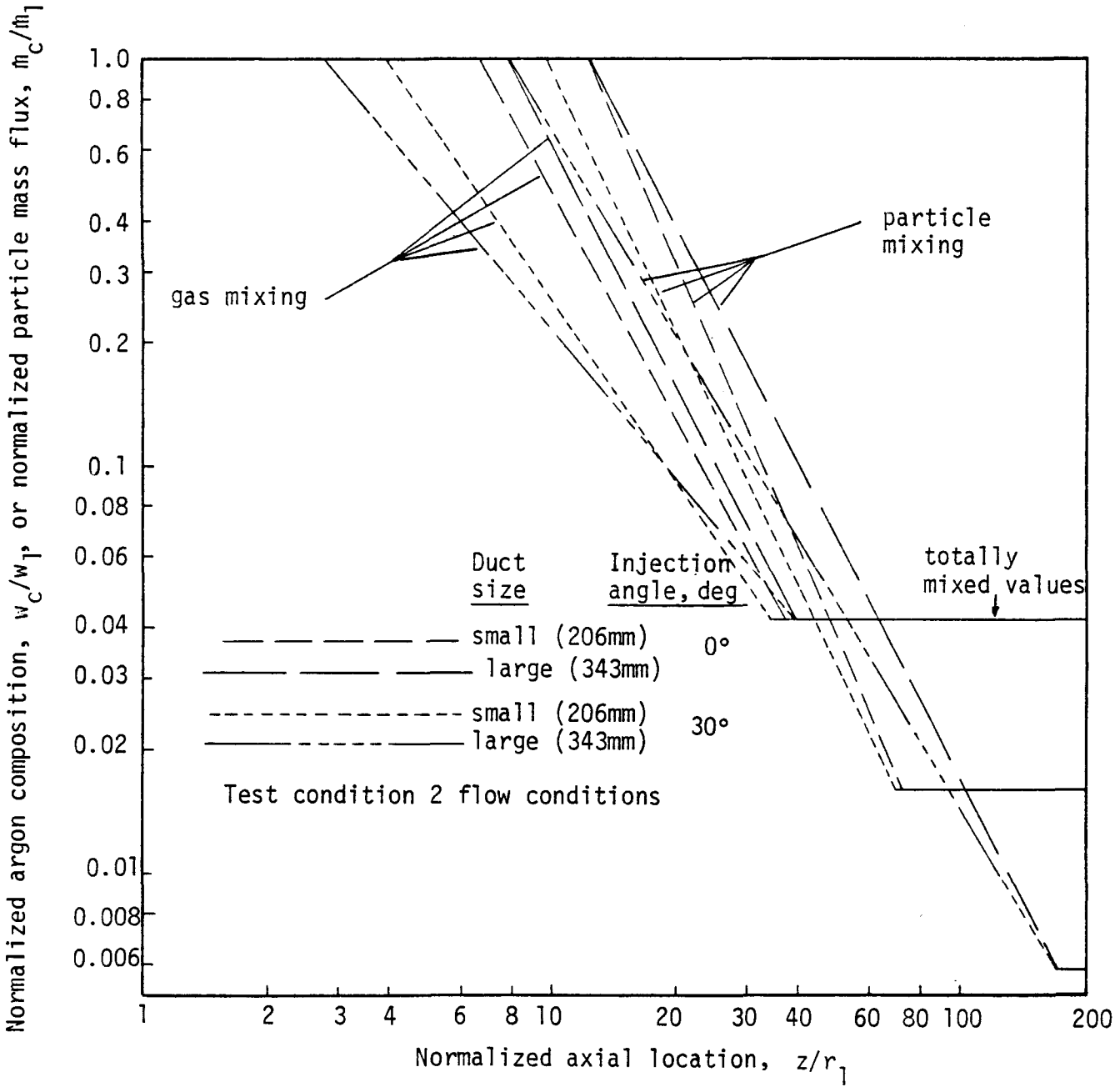

Figure 17. Summary of centerline axial decay plots for coal-dust, cold-flow tests.

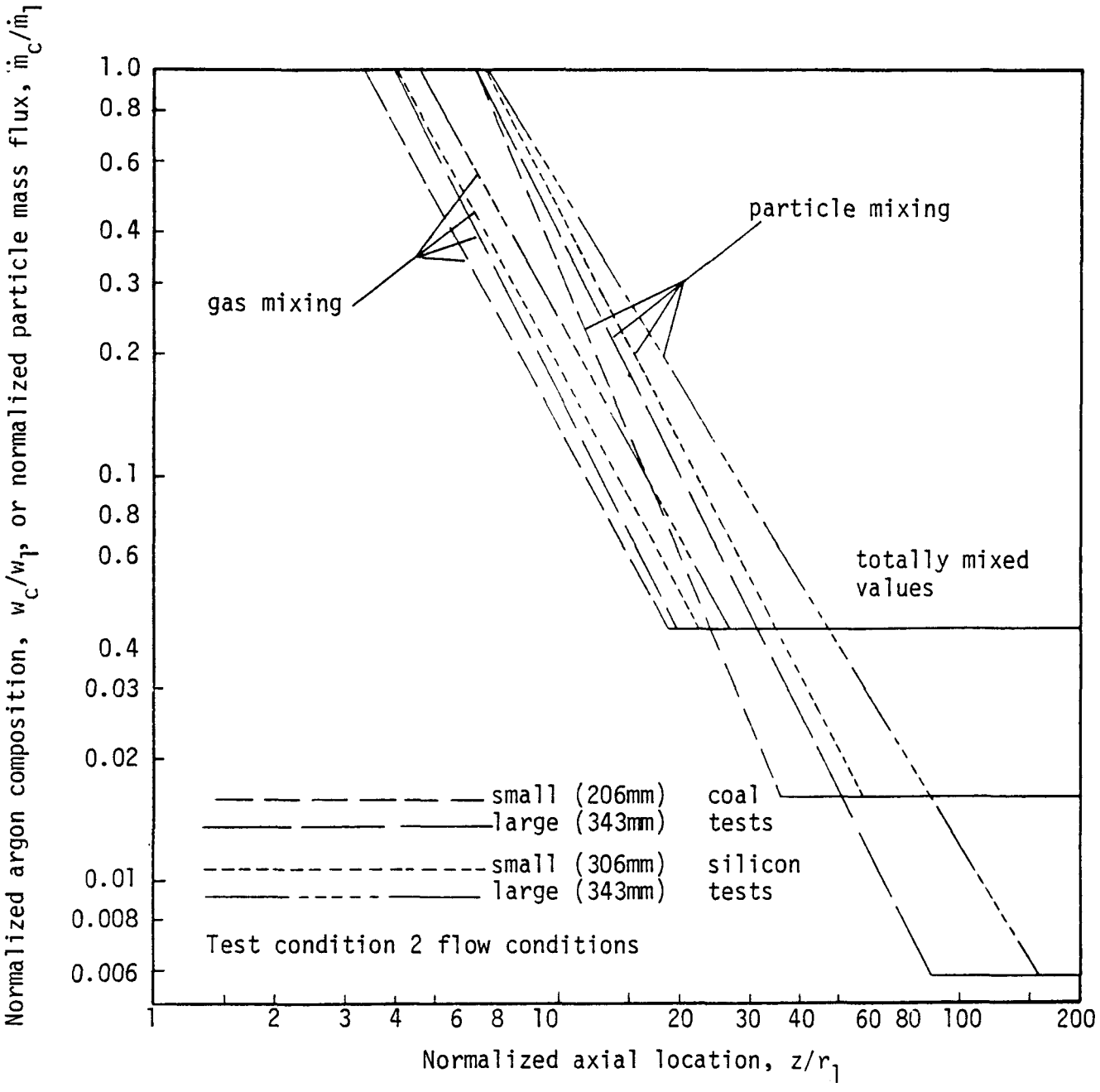

Figure 18. Comparison of coal-dust and silicon centerline axial decay results for parallel secondary injection.

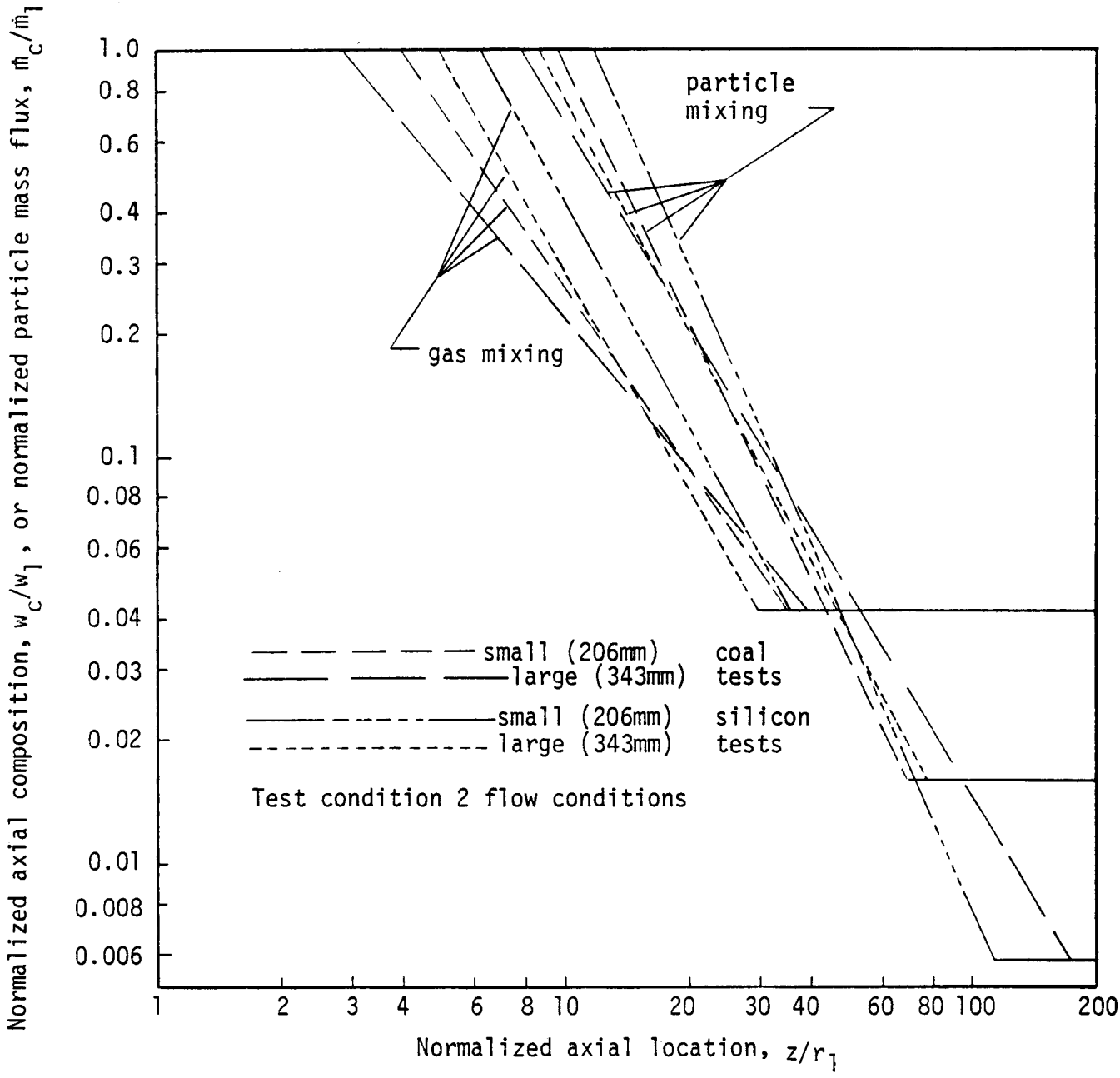

Figure 19. Comparison of coal-dust and silicon dust centerline axial decay results for 30° nonparallel secondary injection.

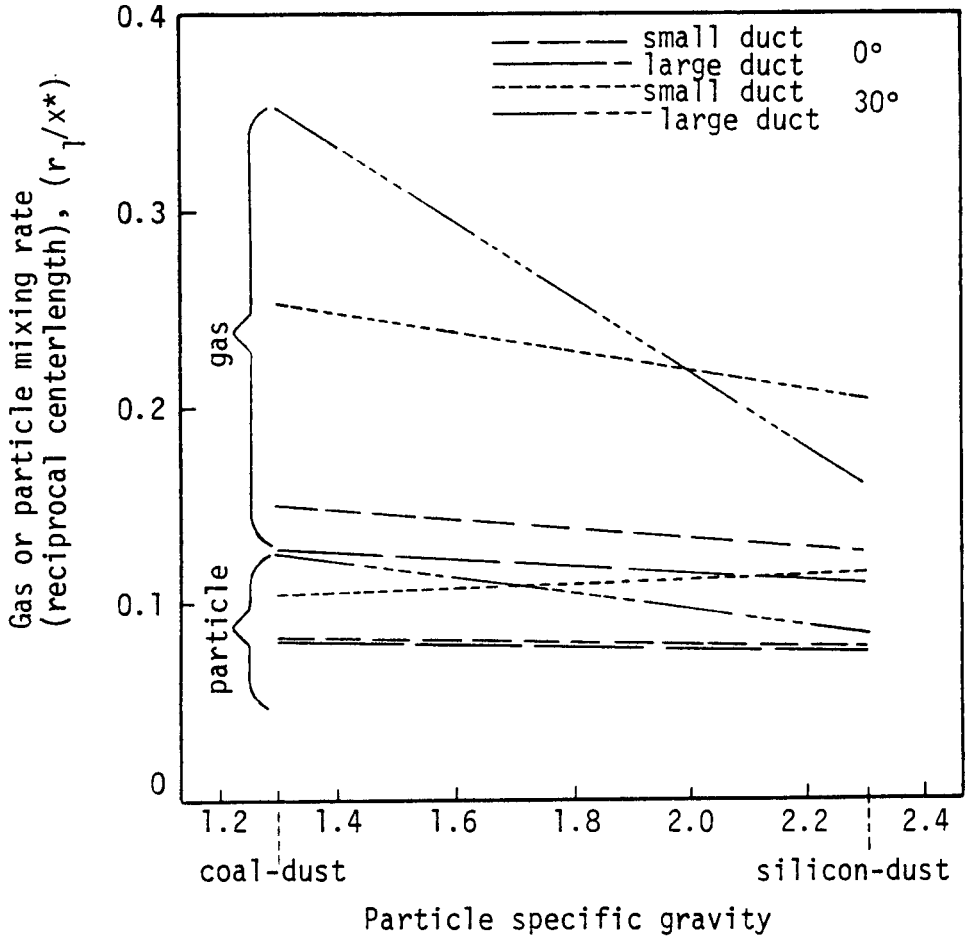

Figure 20. Effect of particle density on gas and particle mixing rates.

TABLE 9

COMPARISON OF MIXING RATES (RECIPROCAL CORE LENGTHS)
FOR COAL-DUST AND SILICON-DUST TESTS

	Injection Angle	Mixing Chamber	Coal-Dust Tests	Silicon-Dust Tests	Coal-Test-to Silicon-Test-Ratio
Gas	0°	Small	0.150	0.125	1.20
	0°	Large	0.128	0.109	1.18
					1.19 (Ave.)
	30°	Small	0.254	0.202	1.26
	30°	Large	0.352	0.160	2.20
					1.73 (Ave.)
					1.46 (Overall gas ave.)
Particle	0°	Small	0.082	0.077	1.07
	0°	Large	0.081	0.075	1.08
					1.07 (Ave.)
	30°	Small	0.103	0.114	0.91
	30°	Large	0.127	0.084	1.51
					1.21 (Ave.)
					1.14 (Overall particle ave.)
					1.30 (Total overall ave.)

TABLE 10

COMPARISON OF MIXING RATES
FROM COAL-DUST TESTS FOR VARIOUS PARAMETERS
(RECIPROCAL CORE LENGTH)

EFFECT OF MIXING CHAMBER

Injection Angle	Type	Small (206mm Diam.)	Large (343mm Diam.)	Small-to-Large Duct Ratio
0°	Gas	.150	.128	1.17
0°	Particle	.082	.081	1.01
				1.09 (Ave.)
30°	Gas	.254	.352	0.72
30°	Particle	.103	.127	0.81
				0.76 (Ave.)
				0.93 (Ave.)

EFFECT OF INJECTION ANGLE

Mixing Chamber Diameter	Type	30° Injection	0° Injection	30°-to-0° Ratio
Small	Gas	.254	.150	1.70
Small	Particle	.103	.082	1.26
				1.48 (Ave.)
Large	Gas	.352	.128	2.76
Large	Particle	.127	.081	1.56
				2.16 (Ave.)
				1.82 (Ave.)

GAS VS. PARTICLE MIXING RATES

Injection Angle	Mixing Chamber Diameter	Gas Mixing Rate	Particle Mixing Rate	Gas-to-Particle Ratio
0	Small	.150	.082	1.83
0	Large	.128	.081	1.57
				1.70 (Ave.)
30	Small	.254	.103	2.46
30	Large	.352	.127	2.78
				2.62 (Ave.)
				2.16 (Ave.)

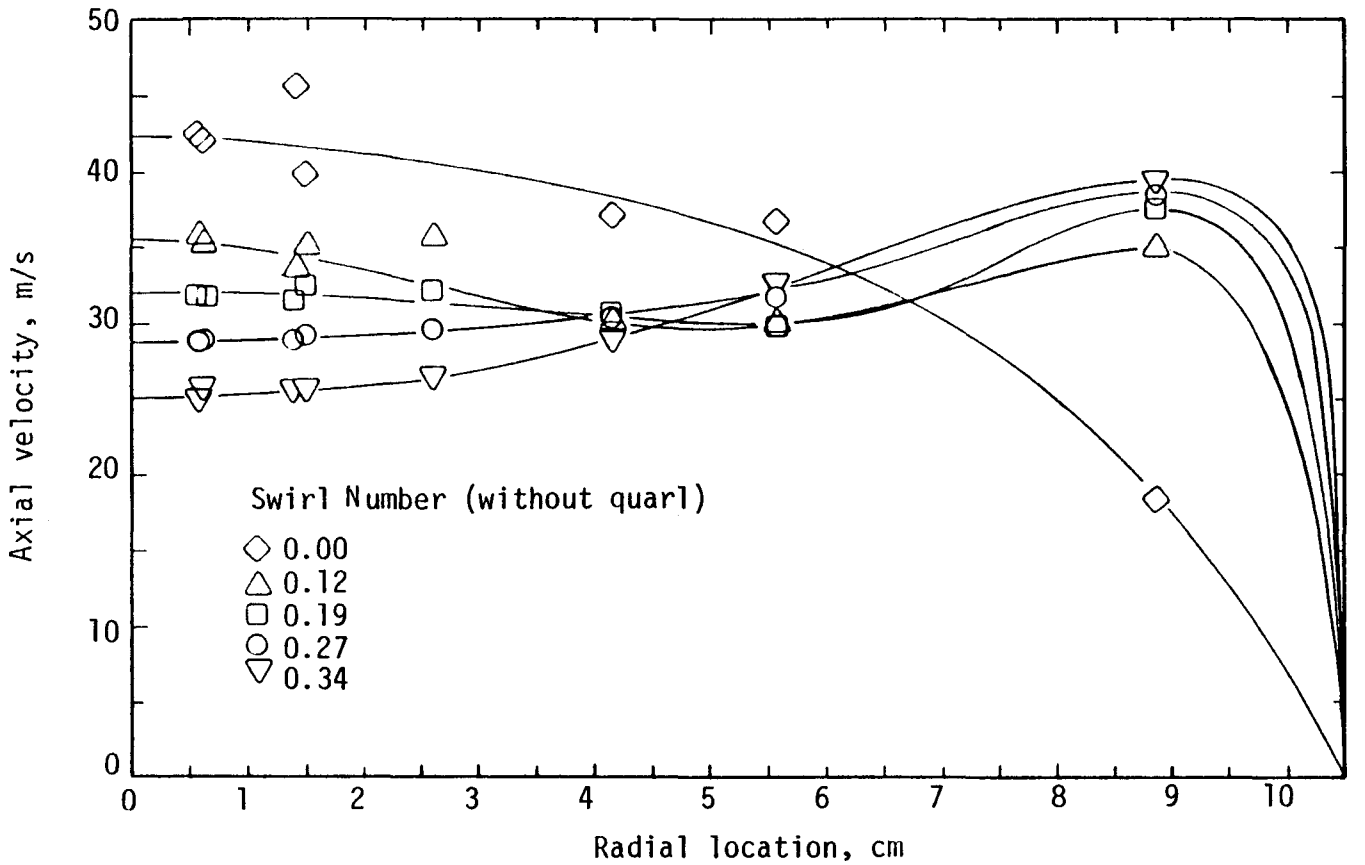

Figure 21. Preliminary cold-flow swirl test results (small (206 mm) duct, axial location of z/r_1 = 25.1, secondary velocity = 41 m/s, primary velocity = 10 m/s).

were determined from pressure measurements obtained with the fixed probe bank.

Another preliminary test was conducted with the standard flow condition, 40% particle loading in the primary, and the maximum secondary design Swirl Number of 3. The normalized axial distance was again 25.1. No velocity measurements could be taken because the fixed probe system did not function properly in the strong cross flow associated with a high Swirl Number. However, gas samples showed that complete, uniform mixing of the gas had been achieved at that axial location.

Because of the unique nature of the swirling flows, a rotating-traversing probe was designed and fabricated for the cold-flow facility as previously discussed. This probe could be located at any radial position and rotated until the probe was aligned to the flow. Thirteen preliminary tests were conducted to check out the operation of the new probe. Initial tests showed that the static pressure taps used initially to align the probe, Figure 22 (a), were not adequately sensitive. The probe is considered aligned to the flow when there is no pressure difference between the two alignment pressure taps. In subsequent tests the alignment pressure taps were modified to measure stagnation pressure. This modification, shown in Figure 22 (b), greatly increased the sensitivity and permitted good probe alignment in most radial locations in the duct under many flow conditions.

Figure 23 shows probe alignment data from two of the preliminary tests where the stagnation-pressure alignment taps were used. The sample probe was left at a fixed radial location and rotated to various angles to observe the resulting pressure difference between the alignment pressure taps. The probe was visually aligned prior to the tests so that an orientation angle of 0^{o} corresponded to the probe being parallel with the axis of the mixing chamber. In the first test, the swirl generator was adjusted for a Swirl Number equal to zero, and the probe was positioned at the center of the duct. An orientation of 0^{o} was expected for proper aligment for this configuration since no swirl was imparted to the secondary jet. Alignment as deduced from pressure balance data was observed to occur at a mechanical position of 3^{o} for this configuration which showed good probe alignment capability. In the second test, the secondary Swirl Number was adjusted to 1.1 and the probe positioned at a radius of 0.102 m. Using the same criteria, the probe was aligned to the flow at 85^{o}. Such a strong tangential component in the flow direction substantiated the need for the rotating probe. Both tests were conducted with the large diameter mixing chamber (343 mm).

In another preliminary test conducted with the small diameter mixing chamber (206 mm), the probe was left at a fixed radial position of 0.076 m and rotated into proper alignment at various Swirl Numbers. Again the stagnation-pressure alignment taps were used. Figure 24 shows the effect of Swirl Number on local flow direction as measured by the orientation angle required to achieve probe alignment. The data showed the increase in the local tangential flow component with increasing the Swirl Number. The discrepancy of about 10^{o} at a Swirl Number of zero for this particular test was caused by mechanical misalignment

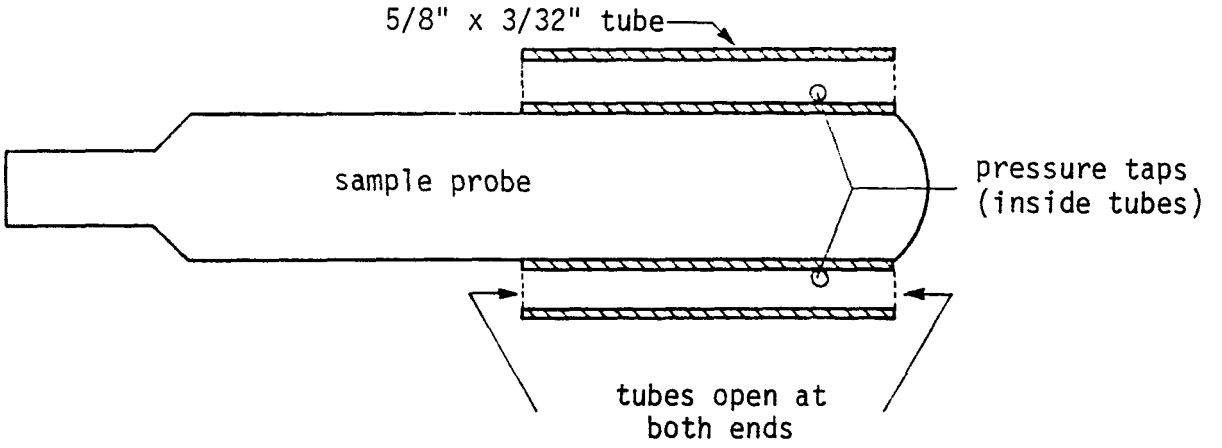

(a) Static-pressure-type alignment pressure taps

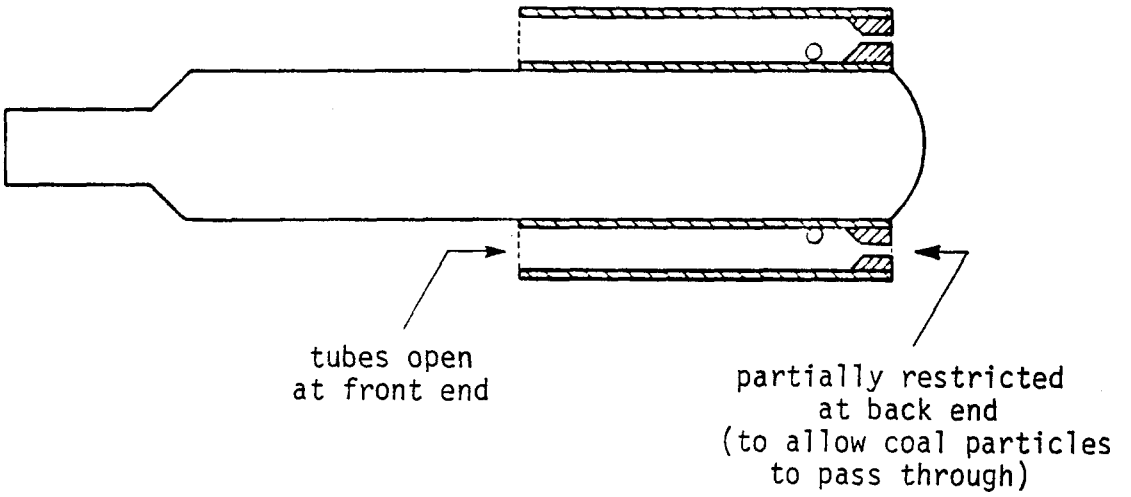

(b) Stagnation-pressure-type alignment pressure taps

Figure 22. Geometry of alignment pressure tap variations used on the cold-flow rotating-traversing probe.

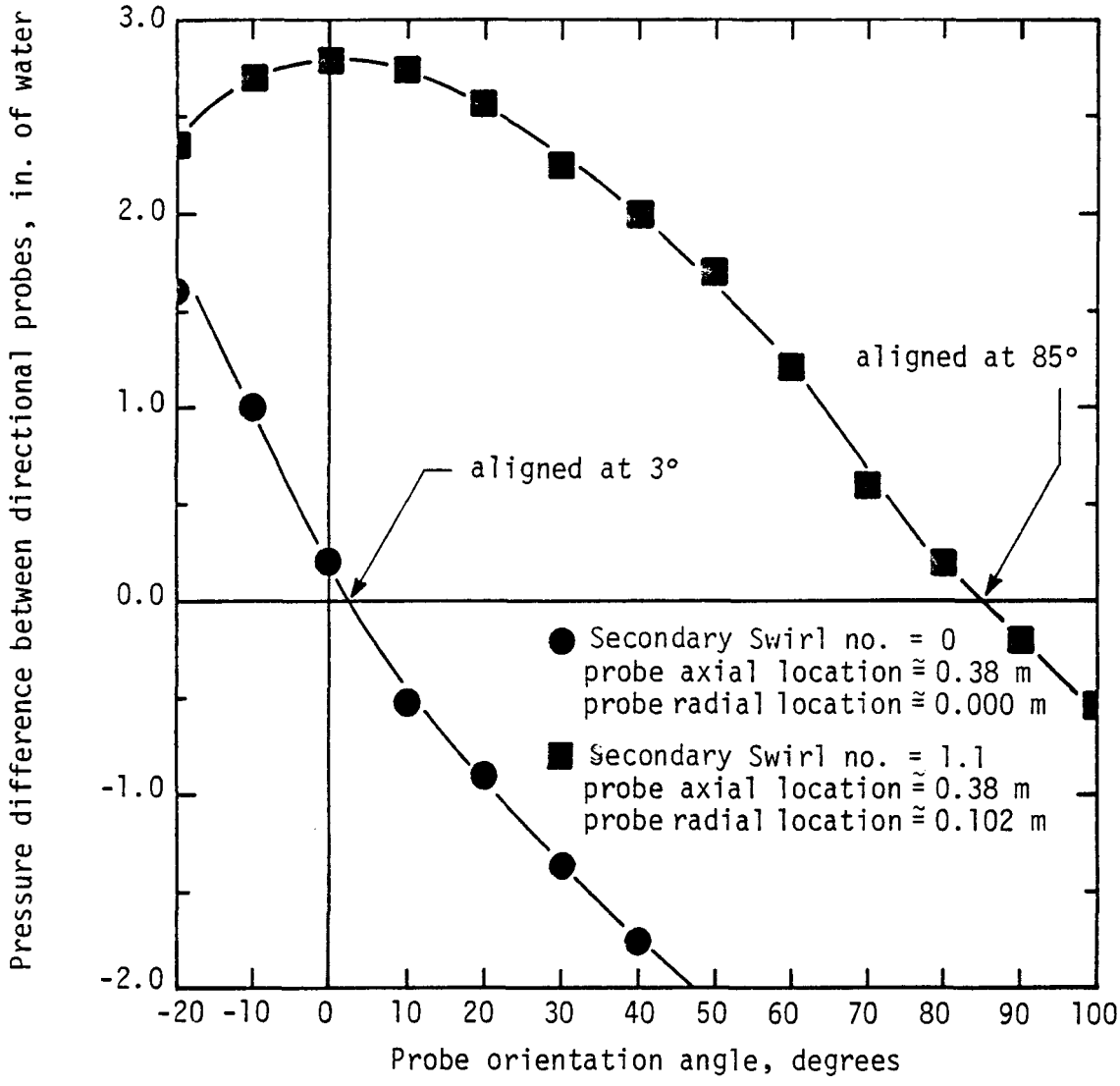

Figure 23. Comparison of response of directional probes on the rotating-traversing probe for two flow conditions. Mixing chamber diameter = 0.346 m .

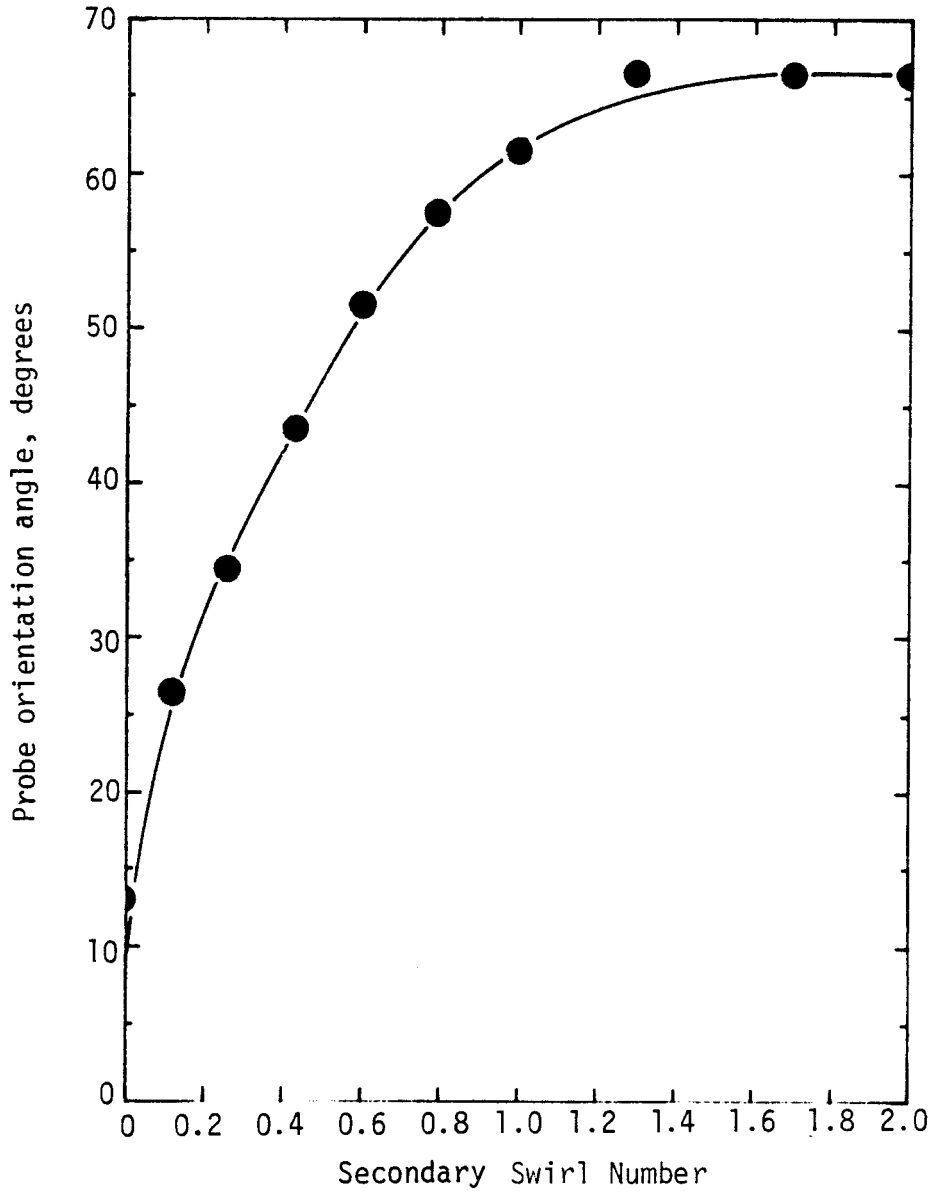

Figure 24. Plot showing effect of swirl on direction of flow (axial location of probe ≅ 0.23 m; radial location of probe ≅ 0.08 m) Mixing chamber diameter = 0.206 m.

of the probe relative to the rotating mechanism. This problem was corrected prior to subsequent testing.

Swirl Test Results A total of 28 cold-flow tests were completed in this part of the cold-flow test program in order to evaluate the effect of swirl in the secondary jet on gas and particle mixing rates. The 28 tests were run at the standard flow condition into the small (206 mm) mixing chamber. Tests at Swirl Numbers of 0, 0.2, 0.4, and 0.6, with and without the quarl section installed, and with or without (gas-only) pulverized coal were performed as summarized in Table 11.

Variables in cold-flow swirl tests were expansion quarl and Swirl Number. It was suggested by Beer and Chigier (13) that the critical Swirl Number for flame stabilization would occur at the transition from weak swirl to strong swirl, that is, at a Swirl Number of about 0.6. Consequently, a Swirl Number of major interest in these tests was 0.6. the lower Swirl Numbers investigated were 0.2 and 0.4.

Some interesting results were observed for the tests at a Swirl Number of zero. The purpose of these tests was to determine the effect of the swirl generator hardware but without swirl on gas and particle mixing rates. These tests were conducted with coal dust as the particlate phase. Three of the tests were run with an expansion quarl, and the remaining tests were run without the quarl. The rigid multiple sample probe bank was used in all of these tests since the secondary jet was not swirled.

Axial decay data from these swirl tests are compared with data from corresponding non-swirl tests (coal dust tests with parallel secondary jet injection and small mixing chamber) in Figure 25. It is apparant that just the swirl generator hardware alone (without any swirl imparted to the secondary jet) altered the characteristics of the secondary jet enough to significantly increase gas mixing rates. Particle mixing rates were also affected, but not to any significant degree.

The results from the tests with secondary swirl are presented in Figures 26 and 27 for gas mixing and particle mixing respectively. These figures compare the centerline gas and particle mixing parameters for Swirl Numbers of 0.0, 0.2, and 0.6 to the equivalent mixing results for parallel injection. The gas mixing results shown in Figure 26 again show the significant increase in gas mixing with the use of the secondary swirl generator at a Swirl Number of zero. This figure also shows that even a small Swirl Number (0.2) will greatly increase the gas mixing rate. At a Swirl Number of 0.6, the gas mixing was essentially completed at the first axial test location ($z/r_1 = 17.4$).

Previous results (5-12) have shown that the centerline gas and particle mixing parameter decay is essentially linear between the core and completely mixed values on a log-log plot. While there was insufficient data in the regions close to the jet-exits from a Swirl Number of 0.6, the 0.2 Swirl Number data suggested that this linear dependence remains. Consequently, axial decay estimates of the gas-mixing parameter were made for both 0.2 and 0.6 Swirl Number data as shown in Figure 26. There was considerable uncertainty regarding this axial mixing as shown

TABLE 11

SUMMARY OF COLD-FLOW SWIRL TESTS

(TEST SERIES 5)

Configuration	With Swirl Generator Swirl No.=0	With Swirl Generator Low Swirl No. No Quarl	With Swirl Generator Low Swirl No. With Quarl	With Swirl Generator High Swirl No. With Quarl
Mixing Chamber Diameter	Small (206mm)	Small (206mm)	Small (206mm)	Small (206mm)
Velocity, (m/s),				
Secondary	38.1 *	38.1*	38.1*	38.1*
Primary	30.5	30.5	30.5	30.5
Flow Rates, 10^{-3} kg/s				
Secondary Air	540	540	540	540
Primary Air	5.5	5.5	5.5	5.5
Primary Argon	16.5	16.5	16.5	16.5
Mole % Argon	75	67-75	67	67
Particle Type (% Loading in Primary)		NUMBER OF TESTS		
Coal (40%)	9	5	5	5
Gas Only (0%)	-	-	4	-

*Nominal axial secondary velocity without swirl.

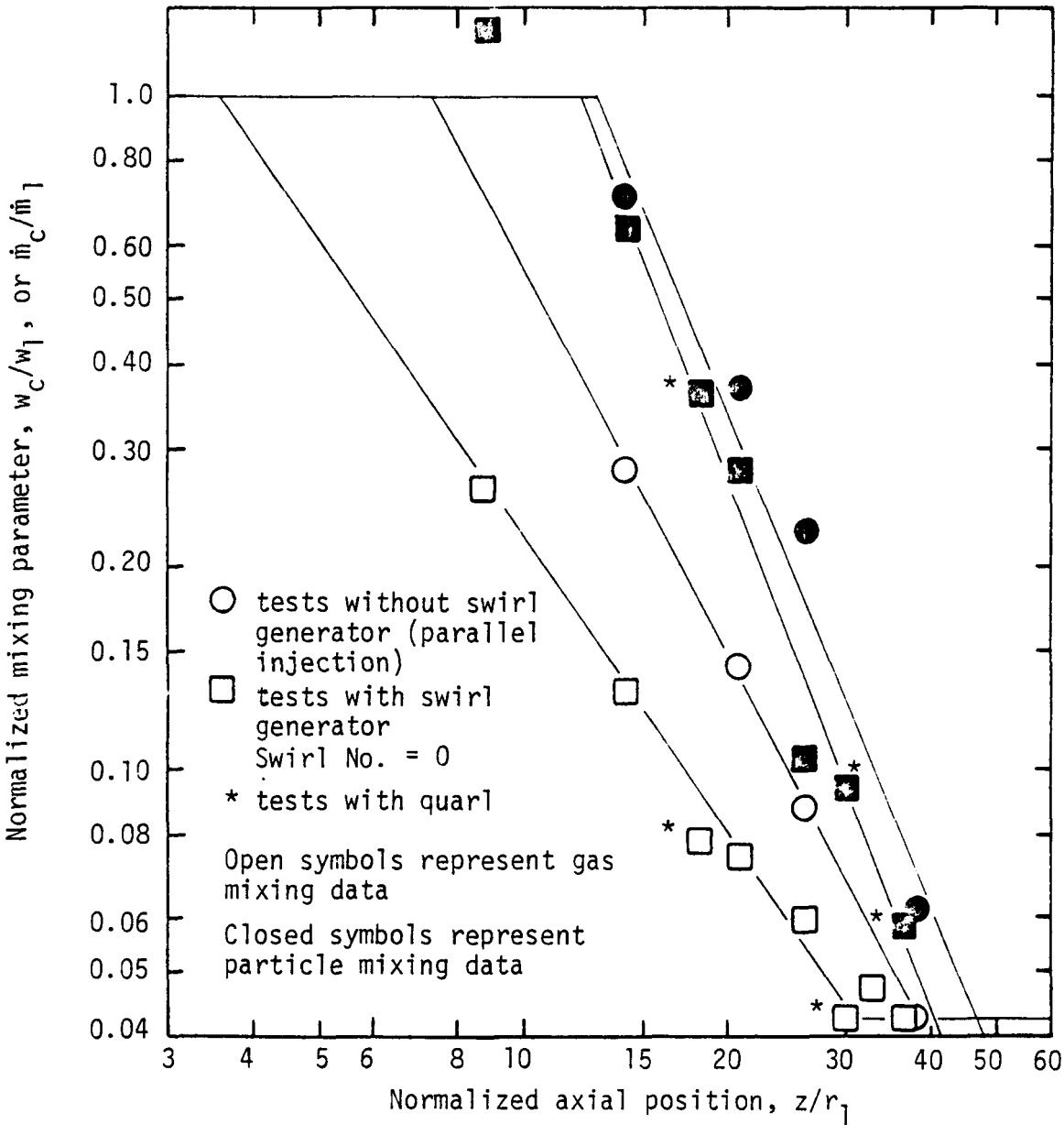

Figure 25. Comparison of centerline axial decay data for coal-dust cold-flow tests with and without swirl generator installed. Flow conditions are standard with small mixing chamber (206 mm diameter). Tests without swirl generator are for parallel secondary injection-tests with swirl generator are for swirl number equal to zero.

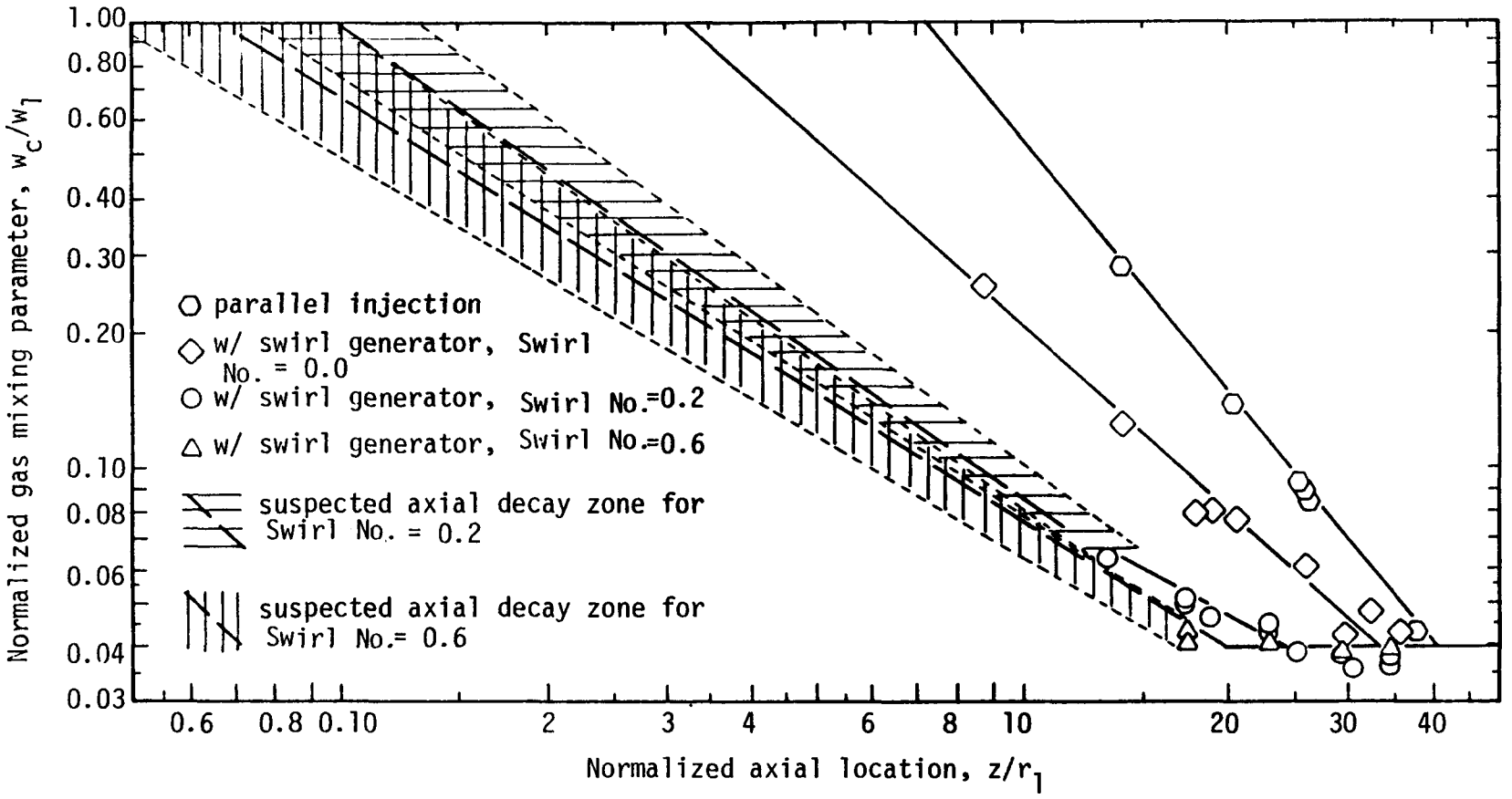

Figure 26. Comparison of axial decay plots of gas mixing parameter for parallel injection and swirled injection at standard flow conditions and small diameter (206 mm) mixing chamber (all coal dust tests).

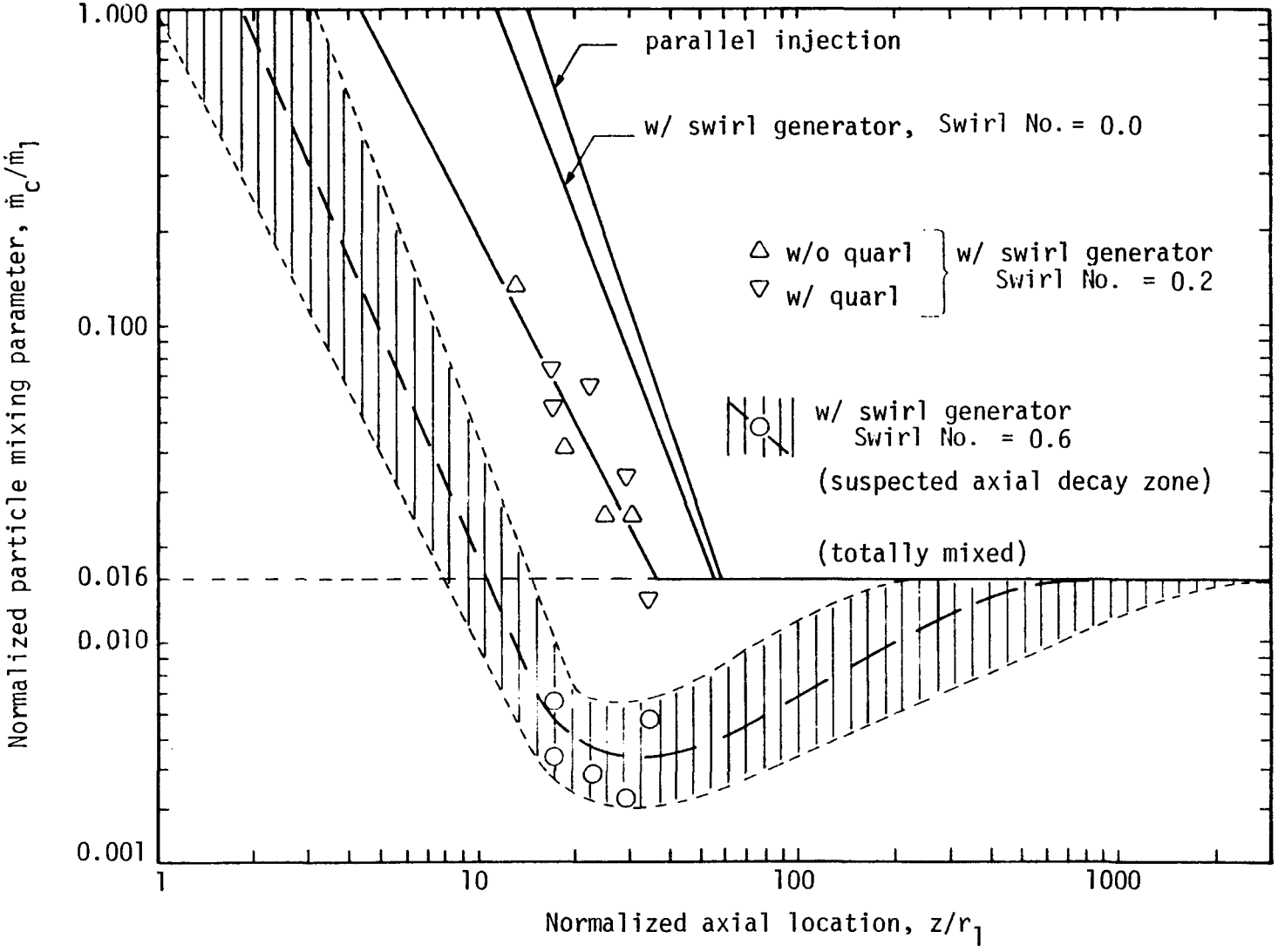

Figure 27. Comparison of axial decay plots of particle mixing parameter for parallel injection and swirled injection at standard flow conditions and small diameter (206 mm) mixing chamber (all with coal dust).

by the banded regions surrounding the decay lines. Nevertheless, it was quite clear that swirl had increased the rate of gas mixing by factors of up to 6, depending on whether the rate increase was based on the completely mixed length or on the core length.

The particle results shown in Figure 27 also showed a very significant increase in mixing rate with secondary swirl. The small effect on particle mixing rate of using the swirl generator at zero Swirl Number is shown again on this figure. An increase of the theoretical secondary Swirl Number to 0.2 causes the particle mixing rate to be increased by a factor of about 2 - 3. The centerline results for a Swirl Number of 0.6 were somewhat difficult to interpret. The centerline values at all of the axial positions where measurements were made showed a mixing parameter value below the fully mixed value. It was clearly evident that the higher Swirl Number of 0.6 had a very major effect on the particle mixing rate. A possible centerline decay curve has been shown on the figure, based on the very limited data. This curve is quite speculative and may not truly represent what was actually happening since strong swirling flows are known to exhibit a region of gas recirculation on the centerline (13). Apparently, the particles are rapidly thrown from the centerline and then mix back toward the centerline.

Additional particle mixing data for a Swirl Number of 0.6 are shown in Figure 28. This figure presents the radial distribution of the particle mass flux at the four axial locations where particle samples were taken. Within the data scatter, it was not possible to differentiate the radial profiles at each of these axial stations. Consequently, a single curve representing the probable radial particle flux is shown. This curve was obtained by fitting a polynomial curve to the data and adjusting the coefficients until 1) a reasonable fit of the data was obtained and 2) an integration of the particle mass flux across the duct matched the primary jet particle feed rate (forced mass balance). This radial profile distribution suggests that the secondary swirl was coupled to the primary jet and that centrifugal effects rapidly moved the particles to the outer regions of the mixing duct. This observation suggested that considerable control of the particle mixing could be achieved at the proper Swirl Number, and that a maximum particle mixing rate would be achieved at some intermediate Swirl Number. It also suggested that at higher Swirl Numbers (greater than 0.6) the particles could be thrown to an outside wall and that mixing between the particles and the gases could actually be delayed.

Further substantiation of the idea that a maximum particle mixing rate could be achieved at some intermediate Swirl Number is found in Figure 29 . This figure presents radial particle flux profiles at Swirl Numbers of 0.2, 0.43, and 0.60. As in the previous figure, a polynomial equation was forced to fit the available data and upon integration match the initial particle feed rate. The shape of the radial profile at a Swirl Number of 0.2 approximates the profiles obtained in previous tests without swirl (see Figure 15 for example). The flux profile obtained at a Swirl Number of 0.43 shows a small peak on the centerline which is below the fully mixed value of 0.016. It then shows a region of reduced particle flux followed by an increase in particle flux near

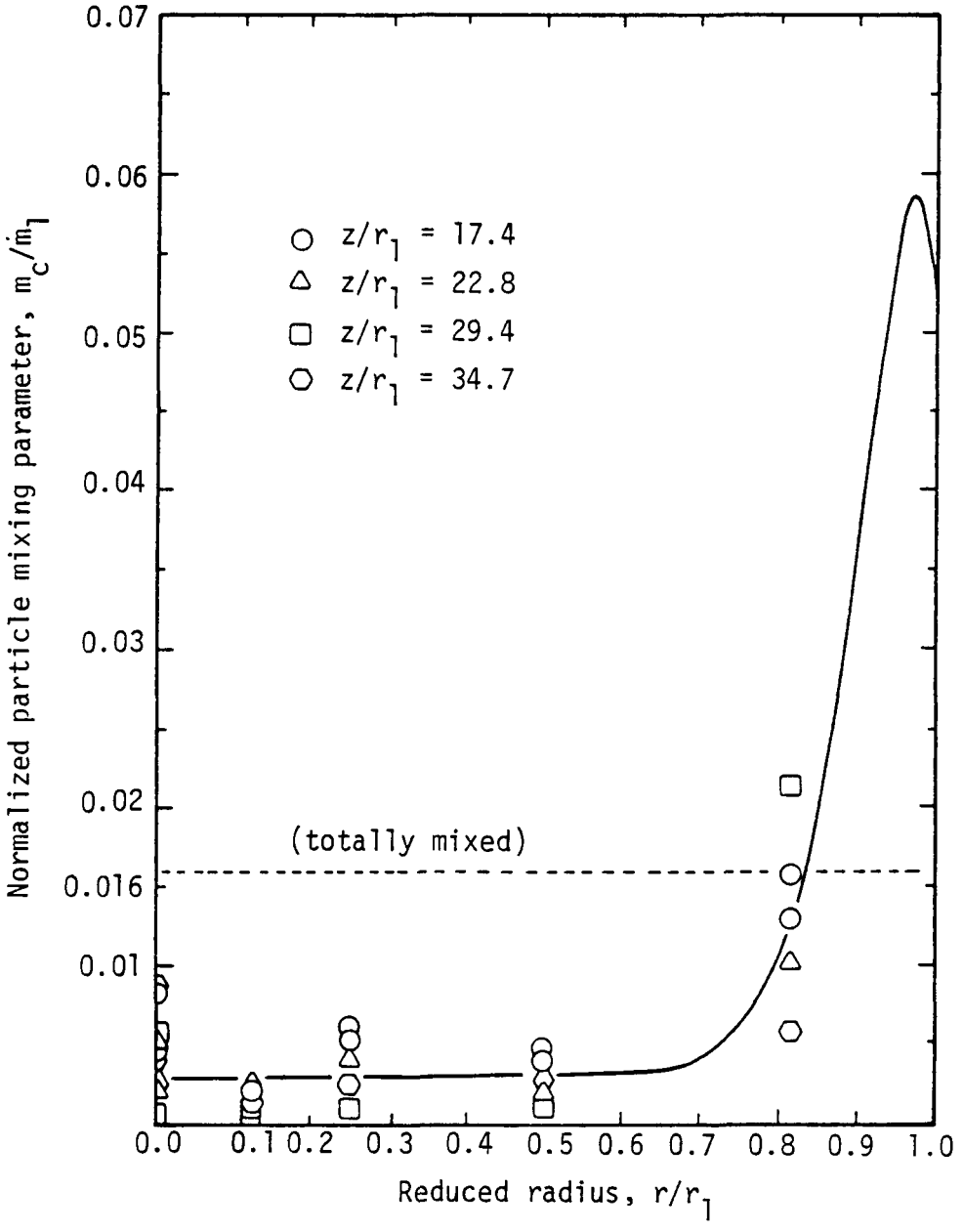

Figure 28. Average radial decay plot of particle mixing parameter for Swirl No. = 0.6, standard flow conditions, small diameter (206 mm) mixing chamber, and coal dust.

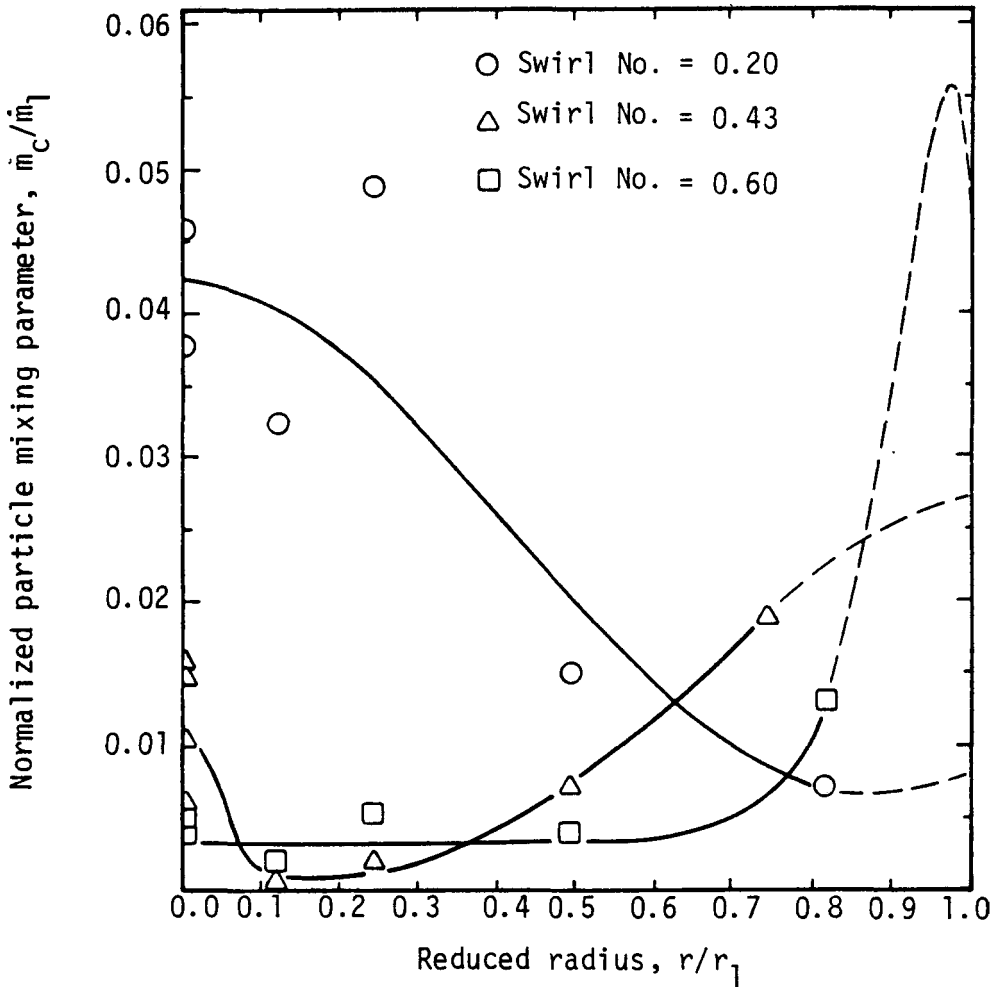

Figure 29. Comparison of radial decay plots of particle mixing parameter for swirled injection, standard flow conditions, small diameter mixing chamber, and coal dust.

the wall. The particle flux curve for a Swirl Number of 0.6 shown on the previous figure is repeated here for comparison. At this Swirl Number, 0.6, the major part of the particles have moved to the outside wall and need to mix back towards the center before complete particle gas mixing can be obtained. It is evident from this figure that considerable control in particle mixing rate can be obtained by careful selection of the flow variables, particle size, and Swirl Number.

Turbulence Intensity Effects The increase in gas mixing rate associated with the swirl generator hardware raised questions regarding the change in secondary flow characteristics associated with the use of this hardware. It was speculated that the installation of the swirl generator had increased the turbulent intensity of the secondary jet even though the secondary velocity was maintained the same. A limited number of tests were made in which an existing hot-wire anemometer was used to check out this postulate. The results from these tests are summarized in Figure 30. This figure shows turbulence intensity values for the primary jet without particles near the centerline (6%) and near the wall (12%). Values are also shown for the secondary jet with parallel injection (17%) and thirty degree angular injection (14% to 17%). The use of the swirl generator however greatly increased the secondary turbulence intensity. At a Swirl Number of 0.0, a turbulence intensity of 38% was measured in the secondary jet. Values at Swirl Numbers of 0.2 and 0.6 were 44% and 32% respectively. It seems clear that a part of the increase in gas mixing rate associated with the swirl generator can be attributed to the higher turbulence level. Consequently, the effect of Swirl Number noted above was obtained by reference to 0.0 Swirl Number but with the swirl generator installed.

This finding which relates mixing rate to turbulent intensity was also noted in the development of the two-dimensional model (see Section 4). The predicted mixing rate was found to be quite sensitive to the assumed levels of turbulence intensity. In as much as turbulence intensity can be controlled by the design of the inlet geometry, this may also prove to be a very effective way of controlling gas mixing rate, independent of particle mixing rate.

E. MAJOR ACCOMPLISHMENTS AND CONCLUSIONS

1. Accomplishments

A number of accomplishments have been completed during the cold-flow test program. Some of the more significant results are summarized below.

1. Successfully adapted the cold-flow, confined jet mixing test facility to operate at conditions which simulate entrained coal gasifiers.

2. Successfully completed three additional test series wherein the effects of geometry and flow conditions on gas and particle mixing rate were measured at conditions that simulate those of entrained coal gasification processes.

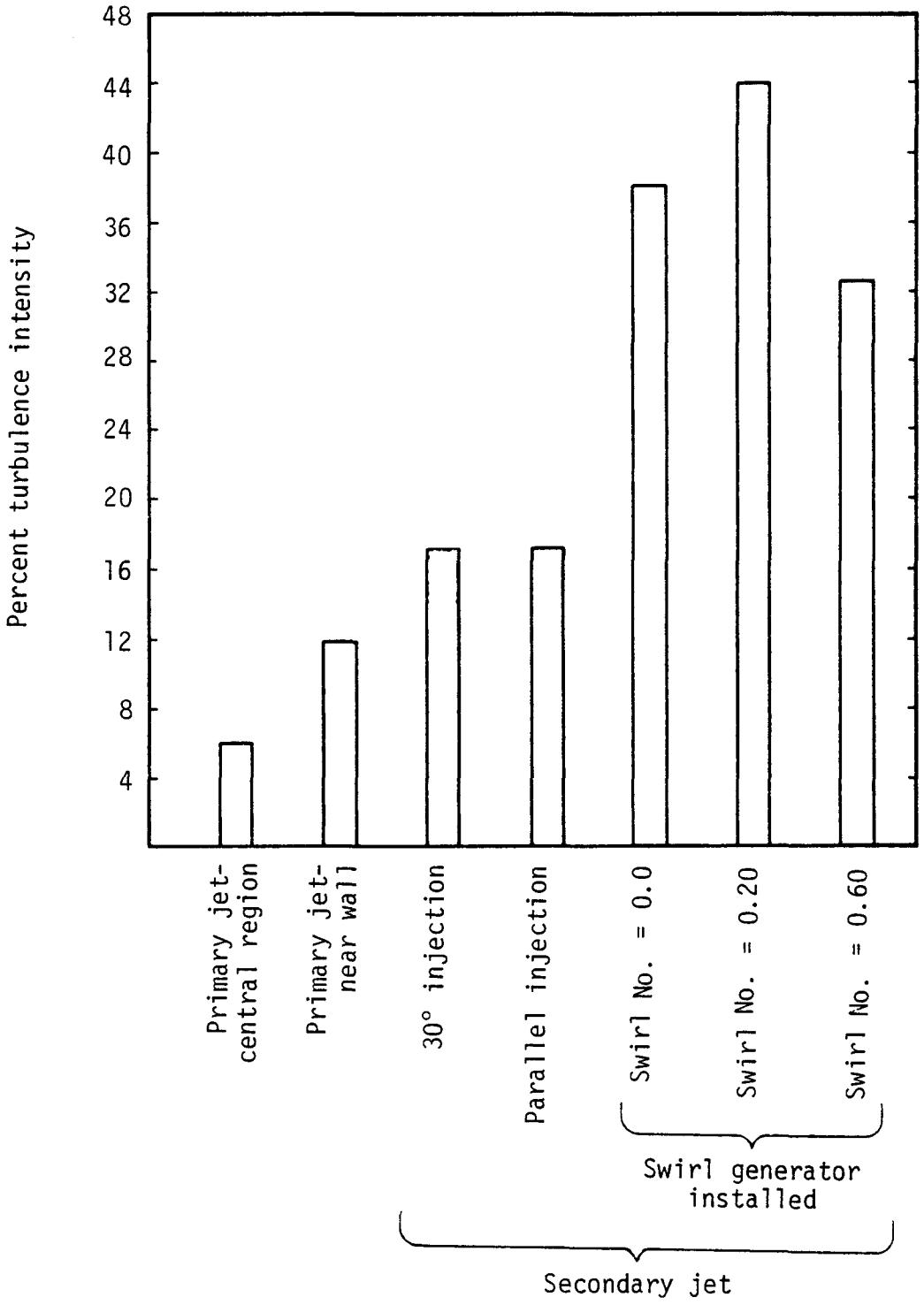

Figure 30. Comparison of turbulence intensities for various configurations for primary and secondary jet streams.

3. Successfully measured radial profiles of gas composition and particle mass flux at various axial positions with and without secondary swirl.

4. Completed fifty-seven cold-flow experiments wherein the combined effects of angular secondary injection with recirculation were investigated.

5. Completed thirty-eight cold-flow experiments wherein combined angular secondary injection and recirculation were investigated with a pulverized coal powder instead of a silicon powder.

6. Designed a moveable-block swirl generator, which was then fabricated and installed on the cold-flow facility. At least eight tests were conducted to ensure the proper operation of the swirl generator.

7. Conducted twenty-eight cold-flow swirl tests: Nine tests at a Swirl Number of zero, 14 tests at a Swirl Number of 0.2, one test at a Swirl Number of 0.4, and five tests at a Swirl Number of 0.6.

8. Designed a rotating, traversing, isokinetic sample probe, which was fabricated and installed in the test facility probe collar to replace the former, rigid, multiple probe bank. (Preliminary tests with a swirled secondary jet had demonstrated the need for a sample and velocity probe which could be aligned to the principal flow direction in swirling flows.)

9. Used the new traversing swirl probe to gather local gas and particle samples in the 19 swirl tests involving non-zero Swirl Numbers.

2. Conclusions

The analysis of Test Series 2 data and the completion of Test Series 3, 4 and 5 have lead to the following significant findings and conclusions.

1. Generally, the gases mixed about twice as fast as the particles. Increases in the gas mixing rates over the particle mixing rates ranged from 77% to 172%. However, in only one case, the small (ca 24 μm) silicon powder size, the measured particle mixing rate was faster than the gas mixing rate.

2. The suspended particulates in the primary gas stream decreased the gas mixing rates. With standard silicon powder present as 40 wt.% of the primary, gas mixing rates were decreased by 15 to 30%.

3. A decrease in the particle size resulted in an increase of both the particle and gas mixing rates. The gas mixing rate increased by 20% and the particle mixing rate increased by 175% when the

small (24 μm) silicon was used in place of the standard (46 μm) silicon.

4. An increase in the secondary-to-primary velocity ratio resulted in a marked increase in the mixing rates of both particles and gases. An average increase in gas mixing of 34% and an average increase in particle mixing of 22% was shown for an increase in velocity ratio from 1.0 to 1.25. Similarly, an average increase in gas mixing of 87% and an average increase in particle mixing of 33% was shown for a velocity increase from 1.25 to 2.0.

5. The effect of mixing chamber size on gas and particle mixing rates was dependent on flow condition and inlet geometry. The observed effects ranged from reductions in mixing rate, to little or no effect, to increases in mixing rate up to a factor of about 2.3. If an increase in mixing rate was noted, the major effect was seen with the small diameter mixing chamber. Larger ducts generally resulted in decreases in the observed mixing rates.

6. The effects of variations in flow parameters on the mixing rates were often more pronounced for the small diameter mixing chamber than for the larger chambers.

7. Use of the 30^{o} nonparallel injection configuration generally resulted in increases in both the particle and gas mixing. Changes in the rate of gas mixing due to nonparallel injection ranged from -5% to 29%, with an average increase of 13%. Similar changes in the particle mixing rates ranged from 6% to 74%, with an average increase of 45%.

8. For the parallel configurations, the influence of flow parameters was much more significant on gas mixing than on particle mixing. The particle and gas mixing rates exhibited independent behavior for the parallel tests.

9. For the nonparallel configurations, the gas and particle mixing rates responded much more equally to changes in the flow parameters. Total mixing duct length had little or no effect on the rates of mixing for this system.

10. The use of the lower density coal dust resulted in somewhat faster mixing rates for both gas and particles for all geometries tested. Gas mixing was increased an average of 19% and 73% for the parallel and 30^{o} injection cases respectively.

11. The installation of a secondary swirl generator caused a higher turbulence level in the secondary stream which increased the gas mixing rate significantly even with no secondary swirl. Little effect was seen on the particle mixing rate, however.

12. The use of even modest amounts of secondary swirl had a very pronounced effect on the mixing rates of both gas and particles. A Swirl Number of 0.2 increased the gas mixing rate by a factor of about 1.4 or 3.3 and the particle mixing by a factor of about

1.6 or 2.9 as deduced by core length or completely mixed length respectively.

13. At a Swirl Number of 0.6, it was impossible to quantify the mixing rate from the core length or completely mixed length from the data taken. It was clear from the data however that the flow pattern had been substantially altered and that the gas was totally mixed by the first axial measurement location and that the particles had been forced away from the centerline toward the outside of the duct.

14. It was evident from the data collected that considerable independent control could be excercised over the gas and particle mixing rates by controlling the secondary jet turbulence intensity and the secondary Swirl Number.

III. ENTRAINED COAL GASIFICATION TESTS

A. INTRODUCTION

Coal gasification has been an available technology for many years. The early history of coal gasification has been well documented by Lowry (14, 15). Coal gasification provided street lights for many cities, and was used to fuel industry through most of the industrial revolution. During that period of time, fixed bed (e.g. Lurgi) and pulverized bed (e.g. Winckler) gasifiers were developed which provided a medium BTU gas but with considerable pollution. After World War II, work to refine the reactors continued and a new reactor type evolved, an entrained flow reactor (15). Entrained coal reactors are of special interest because they have the potential of higher reactor throughput and consequently, lower cost. Also, these reactors are not sensitive to the use of caking or agglomerating coals as are some of the fixed or fluidized bed types.

Bissett (16) provides an extensive summary of the development of entrained gasifiers at the U. S. Bureau of Mines facility in Morgantown, West Virginia during the post World War II years. He also summarizes other entrained gasifier developments which were undertaken during those same years (including, the Koppers-Totzek, Texaco, and Babcock and Wilcox - du Pont gasifiers).

During the late 1950's and early 1960's, natural gas distribution became wide-spread across the continental United States and the need for coal gasification waned. This was unfortunate in light of the serious energy shortages which are now confronting our nation. Beginning in the early 1970's, however, renewed interest in coal gasification developed, and several ambitious pilot plant programs were initiated. These included CO_2 Acceptor, Hygas, Bigas, Synthane, Foster-Wheeler, Babcock-Wilcox, and Westinghouse, gasifiers.

Virtually all of the early gasifier developments came about through an evolutionary process. Reactors were built, operated and modified without a full understanding of the physical and chemical processes involved. Reactors were developed which gave moderate thermal efficiency and an adequate product gas but with considerable pollution. The entrained gasifier reseach after World War II was aimed at developing entrained gasifier reactors for commercial application but little work was done to better understand the complex physical and chemical processes associated with coal gasification and no work was done to understand the mechanisms of pollutant formation.

Over the years, several of the developing entrained processes have not been successful, at least in part, because they lacked the fundamental data and techiques needed for optimum design. Entrained coal processes, including coal gasification, involve the injection of finely pulverized coal, suspended in a gas stream, into a reactor where conversion reactions take place, creating a variety of different products. The basic principles of coal entrainment and reaction are not at all well understood and require considerable study before optimum engineering

designs are possible. The influence of the turbulent mixing characteristics of a particle-laden, reacting, gas stream must be determined before a reaction vessel can best be designed to maximize efficiency yields of desirable products and minimize pollutants and other undesirable effects. Such problems have been identified (1) as among the most critical and key problems which need to be solved in order to improve the design of entrained coal gasifiers. The renewed interest in coal gasification and the stringent environmental contsraints which are imposed by today's society require that a basic understanding of these complex coal conversion processes be obtained.

B. OBJECTIVES AND APPROACH

This report summarizes the work accomplished during the second phase of the entrained coal gasification test program. The objectives of the first phase of this study were reported in detail previously (2) and were summarized in Section I of this report.

The objectives of the second phase of this entrained coal gasification test program reported herein, and in References 17 and 18, were to conduct a series of reacting coal gasification experiments where the extent of gas and particle mixing, the extent of particle reaction, the extent of pollutant formation, gas and char product composition, and temperature and/or velocity would be measured locally. Tests were also to be performed to evaluate the effects of coal feed rate and inlet coal/oxygen steam mixture ratios on flame stability and extent of coal reaction, and to charactrize the effects of such operating variables as pressure, secondary gas temperature, coal particle size, and coal type. Radial profile measurements at several axial locations were to be made in order to map the reaction zones within the reactor.

Additional efforts in support of the program included completion of the non-reactive atmospheric and elevated pressure cold-flow mixing tests initiated under Phase 1, completion of the macroscopic computerized model(s) which describe the reacting coal gasification processes, comparison of the computer model predictions to actual test data and the use of the computer model(s) to make parametric studies to determine relative tradeoffs which result from variation in controllable operating parameters.

The current study included four series of tests. Test Series 1 was a set of system evaluation tests. These tests were performed to establish ignition, preheat, and stable coal reaction operating conditions. Tests were also performed in support of sample probe and sample collection system development. Further tests were performed to determine the allowable coal throughput in the reactor. Test Series 2 was designed to measure the effect of coal/oxygen/steam mixture ratios on the gaseous and solid reaction products, on the extent of coal burnout (carbon conversion), and on the extent of pollutant formation. This set of tests was also designed to establish the flame stability limits for the test coal (a high volatile Utah bituminous coal) in terms of O_2/coal and steam/coal ratios. Test Series 3 was a set of experiments wherein radial profile data were taken at various axial locations within the reactor. These data were used to map the mixing and reacting processess

occuring within the reactor, and to provide important insight into the rates of gas and particle mixing and chemical reactions. Test Series 4 was designed to investigate gas and particle mixing rates at elevated pressure. A series of cold-flow experiments and reacting gasification tests at elevated pressure were to be included in order to measure the effect of pressure on gas and particle mixing rates and on the chemical reaction rates, coal burnout (carbon conversion), and pollutant formation.

The gasifier, which was described in detail previously (2), was designed with interchangeable reactor sections, one of which was a probe section. The probe section, which contained up to five fixed sampling probes located at various radial positions, could be positioned at various axial locations in the combustor. This arrangement allowed both radial and axial sampling over the entire reactor.

The ability to sample both gas and particulates at any given zone in the reactor during gasification operation was an important aspect of the technical approach. The samples were collected with direct water-quenched probes designed specifically for this purpose. Additionally, the introduction of argon trace gas into the primary jet and helium trace gas into the secondary jet permitted the local extent of gas mixing to be determined. A gas chromatograph was used to analyze the gas samples for argon and helium as well as O_2, CO, CO_2, CH_4, H_2 and N_2. H_2O was deduced from a H_2 material balance. A chemi-luminescent analyzer was used to analyze for NO. Selective ion electrodes and Drager tubes were used to analyze for the small amounts of NH_3, HCN, H_2S, and SO_2.

The particulate and quench water materials in the samples were separated from the gas samples. The particulate samples were filtered from the quench water, dried, and analyzed to determine the ash, carbon, hydrogen, oxygen, sulfur and nitrogen content from ultimate analysis. Ash was used as the key particle tracer with ash content being determined prior to and after coal gasification. The local extent of coal burnout is determined from the weight fraction of ash in the sample and the weight reaction ash in the original coal. The weight fraction of ash in the sample was used with the ultimate, elemental analysis of the sample to determine the local extent of pollutant (nitrogen and sulfur) release from the coal char. The particle mass flux was deduced from the mass of particle sample, the probe cross-sectional area, and the sample time. Such detailed information on local properties serves as the basis for interpreting rates of mixing and particle reaction, and therefore the influences of mixing rate on particle reaction rates.

C. TEST FACILITY

The design and fabrication of the gasifier facility has been described in detail elsewhere (2). A schematic flow diagram of the test facility is contained in Figure 31. A more detailed schematic of the reactor is shown in Figure 32. The gasifier was designed to study entrained coal gasification processes at elevated pressures (up to 2150 kPa (20 atm), and was constructed using funds from the phase 1 contract (2) and this study. The gasifier had a primary nozzle diameter

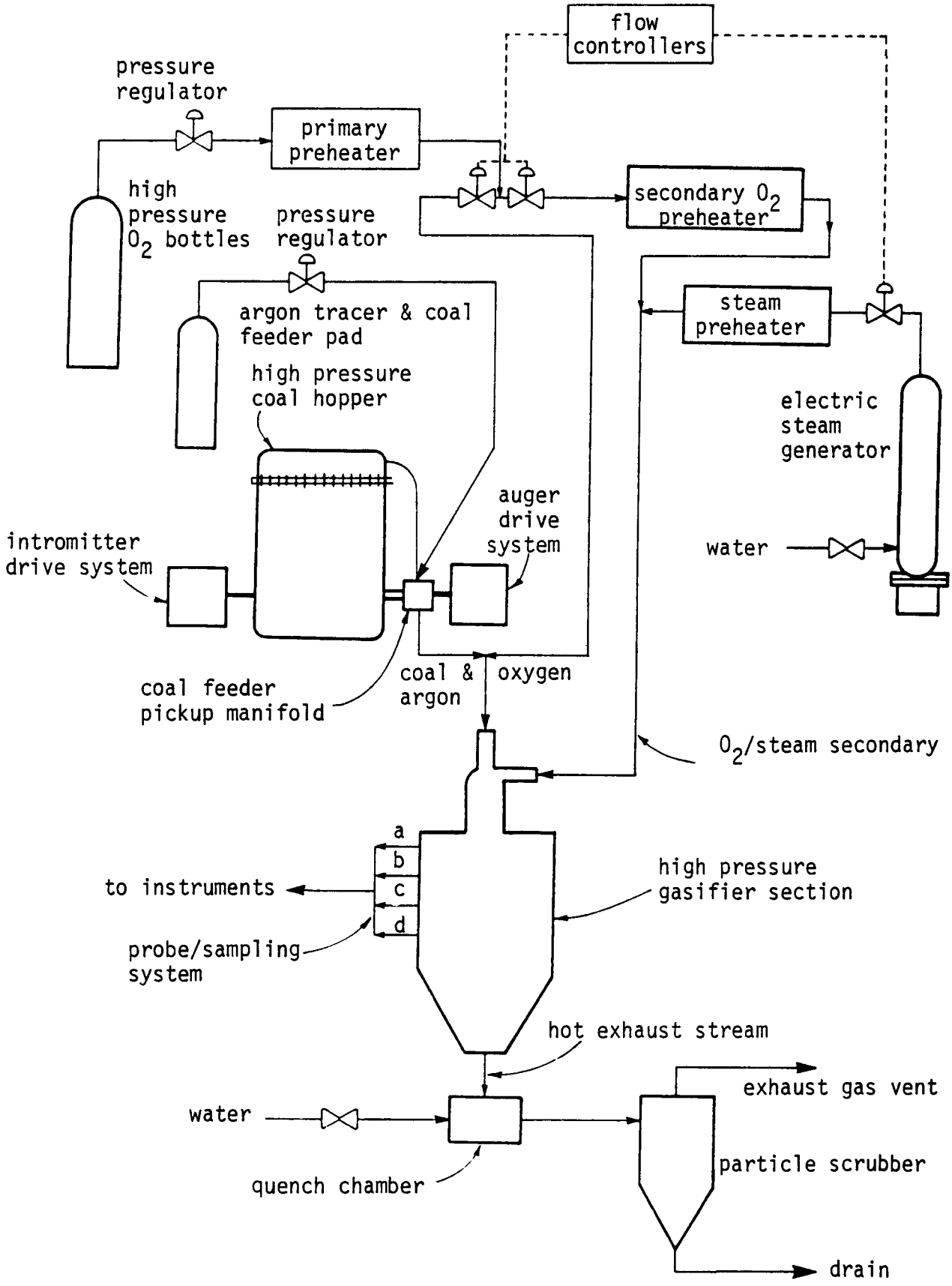

Figure 31. Schematic flow diagram for coal gasification test facility.

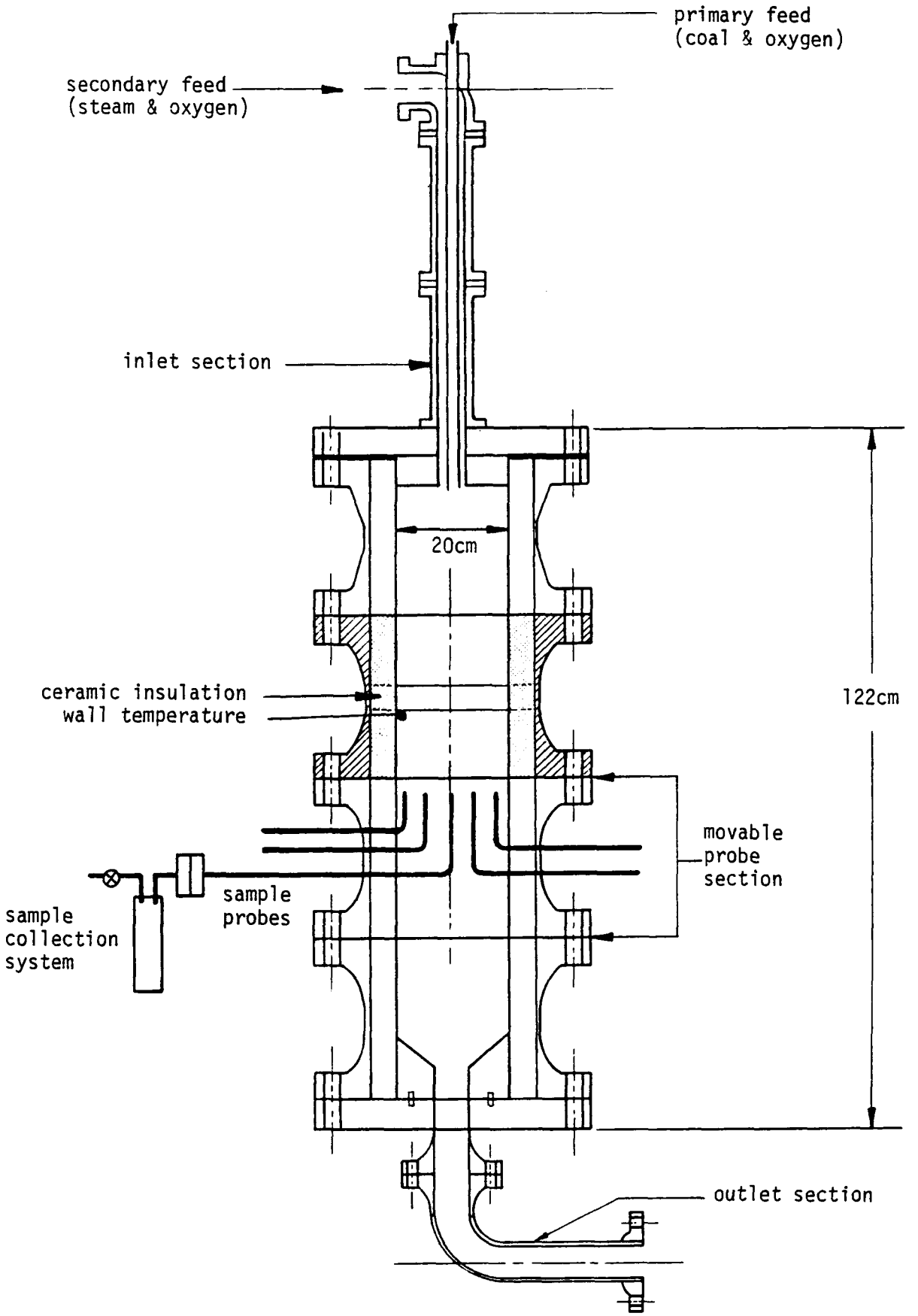

Figure 32. Schematic of high pressure entrained coal gasifier.

of 12.7 mm, and a coal processing capacity of 13.6 to 136 kg of coal per hour.

During the present contract period, the various components of the facility were completed and integrated. The facility was thoroughly checked out and made operable. A total of 114 tests were performed to check facility operation, to develop the sample probe and collection system, and to obtain final test data.

It was necessary to make major modifications to the coal feed system before reliable, steady operation was obtained. In particular, it was found that the original Acrison 105-6 twisted-ribbon-flighted, open-core augers did not give good, reproducible flow at a given feeder setting. Rather, coal dumping was caused by very small pressure imbalances. In addition, it was observed that coal was drawn only from a portion of the auger, instead of over the entire length, which led to funnel flow from the coal bed. A solid-core, variable flight auger (Figures 33 and 34) was designed and fabricated, an overhead stirrer (Figure 34) was installed, and a larger diameter pressure equilibration line was installed in an attempt to resolve the coal feeding problems. These modifications led to stable coal feed with reasonable uniformity and reproducibility and no dumping problem.

Another recurring problem dealing with coal feeding was that of flame propogation back up the primary duct and into the coal feed vessel. Attempts to alleviate this problem by blanketing the coal feeder with an inert gas met with limited success. Subsequent modifications were made in the method used to entrain coal and to blanket the coal vessel. Previously, the primary oxygen was used as the entraining medium. In the modification, the inert gas used to blanket the coal feed tank was also used as the entraining gas; it also served as the primary gas phase tracer. The primary oxygen was brought into the primary duct below the coal pick-off point, where it mixes with the coal and inert gas stream prior to entering the injector section above the reactor. This modification is shown schematically in Figure 31. From rather extensive work in recalibrating the coal feed system, the modifications did not substantially change the coal feeder operation or the calibration. A small pneumatic vibrator was also installed on the primary tube just below the coal pick-off point to reduce the amplitude of pulsations in the coal feed.

A back-pressure regulator was ordered, installed, and checked out. Elevated pressure cold-flow tests demonstrated that stable operation could be maintained at elevated pressures in the reactor. However, no coal gasification tests were performed at elevated pressure.

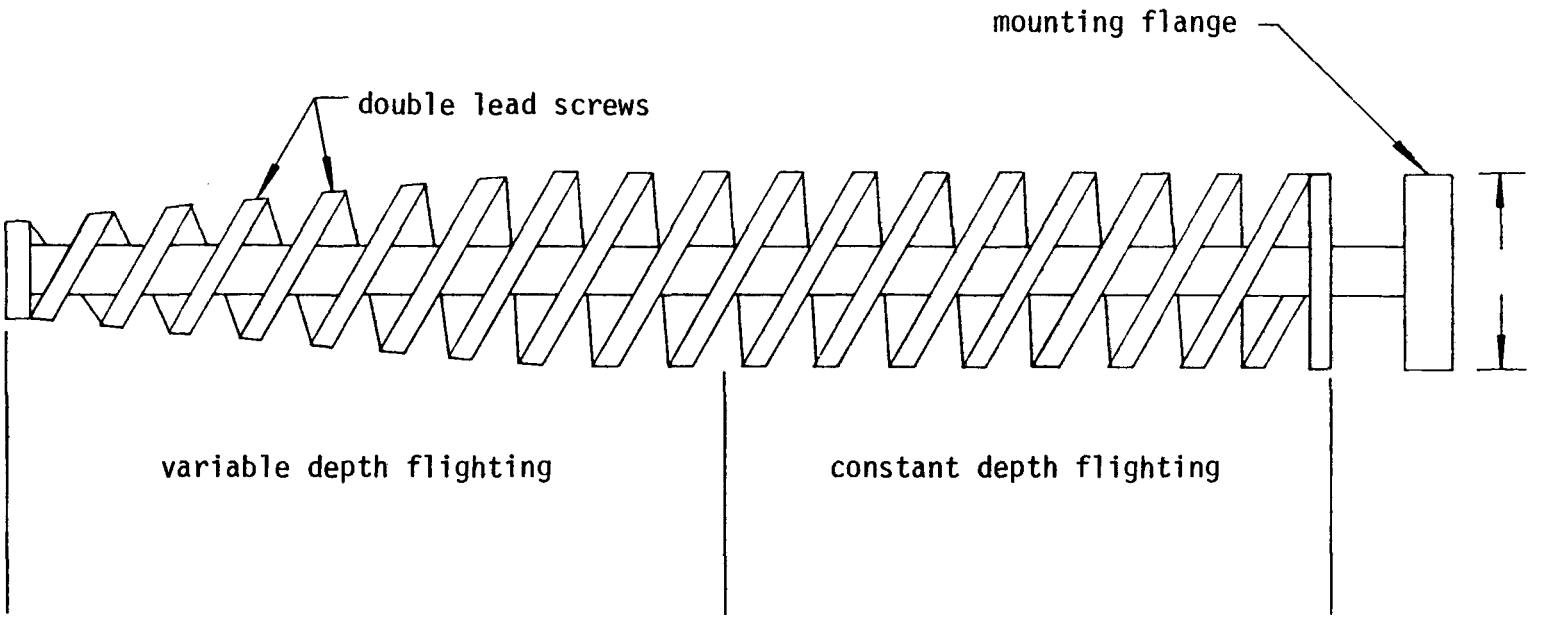

Figure 33. Schematic of modified coal feed augers.

(a) Motor driven stirrer system for coal feeder tank

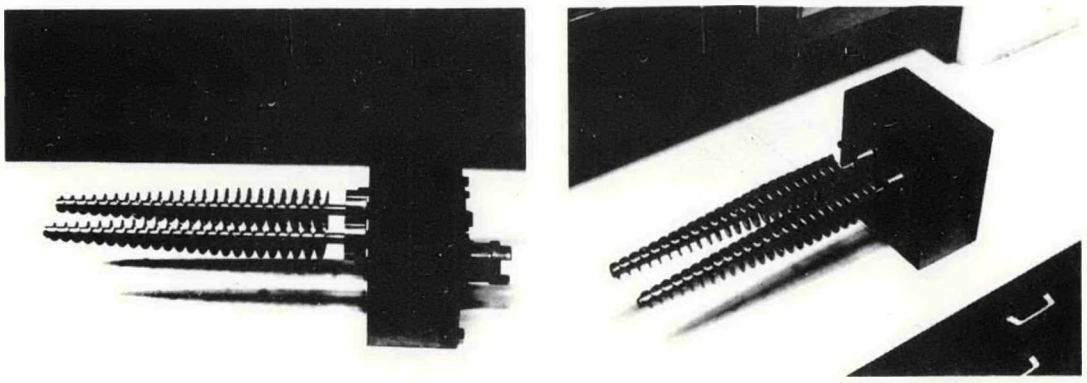

(b) Two views of variable depth, flighted augers for coal feeder.

Figure Components for revised high pressure coal particle feed system.

D. PROBES AND SAMPLE COLLECTION SYSTEM

Considerable effort was expended in designing, fabricating and demonstrating the suitability of a water-quenched probe and total collection sampling system. The probe design, which is shown in Figure 35, was very similar to that described earlier in Phase 1 of this study (2). The sample collection system is shown schematically in Figure 36. The sampling apparatus included the following: 1) up to five 0.32 cm (inner diameter) water-quenched probes made of 316 stainless steel and fixed at various radial locations in a moveable probe section; 2) carbon steel sample collection vessels, one for each probe; and 3) a large nylon sample bag which fits inside each steel collection vessel. A solenoid--actuated valve in the top of each sample collector directs the flow of sample either to bypass, where it is discarded, or to the nylon bag inside the steel collection vessel. The nylon bag prevents contamination of the sample by the steel, and was chosen for its low permeability to the gas phase products. The probe and collection system was designed to meet the following four objectives: 1) to collect a representative sample during an experimental run; 2) to collect gases, solids, and liquids as part of the sample; 3) to require as little manual operation as possible; and 4) to preserve samples in such a way that concentration levels measured give an accurate measurement of the concentration levels that were in the reactor during the experimental run.

Problems which initially plagued the successful implimentation of the sample collection system, such as air contamination of samples, sample bag rupture and absorption of CO_2 in the quench water were all satisfactorally resolved. In addition, collection of all the gas and liquid from a given probe over the known sampling time made it easy to determine the average molar flow rate of the sample gas by a simple application of the ideal gas law, corrected for the amount of liquid collected and the volume of the bag itself.

A modified sampling system for elevated pressure tests illustrated in Figure 37 was also designed and built. The coal-char slurry and gas-phase sample collected in the water-quench probe were separated in a solid-liquid disengager. The gas sample passed through a filter and sensitive metering valve which throttled the gas at reactor pressure down to ambient pressure. The metering valve accurately controlled the gas sampling rate to insure isokinetic sampling. The clean, throttled sample gas would be collected for chromatographic analysis, routed through on-line analytical equipment, and monitored for flow rate. A 5-way ball valve was installed downstream of the disengager to provide water for flushing coal-char residue from the walls of the disengager after tests. This valve also vented the disengager to allow collection of a sample of the gas dissolved in the slurry at high pressure.

Extensive cold-flow tests with a mock-up of this system indicated that the concept was generally adequate for gas flow rates that would be encountered in high-pressure gasifier test runs. However, preliminary tests indicated that a dilute solution could lose up to 15% of the sulfide ion ($S^=$) over a 15 minute period if left in the stainless steel disengager. Stainless steel was found, however, to be much better in this respect than carbon steel or galvanized steel. Possible modifications included

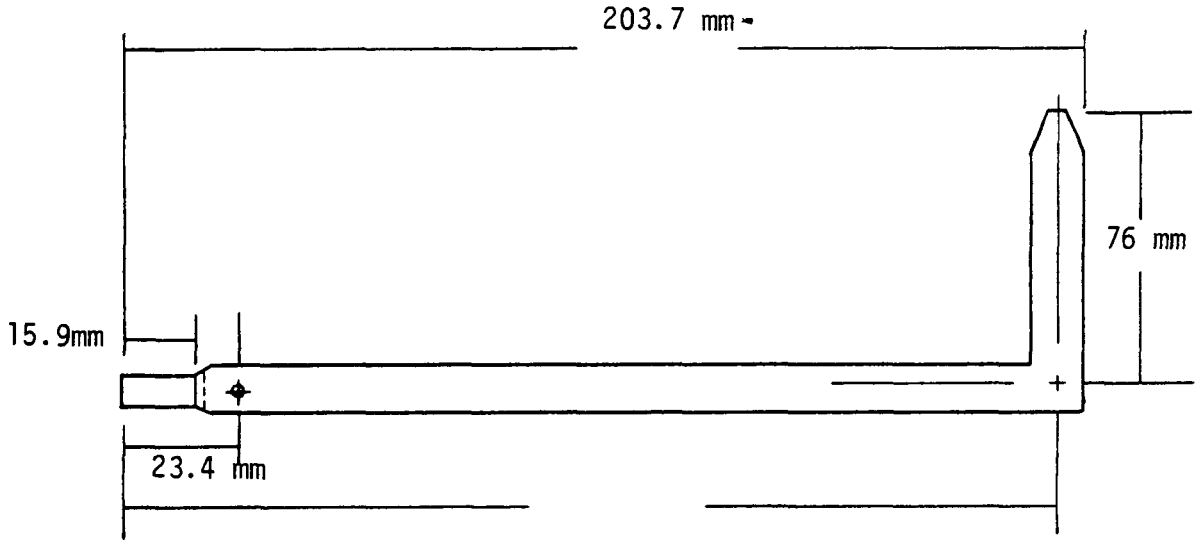

a) Overall probe dimensions

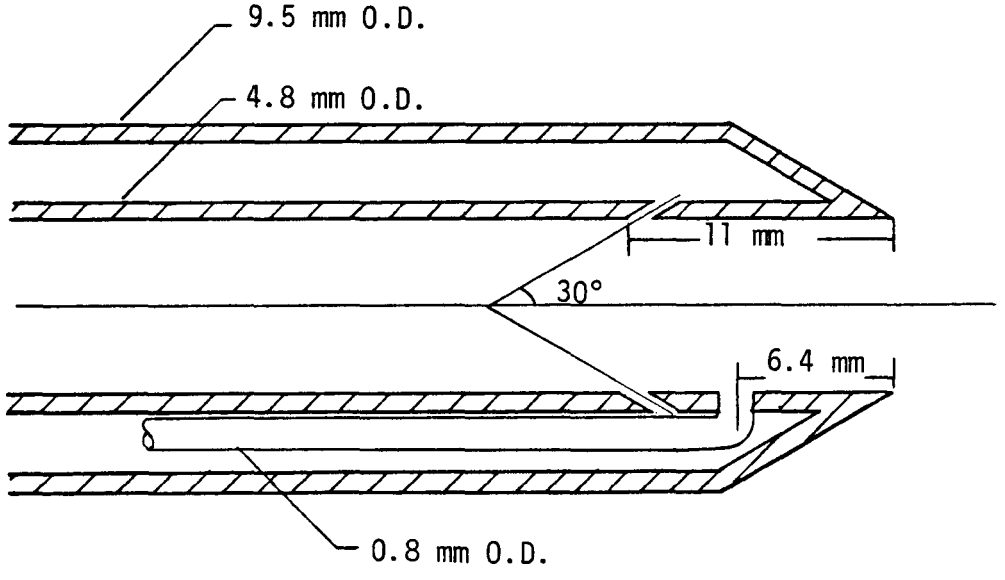

b) Detail of probe tip

Figure 35. Schematics of water quenched sample probe.

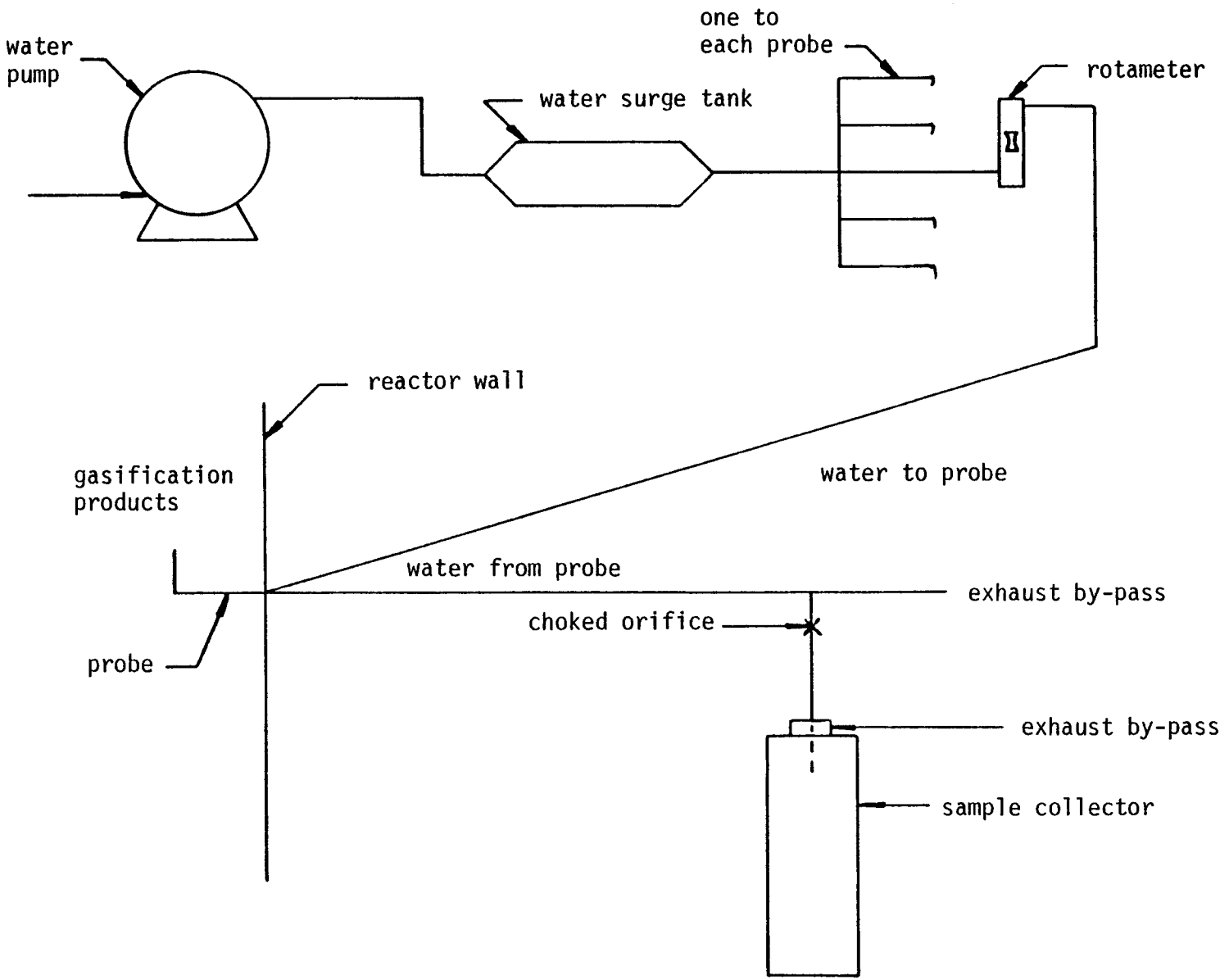

Figure 36. Schematic of sample train.

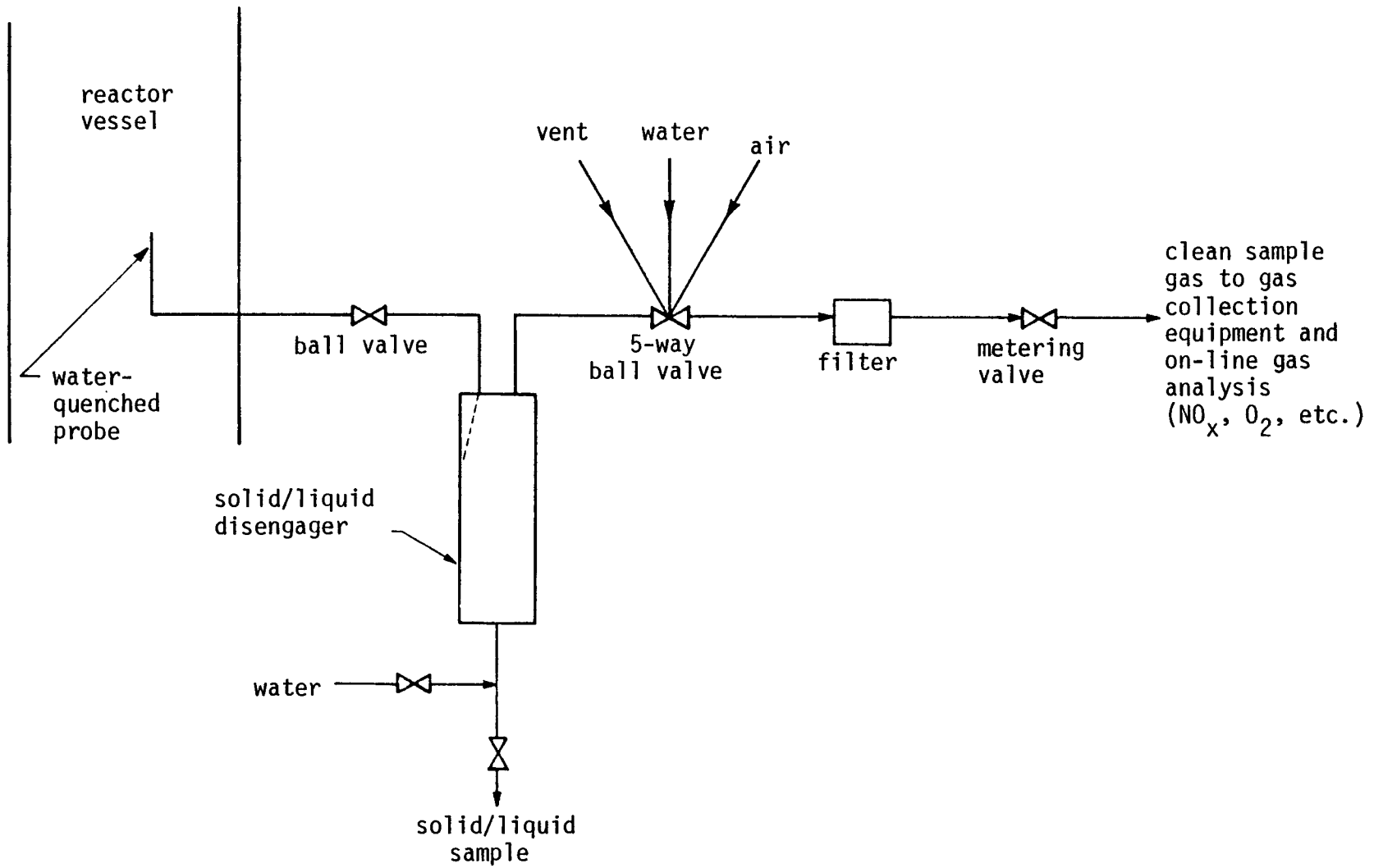

Figure 37. Schematic of modified sample train for high pressure gasification tests.

the addition of a low temperature bath downstream of the disengager to cool the sample gas and remove traces of entrained liquid. No opportunity was available during this study period to evaluate this system at elevated pressures during a gasification test.

E. TEST PROCEDURES

1. Experimental Routine

The test procedures used in the entrained coal gasification experiments have been reported in detail elsewhere (17, 18). Nevertheless, a brief summary of these procedures is included herein. A given gasification test was initiated by identifying the necessary operating conditions. These operating conditions dictated the necessary flows of coal, oxygen, steam, argon and helium in the primary or secondary ducts. Choked flow orifices of proper size for the flows required were placed in the oxygen, argon, and helium gas systems. Appropriate calibration points for the coal feed system and steam feed controllers were determined. The prepared sample collection vessels were brought into the combustion test bay, connected to the sample probes, with the solenoid valves set to bypass. The collection vessels were then evacuated with a vacuum pump.

The test began by establishing cooling water flow to the sample probes, the exhaust cooling spray nozzles in the bottom of the reactor, and the exhaust scrubber. Immediately, the hydrogen/air igniter was started and used to ignite a methane-oxygen flame. Once a stable methane-oxygen flame was established, the igniter was turned off. The methane-oxygen flame was used to preheat the ceramic wall insulation to the high temperature needed to maintain stable coal reaction. This preheating process was continued until thermocouples buried in the ceramic wall indicated that the minimum wall temperature had been reached. At this point the coal feeder was turned on and the coal feed allowed to stabilize. The methane flow was gradually reduced to zero as the coal-oxygen flame continued to preheat the reactor. At this point, the steam flow was initiated and the reactor was allowed several minutes of operation to stabilize and approach steady-state operating conditions. The approach to steady-state was determined by the behavior of the flame as observed through the optical port and by the variation in the wall thermocouple readings.

Once the reactor was determined to be near steady state operation, sampling began. This was accomplished by simply actuating the solenoid valves on the evacuated sample vessels. Sampling ordinarily proceeded for one to two minutes. A measure of the approach to isokinetic sample collection was obtained by monitoring the static pressure difference between the inside of a specific sample probe and the reactor static pressure. Generally, these pressures were within a few inches of water, which implied near-isokinetic collection. At the end of the sample time, the solenoid valve was returned to bypass and the reactor was shut down. The reactor shutdown was accomplished by stopping the flows of coal, oxygen and steam and then introducing a flow of cooling air to accelerate the reactor cool-down. With the reactor shut down, the

sample vessels were disconnected from the sample probes and moved to an instrument room for sample evaluation.

2. Sample Analysis

After the sample collection period, the sample containers were detached, and the contents of each container were analyzed. The sample contained in the nylon bag consisted of three phases; gas, water and char. Basic analysis schemes are illustrated in Figure 38. The gas, liquid, and solid samples collected from within the coal gasifier were analyzed using conventional gas chromatographic techniques, a chemiluminescent NO analyzer and Dräger tubes, selective ion electrodes and an elemental analyzer, respectively. The gas chromatographs used included a two-channel Tracer Model MT-150 instrument with ultrasonic detectors and a Hewlett Packard Model 5830 instrument with a thermal conductivity detector. The elemental analyses on the coal char were performed on a Perkin Elmer Model 240 ultimate analyzer.

Two basic goals were established for chemical analysis of pollutants formed during gasification: to develop methods to determine precisely and accurately concentrations of sulfide, cyanide, and ammonium ions in gasifier probe quench water, and to verify that sample measurements and analyses developed could be used to determine concentrations of H_2S, HCN, and NH_3 in the gasifier. To meet these goals, a series of tests were designed to investigate ion specific electrode analysis of sulfide, cyanide, and ammonium. In addition, experiments were designed to investigate sample decay and sample preservation. Finally the effect of filtering coal particles from quench water samples was examined. A discussion of each part of the sample analysis follows.

a. Gas Analysis

The following gases found in the sample were analyzed by gas chromatography: H_2, He, Ar, N_2, O_2, CH_4, CO, CO_2, C_2H_6, and C_2H_4. Argon and helium inert tracer gases were injected into the reactor to aid in calculating mass balances and in determining the extent of gas mixing. Two gas chromatographs were used in analysis of the above gases; a Tracor model MT-150, and a Hewlett Packard model 5830.

The Hewlett Packard instrument used hydrogen as a carrier gas and was used for analysis of He, N_2, Ar, O_2, CH_4, CO, CO_2, and C_2 hydrocarbons. A schematic diagram illustrating how the analysis took place is shown in Figure 39. The scheme consisted of a Poropak column in a series-parallel arrangement with a molecular sieve column. The gases first passed through the Poropak column. Lighter gases (N_2, O_2, Ar, He, CO) quickly passed through the Poropak column and entered the molecular sieve column. After the light gases entered the molecular sieve column, a solenoid valve activated, automatically trapping the light gases in the molecular sieve column and allowing heavier gases (CH_4, CO_2) to pass onto the thermal conductivity (TCD) detector. Once the heavy gases had passed through the detector, the solenoid valve deactivated and allowed the lighter gases to elute from the molecular sieve column onto the detector.

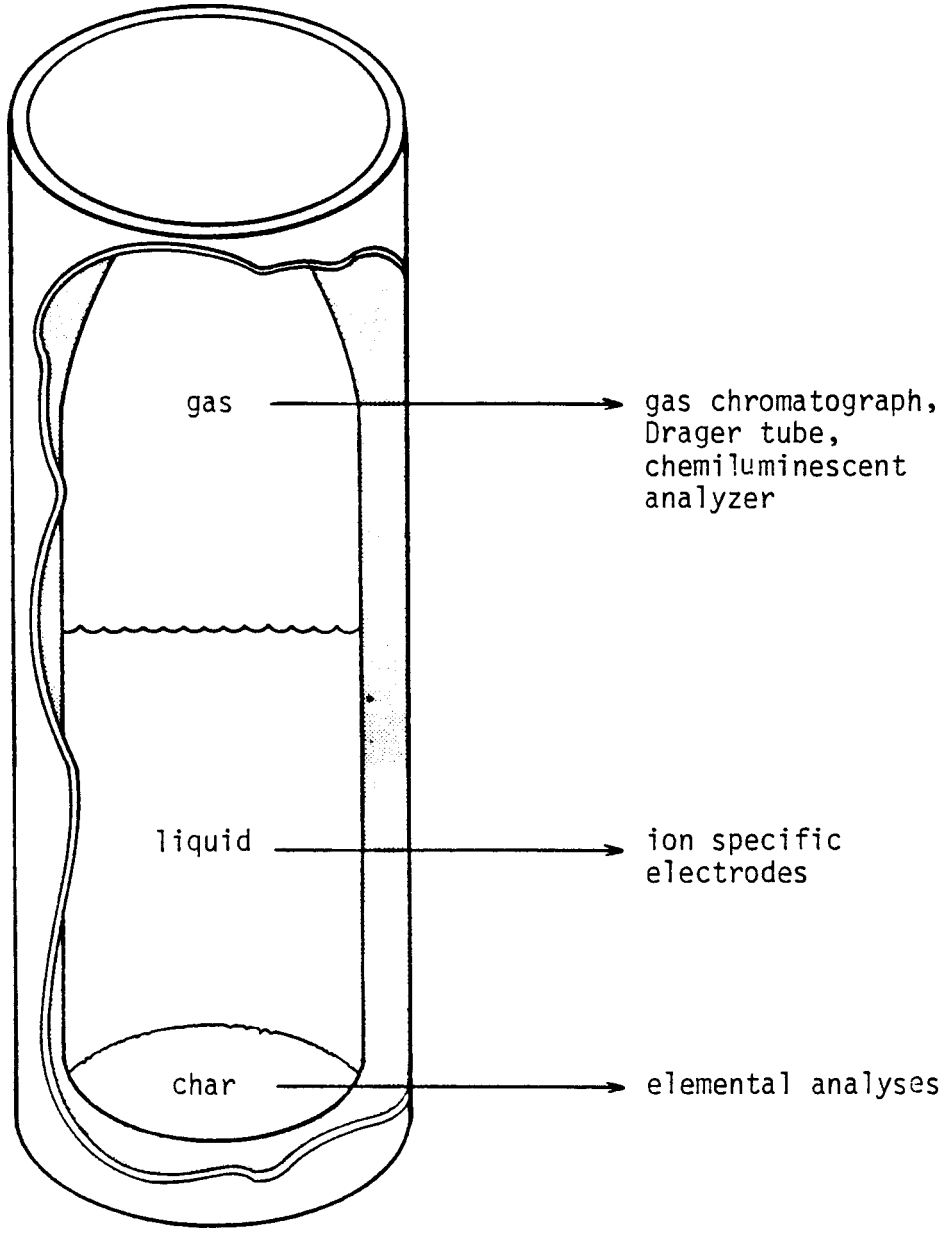

Figure 38. General sample analysis schemes.

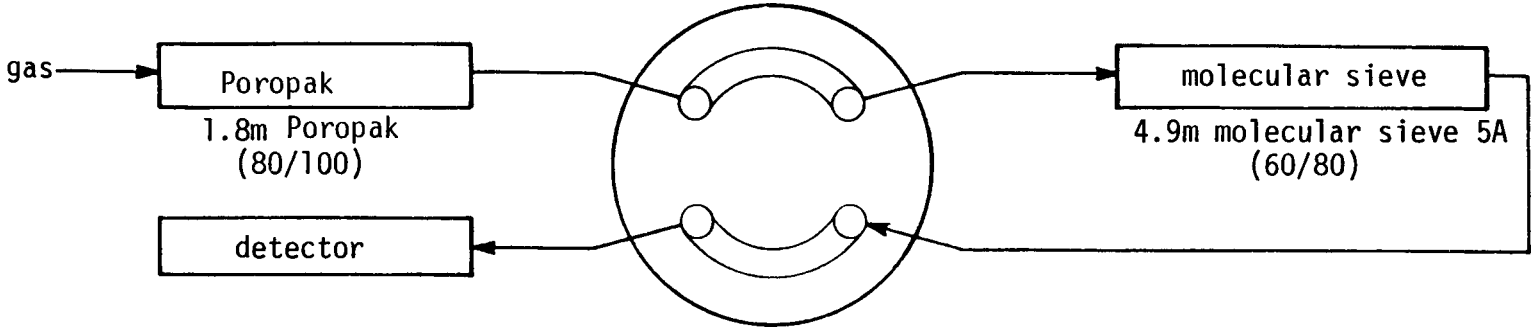

Normal condition: Poropak and molecular sieve in series

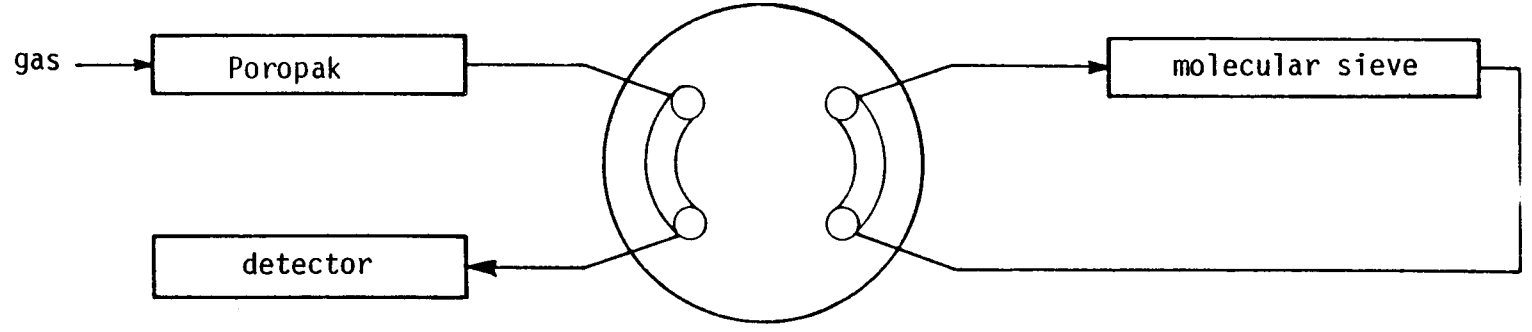

Activated condition: Poropak and molecular sieve in parallel

Figure 39. Hewlett Packard model 5830 gas chromatograph configuration.

The Tracor MT-150 used two channels, both with ultrasonic detectors. One channel used a helium carrier gas and was well-suited for hydrogen analysis. The other channel used an oxygen carrier gas and was well suited for argon analysis. A schematic diagram of the Tracor chromatograph is found in Figure 40. The instrument was versatile and performed analysis of all combustion gases, but the Hewlett Packard chromatograph was automated and facilitated more rapid gas analysis. Hence, the Tracor unit was used mainly for analysis of argon and hydrogen.

Gas collected was also subjected to analysis of nitric oxide (NO) with a Thermo Election Model 10 AR with a chemi-luminescent analyzer (19). In the instrument detector, ozone reacts with NO to form NO_2 in an excited state which emits energy. The intensity of the energy emitted is monitored by a photomultiplier tube located behind the appropriate optical filters to provide a signal that is proportional to the amount of NO present. The NO analyzer was calibrated daily prior to experimental runs using commercial NO in nitrogen standards (Scott Specialty Gases, Tustin, California), and the standard was analyzed repeatedly during the experiment. Earlier work with the instrument confirmed the linearity of the response over a wide range (4). Thus, usually only one gas standard was needed for daily calibration.

Other pollutant gases of interest were H_2S, HCN, and SO_2. It was advantageous to use Drager tubes for the analysis of hydrogen cyanide and hydrogen sulfide. Drager tubes are small inductor tubes containing a chemical compound which has a specific reaction with the pollutant to be measured. As the specified gas sample volume is passed through the tube, a length of the compound in the tube is discolored proportional to the pollutant gas concentration in the sample.

b. Solids Analysis

A Perkin Elmer Model 240 Elemental Analyzer was used for the ultimate analysis of char and coal. It was previously demonstrated that the model 240 could be used for analysis of carbon, hydrogen, nitrogen, and coal ash (4, 20). These results were shown to be comparable to those produced by ASTM procedures (21).

Several techniques for analysis of sulfur in coal were investigated. The technique selected involves combustion of a char or coal sample in an induction coil. The resulting sulfur dioxide is then dissolved and titrated with a potassium periodate solution to a starch end point. This method is known as the Leco Method for Sulfur Analysis. Arrangements were made with the University of Utah to use a Leco instrument to make sulfur analyses of coal and char samples.

c. Quench Water Analysis

Methods were developed to analyze the quench water coming from probes in the gasifier. Such analysis was required to determine concentrations of water-soluble pollutant gases such as H_2S, HCN, and NH_3.

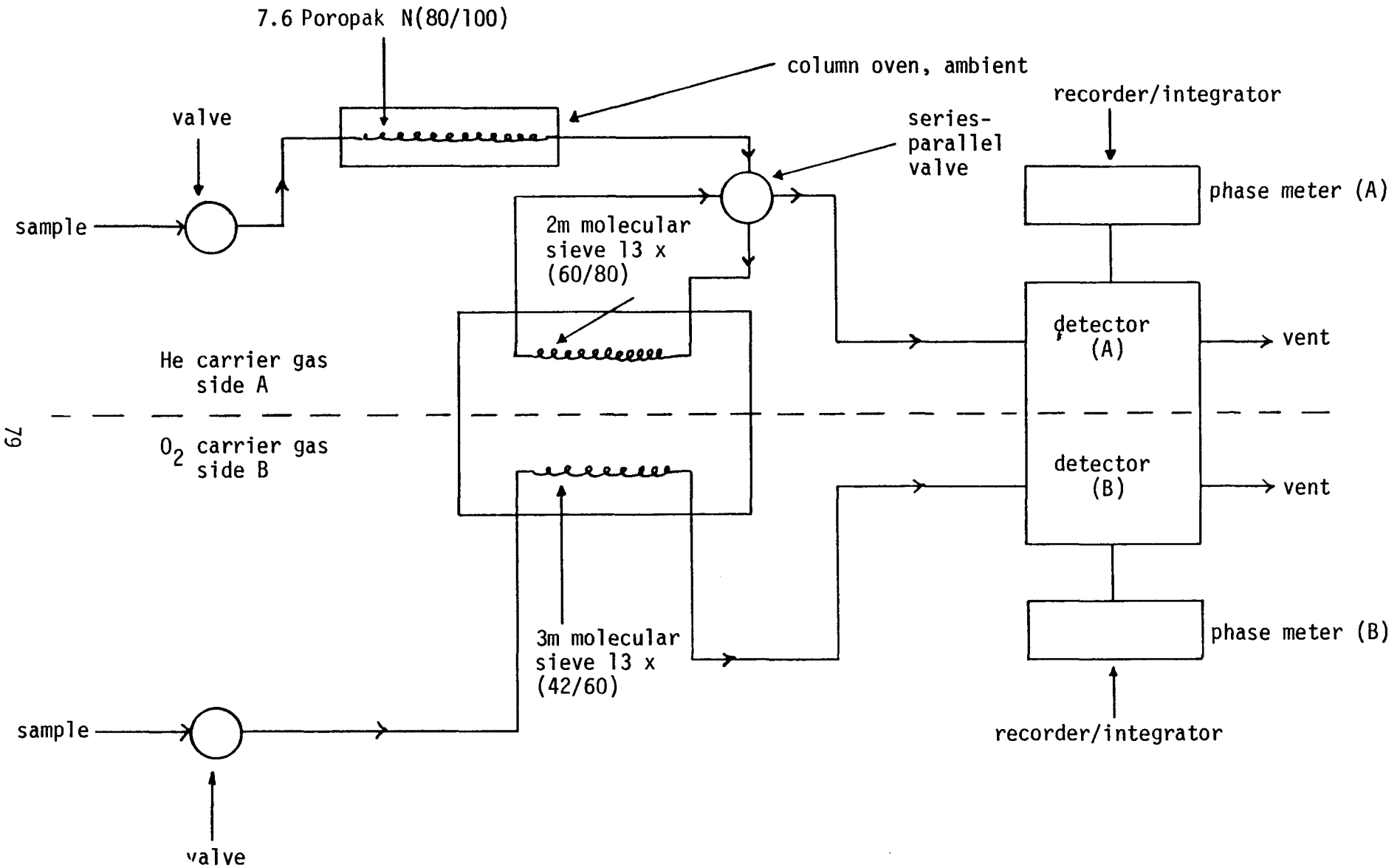

Figure 40. Tracor MT-150 gas chromatograph configuration.

An analysis technique was desired which was quick, thus lessening demands on sample preservation procedures. Simplicity was also required because the chemical analyses would be performed by several individuals with a limited background in analytical chemistry. Finally, it was desired, of course, that the results be reasonably accurate. Consequently, analytical methods involving ion specific electrodes were chosen for analysis of ammonium, sulfide, and cyanide in solution. In order to evaluate the utility of specific ion electrode analysis in probe quench water, several important tests were designed. Price (18) presents a detailed discussion of these tests and their results. A summary of the procedures and key results follows.

Cyanide Analysis. It was first desired to determine how the electrodes would work in solutions in which NH_4^+, CN^-, and $S^=$ were all present. By qualitatively observing performance of the cyanide electrode in solutions of NH_4^+, CN^-, and $S^=$, much useful information was gained. First, it was observed that sulfide at any concentration level strongly interfered with the cyanide electrode. When the cyanide electrode was immersed in a solution containing CN^-, silver ions on the exposed surface of the electrode membrane dissolved causing silver ions within the membrane to move to the surface. This set up a voltage difference proportional to the cyanide level in solution. However, silver ions formed an insoluble sulfide salt if sulfide was present in the solution. Thus, sulfide in solution took the silver out of solution and reacted with silver ions on the membrane surface. Removal of the sulfide from solution before performing a cyanide analysis was thus essential. Luthy (22) recommended the use of either $Pb(NO_3)_2$ or $Cd(NO_3)_2$ to remove sulfide from coal gasification wastewaters. Both $Cd(NO_3)_2$ and $Pb(NO_3)_2$ were chosen for use during tests.

The following precedure was developed for CN^- analysis using specific ion electrodes:

1. A 50 aliquot of the solution was taken.

2. Two ml of .07N $Cd(NO_3)_2$ or $Pb(NO_3)_2$ was added to the aliquot to precipitate any sulfide.

3. One ml of an NaOH solution was added to the aliquot to preserve or fix a constant ionic strength background.

4. The solution was then filtered and diluted to 100 ml with water.

5. The cyanide electrode was then immersed in the solution and a millivolt reading was recorded. The electrode was calibrated by plotting millivolt readings of known standards versus the log of the concentration of the standards which resulted in straight line relationships. Calibrations were performed in detail once per week. Usually only one CN^- standard was needed for daily calibration.

The method was tested by the following experiment. Solutions of 10 mg/l in CN^- and 7.3 mg/l in $S^=$ were prepared, tightly capped, left for one hour, and analyzed according to the above procedure. In three cases, $Zn(C_2H_4O)_2$ was also used as a precipitant. The results are summarized in Table 12. The amount of CN^- found was slightly but not significantly different from the initial amount of CN^- when $Cd(NO_3)_2$ or $Pb(NO_3)_2$ were used to precipitate the sulfide ion. Use of $Zn(C_2H_4O)_2$ did not prove satisfactory because cyanide concentration was significantly reduced. However, a satisfactory method had been found for the removal of sulfide interference.

Ammonia Analysis. Neither sulfide nor cyanide appeared to interfere with ammonium ion determinations. The ammonia electrode used a membrane which was permeable only to gases. The quench water solution was first made basic to convert NH_4^+ to NH_3. NH_3 crossed the membrane where it reacted with OH^- in the electrode filling solution, causing a potential difference relative to a reference electrode. The potential difference was directly proportional to NH_3 concentration. Because the electrode was susceptible to changes every few hours, a standard addition technique based on the Nernst equation rather than a calibration curve was used.

The following analysis procedure has been developed based on this method:

1. A 100 ml aliquot of the sample was obtained.
2. The pH of the sample was adjusted to 13 by adding 10 N NaOH.
3. The potential of the sample was measured with the electrode.
4. 10 ml of a 100 mg/l NH_4^+ solution was added to the sample.
5. The potential was remeasured with the electrode and $(NH_3)_i$ concentration was calculated.

If the sample could not be analyzed immediately, it was preserved by acidifying it with hydrochloric acid. In order to demonstrate the method, three solutions 10 mg/l in NH_4^+ and 7.3 mg/l in $S^=$ were prepared, tightly capped, left for one hour, and analyzed. The results are summarized in Table 13. Amounts of NH_3 found were approximately the same as initial amounts of NH_3.

Sulfide Analysis. It was experimentally observed that the electrode specific to sulfide operated without interference from either NH_4^+ or CN^-. The sulfide electrode had a solid silver sulfide membrane. When the electrode was immersed, silver ions migrated within the membrane, setting up a potential difference which was proportional to the number of sulfide ions in solution.

TABLE 12

EFFECT OF SULFIDE REMOVAL WITH CADMIUM NITRATE, LEAD NITRATE AND ZINC ACETATE

Sample	Concentration, mg/ℓ			
	$[CN^-]^a_{original}$	$[CN^-]^b_{ppt\ with\ Cd(NO_3)_2}$	$[CN^-]^c_{ppt\ with\ Zn(C_2H_4O)_2}$	$[CN^-]^d_{ppt\ with\ Pb(NO_3)_2}$
1	10.0	10.7	7.0	10.0
2	10.0	10.4	6.8	10.1
3	10.0	9.9	6.6	10.6
4	10.0	10.1		9.5
5	10.0	9.9		9.4
6	10.0	10.0		10.3

[a] Initial concentration of CN^- in solution. Attempts to measure CN^- decay without removal proved futile because of rapid electrode poisoning.

[b] CN^- measured with ion specific electrode after sulfide precipitation with $Cd(NO_3)_2$.

[c] CN^- measured with ion specific electrode after sulfide precipitation with $Zn(C_2H_4O)_2$

[d] CN^- measured with ion specific electrode after sulfide precipitation with $Pb(NO_3)_2$.

TABLE 13

EFFECT OF THE PRESENCE OF SULFIDE ON AMMONIUM
(Initial $S^{=}$ was 7.3 mg/l)

Sample	(NH_4^+) Original[a] mg/l	(NH_4^+) after 1 hour[b] mg/l
1	10.0	10.5
2	10.0	10.4
3	10.0	8.9
4	10.0	10.2
5	10.0	10.5

[a] Initial concentration of NH_4^+ in solution.

[b] Concentration of NH_4^+ measured after one hour using the prescribed technique.

The following is the developed procedure for sulfide analysis.

1. A 50 ml aliquot of the sample was selected.

2. The aliquot was diluted to 100 ml with special buffer solution to a pH of 13 with NaOH and ascorbic acid. Disodium EDTA was also added to the buffer to aid in sample preservation.

3. The sample was then measured according to a calibration curve as was described for cyanide analysis.

d. Quench Water Sample Decay Effects

Once the sample container was taken from the gasifier, the sample was sometimes allowed to sit for as long as an hour before analysis. The sample containers were airtight, and they were not exposed to the atmosphere. It was important, however, to understand the various aspects of sample decay over the hour time period. Luthy and co-workers (22) have reported that sulfide and cyanide concentrations decrease rapidly over time in unpreserved coal gasification wastewaters. They observed that cyanide concentrations decreased by as much as 50% in one hour. The decay in sulfide and cyanide concentrations was believed to be due to reactions in which oxygen plays an important role (23). It has also been reported that polysulfide ($S_xS^=$) is reactive with CN^- while $S^=$ alone is not (24). In addition, coal char has a pronounced effect on these reactions (25). So far, the presence of polysulfide has not been detected in fresh, raw HYGAS wastewaters (23). Hence, it appears that sulfide existing in a quench water solution must first be oxidized to polysulfide by O_2 (or another entrained oxidizing agent) for sample decay to occur. It was therefore determined to investigate the effects of oxygen, char, and time on samples from the gasifier.

A series of experiments were undertaken to evaluate the effects that oxygen and char would have on the ion concentration measurements. Price (18) reports the results of these experiments in detail. A brief summary of the results is contained in Table 14. This table reports the average decrease in ion concentration (CN^-, NH_4^+, and $S^=$) observed after one-hour for five separate test conditions. The effect of sample filtration is also shown for the NH_4^+ and $S^=$ ions. The first set of data shown is for the adopted analysis procedures described above. The actual sample decay plots for the adopted analysis procedures are shown in Figure 41 for CN^-, $S^=$, and NH_4^+. It can be seen that the procedures adopted gave quite acceptable results. The next four tests shown in Table 14 evaluate various combinations of char and air. Air, either bubbled through while analyzing or dissolved in the sample prior to analysis, caused significant losses in ion concentration in one hour. Comparison of the char-bubbled air data with no char-bubbled air data also showed that char in the presence of air (oxygen) had a significant effect on the sample decay. Without air, char seemed to have little effect, however. These results generally support the findings of Luthy (22, 23, 25) and Naktes (24).

Table 14 also reports on tests which were made to evaluate the effect of filtration prior to analysis. With CN^-, it was necessary

TABLE 14

SUMMARY OF QUENCH WATER SAMPLE DECAY EFFECTS
WITH SELECTIVE ION ELECTRODES

Procedure	Decrease in Ion Concentration after 1 hour, %		
	CN^{-}[a]	NH_4^+	$S^=$
char - no bubbled air[b]	1.5	0.1	5.6
char - bubbled air	36.1	20.9	24.9
char - dissolved air	4.6	19.1	14.2
no char - bubbled air	23.8	16.2	20.3
no char - dissolved air	9.1	-1.7	5.9
filtration[c]	---	12.8	43.6

[a] In all cases the precipated sulfide is filtered prior to analysis.

[b] Adopted analysis procedure.

[c] Values immediately after filtration.

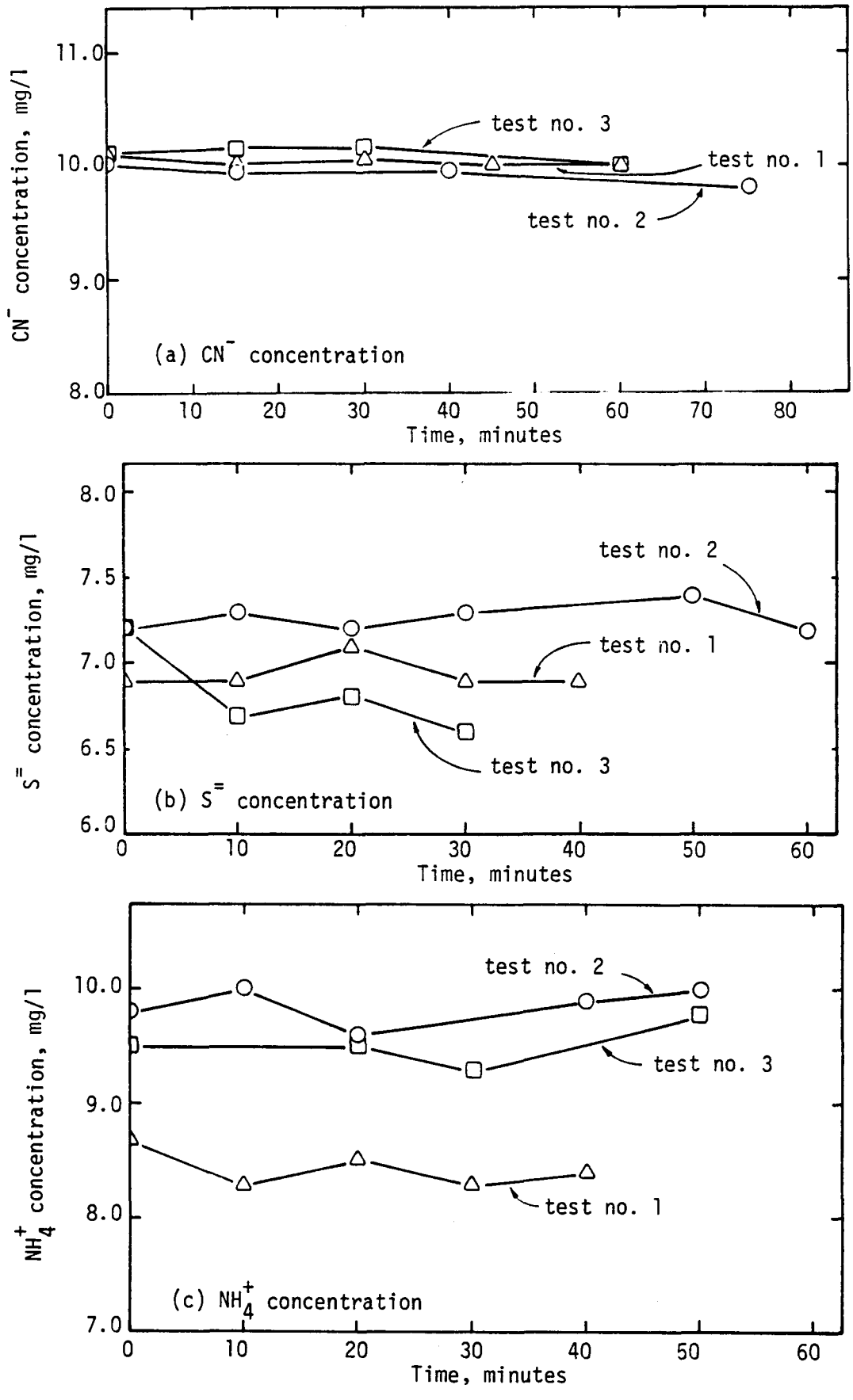

Figure 41. Ion concentration decay for adopted ion specific electrode procedure.

to filter the precipitated sulfide and consequently the char prior to analysis. However, the NH_4^+ and $S^=$ electrodes were found to function in the presence of char. Tests before and after filtration showed considerable NH_4^+ and $S^=$ ion concentration loss as shown in Table 14. Consequently, filtration was not done when analyzing for these two ions.

Three experiments were performed with a standardized gas which contained 873 ppm of NH_3 gas. This standardized gas was introduced into a water quenched probe - sample collection system. The purpose of these experiments was to verify that the sampling and analysis procedures were reliable and yielded accurate results. It was found from these tests that all of the NH_3 was in the quench water with no NH_3 detectable in the gas phase. The NH_3 analysis for the three tests gave 795, 830, and 799 ppm. On average, the analysis was within 64 ppm. At the extreme, the analysis was in error by -8.9%. Similar tests were designed for standard mixtures of hydrogen sulfide and hydrogen cyanide but were not conducted as a part of this study.

In summary, it was found that the developed analysis procedures described above for CN^- (page 80), NH_4^+ (page 81) and $S^=$ (page 84) yielded very satisfactory results so long as care was excerised. This required that the samples be analyzed as soon as possible after collection, and, required careful collection and handling to preclude any contamination by air or other sources of oxygen. Since char was found to exhibit little effect as long as there was no oxygen present, it was unnecessary to filter the samples prior to NH_4^+ or $S^=$ analysis. In fact, filtration introduced appreciable error in the analysis of NH_4^+ and $S^=$. It was necessary, of course, to filter the sulfide prior to CN^- analysis in every case. These developed procedures were used to obtain pollutant concentration data in the coal gasification tests which are described in a following section.

F. DATA REDUCTION

The basic data derived from the gas and particulate analyses were subjected to one of four different methods of data reduction in order to provide meaningful interpretation of the test results. The four reduction techniques involved 1) the individual gas species of the combustion process, including pollutants, 2) particle composition, reaction or burnout, 3) gas mixing and 4) particle dispersion. In conjunction with the various ways of reducing the data, methods for presentation of the results were also developed and are discussed.

1. Gas Mixing

The local extent of gas mixing occurring between the primary and secondary gas streams was determined by use of an argon trace gas injected in the primary stream and a helium trace gas injected into the secondary stream. Mass balances on a sample control volume, for the argon and helium components, permitted the following gas phase mixing parameter to be deduced:

$$\phi_g = m_p/(m_p + m_s) = [W_{Ax}W_{Hs}]/[W_{Ax}W_{Hs} + W_{Hx}W_{Ap}] \quad (1)$$

This mixing parameter includes the effect of additional gas being added to the gas volume by the combustion of coal. Equation (1) can be rewritten by changing the weight fractions to mole fractions to give:

$$\phi_g = [X_{Ax}X_{Hs}M_p]/[X_{Ax}X_{Hs}M_p + X_{Hx}X_{Ap}M_s] \quad (2)$$

The gas data collected in the chromatographic analysis were used directly in Equation (2) to determine the gas mixing parameter (ϕ_g). The mixing parameter ranged from zero in the pure secondary stream to unity in the pure primary stream.

2. Gas Species

In addition to helium and argon concentration determinations, chromatographic analysis of the sample gas yielded concentration data on N_2, H_2, O_2, CH_4, CO, CO_2, and C_2 hydrocarbons. Data relating to these gases were used directly to give molar percentage profiles in the combustor on a water-free basis.

3. Particle Reaction

Particle reaction or burnout was treated using a mass balance on the sample control volume to give:

% Burnout (ash included basis)

$$= (100\%)[1.0 - (\text{ash in coal})/(\text{ash in char sample})] \quad (3)$$

% Burnout (ash free basis)

$$= (100\%)[1.0 - (\text{ash in coal})/(\text{ash in char sample})]/[1.0 - (\text{ash in coal})] \quad (4)$$

This method utilized ash as the inorganic particle tracer. The use of iron, aluminum or titanium in the ash as the particle tracer showed promise for improved accuracy but were not used in this study.

4. Particle Dispersion

The local extent of particle dispersion can be determined by considering a mass balance on the sample control volume. This resulted in a coal mixing parameter similar to that obtained for the gas mixing:

$$\phi_k = M_{kp}/(M_{kp} + M_{gp} + M_{gs} + M_{gk}) \quad (5)$$

$$\phi_k = W_{\alpha x}/W_{\alpha k} \quad (6)$$

To solve this equation and separate m_k into the respective particulate and gas components required the mass of gas (or volume, temperature, pressure and molecular weight) and the mass of particles obtained in the sample collection to be accurately determined. Although total particle and gas samples were taken, the accuracy of the particle mass and gas volume was not adequate to use this method for determining the particle mixing rate. The particle mass flux (deduced from the mass of the collected particle sample, the area of the sample probe and the sample time) ratioed to the particle mass flux in the primary jet has therefore been used as a measure of the relative dispersion rate of the particulate phase in the gas phase. This mass flux mixing parameter incorporates the effects of both particle mixing and coal reaction. Basing this later computation on ash (tracer) mass flux eliminates the effect of coal particle reaction.

5. Char Analysis

The data reduction techniques for the major elements in coal from ultimate analysis use conventional methods. The percent of each element is calculated for the char or coal analyzed and the analysis is normalized to 100% by calculating oxygen by difference. These data are usually referenced to a dry, ash-free basis by dividing the weight fraction of each element by $1.0 - W_{ash}$, where W_{ash} is the weight fraction of the ash. From these data, the fraction of element lost during the reactions can be calculated. This assumes that ash is nonvolatile and nonsoluble, which is not precisely the case (3).

6. Pollutants

HCN, NH_3, and H_2S. Given the volume of gas scrubbed and the amount of water used, the concentration of pollutant from the water can be calculated by the following formula:

$$W_{pg}(ppm) = Q_{pw(ppm)} \times (\rho_\omega V_\omega)/(\rho_g V_g) \quad (7)$$

Limited accuracy of the gas volume caused some uncertainty in these results. The analysis of the pollutants in the gas phase with the Drager tubes is very straightforward. The tubes are calibrated to read pollutant concentration directly at standard temperature and pressure conditions. Corrections were applied to the measured values for the non-standard

pressure and temperature conditions at this laboratory. Water and gas pollutant values were summed to obtain the total pollutant concentrations.

NO_x. A Thermo Electron Model 10 AR NO_x chemi-luminescent analyzer was used to collect the NO_x data reported in this document. The instrument was calibrated and read pollutant concentration in ppm on a dry basis directly without further calculation.

7. Data Presentation

Radial profile plots were made for the gas mixing parameter, each gas species of interest, the extent of coal burnout, and the local particle mass flux in the gasifier at each axial data position. The radial profiles of each property were then interpolated axially to provide a "combustor map". The interfaces of the various regions represent property contours, which provide a map of that property in the gasifier.

Axial decay plots were used to help evaluate the mixing characteristics and reaction rates of the gasification process. For each test condition, centerline data from the various axial locations were plotted in logarithmic coordinates. Previous studies (5-12) have shown that if the value of the centerline parameter and the axial position are both normalized properly and plotted on log-log coordinates, a straight line plot results over the critical area of interest. The linear nature of such plots proves most useful in determining the core lengths which Smoot and Purcell (26) have shown to be inversely proportional to the turbulent mixing coefficient in nonreacting free jets. A core length (z^*/r_1) is defined as the axial distance from the primary stream exit plane to that point were the centerline parameter value begins to decay from its original primary stream value.

The parameters plotted are the gas mixing parameter (ϕ_g), the particle dispersion parameter (δ_k), and the fraction of unreacted coal ($1 - \beta_k$). Normalization to the primary stream value is inherent in the development of these three parameters. The axial distance (z) is normalized by the radius of the primary stream (r_1).

G. GASIFICATION TESTS

There were four separate series of coal gasification experiments performed in this study. They included system evaluation tests (Test Series 1), coal/steam/oxygen mixture ratio and flame stability tests (Test Series 2), reactor mapping tests (Test Series 3), and elevated pressure tests (Test Series 4). A Utah bituminous coal was used in all of the reacting tests. The properties of this Utah bituminous coal are summarized and the results of each test series reported in the following subsections.

1. Coal Properties

The coal used in this study was a Utah high volatile bituminous coal which was provided by Utah Power and Light Co. Extensive evaluation of this coal was reported previously (2). The reader is referred to

TABLE 15

SUMMARY OF TYPICAL PROPERTIES OF UTAH BITUMINOUS TEST COAL

Proximate Analysis (Weight Percent)		Ultimate Analysis (Weight Percent	
Moisture	2.36	Hydrogen	5.66
Volatiles	45.48	Carbon	70.20
Fixed Carbon	43.30	Nitrogen	1.40
Ash	8.86	Sulfur	0.50
		Oxygen*	13.38
		Ash	8.86

Standard Power Plant Grind, 70% - 200 mesh

Average Mass Mean Diameter, 47.3 μm

Surface Area, 161.8 m^2/kg

*Determined by difference.

that earlier report (2) for details. Nevertheless, a summary of typical coal properties is included in Table 15.

Because the properties of any coal tend to be somewhat variable, the practice was adopted of sampling each lot of coal as it was loaded into the coal feeder. Analysis of these samples was then used for that particular set of tests. This provided a more accurate basis for data evaluation.

2. Test Series 1 - System Evaluation Tests

a. Test Program

Several tests were made during this study to evaluate the operation of the experimental apparatus. These included tests to validate igniter operation and stable methane/oxygen flames, coal feeder calibration and operational tests, tests to stabilize coal/ oxygen flames, tests to validate steam boiler flow and control, tests to develop and validate sample probe and sample collection system operation, tests to validate the flow stability of the gas delivery system, and tests for isokinetic sampling. These tests are summarized by objective in Table 16. Some tests had more than one objective. The majority of the tests served to diagnose problems with the sample train, both under cold flow and flame conditions. As indicated above, the sampling system and the water quenched probes were made functional. Ignition was accomplished with hydrogen-air mixture and an electric spark, and preheating used natural gas and oxygen. All of the other components of the facility were checked out and made to function properly.

The gasification facility was initially designed to operate at a coal feed rate of 136 kg/hr for the tests at elevated pressure, and 68 kg/hr for the atmospheric tests. All of the various components of the gasifier were designed around this basis. However, once reacting flow testing was begun at atmospheric pressure, it became apparent that problems with back pressure excursions occurred when the design coal feed rate was attempted. An attempt to pinpoint the difficulty lead to the conclusion that the coal flow rate was too high for stable operation of the reactor at atmospheric pressure. Consequently, as a part of the system evaluation tests mentioned above, experiments at progressively lower coal feed rates were included in the test program in order to empirically determine the highest coal feed rate which would still permit stable reactor operation at atmospheric pressure.

b. Test Results

The system evaluation tests performed in Test Series 1 revealed many operational problems that had to be solved before consistent operation and reproduceable test data obtained. Skinner (17) and Price (18) discuss the problems associated with the reactor and probe sample system development in detail. The operational problems were solved and the gasifier and probe sample system were used to collect final test data which is reported in a subsequent section. Two reactor problems were of some consequence and are summarized below.

TABLE 16

SUMMARY OF GASIFIER SYSTEM EVALUATION TESTS

Objective	No. of Tests Run
Test igniter, stabilizer CH_4/O_2 flame	2
Test coal feeder, stabilize coal/O_2 flame	5
Test steam boiler/flow control	3
Test probe/collection system - cold flow	19
Test probe/collection system - hot flow	38
Test gas delivery system - flow stability	7
Test for isokinetic sampling	5
Test for coal throughput	9
TOTAL	88

Coal Throughput. As mentioned above, early testing at the atmospheric design coal feed rate (2) caused unstable reactor operation. This was evidenced by a progressively increasing reactor operating pressure. The operational behavior of the reactor lead to the conclusion that the design coal feed rate for atmospheric operation was too high. Consequently, a series of gasification experiments were performed at progressively lower coal feed rates (about 55 kg/hr, 39 kg/hr, and 24.5 kg/hr) until stable reactor operation was achieved. Thus, the highest possible coal flow rate was empirically determined which allowed for atmospheric pressure testing, without the difficulty of steadily increasing reactor pressure.

A comparison of the BYU gasifier throughput capacity with other entrained coal gasification systems was made in order to determine if the empirical throughput rates at atmospheric pressure were out of line and to investigate potential feeding problems at elevated pressures. The work of the U. S. Bureau of Mines G-3 gasifier program (27, 28) as summarized by Bissett (16) has shown that the coal throughput of an entrained gasifier can be increased in direct proportion to operating pressure. Consequently, a loading parameter, defined as the coal feed rate normalized to the reactor volume and operating pressure ($lbm/hr\text{-}ft^3\text{-}atm$)[2] was selected as the basis of comparison. Typical throughput data for several entrained gasifiers obtained from Bissett (16) are summarized in Table 17 and Figure 42. The table and figure also include the BYU gasifier design conditions (2) and the atmospheric test conditions where stable operation was achieved. This comparison showed that smaller reactors generally operated at higher throughput levels, and that as reactor size increases, the throughput dropped. While these data were not exhaustive and may not represent the maximum throughput for a given reaction[3], they did represent typical operating conditions for a wide range of reactor sizes and feed rates.

The initial design throughput of the BYU gasifier (120 $lbm/hr\text{-}ft^3\text{-}atm$) as shown in Figure 42, was three to four times the throughput that was obtained in the similar sized USBM G1 and G3 reactors. The initial BYU gasification tests showed that this throughput was too high for stable operation of the reactor. Reduction of the coal throughput to 68 $lbm/hr\text{-}ft^3\text{-}atm$ (39 kg/hr) improved the situation but still resulted in slow increases in reactor pressure during the run. It was not until the coal feed was dropped to 54 lbm/hr (24.5 kg/hr) (throughput of 43.2 $lbm/hr\text{-}ft^3\text{-}atm$) that stable operation was obtained. This value was consistent with the upper limits of the operating curve obtained through the family of throughput data for the various gasifiers shown in Figure 42. Operating experience suggested that the throughput of the gasifier was being limited by the restricted reactor discharge and the inability of the reactor to handle the higher gas flows associated with higher throughput without some increase in operating pressure.

---

[2]The data for the various gasifiers were reported in English units, which were used in this comparison.

[3]Bissett (16) pointed out that the throughput was frequently limited by coal feeder or gas quench/clean up constraints.

TABLE 17

THROUGHPUT OF VARIOUS ENTRAINED COAL GASIFIERS (16)

Reactor	Pressure (atm)	Volume (ft^3)	Coal Feed (lb_m/hr)	Throughput ($lb_m/hr\text{-}ft^3\text{-}atm$)
USBM-G1	1	1.34	52.2-54.3	39.0-40.5
USBM-G2	1	86.0	254-420	3.0-4.9
USBM-G4(5)	1	45.7	402-776	8.8-17.0
USBM-G3	21.3	1.45	1035	33.5
USBM-G3	31.5	1.45	1097-1336	24.0-29.3
KT(La,MO)	1	380	1980-2220	5.2-5.8
Vertical(La,MO)	1	250*	1730-1920	6.9-7.7
B&W-DuPont(Semi)	1	349*	2620	7.5
B&W-DuPont(Comm)	1	1133*	30,000	26.5
Texaco(Early)	14.5	2.0	600	20.7
Vortex	1	9.43	100	10.6
IGT-Cyclone	7	11.65	419-680	5.1-8.3
Ruhrgas-Vortex	1	414	1336-1545	3.2-3.7
KT-2	1	1000	33,330	33.3
KT-4	1	2100	70,833	33.7
Texaco(Recent)	28.9	120*	1060-1480	0.31-0.43
BiGas*	51.9	86.3	7000	1.6
B&W(Proposed)	4.3	3656*	40,000	2.5
Coates-ERI(Early)	5-20	0.139		up to 215
Coates-ERI(Later)	10.2	0.045	40.6-45.0	88.4-98.0
Bell Aerospace	12.2-16.8	0.1818	480-1060	217-347
BYU-Design (2)	1	1.25	150	120
BYU-Design (2)	10	1.25	300	24
BYU-Design (2)	20	1.25	300	12
BYU-Data	1	1.25	54-85	43.2-68

*Estimated

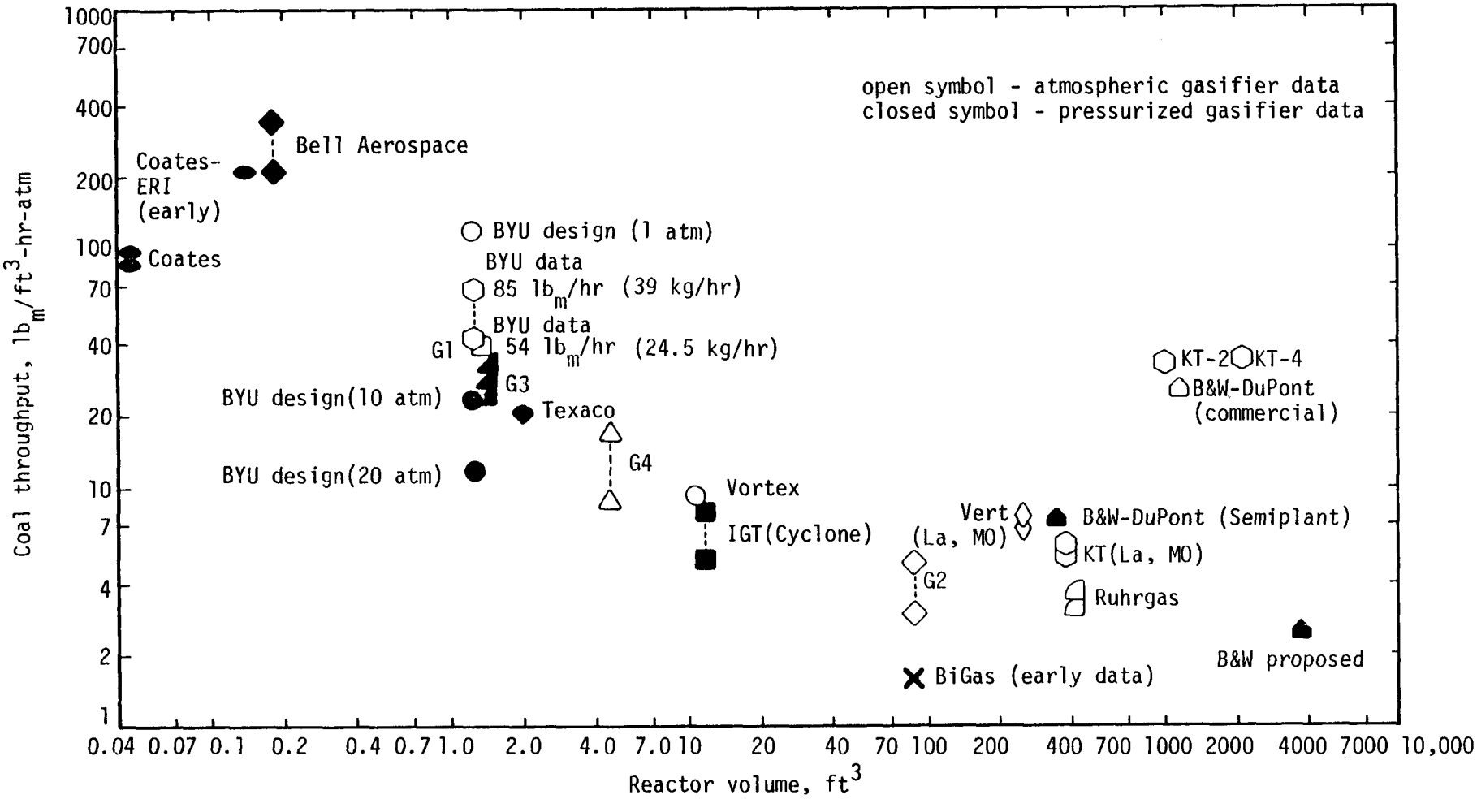

Figure 42. Comparison of the throughput of various entrained coal gasifiers.

The design coal throughputs for operation of the BYU gasifier at 10 and 20 atmospheres are also included in Table 17 and shown in Figure 42. The design throughput for 10 atmosphere operation is very close to the USBM-G3 experience and the 20 atmosphere operation is much less. This suggests that the design throughput for pressurized operation probably would be obtained without difficulty and that higher throughput levels at higher pressures may be possible. However, no elevated pressure gasification experiments were performed in this study.

Coal Feeder Flash Back. The initial design of the coal feeder used an inert gas (argon) to blanket the coal feeder. Oxygen was fed as the entraining medium to the coal feeder discharge and a two-phase stream of coal/oxygen/inert gas was blown through the primary duct in to the reactor. On two separate occasions, a flame propagated back up the primary tube and into the coal feeder. This caused a fire and over pressure in the feeder, which ruptured a safety burst disk. No damage, other than the ruptured burst disk, resulted. It was evident that the introduction of the oxygen at the coal feeder pick off was allowing some oxygen to get back into the feeder creating a potentially hazardous situation. Subsequent to these tests, the coal feed system was modified as described previously. The inert gas was used to entrain the coal at the coal feed pickoff point and the oxygen was not introduced into the primary jet until just before the primary discharged into the reactor. These modifications solved the problem of flame in the coal feeder.

Another constraint became apparent with experience with this reactor. This dealt with the flow rate of oxygen in the primary stream which was required to avoid flame propagation back up the primary feed line. Even though the oxygen was introduced into the primary near the exit, a flame could still propagate up the primary duct to the point of oxygen injection if the velocity in the primary dropped below the critical flame propagation velocity for the particular coal type and coal/oxygen mixture ratio. No difficulties occurred with oxygen flows of greater than 16 kg oxygen/hr and with a flow of Argon of 4.7 kg/hr. When an attempt was made to lower the primary oxygen to 10.7 kg/hr flashback occurred and the stainless steel primary tube was completely melted down in minutes. This placed an oxygen flow rate limitation on the test conditions. As an added precaution, a thermocouple well was machined into the new primary centering ring which was located closest to the injector point, and the temperature at this location was closely monitored in subsequent tests to determine the presence of a flame in that region. Subsequent tests were to be terminated at the first indication of a flame in the primary but no further difficulties were encountered.

3. Test Series 2 - Mixture Ratio and Flame Stability Tests

a. Test Program

A set of equilibrium chemistry runs (29) were made for the Utah bituminous coal being used in order to identify the potential operating region of steam/coal and oxygen/coal mixture ratios for this laboratory gasifier. From these runs, the theoretical cold-gas efficiency was

computed. The peak cold gas efficiency for a given steam and coal feed rate occurred at the oxygen feed rate which just consumed all of the condensed carbon. It was thus possible to identify the locus of steam and oxygen values (kg/kg coal) which gave a peak cold gas efficiency. This locus is shown in Figure 43. This peak cold gas efficiency continually rose toward 100% as the steam and oxygen were varied toward lower reaction temperatures. Thus, the equilibrium temperature can be lowered by variation of the O_2/coal and steam/coal ratios to the point where kinetic limits become very important and reaction may not proceed. The "optimum" operating point from the standpoint of theoretical maximum cold gas efficiency would be at the lowest temperature where stable operation could be maintained on the locus of peak cold gas efficiencies.

Figure 43 also shows constant temperature lines crossing the line of maximum cold gas efficiency. These temperature lines are the adiabatic flame temperature for the particular combination of reactants assumed. No effect of heat loss from the reactor was considered. The data from the Bureau of Mines (6) have shown that heat loss effects generally result in an increased requirement for oxygen. A minimum stable temperature of 1600K would suggest that the "optimum" oxygen and steam quantities for this Utah coal might be about 0.7 lb/lb coal and 0.2 lb/lb coal respectively. However, a point other than "optimum" might be chosen in order to get the CO/H_2 ratio correct for a chemical plant application, to control pollutant emission levels, or to minimize total cost. It is also evident that inefficiencies and kinetic effects in the reaction process would alter these "theoretical" optimum operating conditions. With this information, an experimental approach to map the operating regions of the gasifier was developed. The sample probes were located near the bottom of the reactor. The approach was then to fix the coal feed rate (24.5 kg/hr) and vary the oxygen and steam feed rates in a systematic, parametric manner in order to fully evaluate the effect of these variables on the operation of the gasifier. The test plan was started by setting the oxygen feed to about 1.0 kg O_2/kg coal and then running a series of tests at progressively increasing amounts of steam. Once the conditions at the oxygen feed of 1.0 were characterized, and the upper stability limit of steam flow established, then a new set of tests with varying steam feed rates was conducted at an oxygen coal ratio of 0.83. This was followed by a third set of tests at an oxygen/coal ratio of 0.67[4]. Generally, the three test series were selected to produce operating conditions where many of the entrained coal gasifiers have been operated.

A summary of the design operating conditions for these atmospheric tests is contained in Table 18. Also included in this table for comparison are the initial atmospheric design operating conditions reported in reference 2. The design operating conditions (a through j) reflect the coal feed and primary oxygen flow rate limits determined from the system evaluation tests described above.

---

[4]An O_2/coal ratio of 0.67 was as low as could be used without lowering the primary velocity below the flashback limits or without redesigning and refabricating the primary jet hardware.

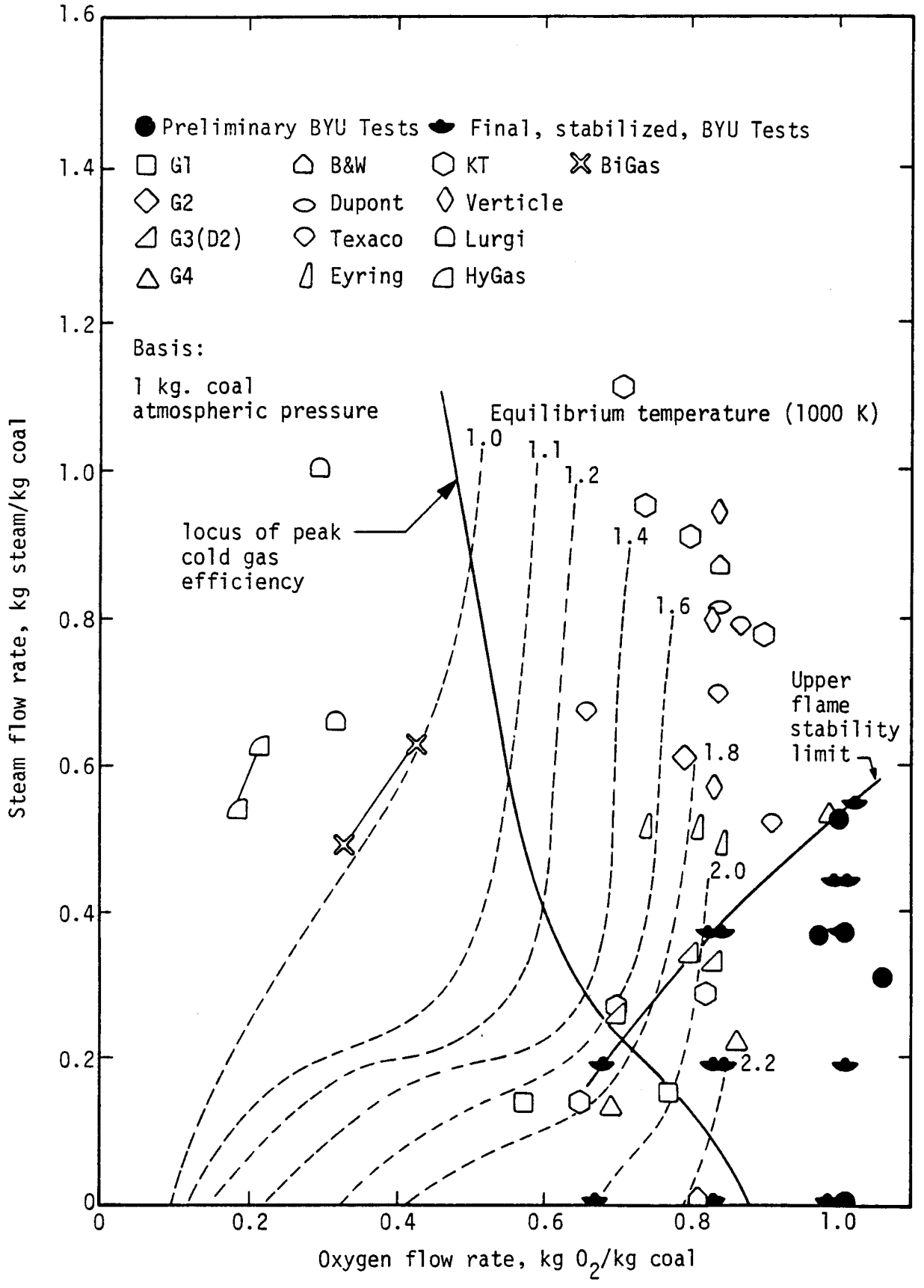

Figure 43. Summary of coal gasification operating conditions.

TABLE 18

TEST CONDITIONS FOR ATMOSPHERIC PRESSURE TESTS

Parameter	Design	a	b	c	d	e	f	g	h	i	j
O_2/Coal, kg/kg	0.56	1.00	1.00	1.00	1.00	1.00	0.83	0.83	0.83	0.67	0.67
H_2O/Coal, kg/kg	0.39	0.00	0.24	0.37	0.44	0.54	0.00	0.24	0.37	0.00	0.24
Primary:											
$\dot{M}$ coal, kg/hr	69.0			24.5							
$\dot{M}_{O_2}$, kg/hr	29.0			16.4							
$\dot{M}_{Ar}$, kg/hr	0.0			4.4							
M_1, kg/hr	97.0		do ←	45.3	→ do						
U_1, m/s	54.2			37.7							
T_1, K	355			355							
Solids, %	70			54							
Secondary:											
$\dot{M}_{O_2}$, kg/hr	9.1	8.1	8.1	8.1	8.1	8.1	3.9	3.9	3.9	0.0	0.0
$\dot{M}_{H_2O}$, kg/hr	26.3	0.0	5.9	9.1	10.8	13.2	0.0	5.9	9.1	0.0	5.9
M_s, kg/hr	35.4	8.1	14.0	17.2	18.1	21.3	3.9	9.8	13.0	0.0	5.9
U_s, m/s	69.4	9.7	22.3	29.2	32.7	37.9	4.7	17.3	24.1	0.0	12.6
T_s, K	589	589	589	589	589	589	589	589	589	589	589

b. Test Results

Twenty-one separate tests were completed to characterize the effects of oxygen/coal and steam/coal mixture ratios on reactor operation, and gasification products produced, including pollutants and coal burnout. The limits of flame stability were also determined, as described above, by progressively increasing the steam flow rate at each of the prescribed oxygen/coal mixture ratios until the flame in the reactor approached extinguishment as determined by visual observations through the optical viewport and from wall temperature measurements. Table 19 summarizes the tests performed at each of the mixture ratios considered. The points where tests were successfully conducted and the limit of flame stability for the coal tested are shown in Figure 43.

Six of the twenty-one tests were considered preliminary (eight test conditions), as problems with reactor stability, sampling and analysis were still being resolved at the time the runs were made. In particular, the gas chromatograph results for CO_2 and CO obtained with the Tracor MT-150 were somewhat unreliable. This was due in part to the fact that the peaks corresponding to these two species tail into each other, and the cutoff point between them was somewhat arbitrary. Fortunately this problem was eliminated with the acquisition of the HP 5830 Chromatograph. The results obtained for the six preliminary tests were run with the sample probes at 94 cm aft of the reactant injection point. In every test, the coal feed rate was 38.7 kg/hr, based on the coal feeder calibrations. The ratio of oxygen to coal feed was nominally set to 1.0 for each of the tests reported, although some slight deviations from this ratio were obtained. Runs at three different ratios of steam to coal feed were performed.

The results of the gas and solid analyses for these preliminary runs are reported in Table 20. Two points should be made about these data. First, part of the deviation in CO and CO_2 results was undoubtedly due to a peak tailing problem associated with the Tracor MT 150 Chromatograph. Second, the nitrogen fractions were, to a large extent, due to contamination of the samples by air. This problem was much less severe in the later tests, which were conducted after the sealing and other problems associated with the sampling system were resolved.

In addition to the runs just discussed, a total of 15 final data tests were run at a lower coal feed rate of 24.5 kg/hr. The data from these tests are summarized in Table 21. In these tests, two to three sampling probes were located 63.5 cm aft of the reactant injectors. Problems with data analysis were resolved prior to these tests, and these test results were considered reliable. The data from these tests, and that which was useable from the preliminary tests are analyzed in the following section.

c. Data Accuracy

Errors in the data include the variation in the coal, oxygen, steam, and argon feed streams; errors introduced because the sample probes are not exactly isokinetic; unsymmetrical flow in the reactor; the partly soluble and volatile nature of the ash particle tracer; probe

TABLE 19

SUMMARY OF ATMOSPHERIC PRESSURE OXYGEN/STEAM/COAL MIXTURE RATIO AND FLAME STABILITY TESTS

Mass Ratio		
O_2/Coal	Steam/Coal	No. Tests
1.0	0.0	5
	0.19	2
	0.37	5
	0.44	2
	0.54*	2
0.83	0.0	1
	0.19	2
	0.37*	2
0.67	0.0	1
	0.19*	1
	Total	23

*Steam/coal ratio at reaction stability limit.

TABLE 20

SUMMARY OF PRELIMINARY COAL/OXYGEN/STEAM MIXTURE RATIO AND FLAME STABILITY TESTS

Test No.	Nominal Test Condition	Actual O_2/Coal kg/kg	Actual Steam/Coal kg/kg	Probe No.	Gas Analysis[1], Mole Percent CO	CO_2	H_2	N_2	O_2	CH_4	Char Ultimate Analysis, Wt. % C	H	N	O+S[2]	Ash	Coal Burnout, %
70a	a	1.00	0.00	1	59.9	4.4	23.2	8.6	1.9	2.0	72.6	-	0.9	1.3	16.3	46.5
				3	59.0	6.7	23.4	8.3	1.7	0.8	68.1	-	0.9	0.3	18.2	53.2
76	a	1.06	0.00	1	47.6	21.8	25.1	3.8	0.8	0.9	No char sample obtained					-
79	a	1.06	0.00	3	56.9	12.3	23.4	4.4	2.0	1.0	69.8	0.2	0.9	4.6	24.5	71.4
85	a	1.03	0.00	3	63.0	7.6	24.5	3.0	1.0	0.9	71.5	0.2	1.2	4.7	22.4	67.9
70b	c	1.01	0.37	1	37.1	20.6	21.2	16.5	3.8	0.8	68.5	0.7	1.0	5.6	24.2	67.4
				3	50.7	4.3	29.8	11.8	2.6	0.8	67.4	0.4	1.0	4.4	26.8	71.6
71a	c	1.00	0.37	1	43.9	3.9	28.1	19.1	3.0	2.0	76.9	0.7	1.0	5.7	15.8	44.5
				3	39.1	8.5	23.6	23.6	4.0	1.3	72.2	0.3	1.0	3.2	23.3	65.7
74	c	1.02	0.37	1	32.6	28.0	14.9	16.5	5.5	2.4	67.2	4.1	1.2	12.6	14.9	46.4
				3	40.2	20.2	28.0	5.0	1.4	5.2	72.1	2.9	1.4	8.4	15.2	47.6
71b	e	1.00	0.53	1	46.3	1.6	31.7	16.9	1.8	1.7	70.0	0.3	1.0	5.0	23.7	66.5
				3	46.3	2.9	30.3	16.8	2.4	1.2	77.0	0.3	1.0	6.2	16.0	45.3

[1]Water-free basis
[2]By difference

TABLE 21

SUMMARY OF FINAL COAL/OXYGEN/STEAM MIXTURE RATIO AND FLAME STABILITY TESTS

Test No	Nominal Test Condition	Actual O_2/Coal kg/kg	Actual Steam/Coal kg/kg	Probe Loc., cm	Flow Rates, kg/hr: Primary Coal	Primary O_2	Primary Ar	Secondary O_2	Secondary Steam	Secondary Temp., °K	Normalized Water-free Gas Analysis, Mole Percent: CO	CO_2	H_2	N_2	O_2	CH_4	Ar
95	a	0.99	0.00	0.0	24.5	16.2	4.4	8.1	0.0	506	46.0	22.4	18.4	2.8	-	1.2	7.5
				3.2							43.4	14.9	16.6	15.7	2.1	0.9	6.5
105	b	1.01	0.25	0	24.5	16.4	4.4	8.4	6.0	383	38.3	32.3	23.6	0.9	1.2	3.3	0.4
				3.2							22.1	59.0	10.2	5.0	2.2	0.6	0.8
				5.0							20.8	59.6	15.7	1.6	1.5	0.2	0.6
106	b	1.01	0.24	0.0[3]	24.5	16.4	4.4	8.4	5.9	475	36.1	18.8	30.7	4.4	3.1	2.6	4.4
				3.2							31.1	41.6	14.4	2.2	2.4	0.6	7.6
				5.0							30.2	41.5	15.1	2.7	2.7	0.6	7.4
94	c	1.00	0.37	0.0	24.5	16.3	4.4	8.1	9.1	567	31.6	33.3	22.5	9.8	na	nd	na
				3.2							9.6	14.3	7.4	63.3	na	nd	na
104	c	1.01	0.39	0.0	24.5	16.6	4.4	8.1	9.5	467	38.7	37.1	19.6	1.5	na	0.8	2.3
				3.2							31.0	49.1	14.4	2.0	na	0.9	2.7
				5.0							31.8	46.8	15.5	1.5	na	1.7	2.7
96	d	0.99	0.47	0.0	24.5	16.1	4.4	8.1	11.4	561	34.4	25.2	21.8	7.1	2.9	1.9	6.9
				3.2							24.9	34.7	25.9	3.6	4.4	nd	6.4
107	d	1.01	0.47	0.0	24.5	16.4	4.4	8.4	11.5	517	36.5	25.8	24.2	2.7	0.6	3.0	7.1
				3.2							20.6	53.4	11.8	2.8	1.4	0.5	9.6
98	e	1.02	0.54	0.0	24.5	16.6	4.4	8.3	13.1	556	34.6	19.9	25.0	1.9	na	8.3	10.3
				3.2							25.1	44.4	17.3	3.1	na	0.5	9.6
				5.0							20.7	53.0	16.0	3.2	na	0.0	6.5
99	f	0.83	0.00	0.0	24.5	16.2	4.4	4.2	0.0	478	46.0	17.9	23.6	3.5	na	1.7	7.4
				3.2							46.7	19.4	22.1	2.4	na	1.3	8.0
				5.0							45.9	19.9	22.9	2.2	na	1.1	7.9
100	g	0.83	0.24	0.0	24.5	16.2	4.4	4.2	5.9	486	38.6	26.0	22.7	2.5	na	2.4	7.8
				3.2							37.7	29.4	21.9	2.2	na	1.3	8.5
103[5]		0.84	0.24	3.2	24.5	10.7	4.4	9.9	6.0	461	21.4	28.9	13.7	30.6	1.2	1.2	3.1
				5.0							22.1	32.0	16.3	24.8	3.4	1.4	na
101	h	0.84	0.39	0.0	24.5	16.3	4.4	4.3	9.4	517	33.7	26.8	20.0	4.1	4.6	2.4	8.3
				3.2							34.8	36.1	20.5	3.1	na	1.5	4.1
				5.0							33.4	36.7	21.6	3.5	na	1.3	3.5
102	h	0.83	0.38	0.0	24.5	16.6	4.4	3.6	9.3	nm	36.2	18.8	29.3	6.9	na	3.8	5.0
				3.2							31.4	36.8	20.2	2.6	na	0.9	8.1
				5.0							30.5	38.5	19.6	2.3	na	1.0	8.0
109	i	0.67	0.00	0.0	24.5	16.3	4.4	0.0	0.0	-	49.2	16.1	21.9	1.9	nd	2.4	8.6
				3.2							49.5	16.1	21.7	2.0	nd	2.1	8.7
				5.0							50.3	14.6	21.9	2.3	nd	2.2	8.7
108	j	0.67	0.24	3.2	24.5	16.7	4.4	0.0	5.9	444	34.1	32.4	16.4	3.3	0.8	1.8	11.2
				5.0							33.6	30.4	21.6	1.9	nd	1.8	10.6

Test No	Char Ultimate Analysis, Wt. %: C	H	N	S	O[1]	Ash	Coal/Element Burnout, Wt. %: Coal	C	H	N	S	O	Pollutants, ppm: H_2S	HCN	NH_3	NO
95	69.3	1.9	1.1	nd	8.6	19.1	67.0	65.0	87.3	70.7	100.0	48.4	389	1431	800	75[2]
	71.1	1.0	1.3	0.4	5.8	20.4	70.0	66.3	93.8	68.2	75.4	62.0	475	1133	788	
105	75.8	2.1	1.0	0.6	11.6	8.9	16.2	9.6	65.8	40.5	19.3	25.7	451	2172	1118	578
	70.0	1.4	1.2	0.3	9.4	17.7	62.0	58.1	88.5	64.9	79.7	69.7	0	281	382	100
	64.9	0.7	0.9	0.5	4.7	28.3	79.3	75.7	96.4	83.0	78.9	90.5	1	337	785	260
106	66.7	3.4	1.5			15.3	54.6	53.6	67.9	48.0			377	1005	1037	na
	66.8	1.0	1.2	0.3	7.9	22.8	72.2	68.9	93.6	72.0	84.3	80.3	116	888	507	690
	63.6	0.6	0.6	0.2	26.0	23.8	73.8	71.6	96.3	86.6	89.9	37.7	97	563	713	560
94	69.6	1.0	1.2	0.6	12.2	15.5	58.0	56.7	91.8	62.6	48.5	70.4	10.5	10.1	195	nm
	73.7	2.6	1.4	0.5	8.0	13.9	52.0	48.8	76.4	51.8	48.3	81.0	-	17.5	179	nm
104	73.2	2.9	1.4	0.5	10.5	11.5	36.8	32.3	63.3	33.1	48.0	48.0	341	2306	856	520
	66.2	1.0	1.0	0.4	7.1	24.3	74.5	71.1	94.2	78.9	80.3	83.4	149	693	1115	510
	72.2	0.6	0.8	0.6	5.6	20.2	67.6	62.0	95.7	78.0	64.5	84.2	263	809	753	470
96	76.4	2.3	1.3	0.6[4]	5.4	14.0	52	47.3	78.9	54.4	45.9	74.7	8.1	187	381	1[2]
	67.4	1.0	1.5	0.1[4]	7.2	22.8	74	71.5	94.6	67.3	96.9[4]	79.1	-	222	503	
107	73.6	2.5	1.3	0.5	11.3	10.8	32.4	27.7	67.0	36.9	44.6	40.4	351	2183	1123	560
	67.4	1.0	1.2	0.3	7.8	22.3	71.4	67.8	93.4	71.8	83.9	80.1	7	408	383	490
98	77.7	1.9	1.3	0.6	8.2	10.3	32.8	27.4	76.9	40.1	18.8	47.3	1010	2300	2170	460
	73.0	1.0	0.5	0.5	17.4	7.6	6.6	7.9	83.9	67.2	-	-	69	1033	1370	na
	66.4	0.6	1.1	0.6	4.6	26.7	78.8	76.0	97.0	80.5	68.1	88.7	55	531	897	1050
99	71.6	1.7	1.1	0.7	9.3	15.6	58.2	55.7	86.0	64.4	41.0	61.0	43	508	187	-
	77.7	1.6	1.4	0.9	2.6	15.8	59.0	52.7	87.4	57.0	23.2	89.3	135	1259	577	210
	73.0	1.0	0.8	0.8	3.8	20.6	70.2	65.3	93.9	79.7	46.8	87.8	472	1166	822	195
100	73.5	2.5	1.9	0.6	8.3	13.2	46.0	40.8	72.3	22.8	45.3	65.4	211	1560	1144	520
	72.5	0.8	1.0	0.7	14.6	10.4	29.8	26.4	89.5	49.3	19.5	23.7	431	1677	1129	780
													23	215	1022	160
	69.5	0.9	0.8			23.9	73.9	69.1	94.4	82.4			155	387[4]	1172	160
101	74.4	3.6	1.9	0.7	9.7	9.7	24.1	18.9	46.7	-	19.8	45.3	186	2477	na	93
	73.3	1.1	1.2	0.6	9.3	14.5	51.8	46.4	89.0	57.2	50.4	65.2	358	1429	848	320
	72.5	0.6	0.8	0.6	11.0	14.5	51.6	53.4	94.3	68.6	47.7	58.6	763	723	1077	315
102				0.7									568	1570	2843	190
	73.4	0.5	0.9	0.4	6.5	18.3	63.3	57.3	95.7	72.2	75.7	80.5	486	641	258	780
	72.8	0.4	1.1	0.7	6.0	19.0	65.2	59.4	96.8	68.5	57.7	82.9	1774	657	437	770
109	75.2	1.6	1.2	0.6	8.3	13.2	46.2	39.6	82.7	51.7	45.6	64.2	1084	2254	1084	540
	77.2	1.2	0.9	0.7	5.9	14.1	50.2	42.0	88.1	64.8	40.6	76.2	1077	2900	1403	500
	77.7	0.8	0.9	0.7	5.2	14.7	52.4	43.8	92.4	66.5	43.0	79.8	714	506	841	410
108	76.8	2.0	1.3	0.6	5.1	14.2	50.4	42.5	79.9	49.7	49.4	79.5	427	867	1695	160
	76.6	0.8	1.1	0.6	6.7	14.2	50.3	42.5	91.7	57.6	49.4	73.1	317	1477	1531	275

[1] By difference
[2] Value at 5 cm radius
[3] Sample probe partially cupped with char
[4] Probably in error
[5] Low primary velocity caused flashback and melted primary tube-data questionable

na - Not available
nd - None detected
nm - Not measured

effects on the reactor flow; uncertain heat loss effects on temperature measurements; and CO_2 dissolution into the quench water. Estimates of the inaccuracies introduced by these various effects are treated in detail in a Ph.D. dissertation by Skinner (17) and an MS Thesis by Price (18), both of which were written as an extention of this study.

d. Data Analysis

Gasification. In an attempt to reduce the data from the various experiments to a common basis, the gas analyses were normalized to a nitrogen-free basis. In most cases, this was a small correction. The presence of large amounts of nitrogen in a few samples could be explained by air dilution problems associated with the sampling or analysis techniques. Radial concentration profiles for the various gas species were plotted versus radial position of the probes and integrated to obtain average species concentrations. An example of such a radial profile is found in Figure 44 for test 98, in which samples at three different radial locations were obtained. Figure 45 shows reproduced results from two different runs (no. 101 and 102) at the same flow rates. Once the average species concentrations were obtained, they were plotted as a function of steam/coal ratio. Figure 46 summarizes these results. The concentrations followed the same trends as that predicted by equilibrium calculations (29), although they did not fall on the equilibrium line. These equilibrium calculations assumed that the elements released from the coal reacted to equilibrium with the gaseous species while the balance of the solid material was inert. Von Fredensdorff and Elliott (30), and Bissett (16), have pointed out that the reactions of carbon with steam and carbon dioxide are not at equilibrium except for 100% steam decomposition.

Figure 47 shows a plot of the hydrogen to carbon monoxide ratio as a function of the steam/coal ratio. There was a tendency, which has been documented previously (16, 30) for an increase in the H_2/CO ratio with increasing steam/coal rates at each oxygen/coal level. Quantitative comparisons with literature values were difficult, since most literature values reported were for exit concentrations, and not for those obtained locally inside the reactor vessel. However, when the hydrogen-carbon monoxide ratio was plotted as a function of oxygen-coal ratio, with the steam-coal ratio as a parameter, as in Figure 48, some interesting trends appeared. For those steam/coal ratios (0.0, 0.24) which were run at all three oxygen-coal levels, there appears to be a maximum H_2/CO near 0.83 kg oxygen/kg coal.

Figure 49 shows the effect of O_2/coal and steam/coal mixture ratios on carbon conversion. The conversion decreased with increasing steam/coal. This trend was observed by others at atmospheric pressure (31). This may be due to reduction in the oxidation reaction rates due to a lowering in the reaction temperature. The values shown for carbon conversion or burnout are probably low because of the ash tracer solubility and devolatilization (3, 4).

Figure 50 (a-d) shows how the various constituent elements in the coal were released as a function of the coal burnout. Carbon, nitrogen, and sulfur were all released at about the same rate as the coal was

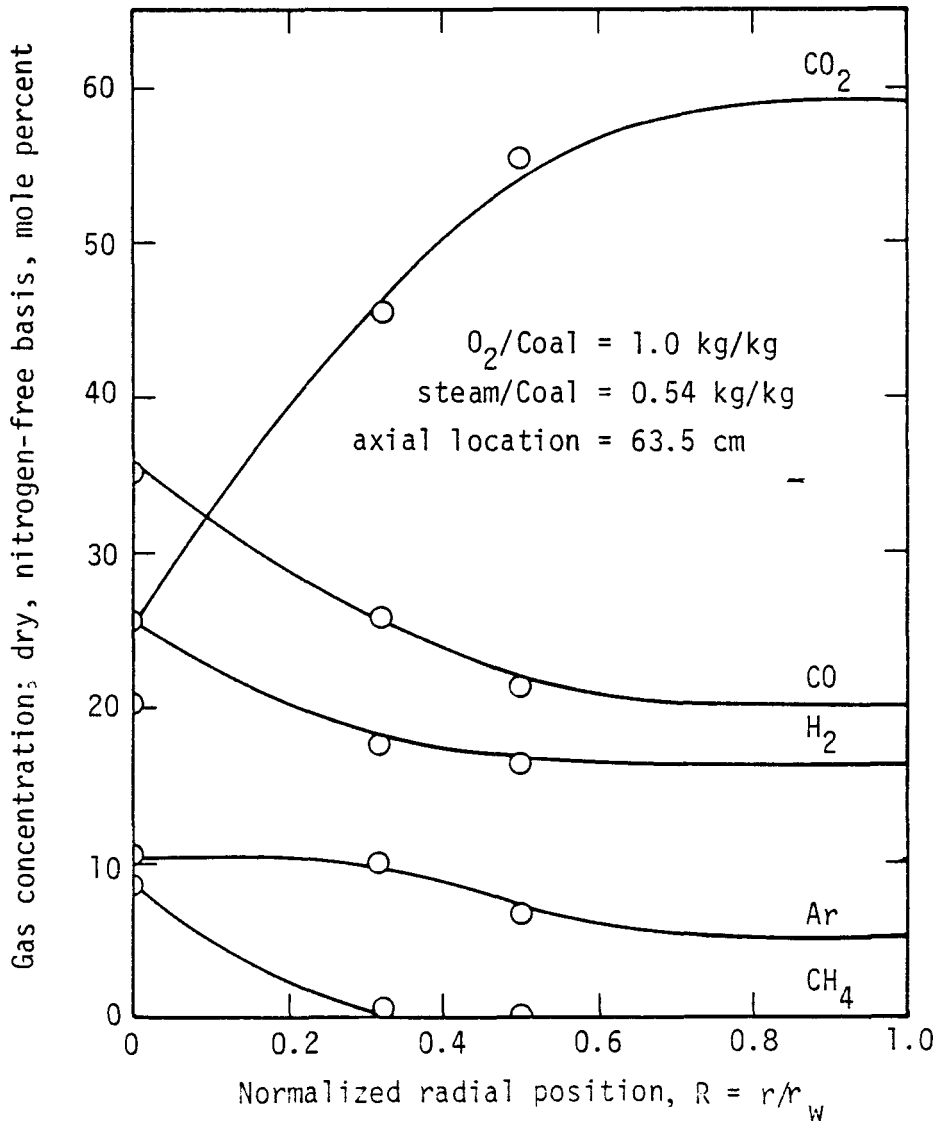

Figure 44. Radial gas concentration profile for test 98

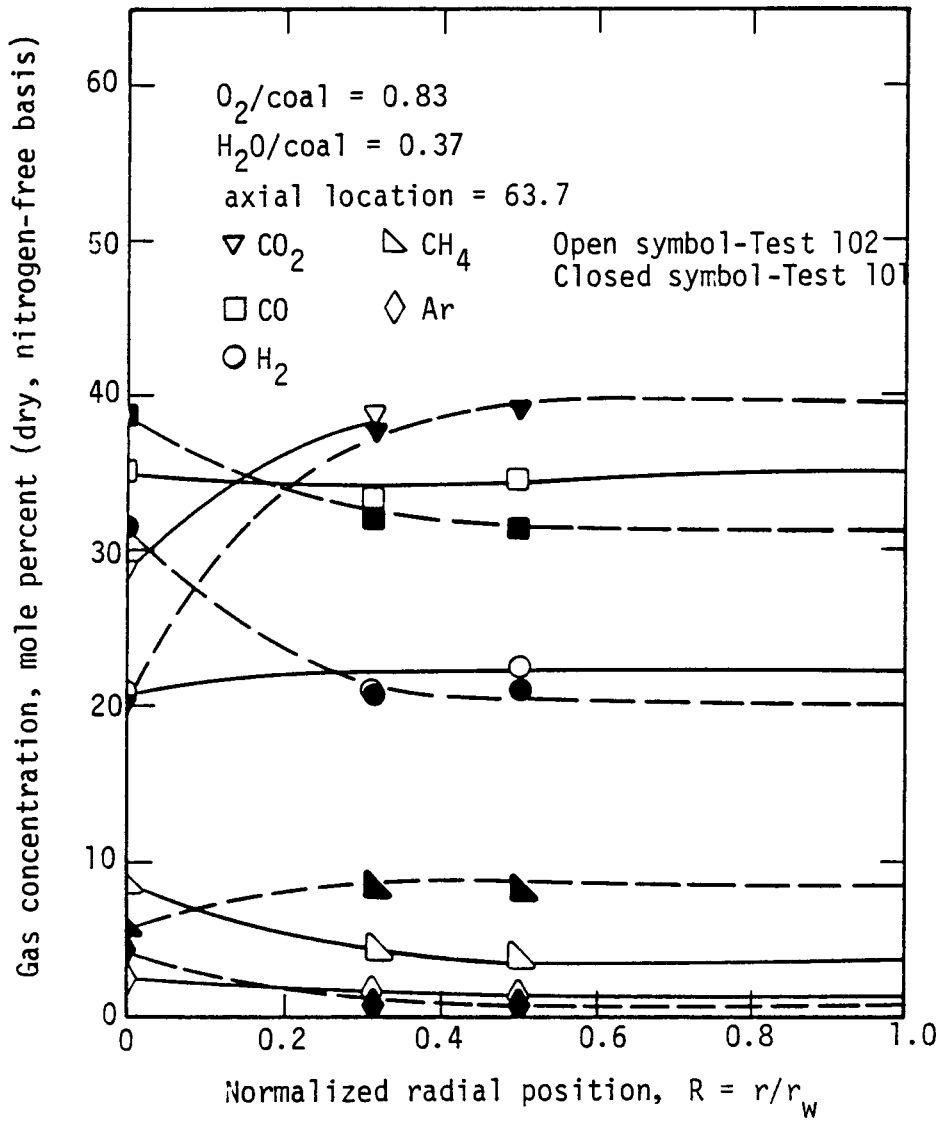

Figure 45. Reproduced test comparison - concentration profiles Tests No. 101 and 102.

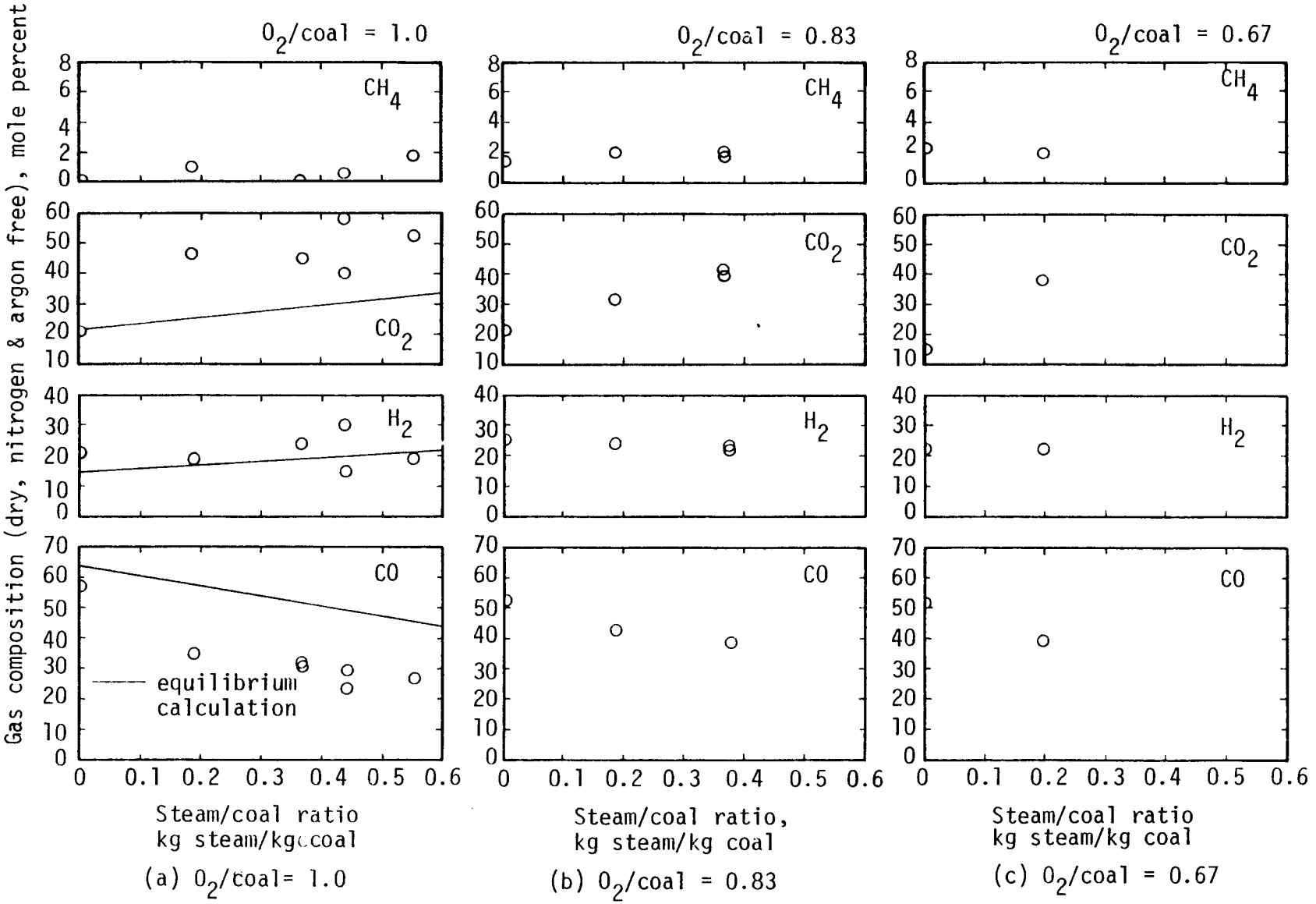

Figure 46. Average gas composition as a function of steam/coal ratio.

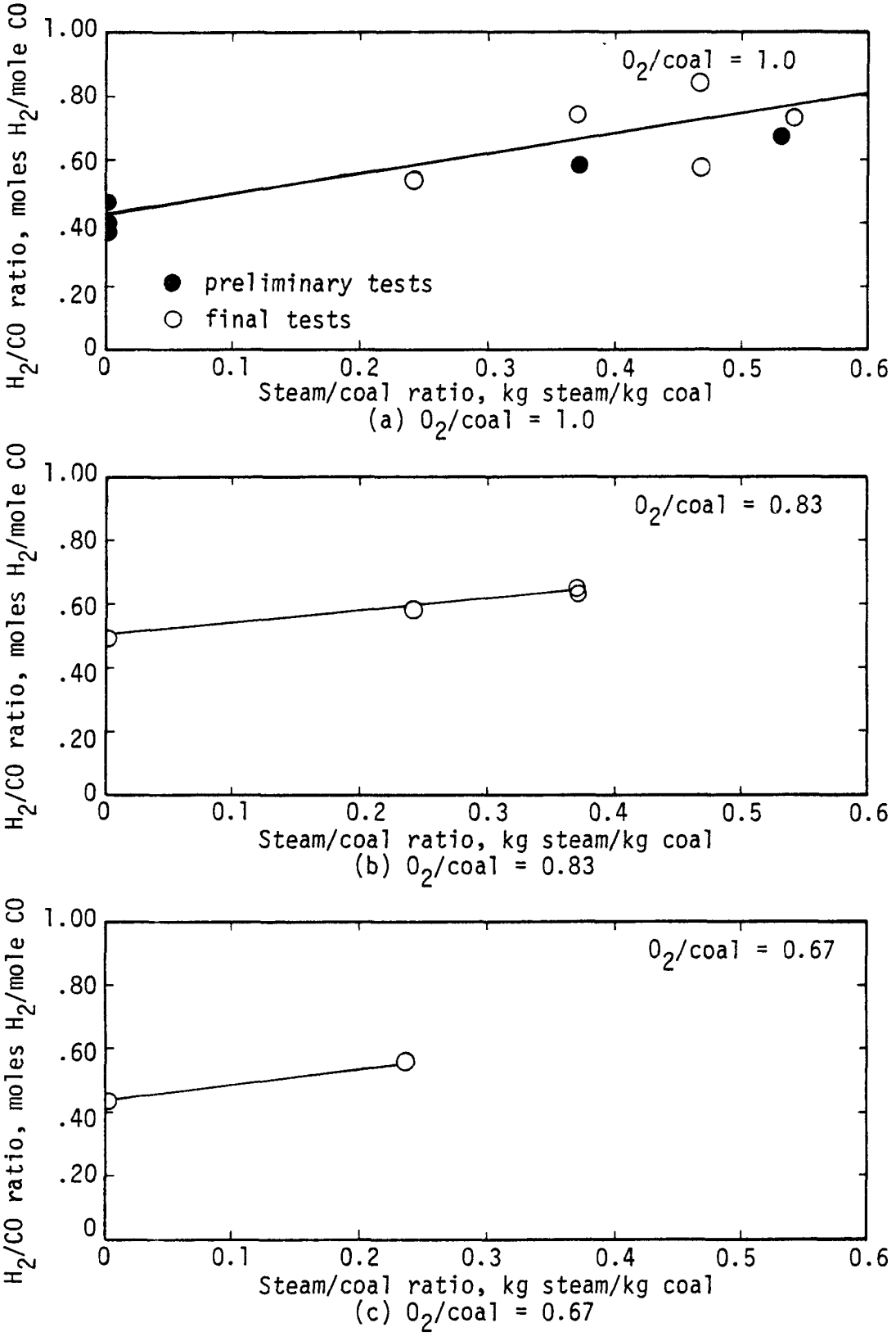

Figure 47. H_2/CO ratio as a function of steam/coal ratio.

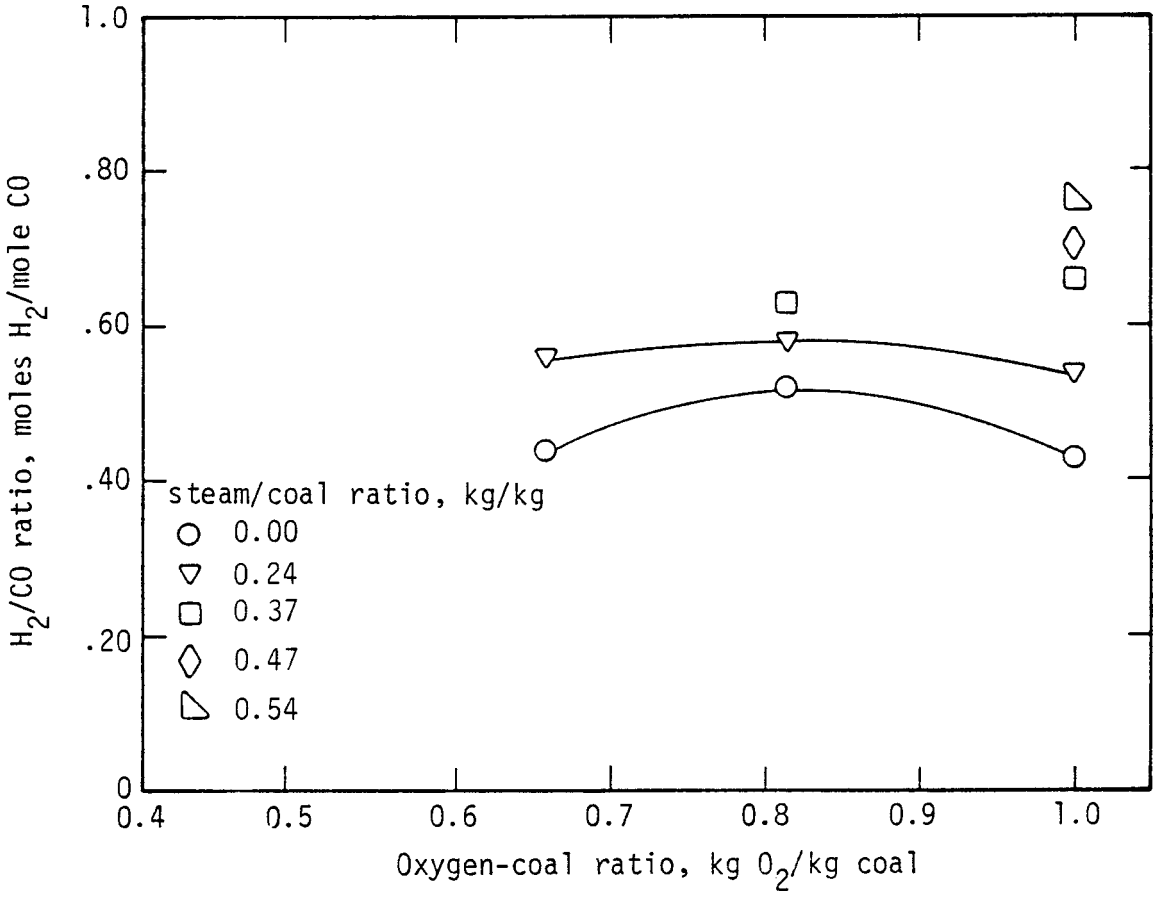

Figure 48. Effect of O_2/coal ratio and steam/coal ratio on H_2/CO ratio in product gas.

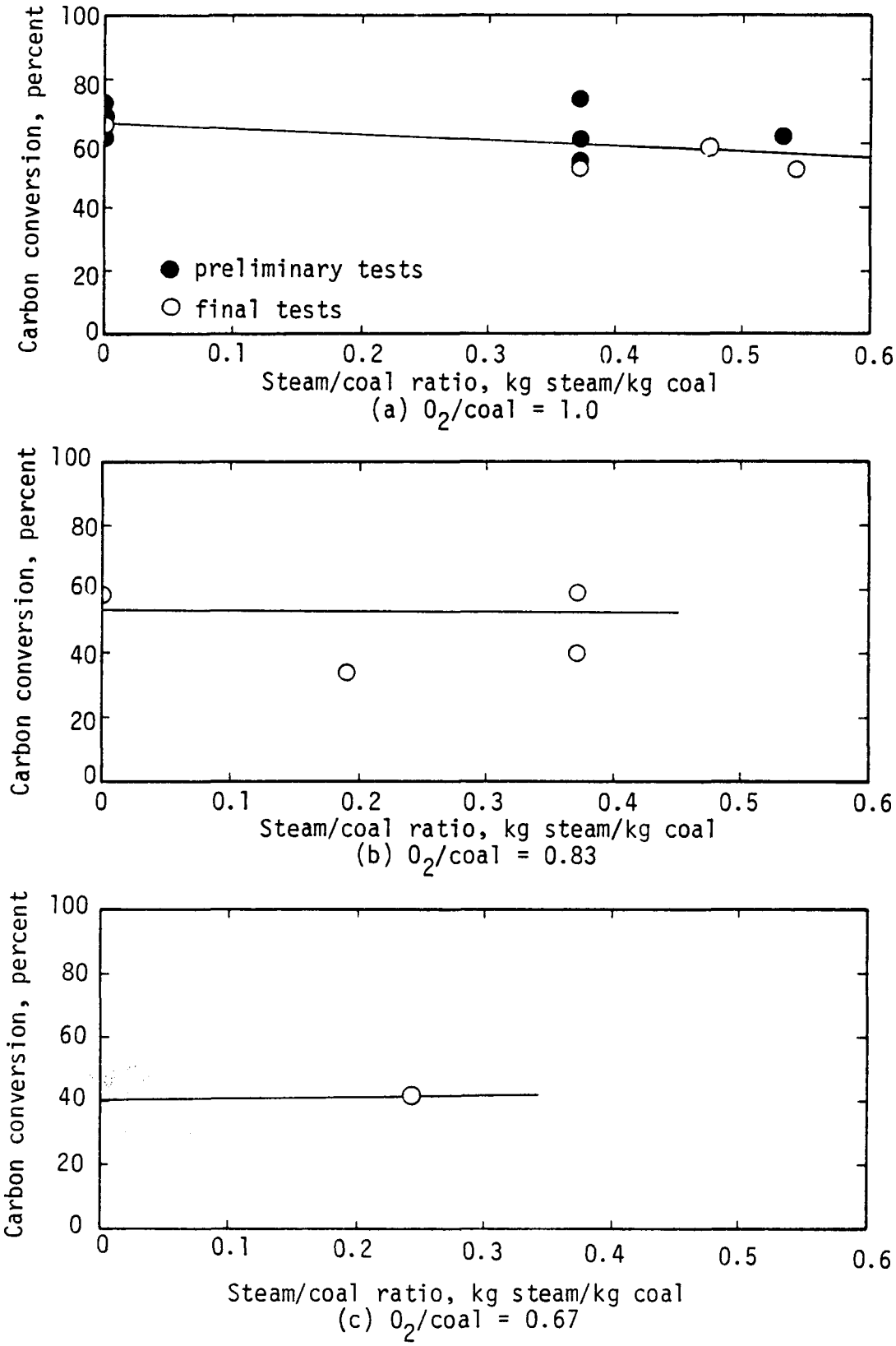

Figure 49. Carbon conversion versus steam/coal ratio.

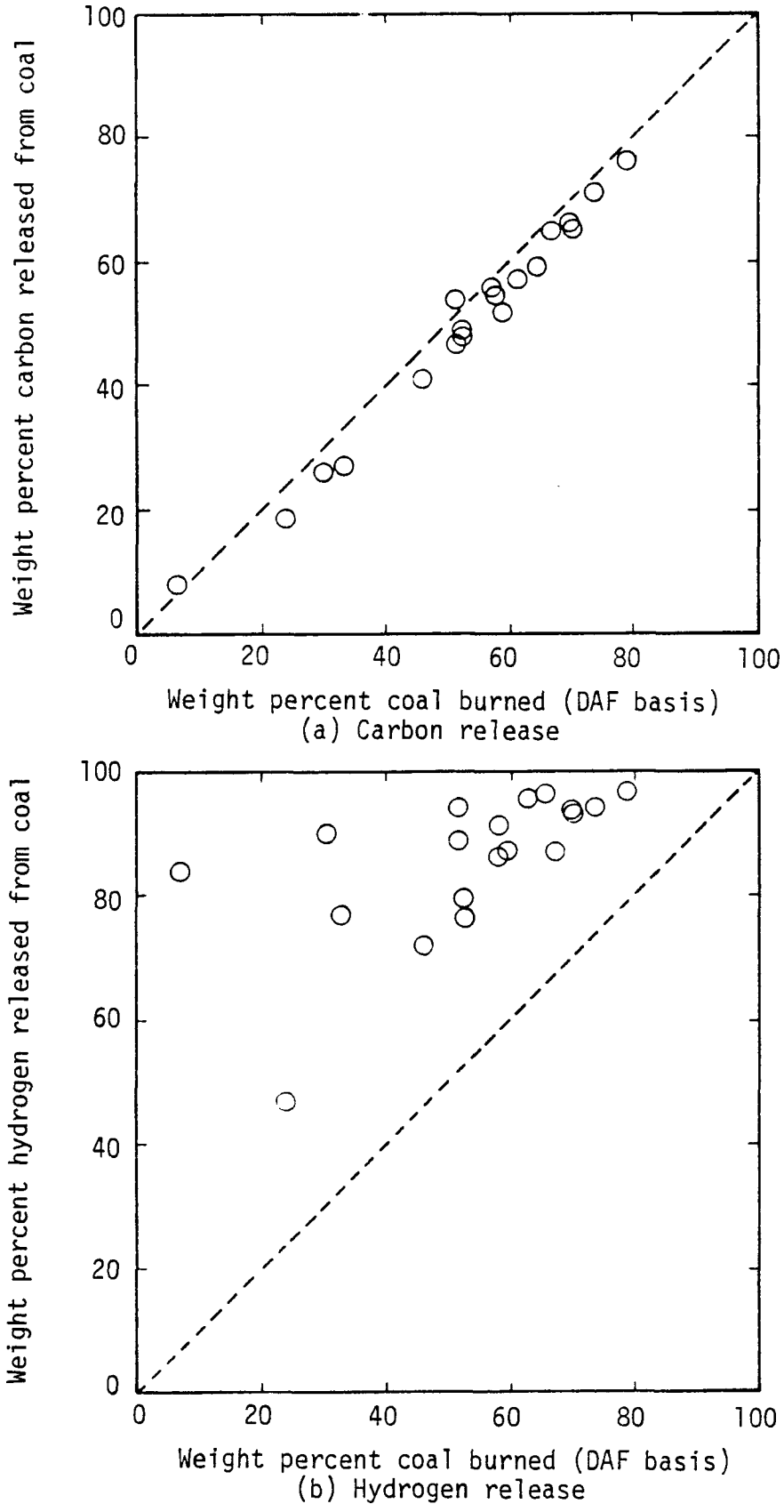

Figure 50. Component release versus coal burnout.

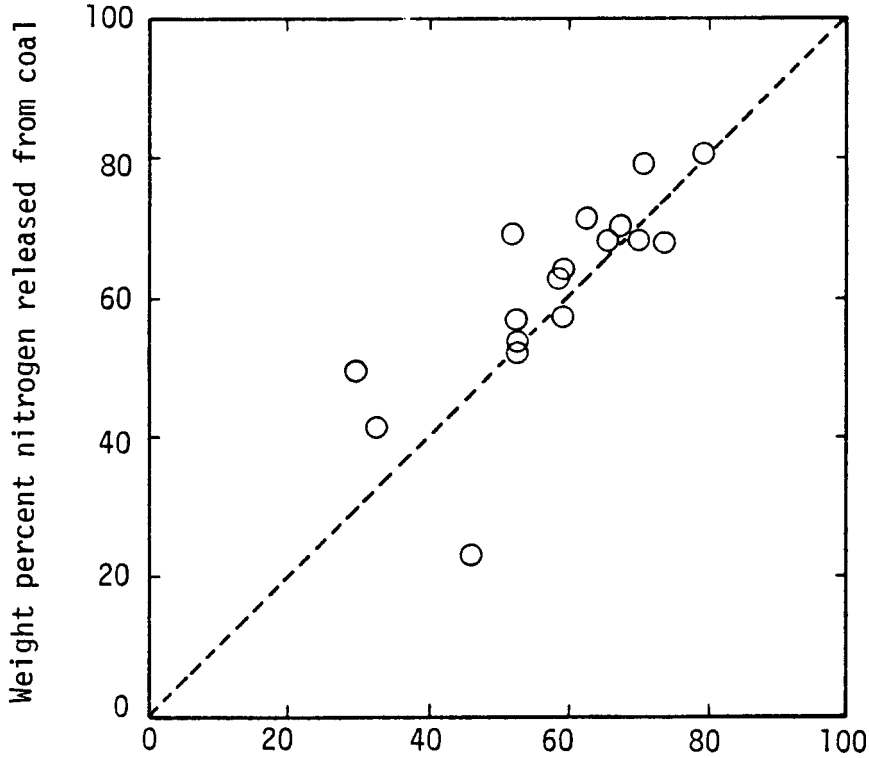

(c) Nitrogen release

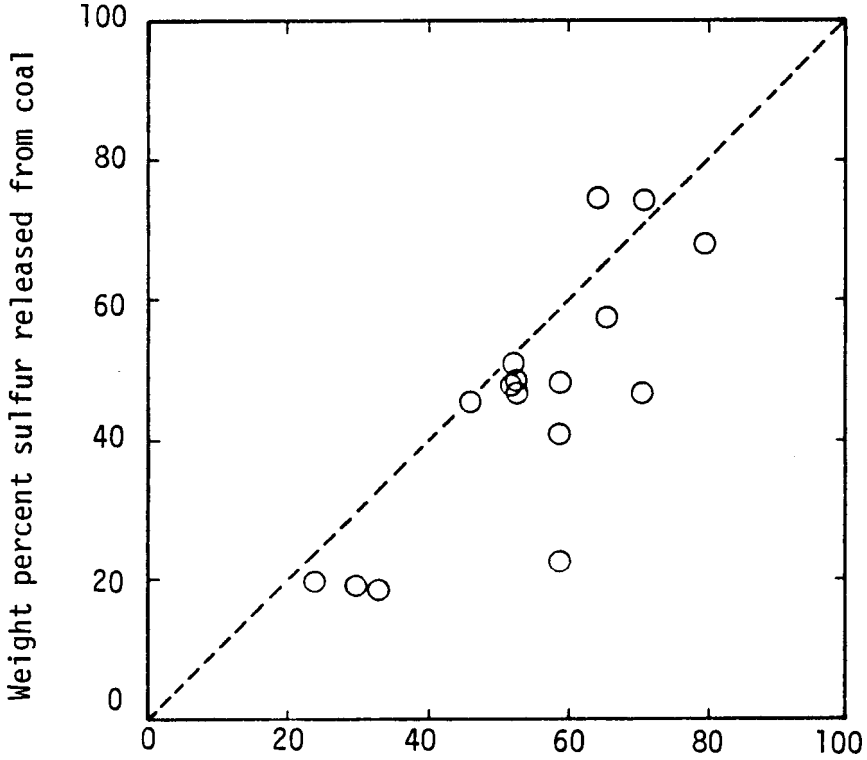

(d) Sulfur release

Figure 50. (Cont.)

burned. However, hydrogen came off much more rapidily. Results obtained in this laboratory for a pulverized coal combustor (3, 4) were somewhat different for hydrogen. For the combustor, the relative hydrogen release rate was lower than for the gasifier.

An important parameter in measuring gasifier performance is the heating value of the gas produced. Figure 51 shows that gas heating value, on an inert-gas free basis, decreased with increasing steam/coal ratio, for each of the oxygen-coal levels studied. Further analysis by Skinner (17) compares these results to literature values. Factors of residence time, in-situ sampling prior to reactor exit, and slow gas/particle mixing are being considered.

Pollutant Formation. Pollutant data from the various tests completed have provided useful information. Areas examined were radial concentration profiles, pollutant concentration minimization, and material balances. Pollutants measured were H_2S, HCN, NH_3, and NO.

Three series of runs were made. Pollutant data were obtained from the set of gasifier experiments as discussed above. As seen in Table 21, the first series was run at an oxygen/coal feed ratio of about 1.00 kg/kg, the second was run at about 0.83 kg/kg and the third was run at about 0.67 kg/kg. In a given series, runs were made at several different steam/coal feed ratios, and the effect of steam on radial concentration profiles was investigated. In most runs, samples were taken with three probes at different radial positions. All of these tests were with the probes at an axial station of 63.5 cm. However, occasonally a probe or sample collection system would plug or otherwise fail to function, leaving a concentration profile with only two data points.

Final pollutant concentration data from five runs made at an oxygen/coal ratio of 1.00 kg/kg were analyzed and the results are shown in Figure 52. The steam/coal ratios examined in this series ranged from 0.0 up to a maximum of 0.54 kg/kg. Higher steam/coal ratios were found to extinguish the flame in the reactor. The radial pollutant concentration profiles tend to become steeper as the steam/coal ratio was increased. In runs with higher steam/coal ratios, pollutant concentrations dropped off dramatically as the wall of the reactor was approached. Pollutant levels were somewhat uniform at lower steam/coal ratios.

Results from the series run at an oxygen/coal ratio of 0.83 kg/kg are summarized in Figure 53. Only three runs were included in this series because steam/coal ratios greater than 0.37 kg/kg extinguished the flame. The run at a ratio of steam/coal ratio of 0.0 kg steam/kg coal produced profiles sloped upward. Pollutant levels were higher toward reactor wall in this run. Concentration tended to level out at a steam/coal ratio of 0.24 kg/kg. The run at a steam/coal ratio of 0.37 kg/kg produced profiles sloped downward, with concentrations toward the outside of the reactor being lower than those toward the center. A similar trend appeared to exist in the runs conducted at an O_2/coal ratio of 0.67 kg/kg, but the two point profile of the two runs summarized in Figure 54 contributed to uncertainty in this observation.

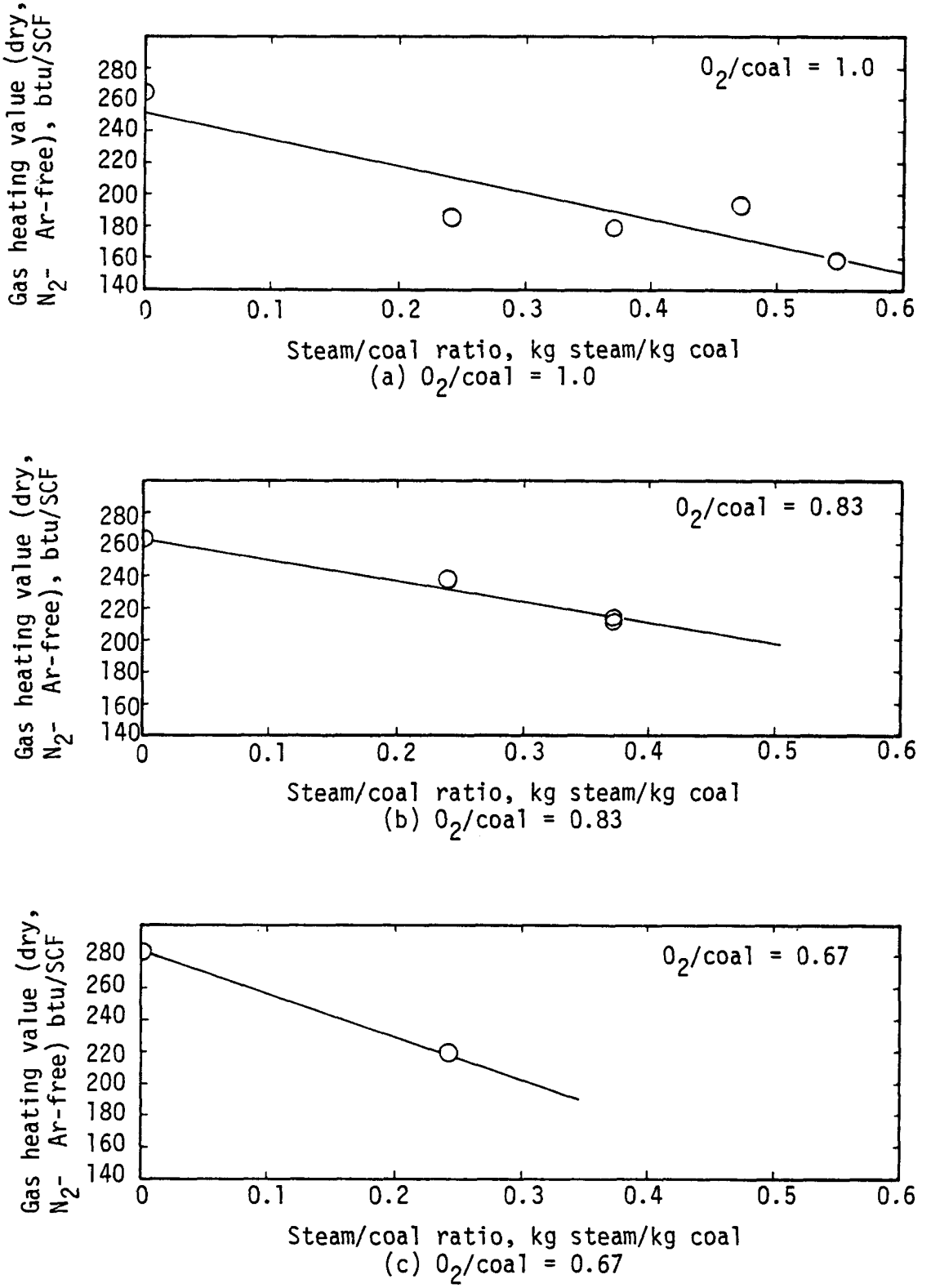

Figure 51. Effect of O_2/coal ratio and steam/coal ratio on gas heating value.

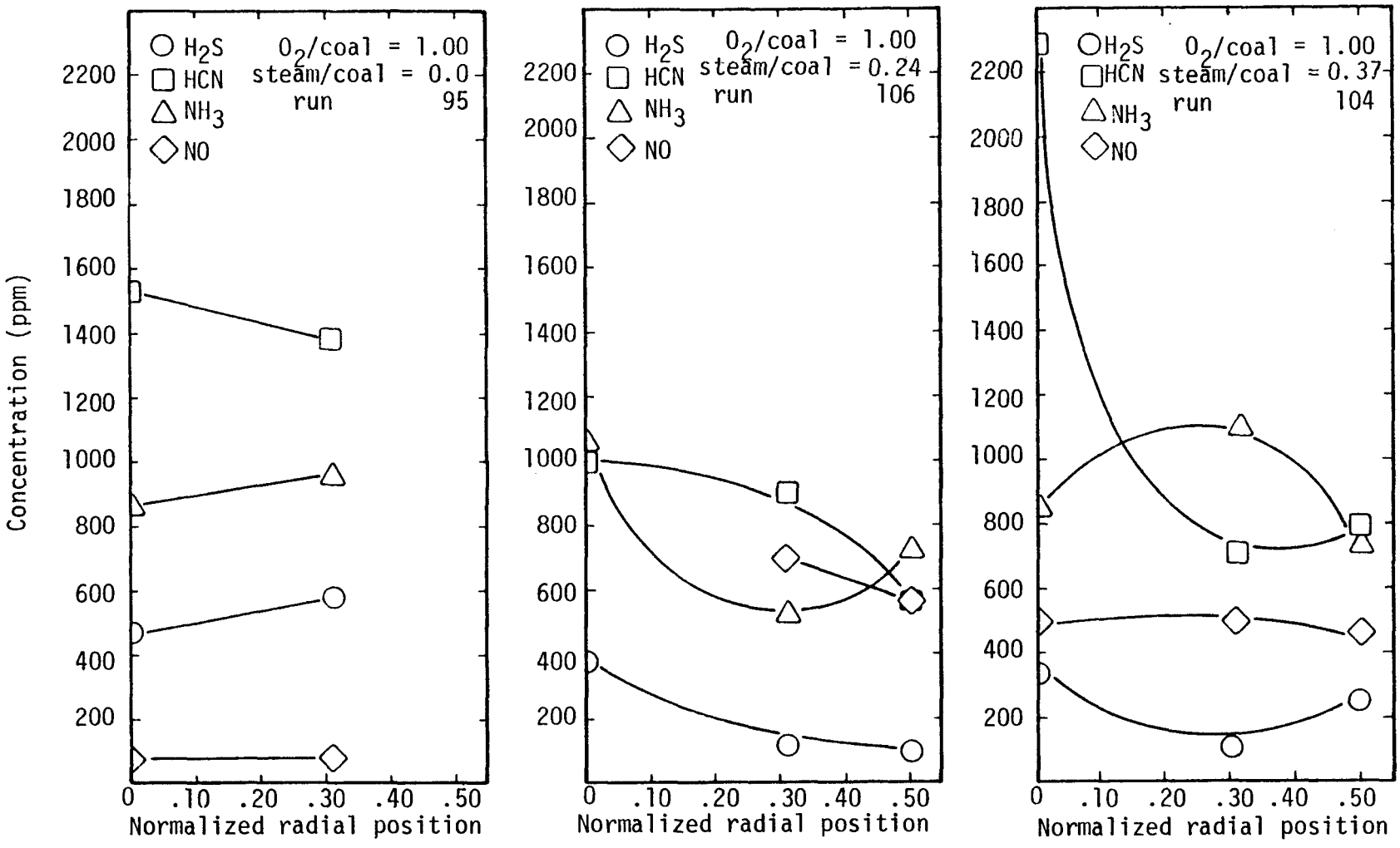

Figure 52. Radial pollutant concentration profiles with increasing steam ratios.

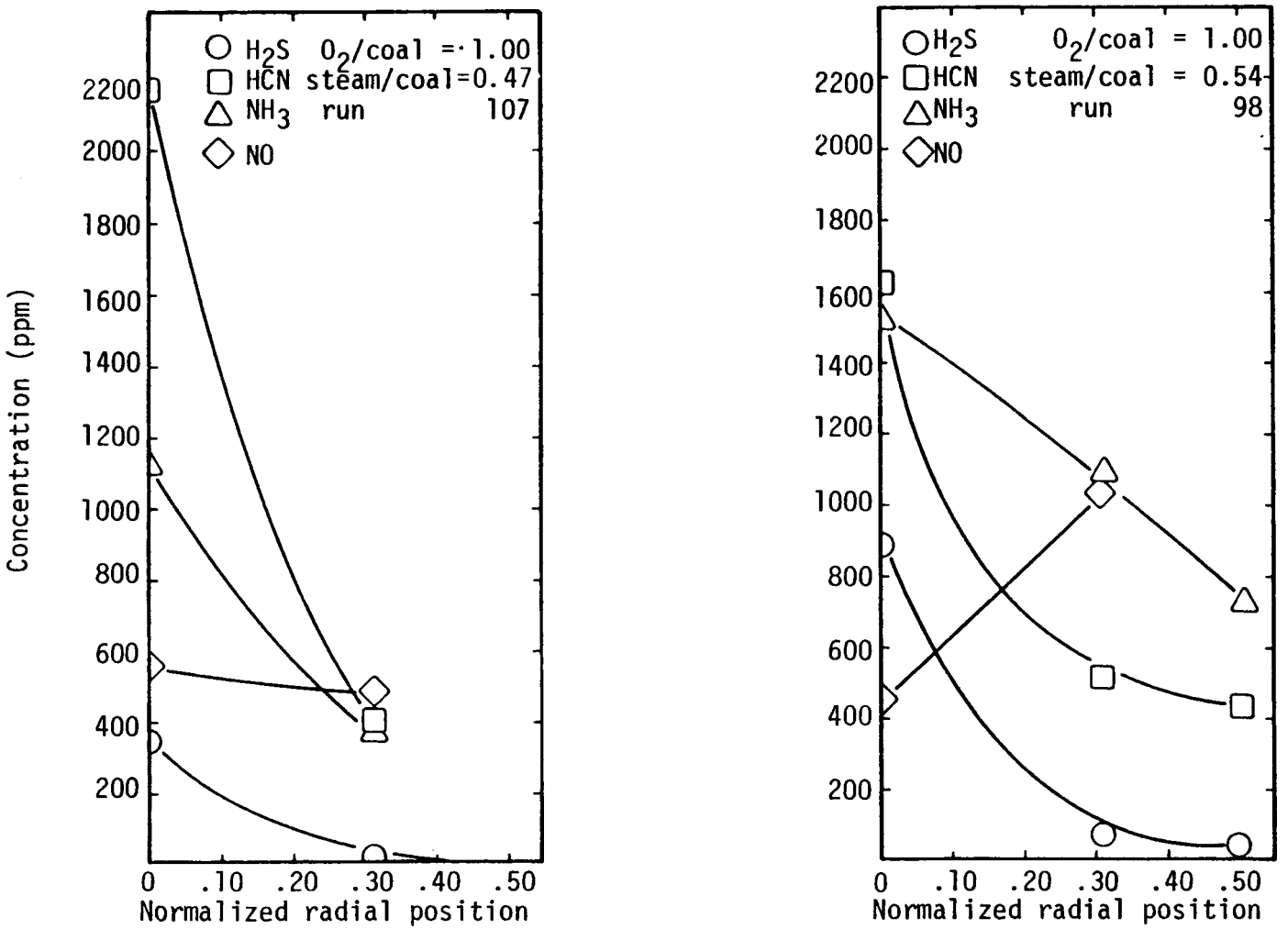

Figure 52. (Cont.)

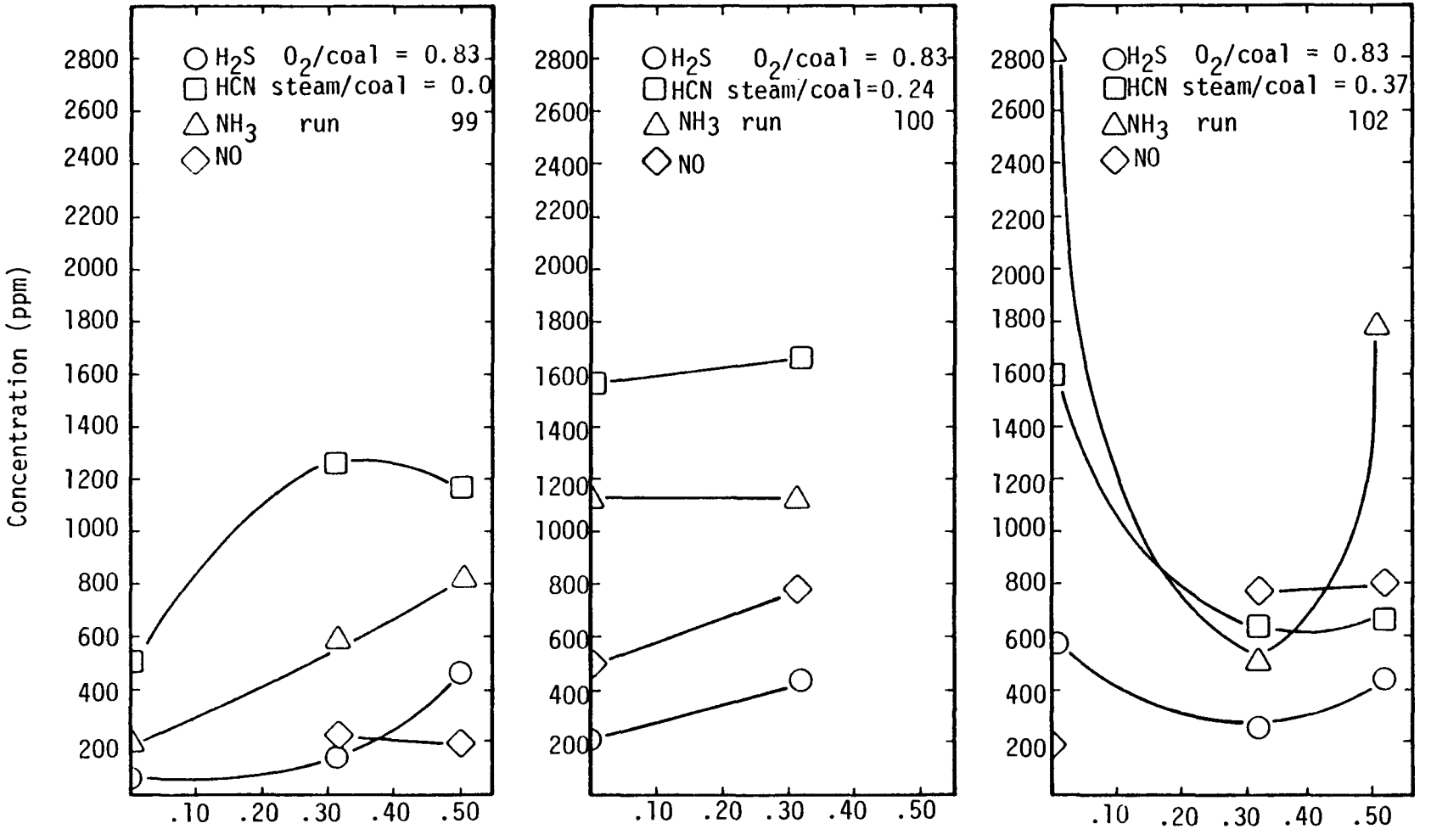

Figure 53. Radial pollutant concentration profiles with increasing steam ratios.

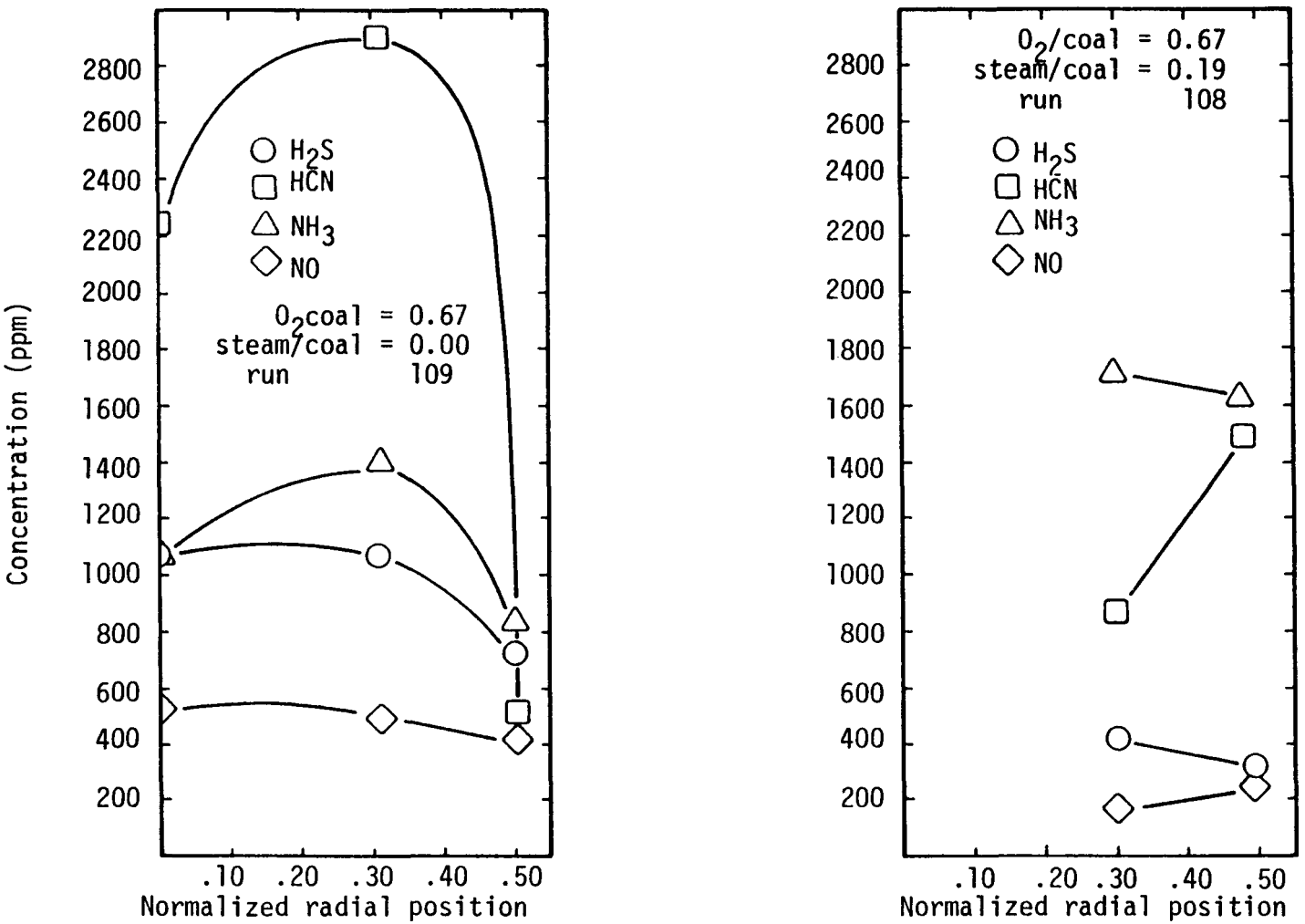

Figure 54. Radial concentration profiles with increasing steam.

Increasing the steam/coal ratios dramatically reduced concentrations of NO, NH_3, HCN, and H_2S toward the outer edge of the reactor. In other words, profiles tended to become steeper with increasing steam. A possible explanation for this could be that steam, injected in the secondary nozzle, had a cooling, quenching effect on formation of pollutants toward the outer edge of the reactor where steam was most abundant.

Data were also examined to determine which O_2/coal and steam/coal mixture ratios produced minimum pollutant levels. The exit gas stream was not sampled. Local samples were taken from within the reactor at a 63.5 cm axial location and at three different radial positions. Steep radial concentration profiles made it impossible to obtain an average concentration from the data. Thus, concentrations were compared on a point-by-point basis. To facilitate comparison, the concentration of each pollutant was plotted against oxygen/coal mass ratio for each given steam/coal ratio. Pollution concentration results for a steam/coal ratio of 0.0 kg/kg are summarized in Figures 55 and 56. From Figure 55(a), the minimum H_2S concentration levels were found at an oxygen/coal ratio of about 0.83 kg/kg. From Figures 55 (b) and 56(a), the minimum levels of HCN and NH_3 concentration were also found at an oxygen/coal ratio of about 0.83 kg/kg. However, the minimum levels of NO, Figure 56(c), found at an oxygen/coal ratio of at least 1.0 kg/kg. Interpolation between these results, and similar analyses of the 0.24 and 0.37 steam/coal ratio data produced the results shown in Table 22 where the operating conditions for minimum pollutant levels for each pollutant are summarized. Operating conditions for minimum pollutant formation for all pollutants measured tend to be at lower steam/coal ratios and higher O_2/coal ratios, there was no "best" condition observed however, which applied to all pollutants. Production of each pollutant tends to minimize at different, unique, conditions.

Material balances were employed in order to determine accuracy of the data and the extent of pollutant formation from coal impurities. From the analysis of coal char samples presented above, the amount of sulfur or nitrogen released from the coal was calculated. This information, combined with gas analysis data was used to determine the fraction of the sulfur or nitrogen released from the coal which was converted to form a given pollutant. The results of this analysis are summarized in Table 23. Fractional conversions to H_2S appeared to be somewhat low. It was believed, however, that SO_2 was formed from most of the remaining sulfur. No SO_2 measurements were taken during the mixture ratio tests. Subsequent tests, which were taken to map the reactor characteristics and which are discussed in a following section, confirm that large amounts of SO_2 were formed.

Potential concentrations of molecular N_2 and SO_2 liberated from the coal were also estimated from material balances. It was assumed that all coal nitrogen not found in coal char, HCN, NH_3 or NO was in molecular N_2. It was further assumed that all sulfur not found in char samples or H_2S was in the form of SO_2. Resulting estimated concentrations of N_2 and SO_2 are summarized in Table 24. Results suggest that SO_2 is a more predominant sulfur species than H_2S for these test conditions. Further, results suggest that the conversion of fuel-nitrogen in the gasifier to N_2 varies from 35-97%, depending upon test condition and

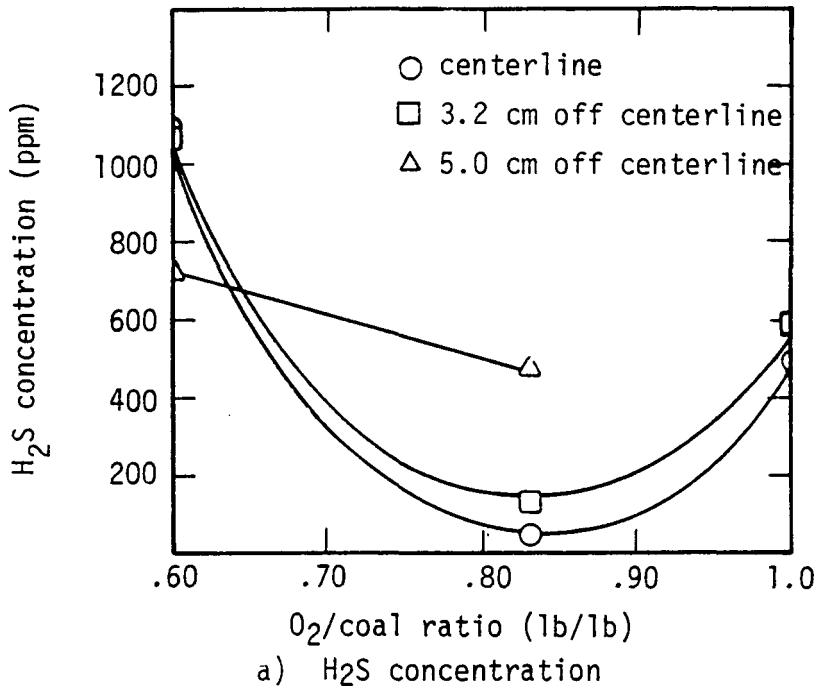

a) H_2S concentration

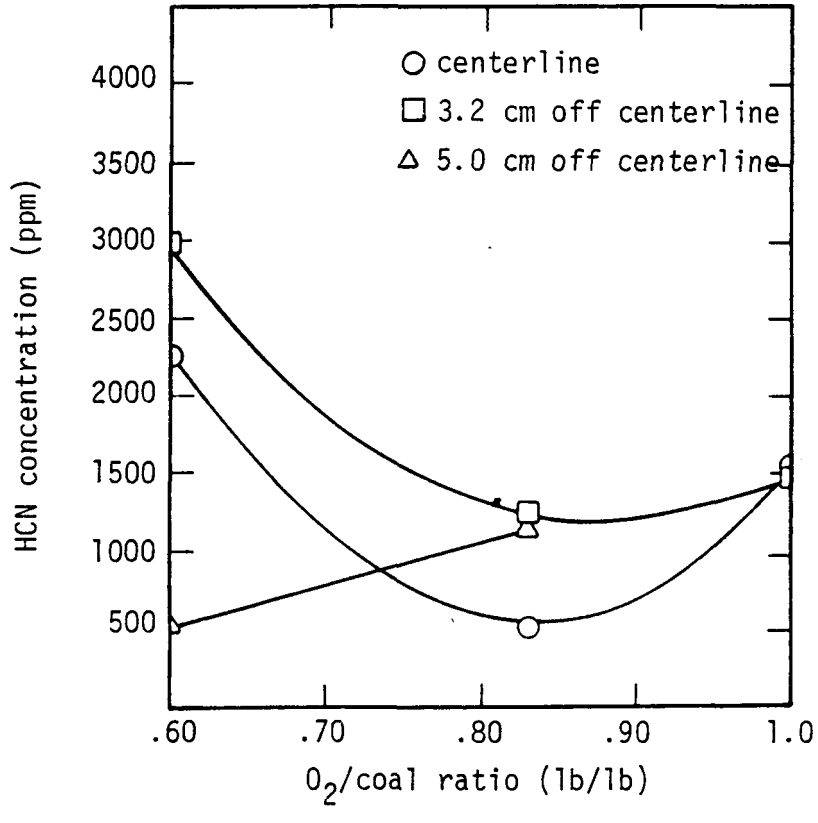

b) HCN concentration

Figure 55. Effect of O_2/coal ratio on H_2S and HCN pollutant formation (steam/coal = 0.0).

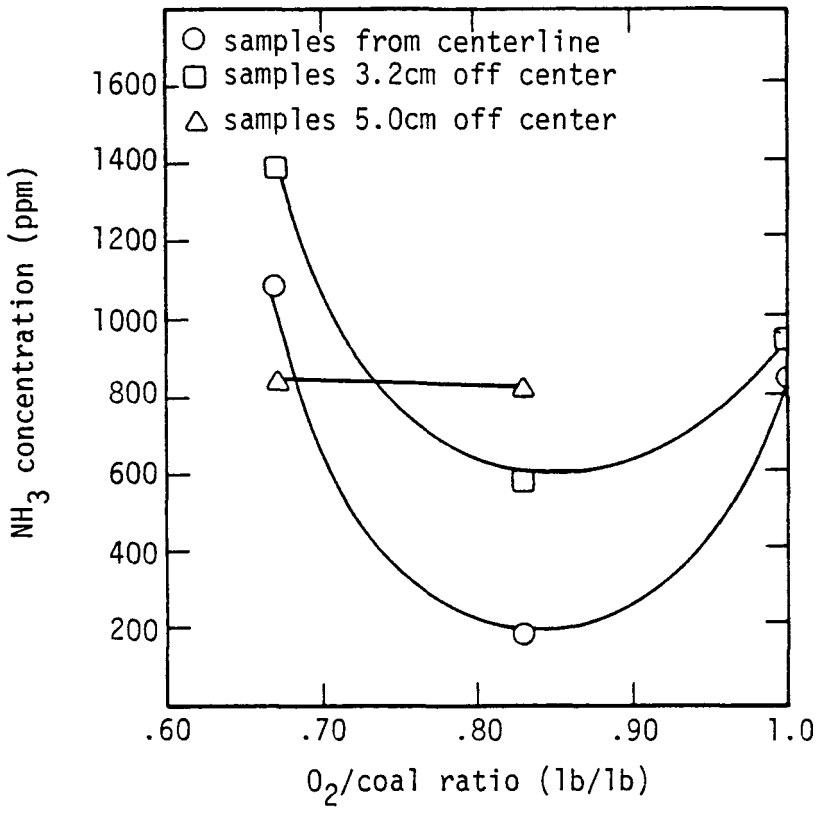

a) NH_3 concentration

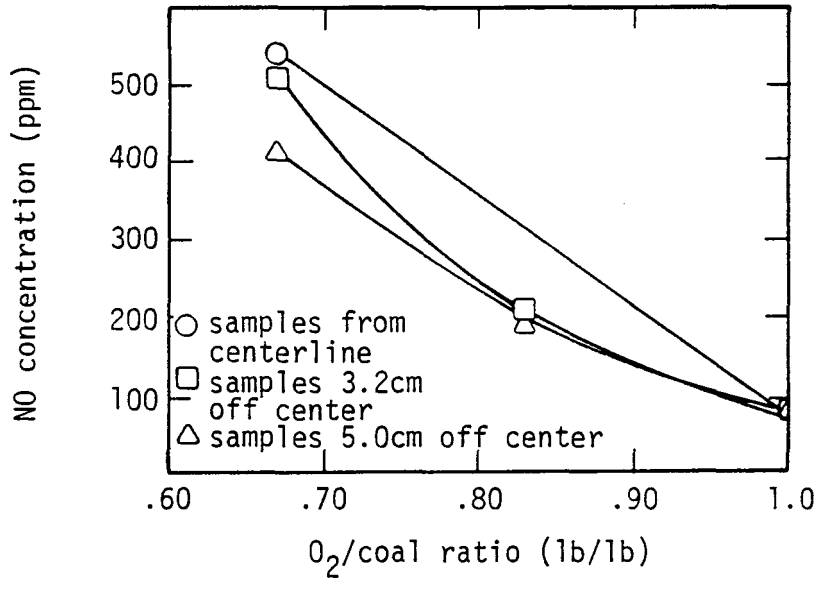

b) NO concentration

Figure 56. Effect of O_2/coal ratio on NH_3 and NO pollutant formation (steam/coal = 0.0).

TABLE 22

SUMMARY OF OPERATING CONDITIONS FOR MINIMUM OBSERVED POLLUTANT FORMATION

Pollutant	Operating Conditions for Minimum Pollutant Formation O_2/Coal	Steam/Coal	Probe Location, cm	Pollutant Level, ppm
H_2S	1.00	0.24	0.0	377
			3.2	116
			5.0	97
HCN	1.00	0.24	0.0	1005
			3.2	888
			5.0	563
NH_3	0.83	0.00	0.0	187
			3.2	577
			5.0	822
NO	1.00	0.00	0.0	
			3.2	75[a]

[a]Probe located at about 1.6 cm

TABLE 23

FRACTIONAL CONVERSION TO POLLUTANTS

F = Fractional Conversion of N or S from coal to pollutant indicated

Run #	Probe	F_{H_2S}	F_{NH_3}	F_{HCN}	F_{NO}
95	1	0.073	0.067	0.121	0.005
95	3	0.143	0.094	0.135	0.007
98	1	0.015	0.099	0.105	0.030
99	1	0.073	0.015	0.040	
99	3	0.162	0.047	0.103	0.017
99	4	0.061	0.060	0.085	0.014
100	1	0.038	0.159	0.217	0.072
100	3		0.061	0.091	0.042
101	3	0.141	0.064	0.108	0.024
101	4	0.359	0.068	0.046	0.020
102	3	0.086	0.037	0.049	0.059
102	4	0.062	0.144	0.053	0.063
104	1	0.042	0.081	0.218	0.049
104	3	0.023	0.081	0.050	0.037
104	4	0.043	0.048	0.052	0.030
106	1		0.138	0.134	
106	3	0.017	0.043	0.075	0.059
106	4	0.015	0.055	0.044	0.043
107	1	0.050	0.094	0.182	0.047
107	3	0.001	0.032	0.034	0.041
108	3	0.064	0.145	0.075	0.014
108	4	0.214	0.139	0.134	0.025
109	1	0.227	0.164	0.341	0.082
109	3	0.067	0.090	0.185	0.032
109	4		0.055	0.033	0.027

TABLE 24

N_2 AND SO_2 LEVELS ESTIMATED FROM N AND S MASS BALANCES

Run No.	Probe No.	$[N_2]$ (ppm)	F_{N_2}	$[SO_2]$ (ppm)	F_{SO_2}
95	1	5140	0.807	6050	0.927
95	3	4040	0.764	3520	0.857
98	1	5920	0.765	4000	0.985
99	1			2920	0.927
99	3	5110	0.833	1710	0.838
99	4	5740	0.841	2440	0.939
100	1	1990	0.552	3230	0.962
100	3	7470	0.806		
101	3	5300	0.804	5460	0.859
101	4	6830	0.866	4650	0.641
102	3	5680	0.855	6560	0.914
102	4	4560	0.740	4640	0.938
104	1	3460	0.652	7770	0.958
104	3	5760	0.832	6480	0.977
104	4	7180	0.870	5850	0.957
106	3	4820	0.823	6440	0.983
106	4	5540	0.859	6590	0.985
107	1	4050	0.677	6730	0.950
107	3	5410	0.893	6530	0.999
108	3	4450	0.766	5930	0.936
108	4	4660	0.702	4620	0.786
109	1	1370	0.413	1940	0.773
109	3	5430	0.693	3670	0.933
109	4	4820	0.885		

probe location. Calculated values of N_2 coming from coal were two to three orders of magnitude less than actual N_2 concentrations measured due to N_2 dilution from the window coolant and other trace nitrogen impurities in feed gases, etc. High calculated SO_2 levels indicate the necessity of careful SO_2 measurement in future studies.

Comparison of pollutant data from this study with previous work was somewhat difficult. Reactors operated by others all differ in various ways. In addition, previous reactors measured pollutant concentrations in the exhaust product gas while measurements for this study were made at discrete points within the reactor. The most similar reactor to the BYU gasifier was the G1 gasifier operated by the Bureau of Mines in the 1950's. Bissett reports data from this reactor at similar operating conditions to those used in the BYU study (16). Concentration levels of H_2S were found to be around 3000 to 4000 ppm in the G1 gasifier for a run at a 52 lb/hr coal rate. The O_2 coal ratio was 0.77 kg/kg, and the steam/coal rate was 0.15 kg/kg. The coal used was 2.7 percent by weight in sulfur. Coal used in the BYU study was about 0.5 percent sulfur. If one assumes H_2S concentration to be proportional to sulfur concentraton in the feed coal, H_2S concentration in the G1 gasifier would be around 750 ppm if coal used in the BYU study was used in the G1 gasifier. Such levels of H_2S are comparable to those found in the BYU gasifier.

4. Test Series 3 - Reactor Mapping Tests

a. Test Program

The objectives of the reactor mapping tests were to measure the local gas composition, particle composition and particle mass flux throughout the entrained coal gasifier. These measurements were made in order to determine the gas and particle mixing rates, and the rates of gas and particle chemical reaction. Five separate tests were performed with the probe collar located at various axial locations ranging from the bottom-most position in the reactor to a location near the top of the reactor. Sample probes were located at five specific radial locations from the centerline of the test section to near the reactor wall.

The extent of mapping was somewhat limited because of probe plugging problems associated with test locations near the primary jet exit. The coal flux was high and the coal was very sticky in these regions. Consequently, the probes near the centerline plugged very rapidly and even capped over in some cases which prevented complete data from being obtained.

Test condition g (O_2/coal = 0.83 and steam/coal = 0.24) was selected for the mapping tests, based on an analysis of the mixture ratio test results presented in the previous section. This gave a good carbon conversion, a good gas heating value, and near minimum pollutant production. The coal gasifier also operated very stably at these conditions. As with the mixture ratio tests, the coal feed rate was set at 24.5 kg/hr.

b. Test Results

Five separate tests were completed to map the local properties within the coal gasifier. Tests were performed at axial locations of 33 cm, 48.3 cm, 63.5 cm, and 94 cm. A second reproducability test was performed at 63.5 cm. The composition of the gaseous products, pollutants, char, and other pertinent test results are summarized in Table 25 for each of these tests.

c. Data Accuracy

Skinner (17) and Price (18) have reported a comprehensive accuracy analyses of the gasification and pollutant results respectively.

d. Data Analysis

Gasification. As in the previous section, the gas analysis data were normalized to a nitrogen free basis in order to have a common basis of comparison. The concentrations of trace gases, He and Ar, were used to calculate the extent of gas mixing at each of the radial and axial locations in the reactor where measurements were taken. Figure 57 presents the resulting radial profiles. The characteristic radial profiles which have been seen in previous studies (3-12) were observed. The profiles obtained at 33 and 48.3 cm show evidence of gas recirculation near the reactor wall, with the profiles becoming flatter toward the end of the reactor. At 94 cm the profile is completely flat, indicating total gas phase mixing at that point. The profile at 63.5 cm is also quite flat. The data obtained from both runs at 63.5 cm are included to give an idea of the reproducibility of the data for different runs. For the given test condition (g), the gas mixing parameter would vary between 0.66 and 0.68 for complete gas mixing, due to minor variations in reactant flow rates from run to run.

Figures 58-61 present the radial profiles obtained for the principal gaseous products (CO, H_2, CH_4, and CO_2) at each of the axial test locations. The zone within the reactor where the major part of the reactions took place is easily identified. It appeared that the extent of reaction was approximately proportional to the extent of gas mixing. This can be seen by comparing the gas mixing profiles, Figure 57, with the amount of CO_2 produced as shown in Figure 61. This result is different from the coal combustor (3,4) where the gases were completely mixed before any significant coal reaction occurred.

Figure 62 presents the radial profiles of coal burnout (carbon conversion) for the four axial positions tested. The increase in burnout towards the bottom of the reactor and near the outer walls is apparent. It should be recalled that the burnout data were based on an ash tracer and the actual burnout results may be somewhat higher because of ash volatility and solubility effects. The coal burnout at the lowest axial position, 94 cm, can be seen to be nearly uniform across the entire reactor, at about 58%.

A measure of the radial particle dispersion at each axial test location is shown in Figure 63. This figure plots the local particle

TABLE 25

SUMMARY OF FINAL AXIAL MAPPING TESTS (TEST SERIES 3)

Test No.	Actual O_2/Coal kg/kg	Actual Steam/Coal kg/kg	Flow Rates, kg/hr: Primary Coal	Primary O_2	Primary Ar	Secondary O_2	Secondary Steam	Secondary He	Secondary Gas Temp, °K	Test Axial Location, cm	Probe Radial Location, cm	Normalized Water-free Gas Analysis, Mole Percent: CO	CO_2	H_2	N_2	O_2	CH_4	Ar	He
110	0.84	0.24	24.5	16.6	4.4	4.0	5.9	0.1	460	63.5	0.0	36.6	25.5	22.2	2.1	nd	2.4	8.4	2.8
											1.3	36.1	25.8	22.1	2.5	nd	2.4	8.4	2.8
											2.8	34.1	26.9	16.2	3.7	nd	1.1	9.4	3.7
											5.6	31.4	33.3	18.9	2.2	nd	0.8	9.5	3.9
											8.9	32.3	31.3	20.2	2.0	nd	1.2	9.2	3.6
111	0.85	0.25	24.5	16.5	4.4	4.3	6.0	0.1	460	63.5	0.0	37.9	26.6	20.8	2.2	nd	2.0	8.3	2.2
											1.3	38.6	26.3	21.7	2.2	nd	2.1	7.0	2.2
											2.8	36.6	25.7	19.9	2.8	nd	2.7	7.3	2.4
											8.9	35.4	30.2	19.2	2.3	nd	2.0	8.5	2.5
112	0.88	0.24	24.5	16.5	4.4	5.0	5.9	0.1	460	94	0.0	36.2	28.0	22.1	1.6	nd	2.0	8.1	2.1
											1.3	36.0	27.3	21.9	2.7	nd	2.0	8.0	2.1
											2.8	35.9	27.4	21.5	3.2	nd	1.8	8.2	2.1
											8.9	36.5	27.3	22.1	2.0	nd	1.7	8.2	2.1
113[2]	0.85	0.24	24.5	16.5	4.4	4.3	5.9	0.1	489	33	0.0	35.7	12.2	35.9	5.1	nd	6.6	4.0	0.5
											1.3[4]	36.1	11.3	27.3	13.1	1.6	4.8	5.1	0.6
											5.6	26.7	40.6	16.7	3.6	nd	0.8	7.6	4.0
											8.9	35.5	25.0	24.8	2.9	nd	0.6	8.0	3.1
114[3]	0.84	0.24	24.5	16.3	4.4	4.3	5.9	0.1	472	48.3	0.0	37.8	14.3	30.6	4.5	0.3	7.0	4.7	0.9
											1.3	37.7	17.0	29.7	4.9	nd	3.0	6.6	1.1
											2.8	31.5	36.9	15.1	3.3	nd	0.5	9.7	2.9
											5.6	22.9	46.3	11.8	4.5	nd	0.4	10.0	4.0
											8.9	30.3	36.9	16.8	2.7	nd	1.0	9.3	3.0

Test No.	Char Ultimate Analysis, Wt. %: C	H	N	S	O[1]	Ash	Coal/Element Burnout, Wt. %: Coal	C	H	N	S	O	Pollutants, ppm: H_2S	HCN	NH_3	NO	SO_2
110	69.5	3.1	1.4	0.57	14.3	11.6	37.3	36.1	60.7	34.9	41.2	29.8	395	1812	818	550	891
	73.8	2.4	1.2	0.60	11.1	10.9	32.8	28.0	67.4	42.3	34.1	42.0	106	2139	1008	350	464
	74.0	1.4	1.1	0.31	7.2	16.3	58.0	51.9	87.9	63.6	77.2	74.8	237	1346	937	370	1363
	71.7	0.9	1.0	0.38	6.1	19.9	67.0	61.7	93.5	72.5	77.1	82.5	244	745	875	590	1196
	73.2	0.7	0.9	0.37	8.9	15.9	56.6	51.1	93.4	68.7	72.2	68.1	808	1318	1178	600	2351
111	75.3	2.6	1.3	0.57	8.9	11.3	35.9	29.5	66.3	36.5	39.6	55.1	526	1840	745	550	931
	70.9	3.0	1.7	0.59	10.5	13.3	46.5	43.3	67.2	30.7	46.9	55.0	384	1956	962	490	945
	72.5	1.0	0.7	0.69	10.3	14.8	53.0	48.1	90.5	74.9	44.2	60.3	844	1631	888	430	1229
	71.5	0.5	0.6	0.66	6.3	20.4	68.1	62.8	96.2	83.6	61.3	82.4	1003	1781	1291	490	2714
112	74.1	1.3	0.8	0.76	7.1	15.9	56.5	50.3	88.6	71.7	42.8	74.6	889	1208	915	480	1966
	75.2	1.7	1.3	0.72	5.2	15.9	56.8	49.9	84.5	56.9	45.8	81.4	585	1451	989	300	1569
	76.0	0.8	0.8	0.73	12.5	9.2	na	na	na	na	na	na	491	1120	1190	350	1701
	75.7	0.6	0.9	0.68	5.5	16.6	58.8	51.5	95.1	69.7	51.0	81.1	956	1396	1028	380	2876
113[2]	na	na	na	na	na	na	na	na	na	na	na	na	2458	2597	4080	120	746
	na	na	na	na	na	na	na	na	na	na	na	na	na	na	na	na	na
	73.4	0.5	1.1	0.46	2.2	22.3	71.5	65.1	97.0	73.6	75.3	94.4	135	725	3599	440	97
	74.7	0.4	1.0	0.59	5.3	18.0	62.6	55.9	96.5	70.2	60.8	83.2	812	945	3440	360	778
114[3]	68.1	4.5	1.5	na	na	12.3	41.6	41.2	47.0	36.3	na	na	1379	3334	2653	130	2920
	72.2	3.2	1.4	0.65	14.9	7.7	na	na	na	na	na	na	7	2284	1145	230	730
	71.7	2.0	1.2	0.59	11.9	12.6	43.3	39.7	63.8	50.3	44.0	46.2	1	653	553	390	nd
	66.8	0.7	1.1	0.31	7.0	24.1	74.2	70.6	95.9	75.6	84.6	83.5	1	344	495	370	nd
	75.6	0.6	1.0	0.36	3.2	19.2	65.5	58.1	95.8	70.7	98.1	90.5	610	1408	1056	640	1869

[1] By difference

[2] Probes at 0.0, 1.3, and 2.8 cm capped over with particles. Very little gas sample obtained (especially at 2.8 cm) and no particles

[3] Probes at 0.0 and 1.3 cm partially plugged

[4] Did not have sufficient gas sample to complete pollutant analysis

na not available
nd not detected
nm not measured

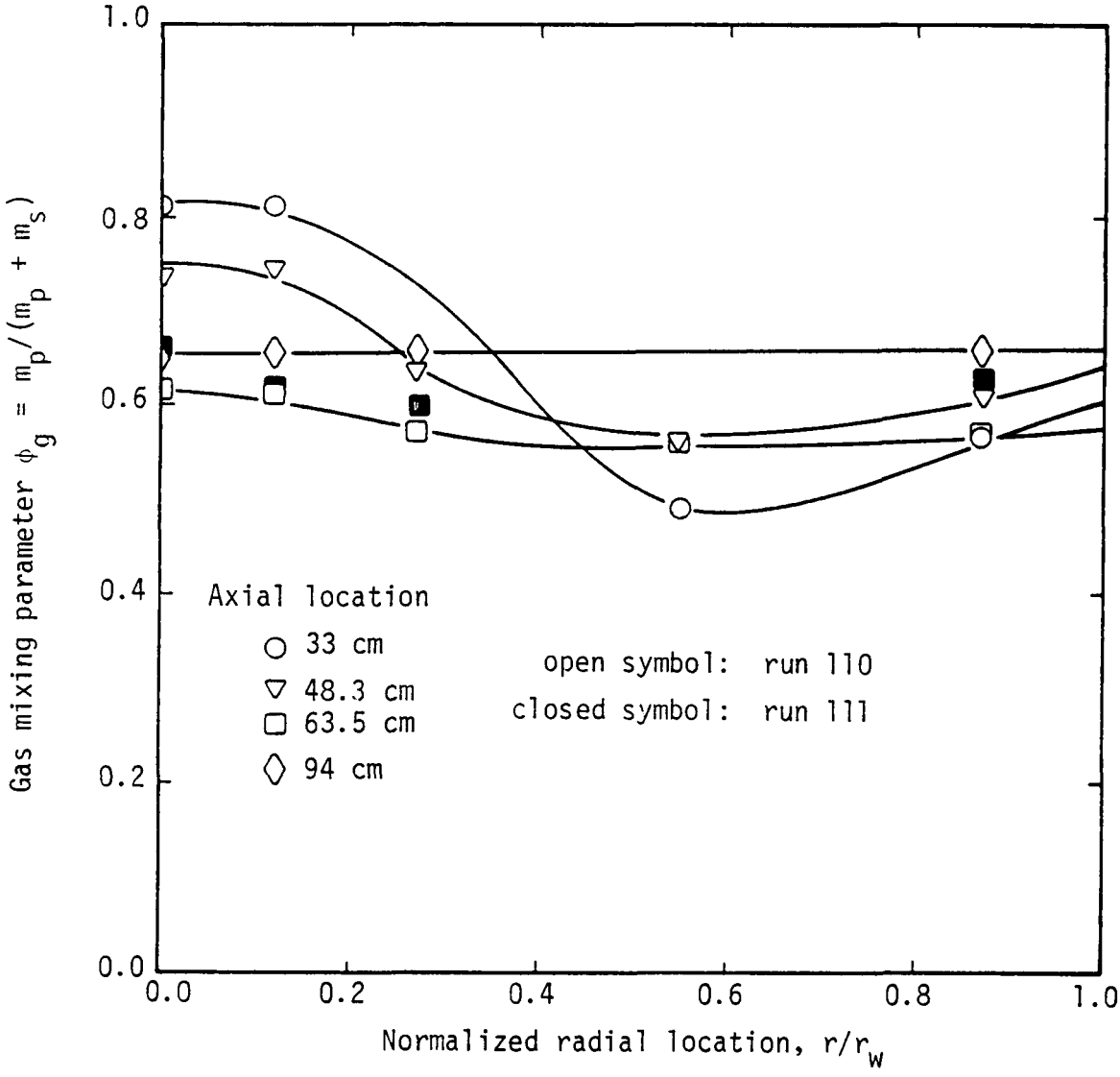

Figure 57. Radial gas mixing profiles.

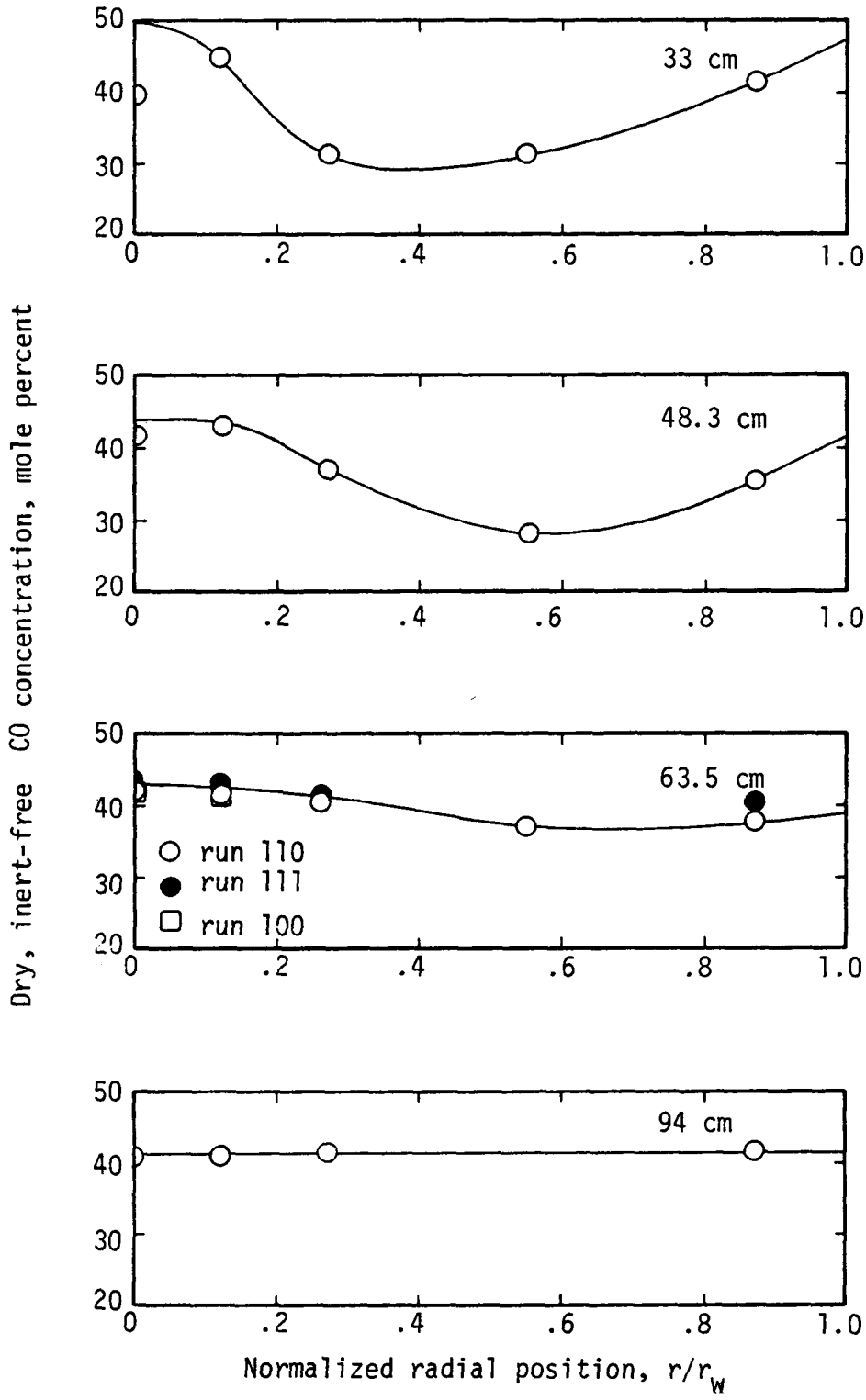

Figure 58. Radial profiles of carbon monoxide at specified axial locations.

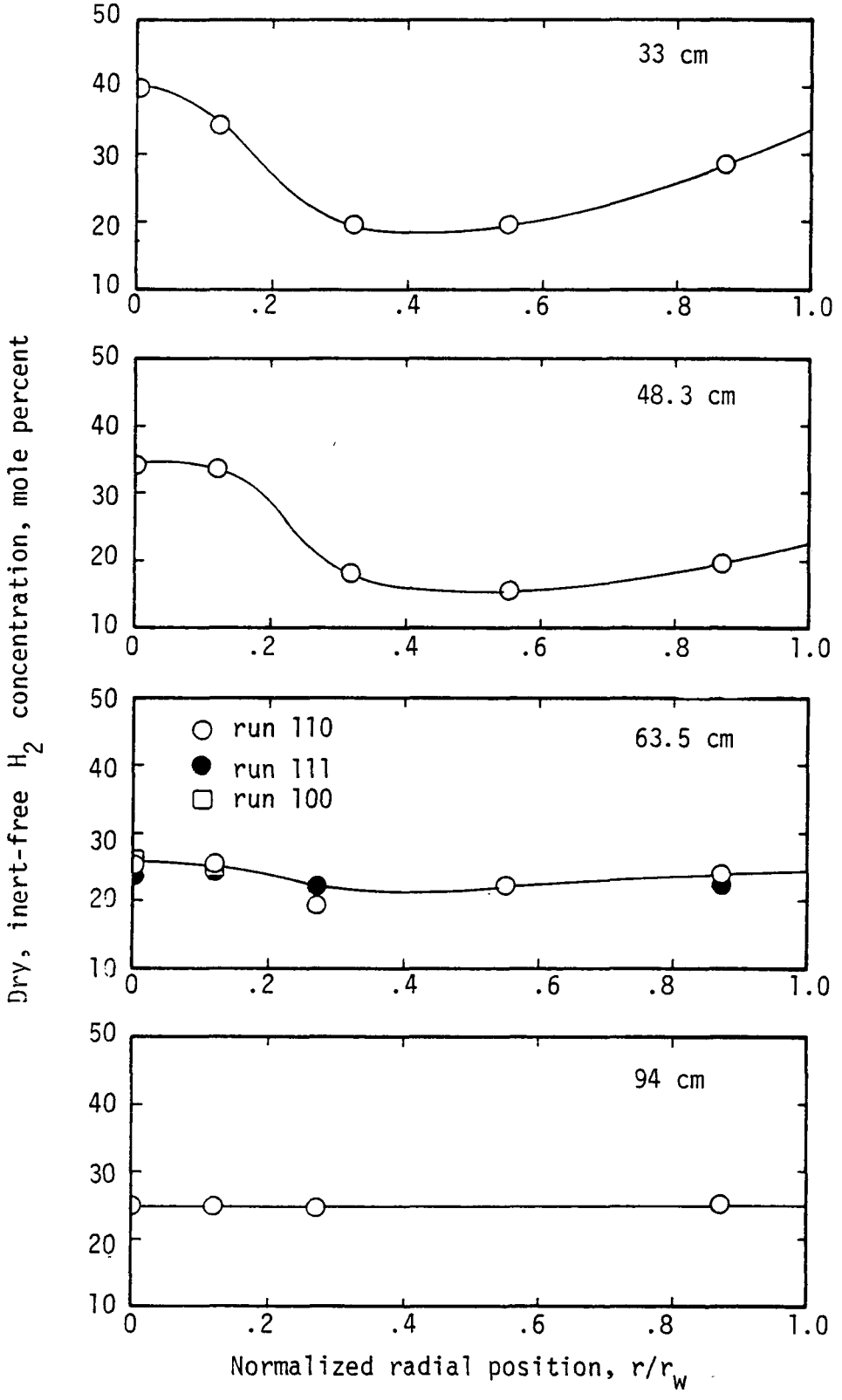

Figure 59. Radial profiles of hydrogen at specified axial locations.

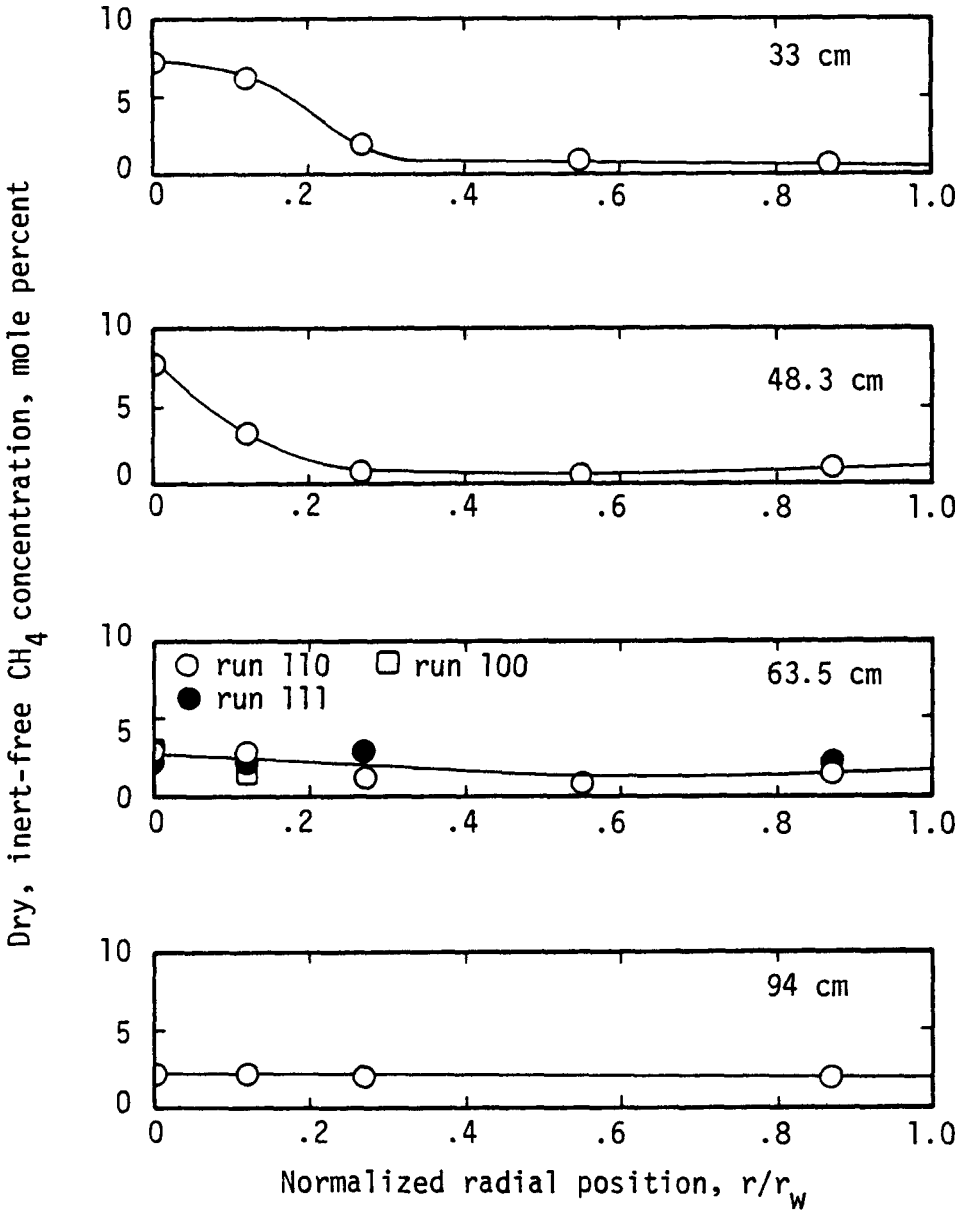

Figure 60. Radial profiles of methane at specified axial locations.

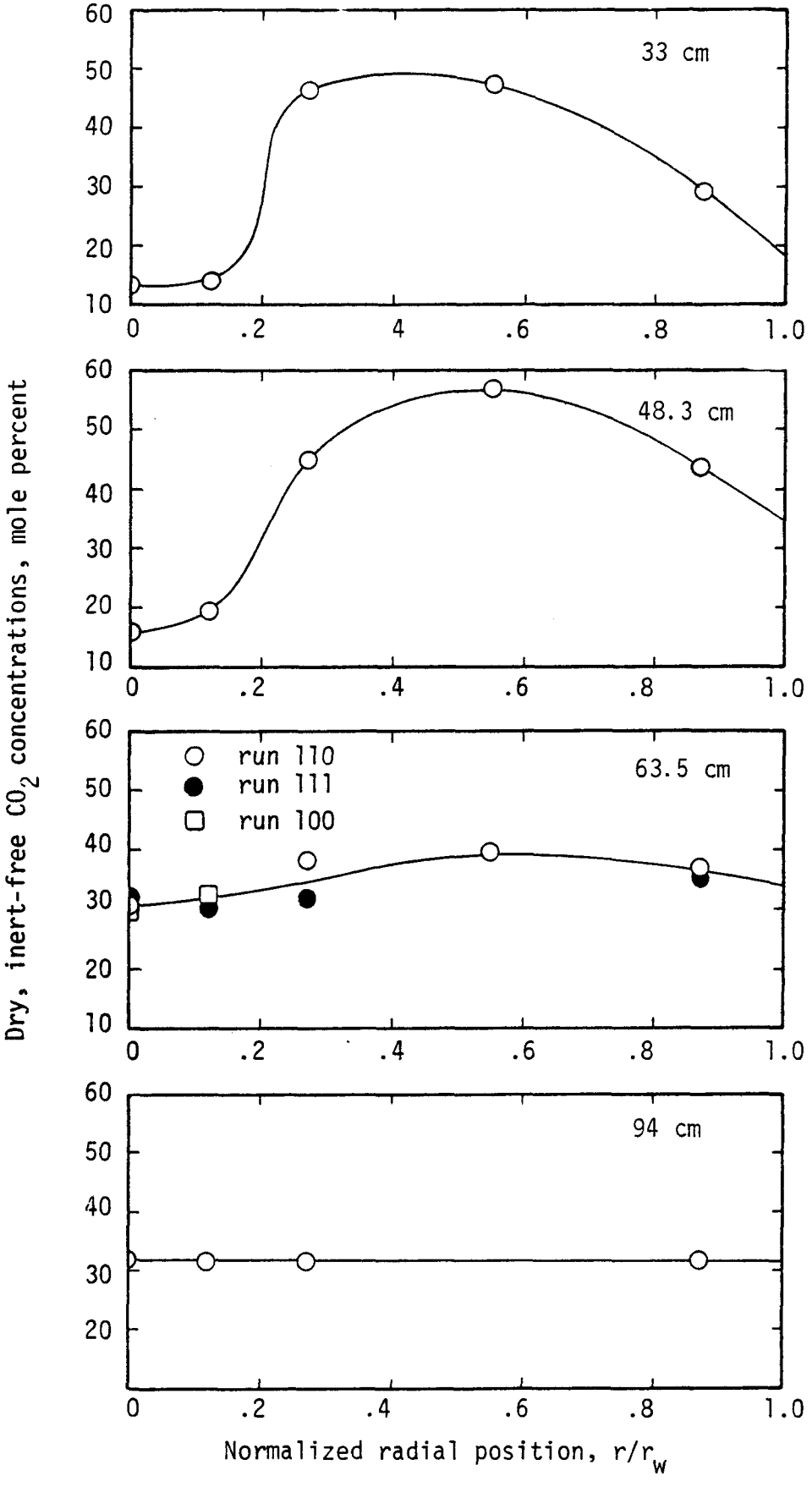

Figure 61. Radial profiles of carbon dioxide at specified axial locations.

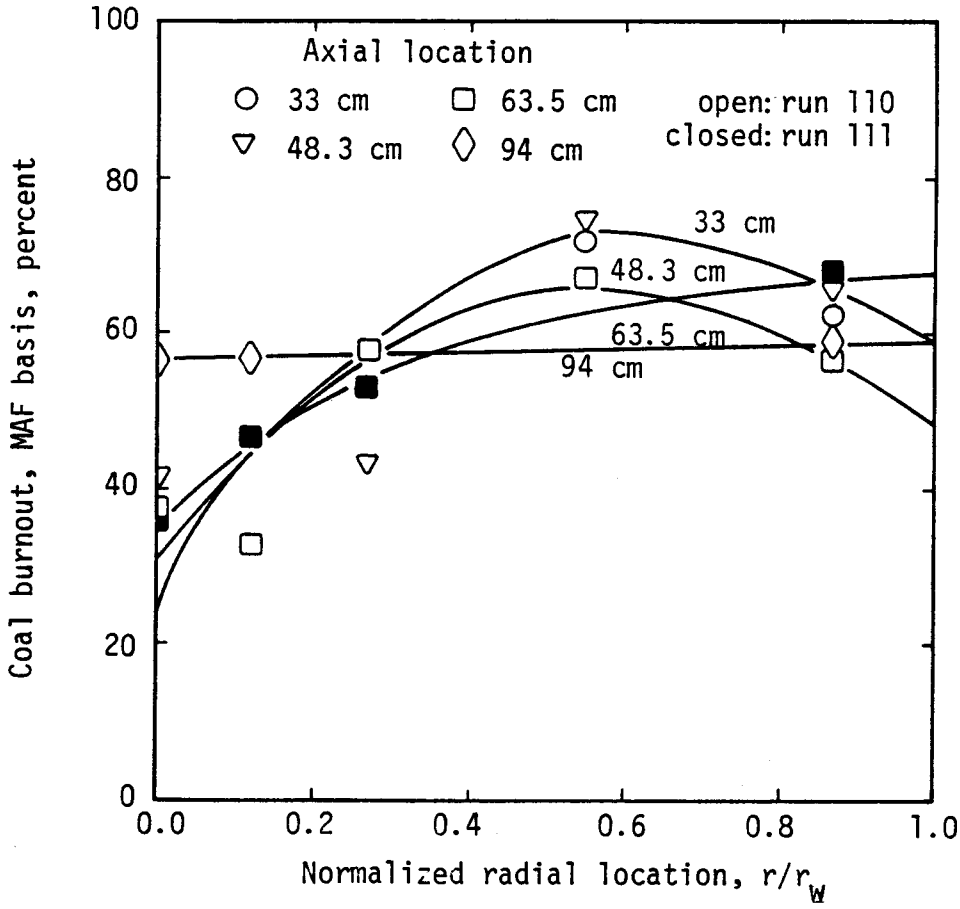

Figure 62. Coal burnout profiles.

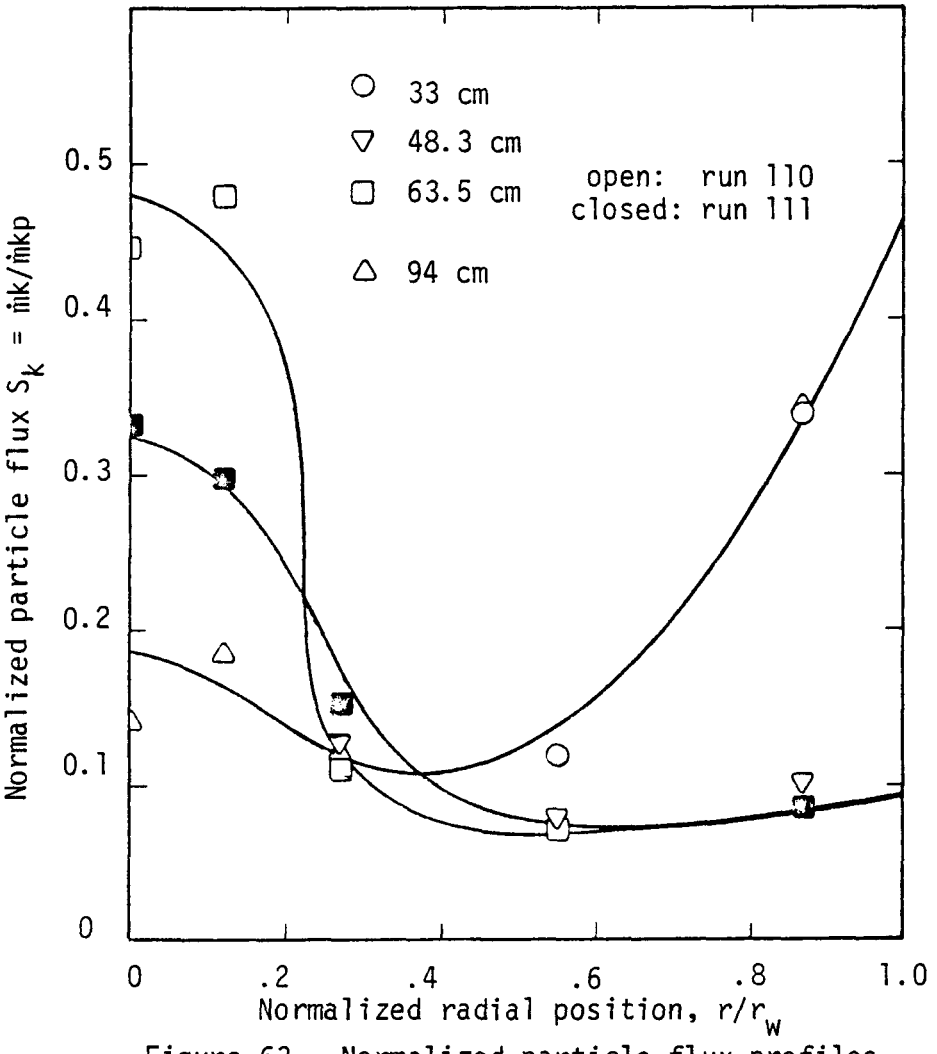

Figure 63. Normalized particle flux profiles.

mass flux normalized to particle mass flux in the primary jet, and includes both particle mixing and particle reaction effects. This particle dispersion parameter would approach a value of about 0.00031 for a fully reacted, fully mixed particle phase. These results suggest that the particles were not well mixed by the reactor exit. However, this is subject to considerable uncertainty, since material balances indicated that particle sampling was not nearly isokinetic.

It has been found (2-12) that the centerline decay of the gas mixing parameter, and the particle dispersion parameter can be used to obtain a measure of the gas and particle mixing rates. This technique was applied to both the gas and particle data obtained in these mapping tests and is shown in Figures 64 and 65. Figure 64 compares the centerline decay of the gas mixing parameter obtained in the coal gasifier with data from a similar-sized coal combustor with close to the same reactant feed rates (3). The data indicate very similar gas mixing trends but show that the mixing rate in the gasifier was somewhat less rapid than in the combustor. Similarly, Figure 65 compares the rate of particle dispersion and reaction in the gasifier to similiar data from the coal combustion (3). From these data, it appears that the coal in the gasifier generally dispersed and reacted less rapidly than in the combustor.

Pollutant Formation. Concentration levels of five pollutants, H_2S, SO_2, HCN, NH_3, and NO, were measured in each of the reactor mapping tests. The local concentrations are presented in Figures 66 (a-e) as a function of radius and at each axial test location. The effects of mixing and reaction on the formation of each pollutant is readily apparent. It can be seen from Figure 66 (b) that the major part of the H_2S is formed in the fuel-rich regions of the reactor. A significant amount of SO_2 is also formed in the fuel-rich regions as shown in Figure 66(f) but the major part is formed as the fuel is more totally consumed. The radial profiles for NH_3, HCN, SO_2, and H_2S show a sharp rise in concentration level toward the reactor wall, indicating the possiblity of recirculation within the reactor, and/or significant wall effects.

The formation of the nitrogen pollutants, HCN, NH_3, and NO closely parallel the results observed in the coal combustion study (3, 4). In general, however, the levels of HCN and NH_3 are larger than the levels in the combustor, and the level of NO tends to be smaller.

Axial interpolation of the radial profile data permitted pollutant maps of the gasifier to be constructed. These maps present pollutant iso-concentration lines within the reactor and give a qualitative measure of the regions within the reactor where a given pollutant is formed. Two example maps are shown in Figure 67 for H_2S and HCN. In general, the H_2S and HCN pollutants were both formed in a fuel-rich region of the flame where coal is pyrolyzing and excess quantities of hydrogen were measured. In addition, both maps show clearly the presence of recirculation, thus confirming that which was observed from the radial profiles. Price (18) has reported an extensive evaluation of these pollutant results and the reader is referred to that reference for more detail.

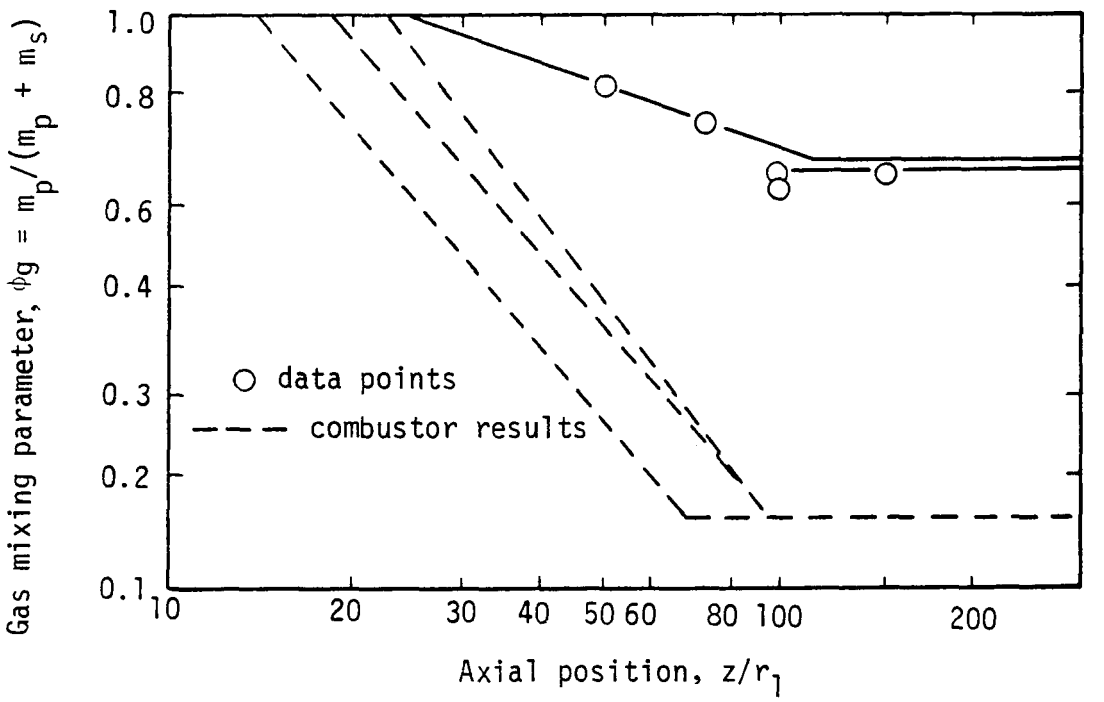

Figure 64. Axial gas mixing profile (O_2/coal = 0.83, steam/coal = 0.24).

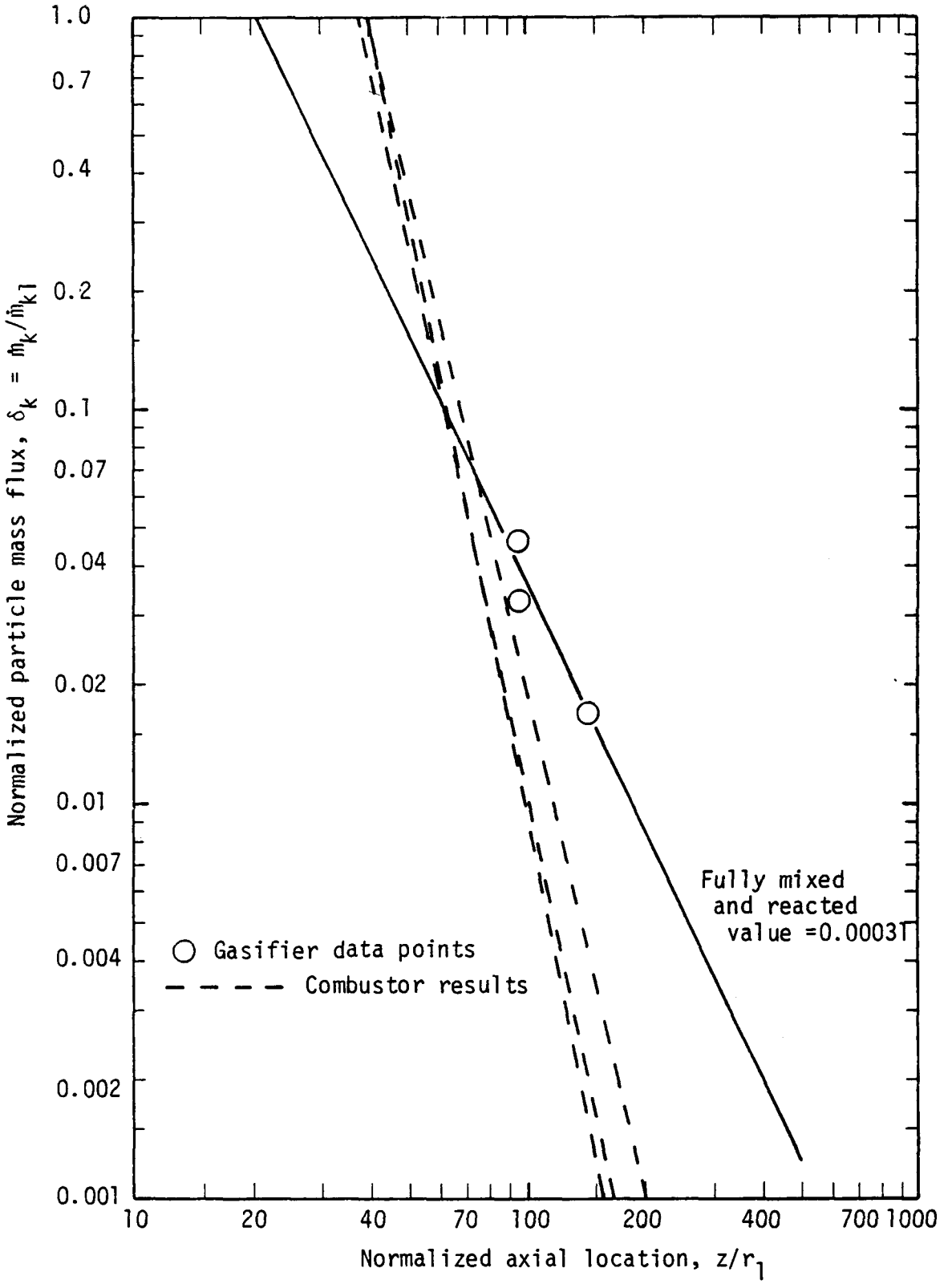

Figure 65. Normalized particle axial decay.

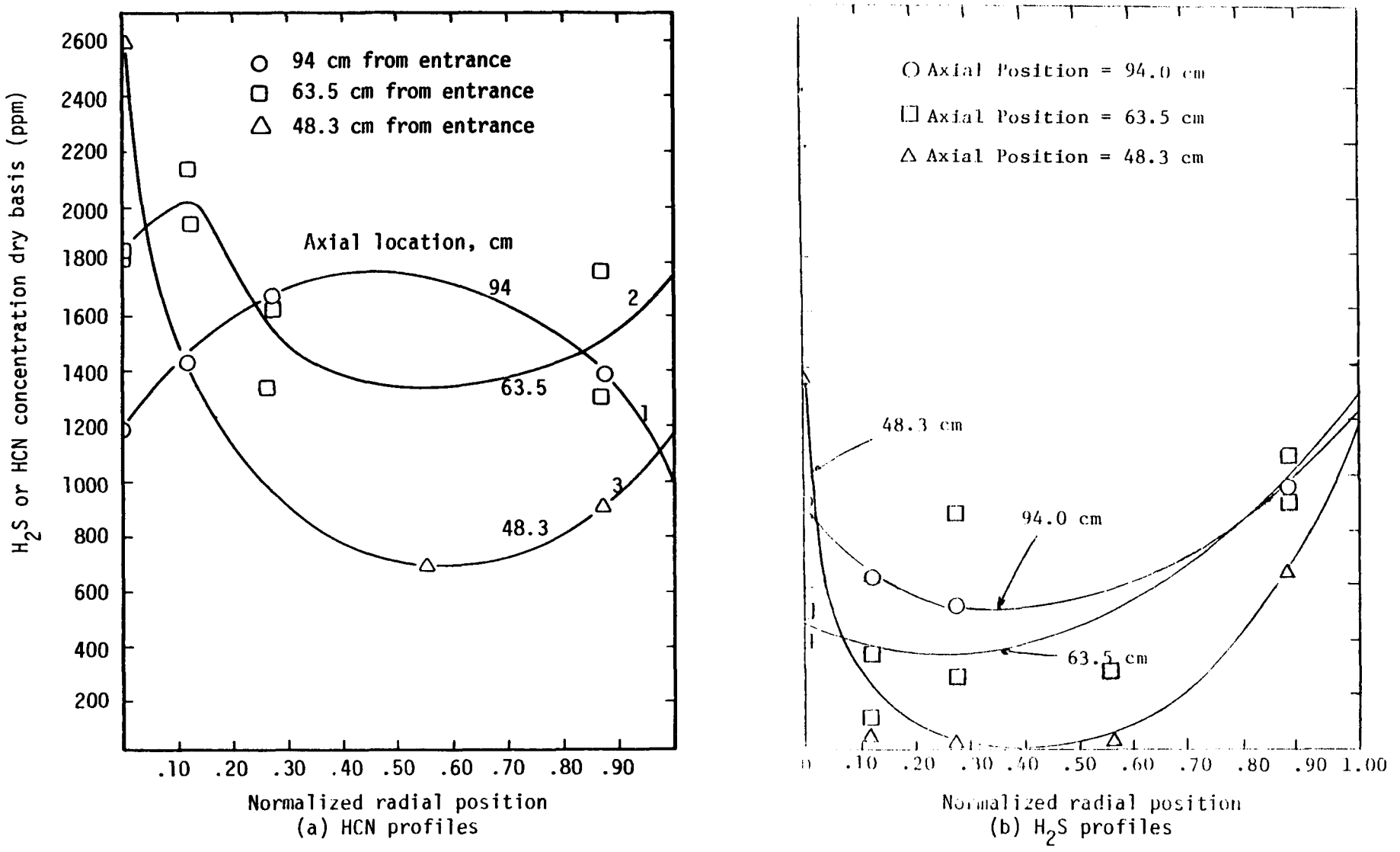

Figure 66. Pollutant concentrations at various radial and axial locations (dry basis).

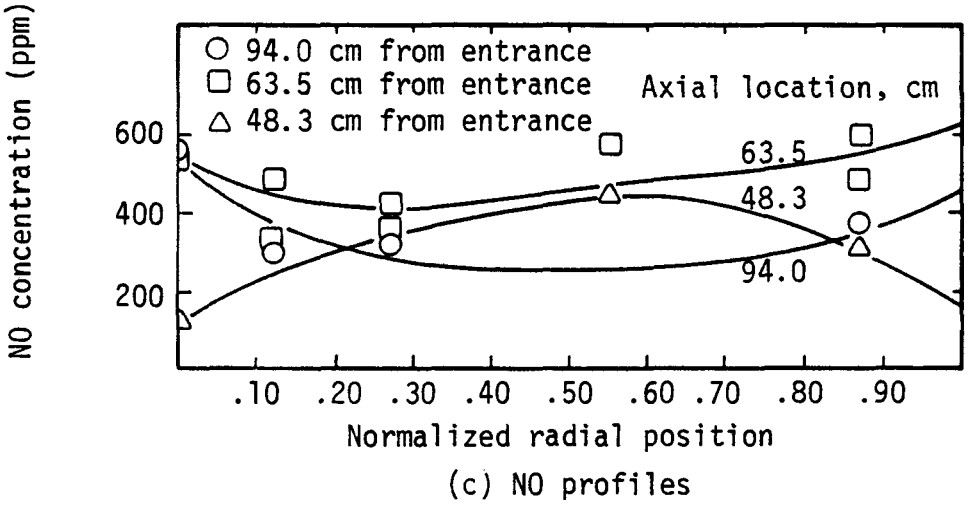

(c) NO profiles

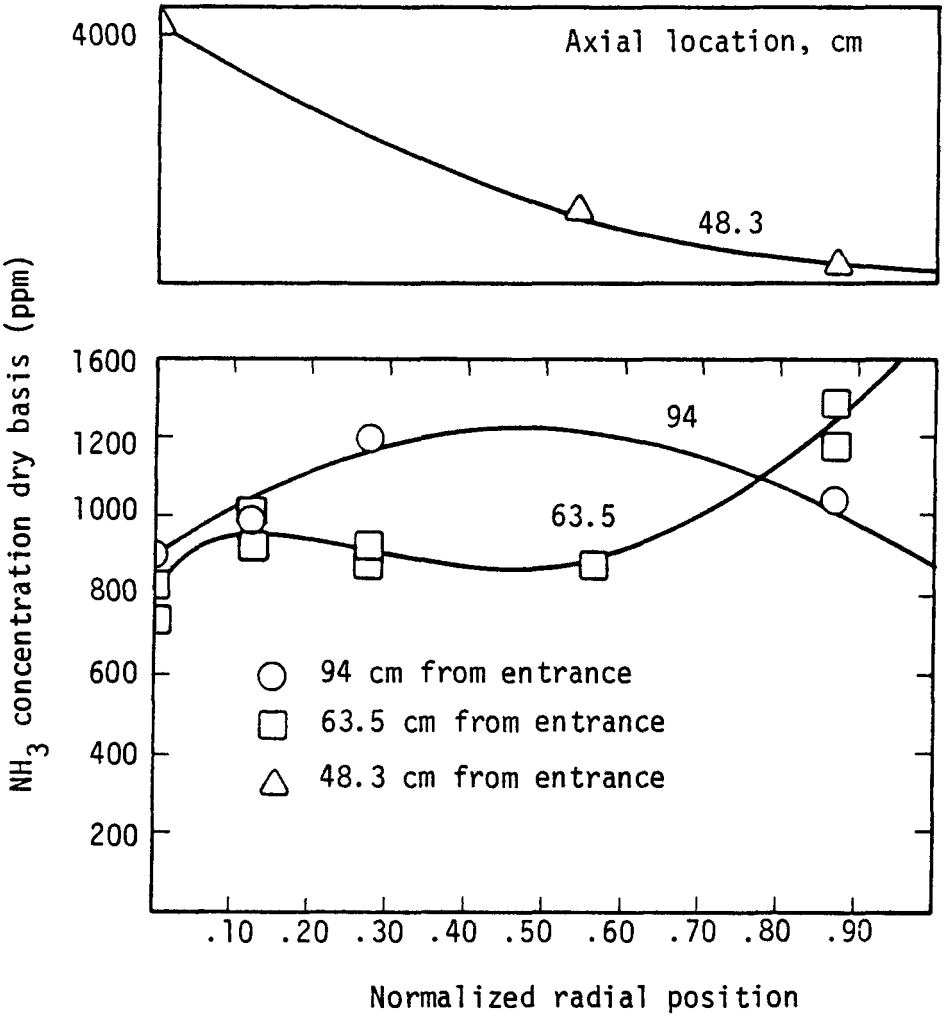

(d) NH_3 profiles

Figure 66. (Cont.)

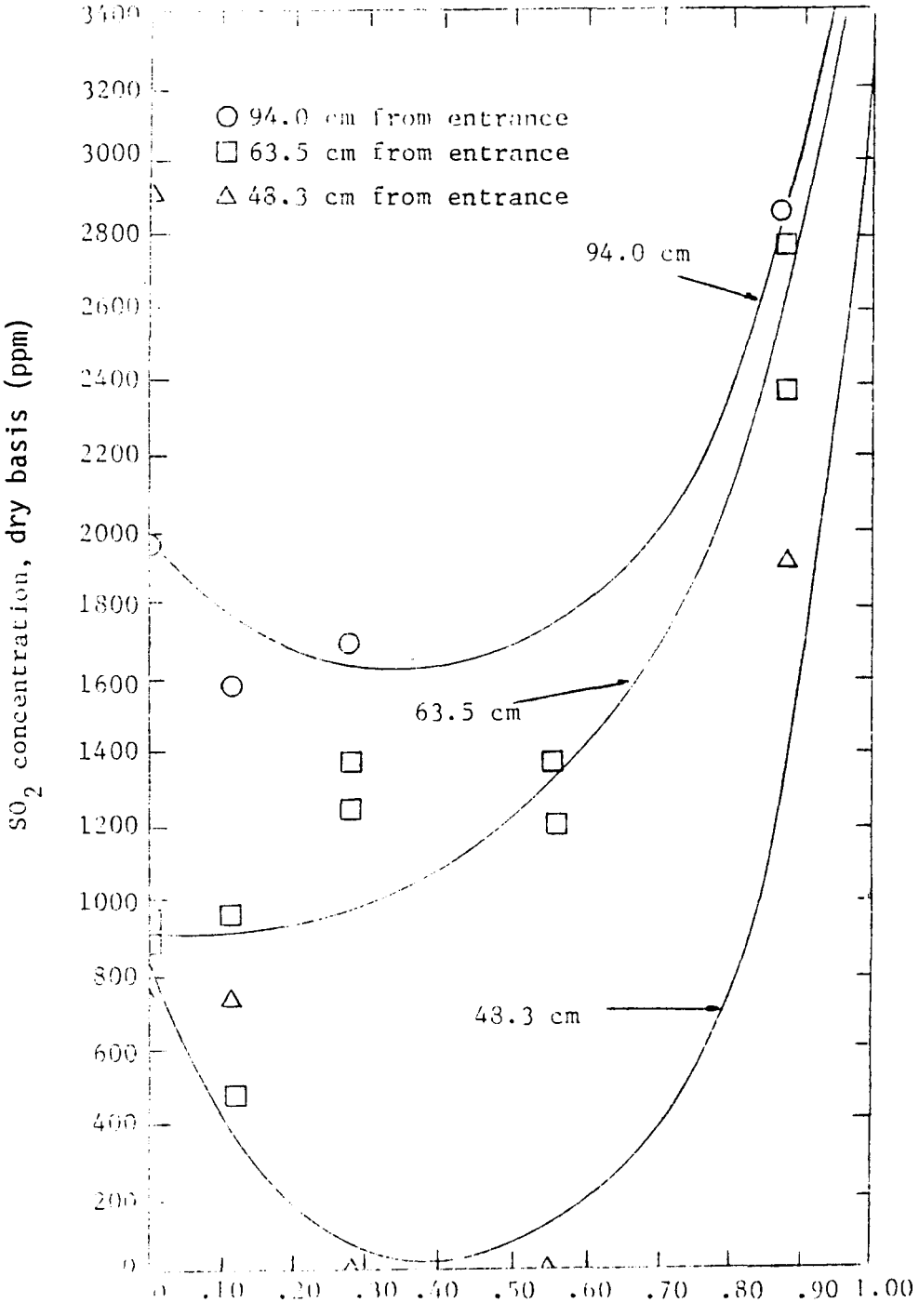

(e) SO_2 profiles

Figure 66. (cont.)

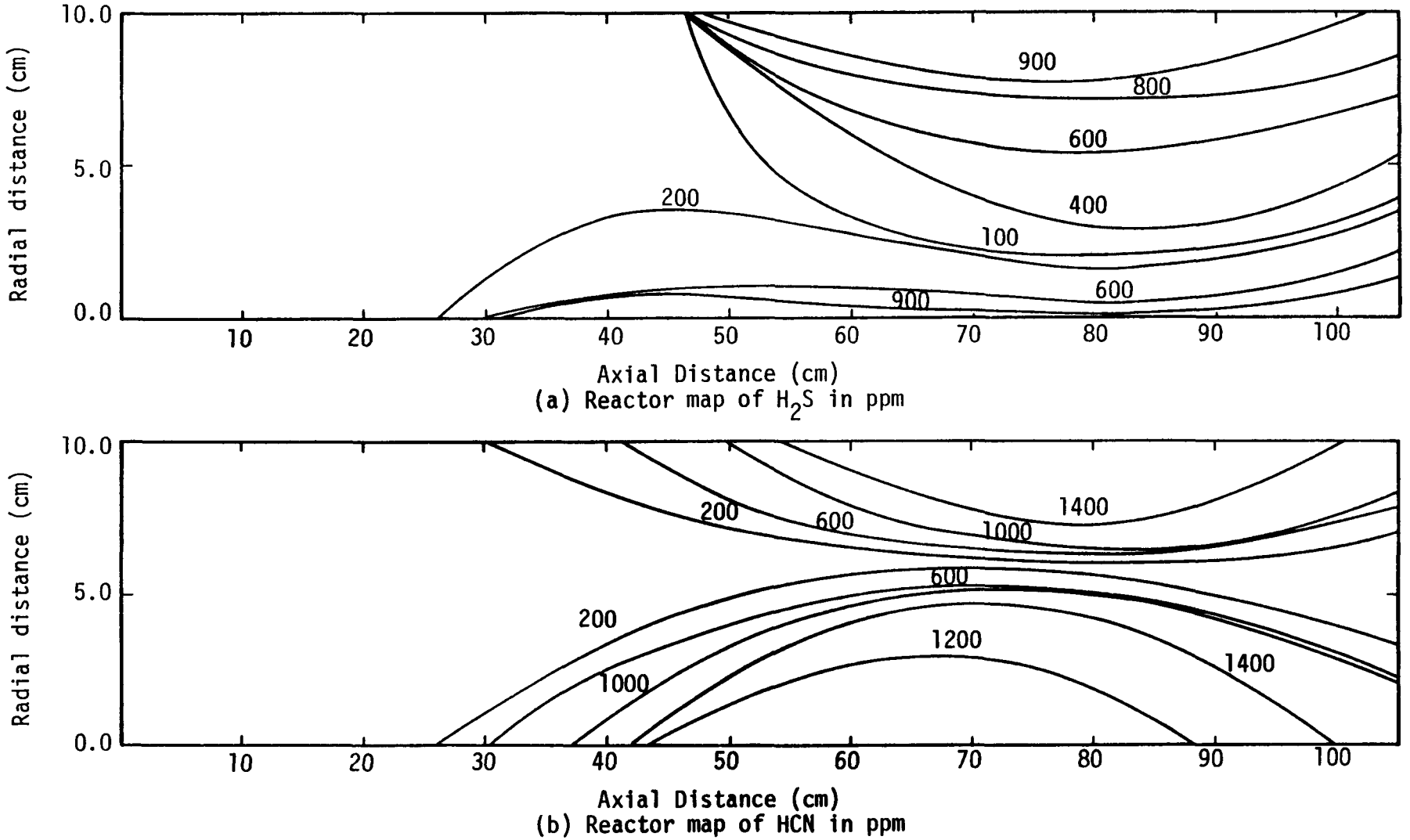

Figure 67. Selected pollutant reactor maps.

Material Balances. In performing material balances with data from the mapping study, it was discovered that sampling had not been isokinetic. Briefly, too much gas and particles were collected for sampling to have been isokinetic. Particle mass fluxes, when integrated over the area of the reactor, gave calculated coal feed rates which were too high. Correction was made for this situation by using a ratio of the calculated coal feed rate to the actual coal feed rate to calculate the amount of gas and particles which should have been sampled had the sampling been isokinetic. With this correction, mass balances were performed successfully. Approximately 80% of the sulfur was accounted for in the measured char-S, SO_2 and H_2S. Approximately 50% of the nitrogen was accounted for as char-N, HCN, NH_3, and NO. Most of the missing fuel nitrogen likely formed N_2. Thorough discussions of material balances for the reactor are reported by Skinner (17) and Price (18).

5. Test Series 4 - Pressurized Tests

a. Test Program

The objective of this test series was to investigate the effect of operating pressure on the gas and particle mixing rates and to obtain some basic gasification data at elevated pressure. As a first-step, a series of cold-flow experiments were planned in the entrained coal gasifier. The investigation of pressure effects on mixing rates required the use of the gasifier vessel because it was the only facility capable of operation at elevated pressure. The cold-flow experiments were also to serve as system evaluation tests to check-out the operation of the reactor probes and sampling systems at elevated pressure.

The program planned for elevated gasification experiments was patterned after the program used in the mixture ratio tests discussed above. Briefly, an O_2/coal ratio was to be set (e.g. O_2/coal = 1.0) and the steam/coal ratio was to be varied from 0.0 up to the maximum that would sustain reaction. Tests were planned at the same O_2/coal ratios used in the atmospheric mixture ratio tests namely 0.67, 0.83, and 1.0. Initial testing was to be accomplished at an intermediate pressure of 75 psia in order to gain experience in pressurized operation and to validate reactor and sample system operation. Additional tests at 150 psia and 300 psia were also considered. However, the extensive gasification test program conducted at atmospheric pressure precluded all but some preliminary atmospheric cold-flow experiments from being conducted.

b. Test Results

Twenty-two cold-flow experiments were performed in the coal gasification reactor. Six atmospheric cold-flow tests were conducted to check out the high pressure gasifier test facility, the probes and the sample collection system. Twelve additional atmospheric tests were conducted to check the accuracy of the sample collection system and to determine mixing rates in the coal gasifier at atmospheric conditions. A summary of objectives and general results for these tests is presented in Table 26.

TABLE 26

SUMMARY OF COLD-FLOW TESTS IN LABORATORY GASIFIER

Test No.	Objective	Results
1	Test control values, probes and sampling system - Gas only Probe collar at the 64 cm(a)	Control valves worked well. No sample in sampling system due to pressure inside sampling tanks. Evacuate tanks next time.
2	Test probes and sampling system - Gas only	Sample obtained. Wide variance in samples from chromatograph
3	Improve sampling system and gas chromatograph technique - Gas only	No. 3 sample bag leaked. Upstream orifice pressures not great enough
4	Obtain sample with new upstream conditions - Condition I(b) Gas only	Sample obtained. Data were not consistent.
5	Obtain sample - Gas only Condition I	Sample obtained. Gas chromatograph technique improving.
6	Condition II(c) - Gas only Obtain sample	Sample obtained. Accuracy of data improving.
7	Duplicate test 5	Fair consistency of data. The gas was well mixed.
8	Duplicate test 7	Better consistency.
9	Duplicate test 8	Good consistency. Need move probe collar up.
10	Probe collar at 33 cm(d). Test for core length - Gas only Condition I	Obtained good sample. Air-argon well mixed.
11	Obtain sample - Gas only Condition II	Sample obtained. Argon-Air well mixed.
12	Duplicate test 10	Sample showed good consistency. Air-argon well mixed. Need to move probes up.
13	Probe collar moved to 18 cm(e) Obtain sample - Gas only Condition I	Sample obtained. Air-argon well mixed. Slight profile. Recirculation observed.

TABLE 26 (Cont.)

Test No.	Objective	Results
14	Obtain sample at Condition II - Gas only	Sample obtained. Slight profile. Recirculation observed.
15	Duplicate test 14	Good consistency of data with test 14. Small profile. Need to move collar up.
16	Duplicate test 13	Good consistency with test 12. Small profile. Need to move collar up.
17	Probe collar moved to 2.5 cm Obtain sample - Gas only Condition II	Sample obtained. Profile obtained. Recirculation ovserved.
18	Condition I - Gas only Obtain sample	Sample obtained. Good profile. Recirculation observed. Need to sample between 2.5 cm and 18 cm
19	Test back-pressure regulator	Leaks of air in reactor connections.
20	Test back-pressure regular up to 45 psig	Regulator worked fine. Small leakage in the reactor system.
21	Test reactor, air control system, and regular up to 90 psig	Unable to reach 90 psig due to leak in scrubber.
22	Test up to 90 psig	Regulator worked fine. Small leaks in reactor

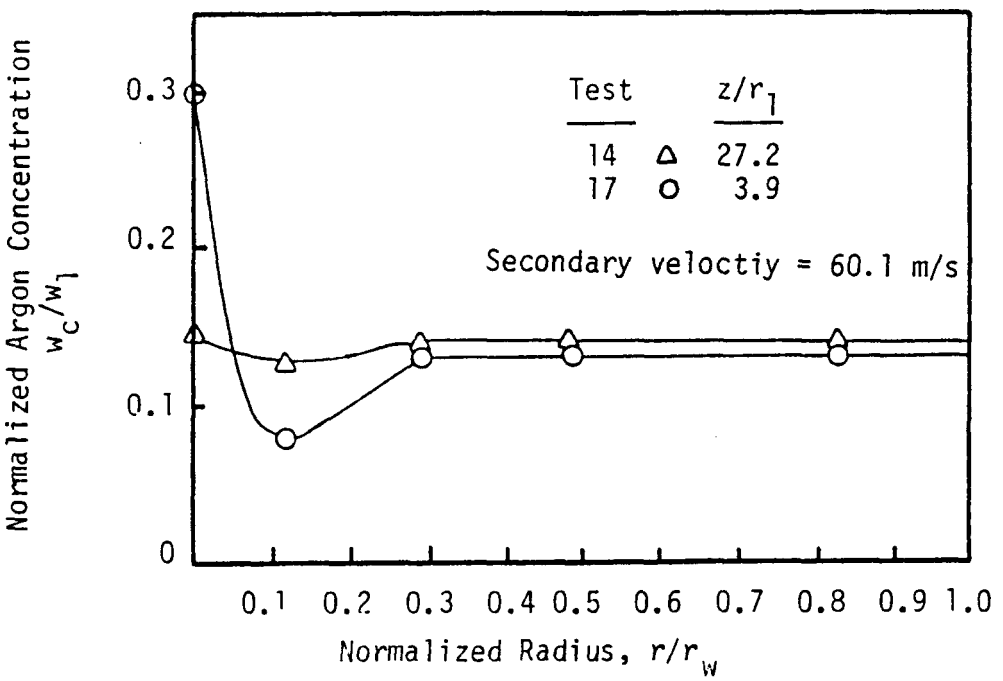

Figure 68. Preliminary radial decay plot for air argon mixing in the coal gasifier.

Several modifications were made to the existing air supply facility to handle high pressures for the high-pressure, cold-flow coal air tests. Pipe fittings and pressure gauges were installed that were suitable for the desired pressure range. Transducers, thermocouples, switches and wiring were designed and installed in the existing air flow control apparatus in order to have accurate control over high pressure air flow. The final pressure in the reactor was controlled with a back-pressure control valve.

Four preliminary tests were completed to check out the system (high pressure controls, coal gasifier, water scrubber and back-pressure regulator) at pressures of 45 psig and 90 psig. The objectives and results for these pressurized tests are also summarized in Table 26.

Preliminary radial gas composition profiles were obtained for atmospheric tests with primary and secondary velocities of 38.5 and 60.1 m/sec respectively, and are shown in Figure 68. These results show that essentially complete gas mixing was obtained by the axial location of 18 cm ($z/r_1 = 27.2$).

H. MAJOR ACCOMPLISHMENTS AND CONCLUSIONS

1. Accomplishments

The following accomplishments were completed in the coal gasification test program:

1. The design, construction, and check out of a unique, highly instrumented, laboratory-scale entrained coal gasifier.

2. The development of workable, water-quenched sampling probes and a gas-liquid-solid sample collection and analysis system.

3. The ignition and stabilization of methane-oxygen diffusion flames in the gasifier which are used for reactor preheat.

4. The ignition and stabilization of coal-oxygen and coal-oxygen-steam diffusion flames in the gasifier.

5. The demonstration of the operation of the laboratory gasifier to obtain reliable data on reaction and mixing rate processes.

6. The completion of a total of 114 tests to check out various components of the system, to develop the sample probes and sample collection system and to collect test data.

7. The collection of final gasification test data (15 tests) at various operating conditions (O_2/coal and steam/coal ratios) near the reactor exit.

8. The collection of final gasification test data (5 tests) at five different radial locations and four different axial locations to map the gas and particle mixing rates and chemical reaction rates within the reactor.

9. The completion of 22 preliminary cold-flow mixing tests in the gasifier to prove cold-flow sampling techniques and validate reactor operation at elevated pressure.

10. The development of a technique for measuring local gas-particle mixing rates in a reacting system.

11. The development of data analysis methods for presentation and comparion of local gasification data.

12. The use of collected data from the entrained coal gasifier to:

    a. Determine the relative rates of release of the individual coal components (C,H,N,O.S).

    b. Measure the extent of coal burnout at a location near the reactor exit for various O_2/coal and steam/coal mixture ratios and at various radial and axial locations within the reactor at a specified test condition.

    c. Evaluate the effect of O_2/coal and steam/coal ratios on gas composition, H_2/CO ratio, carbon conversion, and gas heating value.

    d. Evaluate theoretically-formulated computer codes which model the gasification processes.

13. Determination of pollutant gas concentrations in the entrained flow gasifier:

    a. Demonstrated the utility of specific ion electrodes in analysis of CN^-, S, and NH_4^+.

    b. Showed the effects of filtration on concentrations of $S^=$, CN^-, and NH_4.

    c. Investigated the effects of oxygen and char on concentrations of $S^=$, CN^-, and NH_4^+ in aqueous solution.

    d. Developed a workable scheme for the analysis of quench water coming from sample collection vessels.

    e. Determined reactor operating conditions which yielded minimum formation of H_2S, HCN, NH_3, and NO pollutants.

Conclusions

Specific conclusions and observations from the laboratory-scale entrained gasifier data collected and analyzed during this research study are summarized below and in detail by Skinner (17) and Price (18):

1. There are significant radial gradients in coal particle flux, coal burnout, gas composition, and pollutant composition at the near exit position tests (63.5 cm from injection).

2. Evidence of recirculating flow was observed in the upper regions of the reactor.

3. Hydrogen is released from the coal more rapidly than carbon. Sulfur and nitrogen are released at essentially the same rate as carbon.

4. Individual coal component release (including C, H, N, O, S) did not appear to vary greatly from one test condition to another the release seems to depend principally upon the extent of coal burnout.

5. Gas mixing which was not completed until near the exit of the reaction (ca 94 cm) had an influence on the extent of reactions in the gas phase and on the particle reactions.

6. Particle dispersion and reaction were not completed within the length of the reactor which lead to incomplete particle burnout.

7. The maximum coal throughput for stable reactor operation at atmospheric pressure (24.5 kg/hr) is consistent with the previous experience of the Morgantown G1, G3, and G4 coal gasifiers as well as others.

8. Flame stability limits of the reactor were a function of mixture ratios and ranged from 0.24 kg steam/kg coal at an oxygen ratio of 0.6 kg O_2/kg coal to 0.54 kg steam/kg coal at an oxygen ratio of 1.0 kg O_2/kg coal.

9. Major nitrogen pollutant species observed in the gasifier were NH_3, HCN, and NO which ranged in level from 258 to 4080, 10 to 3334, and 1 to 1050 ppm respectively, depending on operating conditions and location within the reactor. In the mapping tests, about 50% of the fuel nitrogen was accounted for which suggested significant N_2 formation.

10. The levels of H_2S pollutant for all final tests and SO_2 pollutant for selected final tests ranged from 0 to 2458 and 0 to 2920 ppm respectively, depending on operating conditions and location within the reactor. In the mapping tests, about 80% of the fuel sulfur was accounted for.

11. The dry, inert-free gas heating values ranged from about 160 Btu/scf to 280 Btu/scf while the carbon conversion ranged from about 42% to 70% depending on operating condition.

IV. ENTRAINED GASIFIER MODELING

A. OBJECTIVES AND APPROACH

In order to optimize design of coal gasifiers, a better understanding of the detailed mechanisms within the reactor is needed. The development of a theory for such a system in the form of a numerical computer model helps not only with understanding and interpretation of data but is an essential tool in engineering design optimization.

Past technology for describing and analyzing pulverized coal reaction systems relied heavily on empirical inputs for the complex flow and chemical reactions occurring while more formally treating the radiative heat transfer effects. The objective of this study was to develop working computer models to help in interpreting experimental data and in designing combustion and gasification systems. The specific models developed were: 1) a one-dimensional pulverized coal combustion or gasification model, and 2) a two-dimensional, axi-symmetric, turbulent gaseous combustion model as a basis for a two-dimensional coal gasification model. These models were evaluated by comparison with experimental measurements obtained at this Combustion Laboratory and with other measurements.

B. ONE-DIMENSIONAL CODE

1. Background

1-DICOG (1-DImensional Combustion Or Gasification), the one-dimensional, steady-state model describing pulverized coal combustion and gasification, was initiated under previous EPRI and ERDA contracts (2-4). While emphasis was placed on the description of the coal reaction processes and gas-particle interactions, one-dimensional fluid mechanics and particle-particle, particle-wall radiation were included. Moisture vaporization from the coal particles, multi-step coal pyrolysis, and heterogeneous char oxidation by multiple oxidizers were modeled for poly-dispersed coal particle sizes or types. Although the formulation was one-dimensional, mixing rates of primary and secondary streams and recirculation within the reactor were accounted for as specified input. The resulting model predicts thermal, chemical and physical histories for both the gaseous and particle phases. Gas phase reactions were assumed to be in local chemical equilibrium. The solution technique used predictor-corrector methods for integration of the ordinary non-linear differential equations, which were coupled with a number of auxiliary algebraic equations. An iterative approach was required for the radiant heat transfer calculations by the zone method. Stiffness in differential energy equations was overcome by a pseudo steady state method when needed. The generalized nature of the model allowed for calculation of both coal combustion and coal gasification characteristics.

Complete documentation of the model including solution techniques and user's information is included in Volume 2 of this report, the 1-DICOG

User's Manual. For this reason, and since the code developed was reported in detail in a previous report (4), the detailed documentation is not repeated here. A summary of code applications accomplished during this study is presented below.

2. Summary of Model Predictions

1-DICOG has been applied to predicting characteristics of laboratory and industrial pulverized coal combustors and entrained coal gasifiers. In particular, model predictions have been compared to profile measurements from the B.Y.U. laboratory scale pulverized coal combustor and entrained coal gasifier. Computations have also been made for the BI-GAS Gasifier, the Coates Gasifier, the first stage of a Babcock and Wilcox staged combustor, and the gasification stage of an industrial design for a hydroliquifaction process. Selected experimental measurements have also been compared with model predictions.

A brief summary of all final converged predictions made with 1-DICOG is shown in Table 27. This does not include any of the computations required for model development or debug, nor does it show any of the unsuccessful computer runs. A total of fifty converged runs were made and are shown in this table.

Laboratory Gasifier Predictions. Preliminary model predictions based on initial design operating conditions (2) were made for the BYU Rate-Resolution Gasifier (see Section 3). These calculations shown in Figures 69 and 70 indicated that with a single coal particle size of 60 μm, char burnout was not quite complete in the gasifier length of 1.12 m. These results also indicated that gasification in the laboratory reactor was affected by the mixing and recirculation processes. Also, pyrolysis and subsequent oxidation of the pyrolyzate is very rapid in the gasifier. Oxygen was depleted during devolatilizaton, and the oxidation of the char with steam and carbon dioxide followed slowly.

Industrial Gasifier Predictions. Foster-Wheeler Energy Corporation has considered the design of a hot-flow model of a two-stage, entrained-flow gasifier under DOE contract EX-76-C-01-1521. The unit is to have a coal feed charge rate of 680 kg/hr (1500 lb/hr) and operate at approximately 1480 kPa (200 psig). This version is directed toward the production of low-BTU gas to serve as fuel for gas turbines. In cooperation with Foster Wheeler Energy Corporation, the 1-DICOG code was used to predict the behavior of the first stage. This application of the code furthered the model development in three ways. First, it showed that the model could be applied to larger scale equipment. Secondly, model development was advanced to allow for char feed. Previously, only coal with some volatile component had been used in the model. The Foster Wheeler gasifier stage used char feed which had already been completely devolatilized. Finally, the predictions for poly-dispersed coals made for Foster Wheeler included 1000 μm particles. The results shown in Figures 71 and 72 dramatically illustrate the effect of such large particles in entrained flow systems. The relatively slow heating of these particles retarded the entire system. The burnout of these large particles was insignificant.

TABLE 27

SUMMARY OF 1-DICOG PREDICTIONS

Reactor	Total Number of Predictions	Comments
BYU combustor	35	9 predictions to study effect of particle size distribution 6 predictions to study recirculation and/or secondary mixing 4 predictions to examine effect of different model options 10 predictions to evaluate controlling rate processes and/or effect of rate constants 6 predictions to study pollutant issues
BYU gasifier	2	1 calculation for premixed system and 1 prediction with secondary mixing and recirculation
Foster-Wheeler gasifier	5	Parametric studies on effect of wall temperature, particle burnout model, and size distribution
BI-GAS gasifier	2	Radiation calculated as a diffusion process
Coates gasifier	1	Two expansions in reactor geometry with different wall temperatures
Babcock and Wilcox combustor	3	Studied effect of recirculation, different oxidizers, particle size distribution
Industrial hydro-gasification stage	2	Studied effect of hydrogasification rate constants
Total	50	

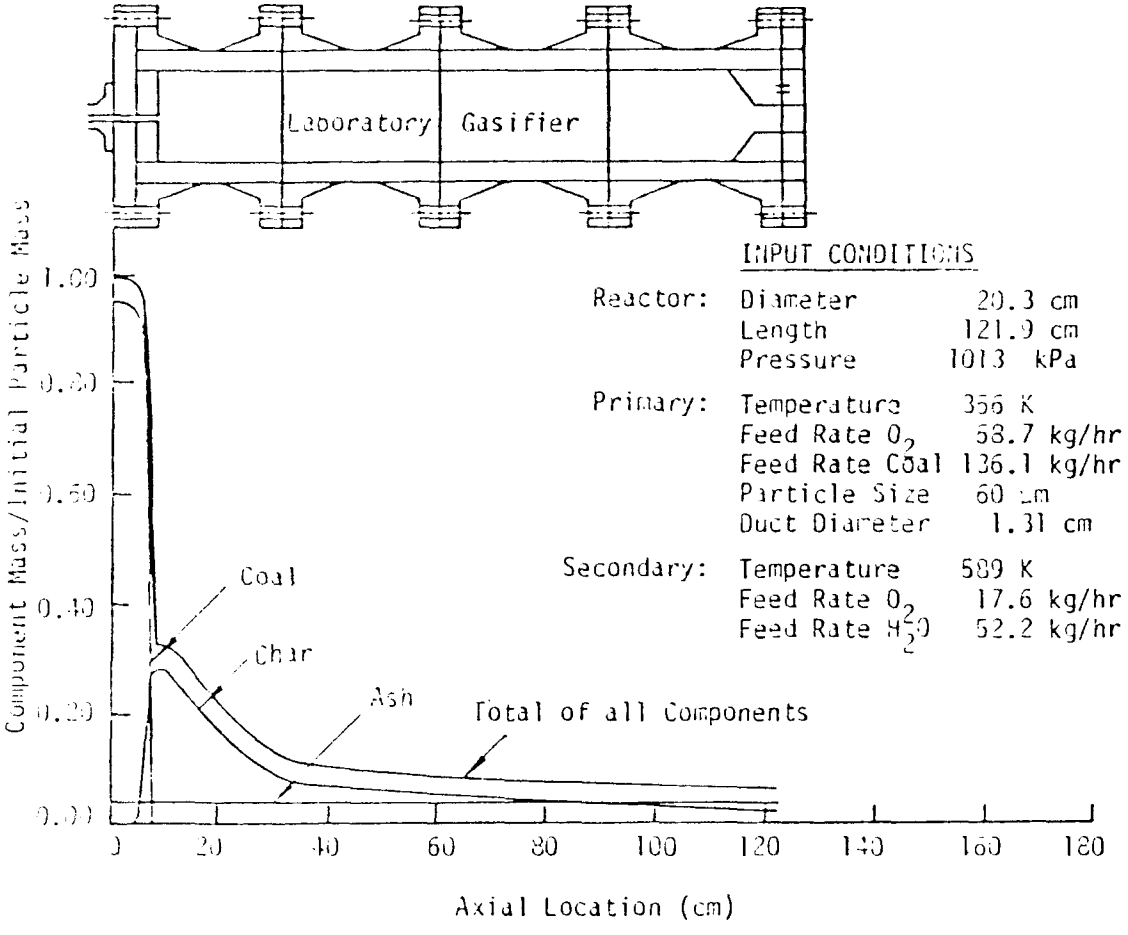

Figure 69. Predicted particle mass history for laboratory gasifier.

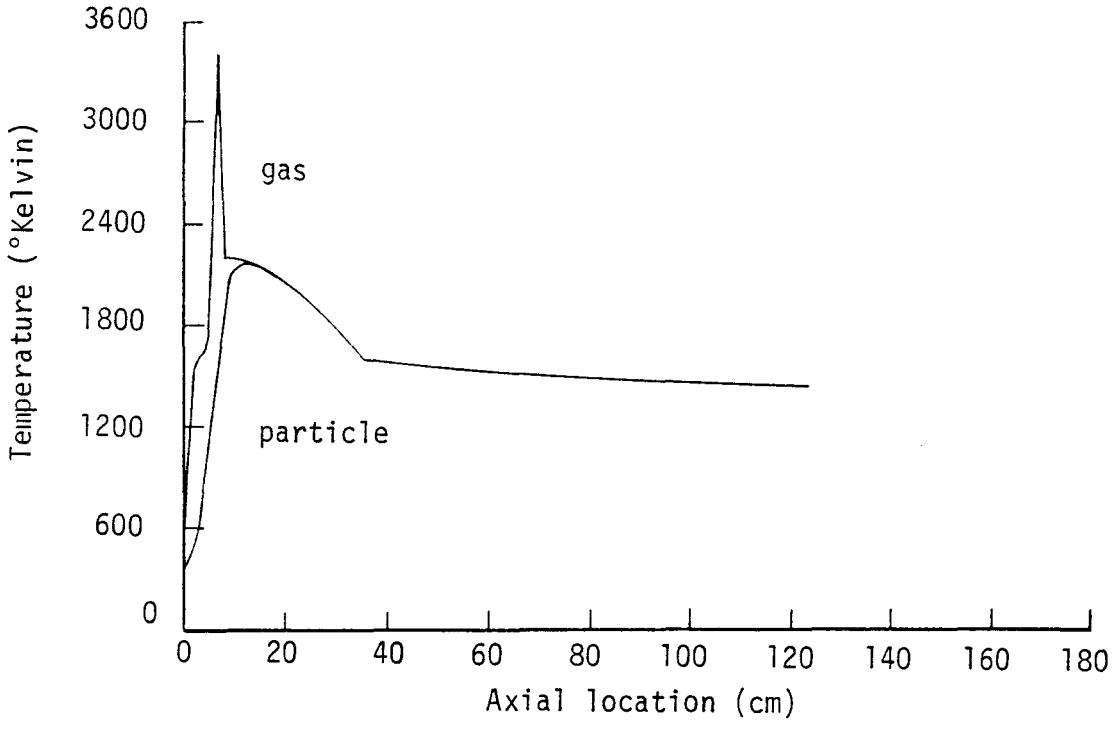

(a) Particle and gas temperature

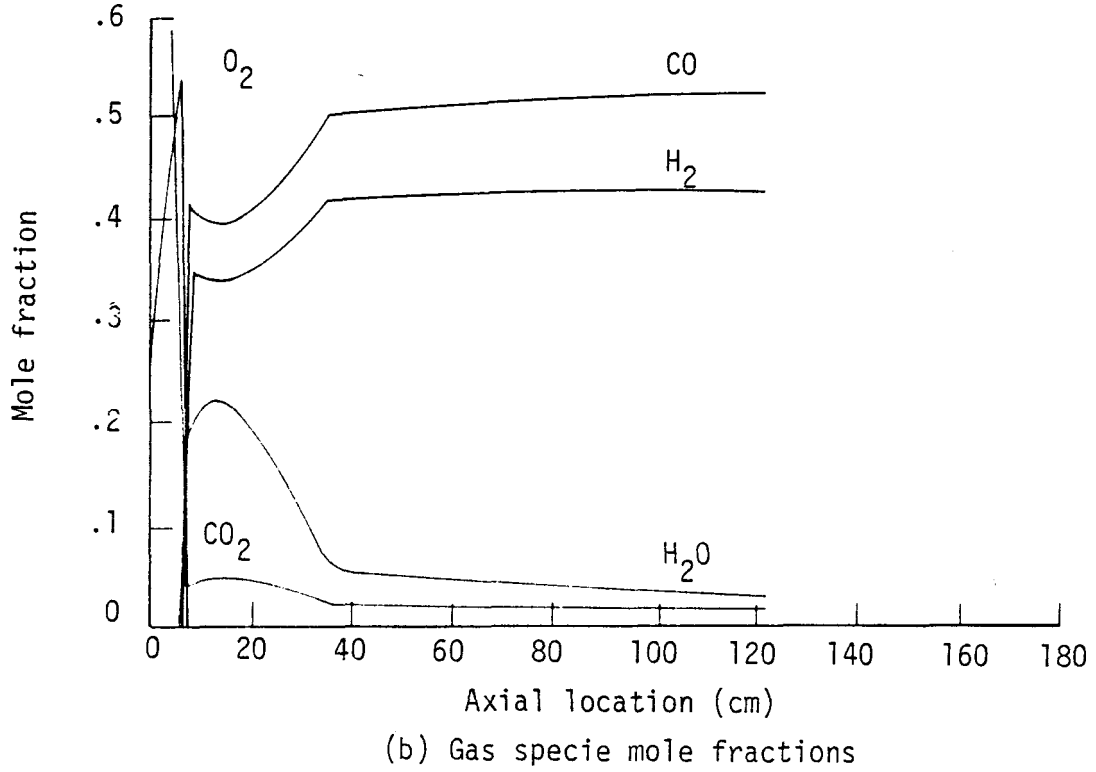

(b) Gas specie mole fractions

Figure 70. Predicted temperature and species profiles for laboratory gasifier

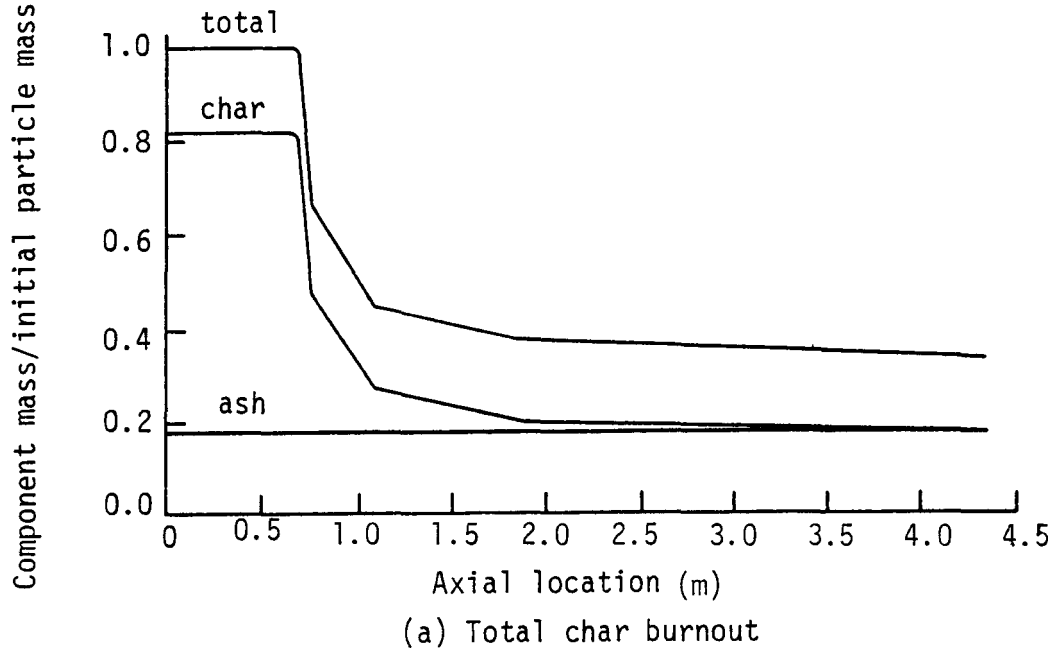

(a) Total char burnout

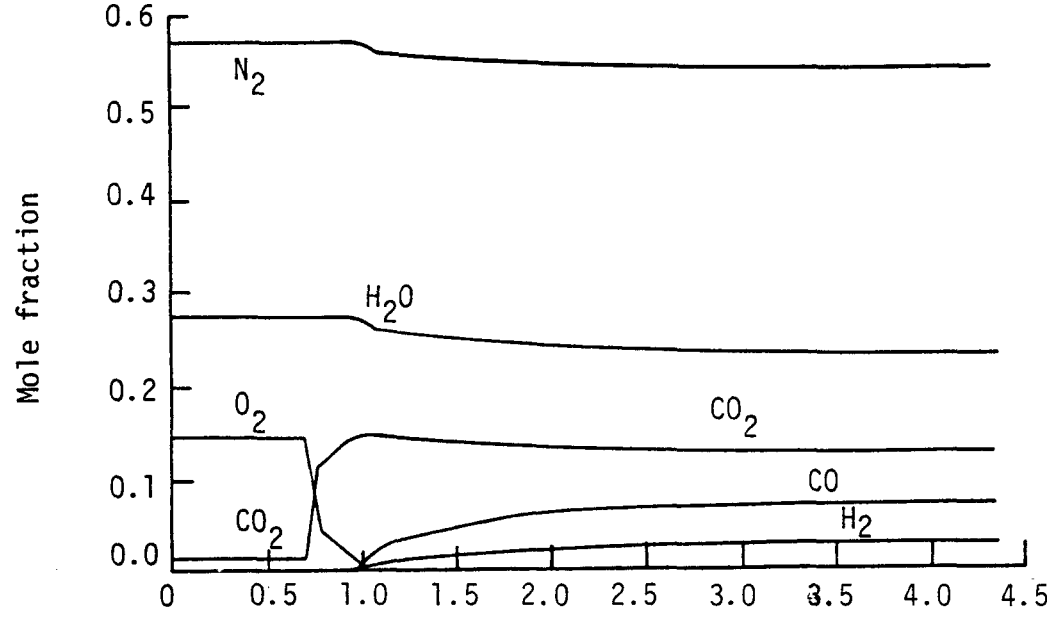

(b) Gas composition

Figure 71. Predicted particle mass and gas composition for Foster-Wheeler gasifier.

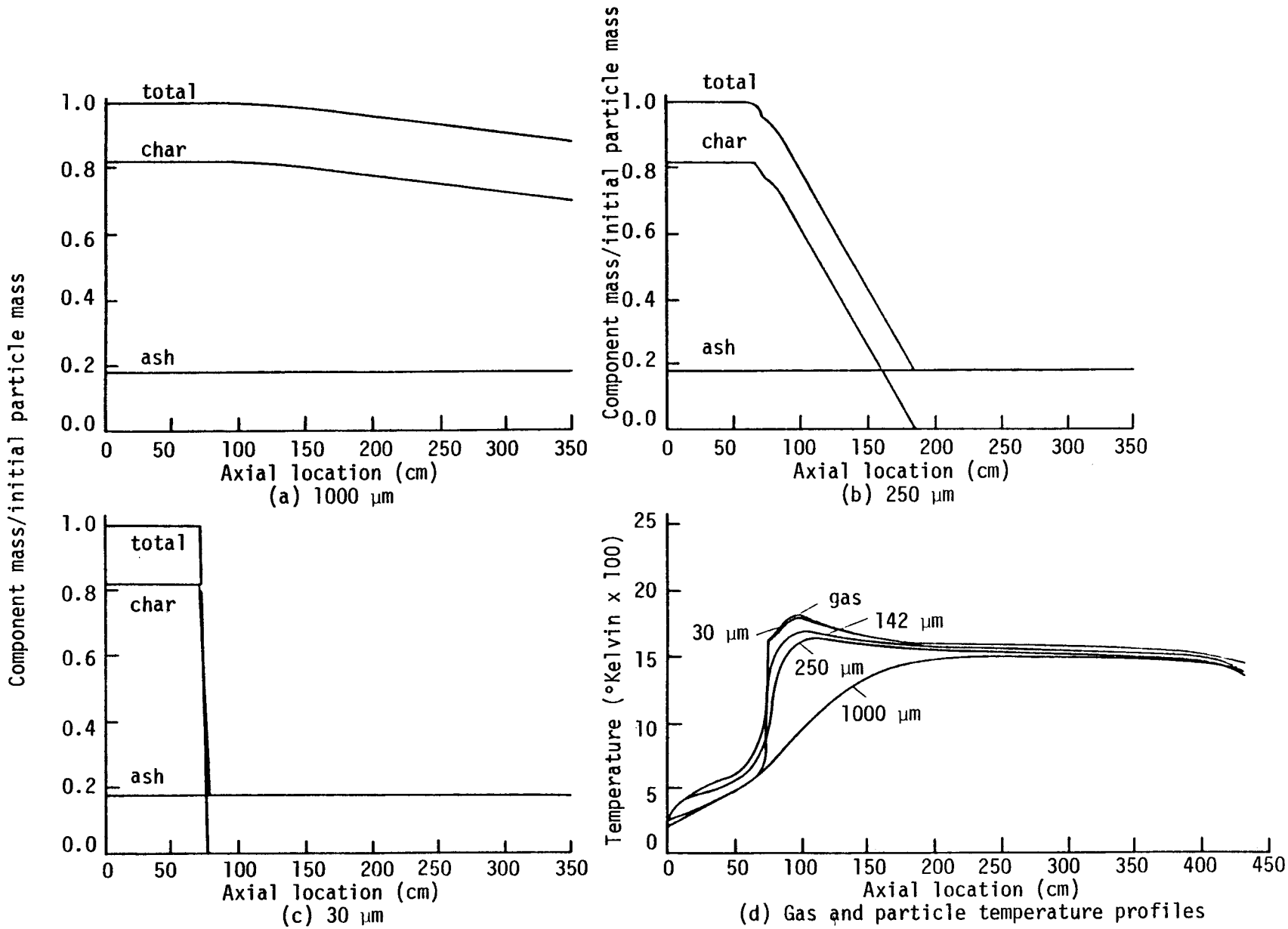

Figure 72. Predicted mass history and temperature for various particle sizes in Foster-Wheeler gasifier.

Comparison with Laboratory Combustor Data. The Rate-Resolution Combustor is a laboratory scale, pulverized coal combustor developed at the Brigham Young University Combustion Laboratory. Detailed test results are discussed by Thurgood (32).

Figure 73(a) shows model predictions for polydispersed particles (five separate particle sizes) compared with laboratory combustor measurements of coal particle burnout as a function of reactor length. The experimental points were determined by integrating the measured particle mass flux over the cross sectional area at each of the five axial stations. These points are then compared with the predicted total particle mass history. Figure 73(b) shows the measured and predicted gas phase mole fractions for the same case. Experimental gas mass flux measurements were not available so the points plotted depict a radial average of the mole fractions.

The reason for such good agreement between laboratory measurements and predictions by 1-DICOG was thought to be due in part to the one-dimensional nature of the laboratory combustor. By virtue of its size and feed rate, the combustor was found to have rapid mixing of primary and secondary gases. Particle ignition occurred later in fully mixed gas environment and particle combustion was thus not significantly affected by the gas mixing and recirculation processes. This experimental observation was supported by performing 1-DICOG calculations with different mixing and recirculation parameters. No predicted effect of these variables on coal burnout was observed.

These calculations and measurements were performed for a high volatile B-bituminous Utah coal from the Deseret Mine. The proximate and ultimate analysis of this coal were given previously in Section 3 and were reported in detail in Ref. 3. Five size classifications were used in 1-DICOG with the mass flow rates and particle diameters of each chosen to closely match the measured continuous distribution (3). Figure 74 shows large (85 μm), medium (50 μm), and small (15 μm) particle histories for three of the five particle classifications used in the prediction of 85 μm, 65 μm, 50 μm, 30 μm and 15 μm particle diameters. The respective mass flow rates of each were 0.6 g/s, 1.1 g/s, 1.1 g/s, 0.6 g/s and 0.2 g/s. The predicted gas and particle temperature histories for this same calculation are also shown in Figure 74. The mass mean diameter of this particle distribution is 55 μm while that of the measured distribution was 47 μm. During the calculation of the poly-dispersed system, the importance of an accurate particle size distribution was noted. Weighting the small particles too heavily, for example, shifted the point of coal dust ignition much closer to the reactor inlet.

The coupled effects of all particle sizes were included in the computation. During the first 70 cm, the particles were heated by radiation from the hot reactor walls and from hot downstream particles. Moisture vaporization was very rapid in the very early regions of the reactor. Devolatilization began at about the same time for all particles and was completed very rapidly. As the raw coal devolatilized, it gave off gas phase products which were further reacted in the bulk gas phase and the temperature rose sharply. The devolatilization process also formed the residual char which rose to a peak at the point of complete

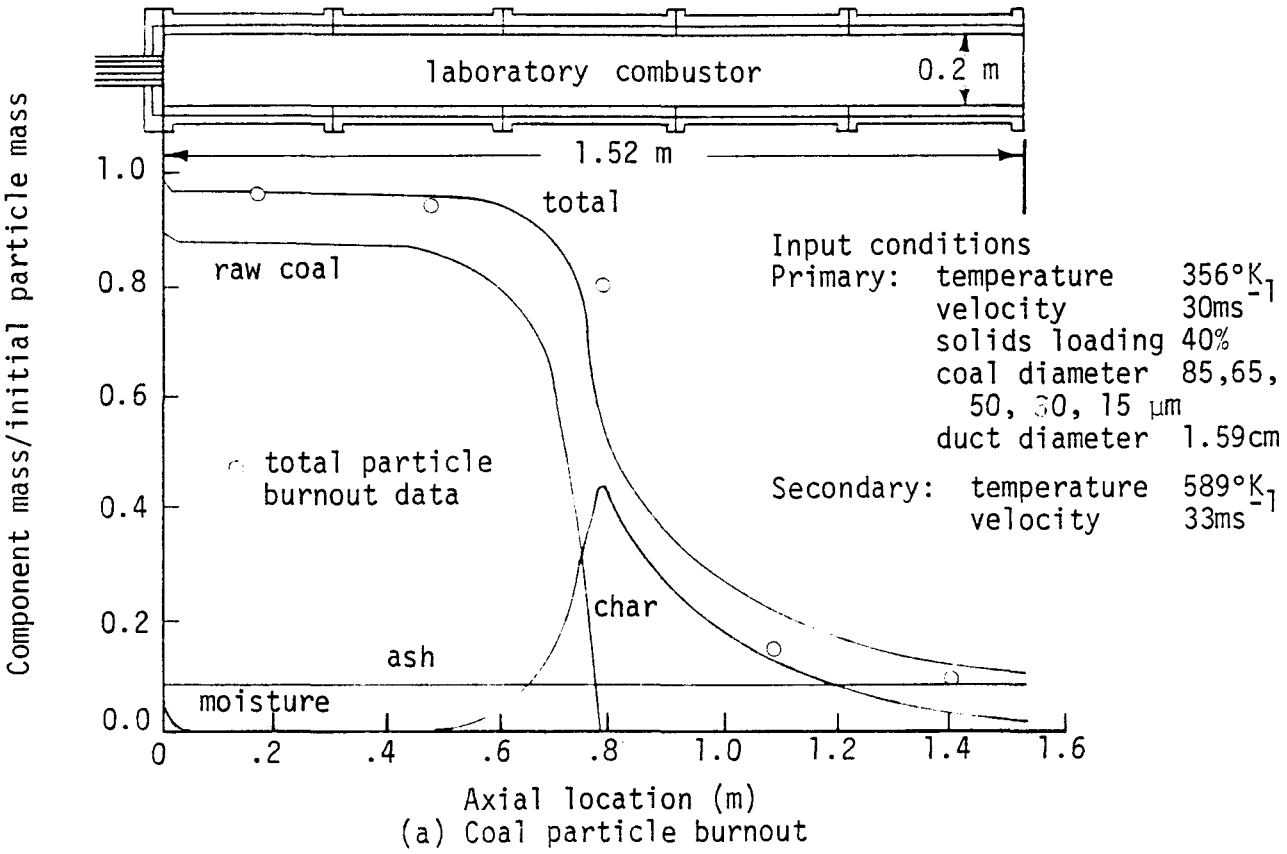

(a) Coal particle burnout

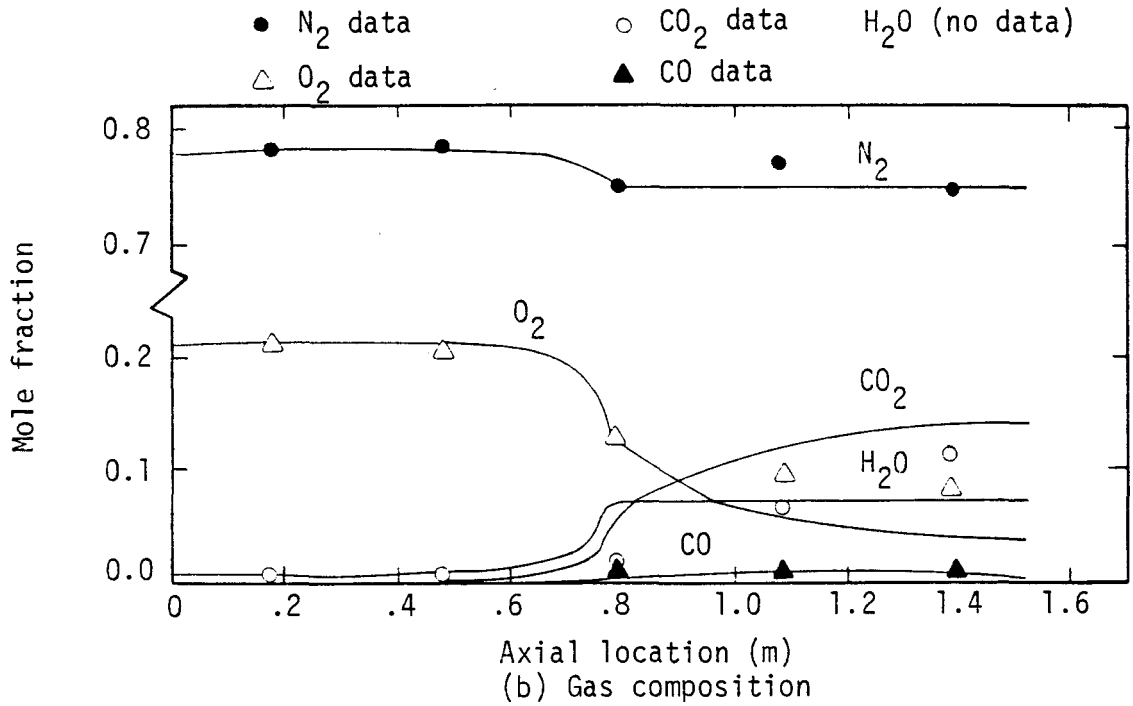

(b) Gas composition

Figure 73. Prediction and measurement of coal particle burnout and gas composition for poly-dispersed particles in BYU combustor.

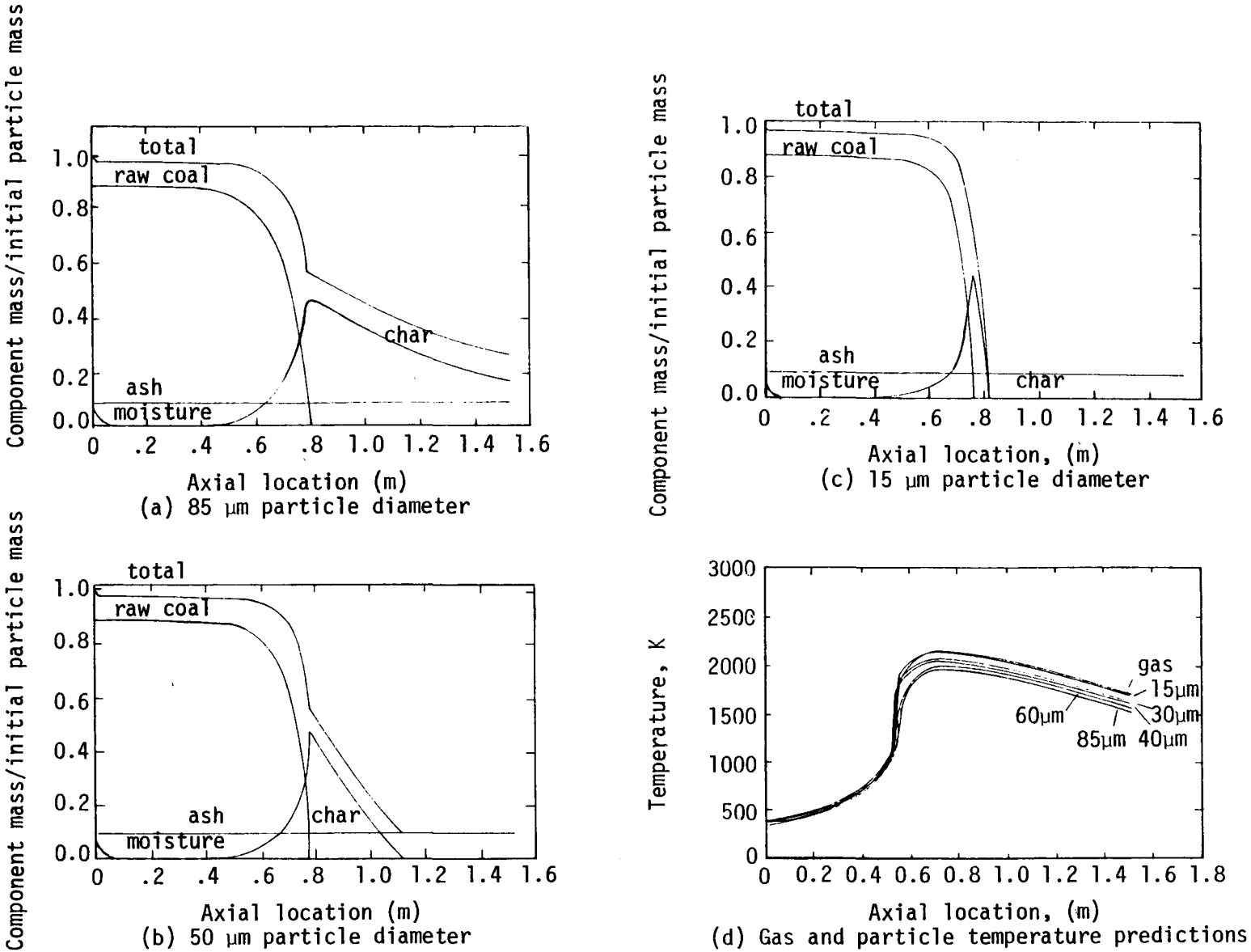

Figure 74. Predictions of particle burnout and temperature in poly-dispersed systems.

devolatilization. Heterogeneous char oxidation took place at vastly different rates for each particle size. Small particles burned out quickly while the larger particles were not burned out even at the end of the 1.52 meter reactor. This overall qualitative process was also observed by measurements made by the International Flame Research Foundation at Ijmuiden (33), as well as confirmed by the BYU measurements (3, 4). The heat-up time was much shorter in the Ijmuiden furnace, probably due to a large recirculation zone allowing convective heating from the hot recirculated combustion products.

Implications of mono-dispersed particle calculations were introduced in an EPRI final report (3) where a calculation was reported for a mono-dispersed particle size (i.e. only one particle size classification) of 60 um. The predicted particle mass history as well as the gaseous mole fraction histories were presented with the same experimental data points of Figures 73. Although, for this case, there were no substantial predicted differences between the results for the mono-dispersed and poly-dispersed systems, particle size distribution is known to be very important. For this particular poly-dispersed calculation, the large and small particle sizes tended to offset each other and the resulting system acted similar to a monodispersed particle size calculation of particles near the mass mean diameter. The calculations for poly-dispersed coal dust did reveal added information about the combustion process. For example: 1) devolatilization rates were fast and were nearly the same for all particle sizes, and 2) char burnout rates were very different for each particle size. Small particles burned out more rapidly than large particles.

Experimental studies were also conducted on coal dust particles of a smaller mass mean diameter to investigate particle size effects (32). The measured mass mean particle diameter of this smaller particle size was 20 um. 1-DICOG was used to predict behavior of these results with a distribution of three particle sizes of 10 um, 20 um and 30 um. The total particle mass history is shown in Figure 75(a). The entire combustion process occurred much sooner in the reactor for these small particles than for the larger mean size distribution. Measurements and predictions agreed very well. Again the recirculation zone did not contribute to the reaction process and thus the reaction zone was near one-dimensional in nature. More experimental data would be helpful to better define the limits of the curve; however, the first experimental point was in a crucial location. Gas phase mole fraction histories are shown in Figure 75(b). The comparison of theory and measurement is limited by the lack of local flux data as in the case with larger particles. The gas comparison is not as good as the solid comparison. Thurgood (32) has discussed in detail the implications of these computations and measurements particularly as pertaining to the relative rates of the processes involved (i.e. initial heatup, devolatilization, char oxidation, etc.).

Comparison with Laboratory Gasifier Data. In conjunction with the laboratory test data in Section 3, 1 DICOG was applied to predicting the performance of the gasifier operating under the conditions of Test No. 96 reported in Table 21 (O_2/coal ratio of 0.99 and steam/coal ratio of 0.47 kg/kg). The prediction was made with three discrete particle

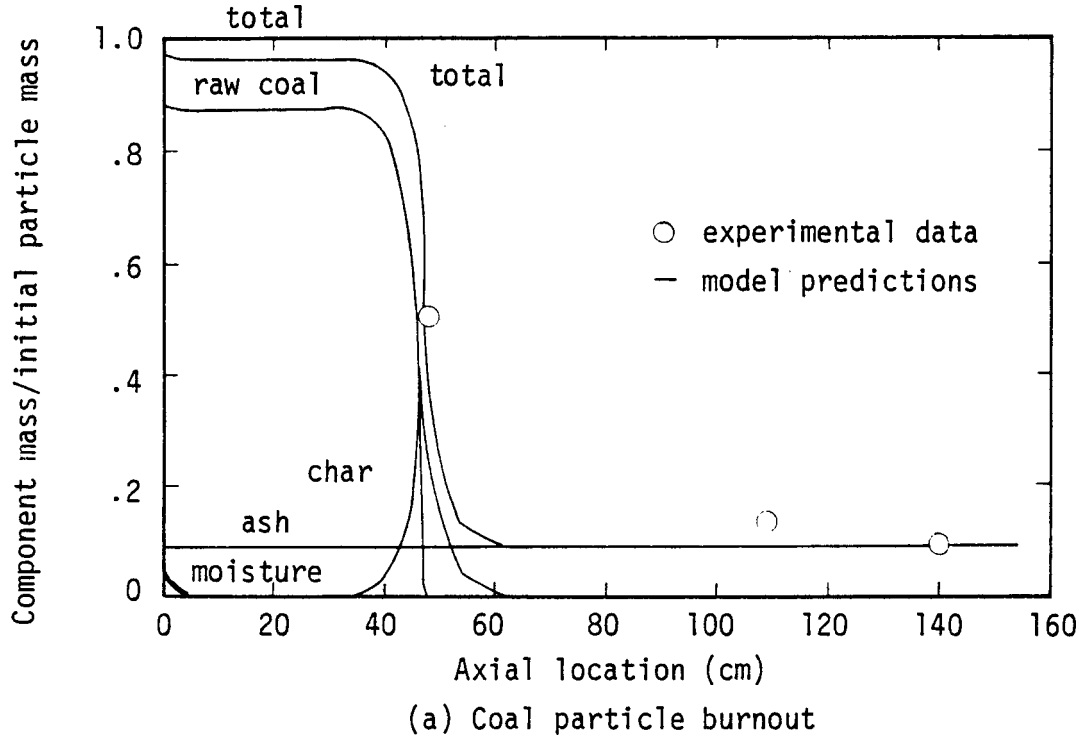

(a) Coal particle burnout

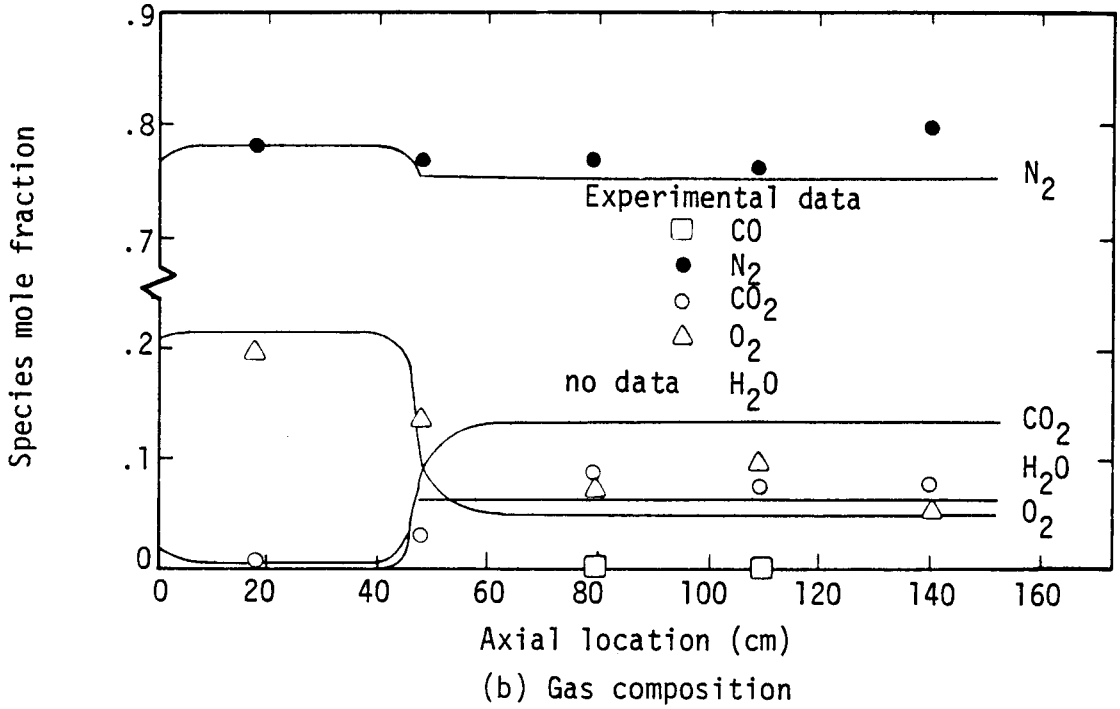

(b) Gas composition

Figure 75. Predictions and measurements of coal particle burnout and gas composition for small particles in BYU combustor.

size classifications of 21, 41, and 70 μm to simulate the overall distribution. Figures 76 and 77 show the predicted particle mass and gas composition histories, and the temperature and individual particle size mass histories for the computation, respectively. The presence of the O_2 in the primary stream allowed for rapid heating as the early released volatile matter reacted to completion. The temperature rose quickly to allow for early devolatilization, aided by the recirculation process. According to the theory, this flame was recirculation stabilized and not radiation stabilized, as was the case in the combustor. This effect could only be approximated in this one-dimensional application. Arbitrarily, 20% of the total gas mass flow was recirculated in this prediction. The limited measurements obtained at an axial position of 63.5 cm are shown on the graphs. Since only two radial samples were available, both taken near the centerline, it was not possible to obtain a properly integrated average for the solids burnout or gas phase composition. Measurements from both probes are plotted for comparison. Even though agreement between theory and experiment was poor, the theory was useful in identifying the basic trend through the gasifier. The poor agreement was probably due to: 1) limitations in the 1-D code to predict recirculation phenomena, and 2) the absence of sufficient radial data to obtain an integrated average.

These comparisons were preliminary. A significant amount of additional detailed profile data on gas mixing rates, particle dispersion, coal reaction, gaseous species and pollutants were reported in Section 3. These results provide an important data base for evaluating the one-dimensional code.

Coates Gasifier Predictions. 1-DICOG was formulated to handle either combustion or gasification conditions. Coates (34) has constructed an experimental gasifier designed with a continuous throughput capacity of up to 45 kg (100 lb) of coal per hour at pressure of up to 20 atmospheres. The gasifier has a downflow configuration with a combination quench/heat recovery stage located immediately below the gasifier stage. Figure 78 shows a idealized schematic of the reactor system with data pertaining to one particular experimental run. 1-DICOG was used to predict the performance of the gasifier with these input data. The geometry of the reactor required some minor modifications in the computer code. The injection of air, steam, recycle gas, and coal were assumed to be premixed and then expanded into the initial chamber at a 20^{o} growth angle. The stream leaving the initial reactor section was again expanded at a 20^{o} growth angle with negligible recirculation into the final chamber. The boundary conditions were given as a heat flux of 12,100 J/S (2900 cal/s) for the first chamber and constant temperature cold wall at 339K for the second section. Since 1-DICOG was coded for a constant temperature boundary condition the wall temperature was found through an iterative procedure. The wall temperature used in the first chamber in the theoretical predictions to achieve the specified cooling rate was 1000 K. Predicted profiles for a monodispersed system are shown in Figure 79. Experimental measurements were not available for local comparison inside the gasifier but Figure 79 compares experimental observations and theoretical predictions for the exhaust gas composition. It was noted that all of the sulfur in the coal was experimentally observed as H_2S whereas the model only considered the formation of SO_2 for this particular predic-

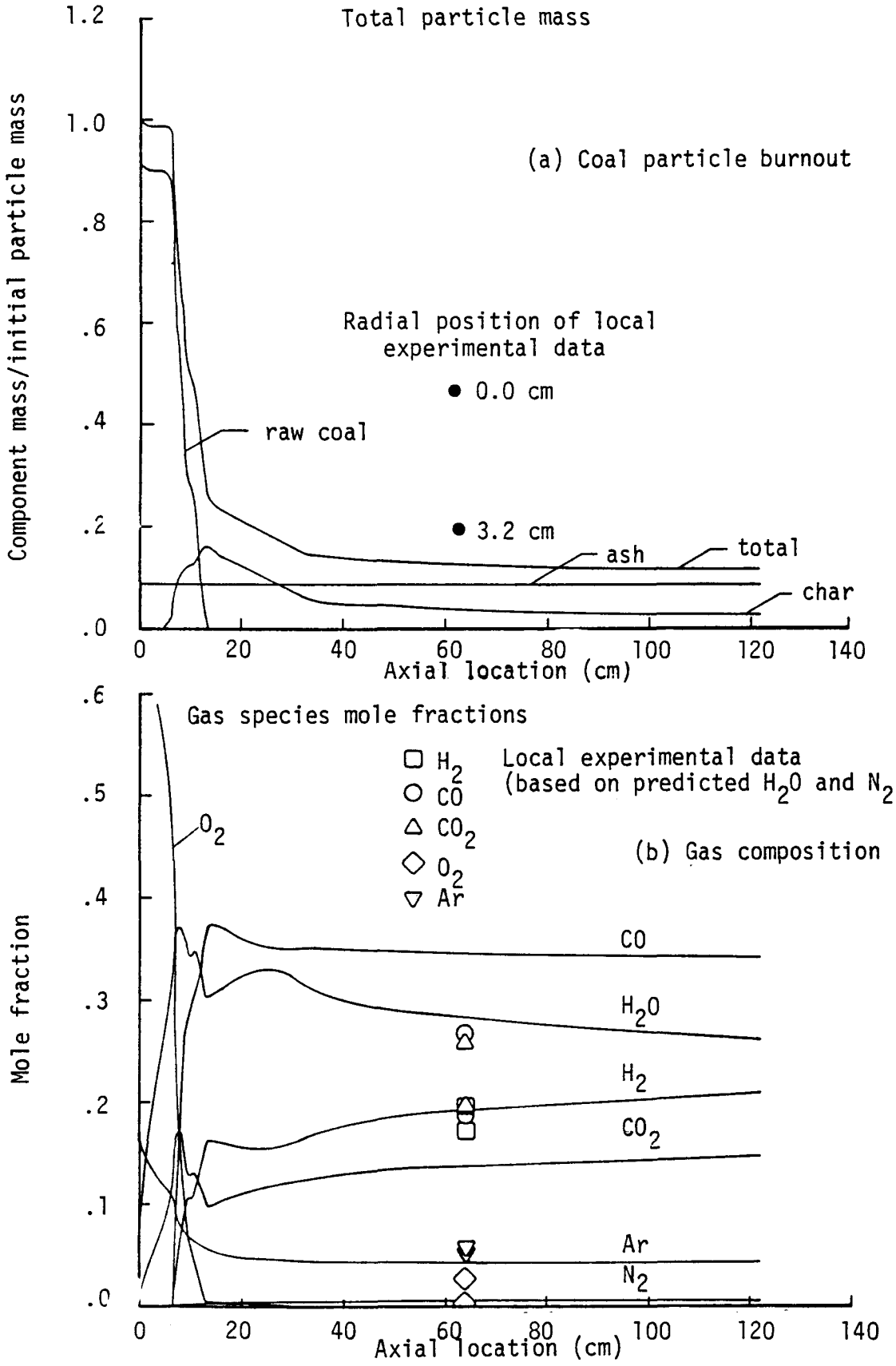

Figure 76. Preliminary comparison of predictions and measurements of coal particle burnout and gas composition for poly-dispersed coal particles in the BYU gasifier.

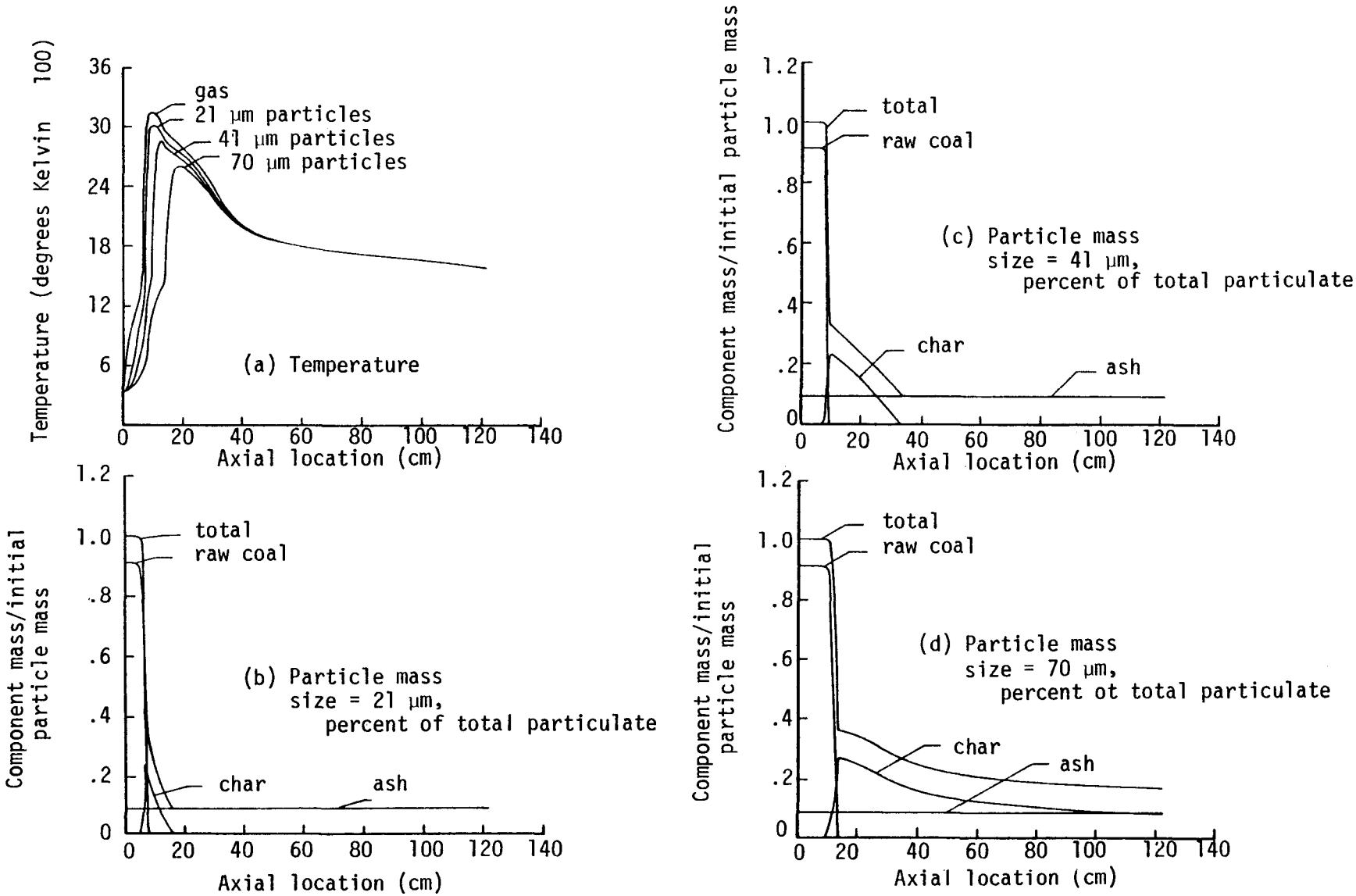

Figure 77. Predictions of temperature and particle mass for poly-dispersed coal particles in the BYU gasifier.

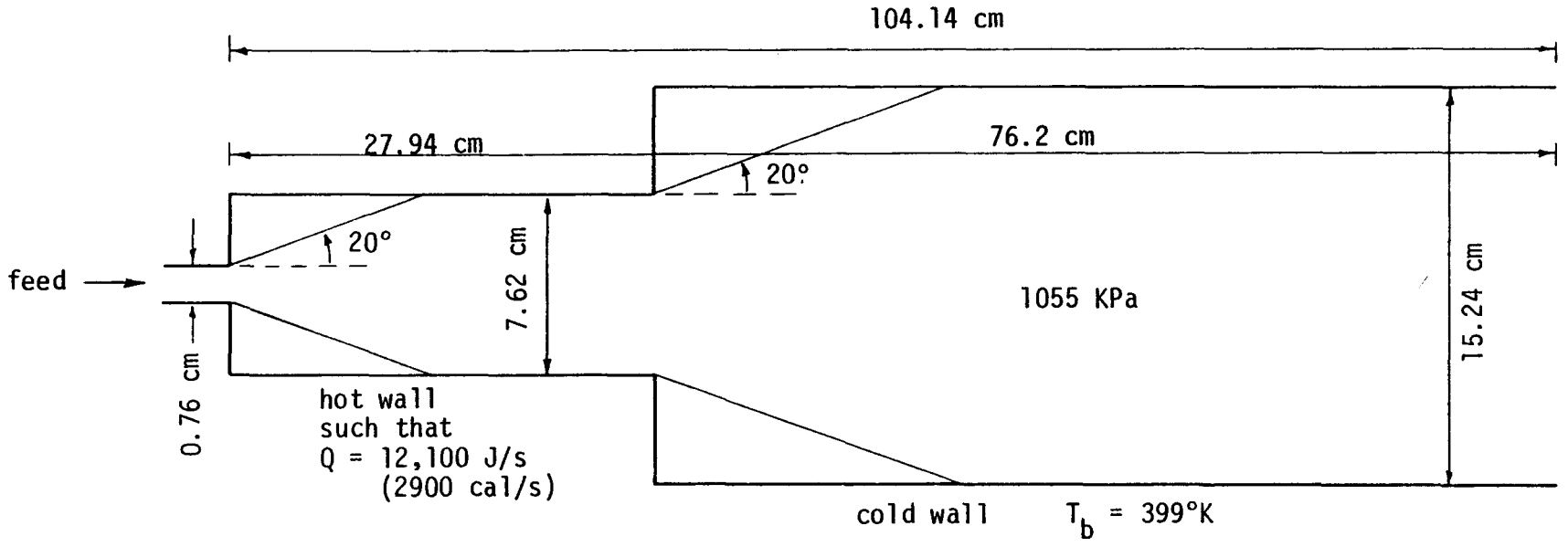

Feed, Kg/hr	
coal	20.5
oxygen	16.8
steam(561K)	7.9
recycle gas	4.7
total	49.9

steam make
37.2 Kg/hr
1172 KPa sat.
water rate
51.7 Kg/hr

Coal high heating value 12,600 BTU/lb

Coal analysis	(Wt. %)
carbon	69.4
hydrogen	5.5
oxygen	11.6
nitrogen	1.4
sulfur	0.6
ash	10.5
moisture	1.0
	100.0

Figure 78. Schematic of 1-DICOG configuration for Coates gasifier (34).

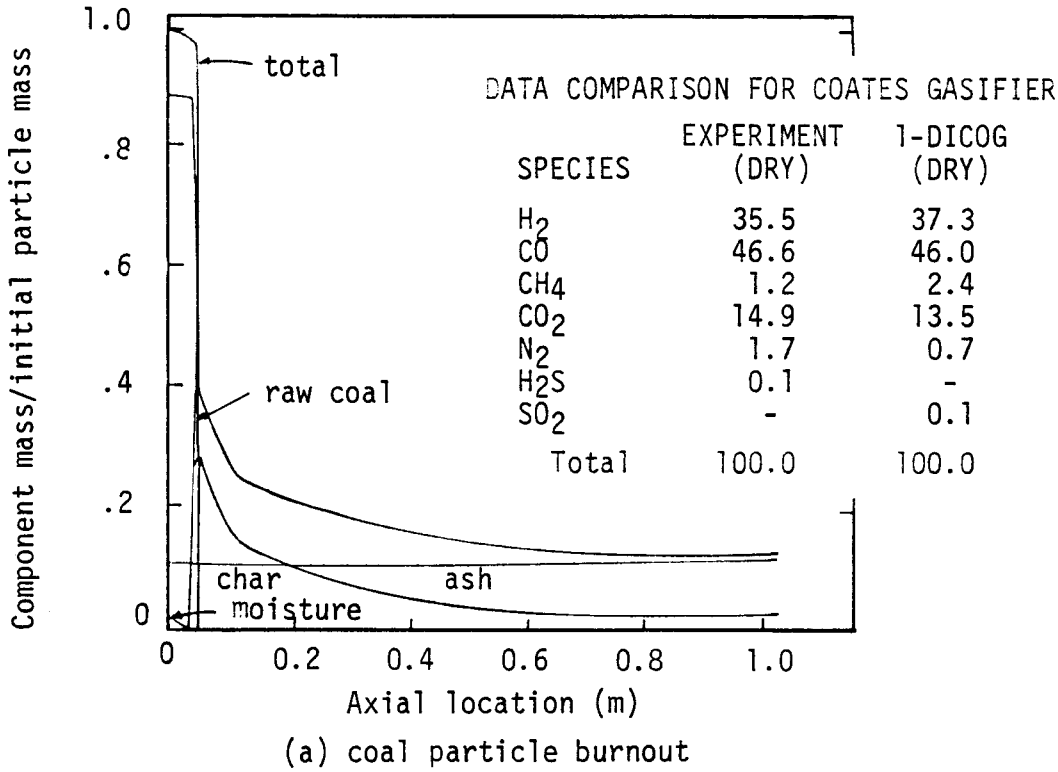

(a) coal particle burnout

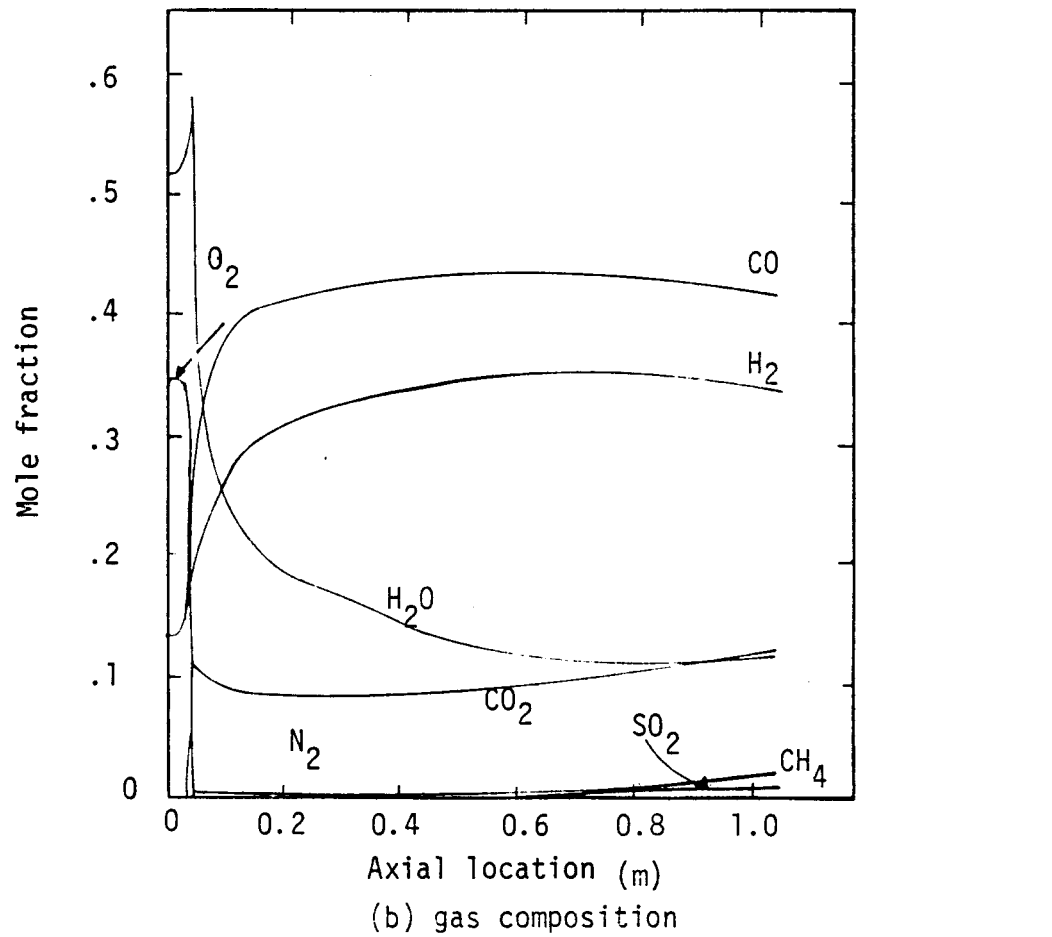

(b) gas composition

Figure 79. Prediction of coal particle burnout and gas composition for Coates Gasifier.

tion. Predicted results were considered to be very good. Experimentally, 91.8% of the input solids were reacted. 1-DICOG predicted 87.9% burnout. There appears to be some inconsistency in the experimental solids data since 10.5% of the input coal is analyzed as ash; thus, 89.5% burnout is the theoretical ash included burnout without significant ash volatilization. The predicted flame front was only lifted from the burner exit by a few centimeters.

Predictions for Babcock and Wilcox Combustor. Babcock and Wilcox is seeking to limit NO_x from coal-fired boilers by delaying fuel/air mixing in a staged combustion process (35). The first stage of this system initiates pyrolysis and oxidation in a fuel rich environment. With the cooperation of Babcock and Wilcox, 1-DICOG was applied to this stage of the combustor. The reactor geometry was composed of a primary jet of pulverized coal entrained in an air stream encircled by an annular jet of preheated secondary air. This co-axial jet dumps into a rectangular box. The input conditions for a Pittsburgh seam 8 bituminous coal are summarized in Figure 80. Since limited information was known about the particle size distribution, a mono-dispersed system was used. The actual burner operates by swirling the secondary air. Plug flow was assumed from the onset in a completely premixed system.

Predicted particle and gas temperature profiles, particle mass profiles and gas phase mole fraction profiles are shown in Figure 80. Ignition was predicted very late in the reactor. This was due to the cold wall temperature of 422 K. The experimentally observed ignition was very much earlier in the reactor. The flame was probably very close to being attached to the burner. Experimentally observed gas temperatures and oxygen mole fractions are shown in Figure 80. Agreement was not good. The inconsistency between experimental and theoretical observations was possibly due to the one-dimensional approximation. The swirling jet in the box furnace has multi-dimensional fluid mechanics effects. Strong recirculation and the effects of swirl could increase the initial heat-up beyond that predicted by the premixed plug flow computation.

BI-GAS Gasifier Prediction. In all the applications discussed thus far, the zone treatment for radiative transfer was used. An example where the optical depth was too small for this treatment is shown in Figure 81. These computations are for a 1 kg/s solids loading, high pressure (80 atm), BI-GAS gasification system (36). In such systems, greatly improved computational efficiency was achieved by treating radiation as a diffusional process as discussed in the User's Manual, Volume 2. This stage of the gasifier was also char-fed and 1-DICOG was applied using mono-dispersed particles of 60 μm diameter. Figure 81 shows a very sharp flame front in this high pressure, high solids loading system, even without the volatile products available for gas phase reaction.

Shrinking Particle Predictions. All the applications to this point emphasized one particular burnout model for heterogeneous oxidation. This was the constant diameter model where the particle diameter was taken to remain constant during char oxidation as opposed to the shrinking particle option where the solid density is assumed constant and the diameter changes accordingly. Both options were examined with 1-DICOG

Pittsburghseam 8 coal
38 μm particle diameter
29.7 x 10^6 J/kg heating value

Conditions	Primary	Secondary
Air flow, g/s	72.6	215
Coal flow, g/s	39.0	-
Temp. K	328	589
Jet diameter, cm	7.6	19.1

Reactor is 71 cm diameter x 142 cm long.

(a) Input conditions

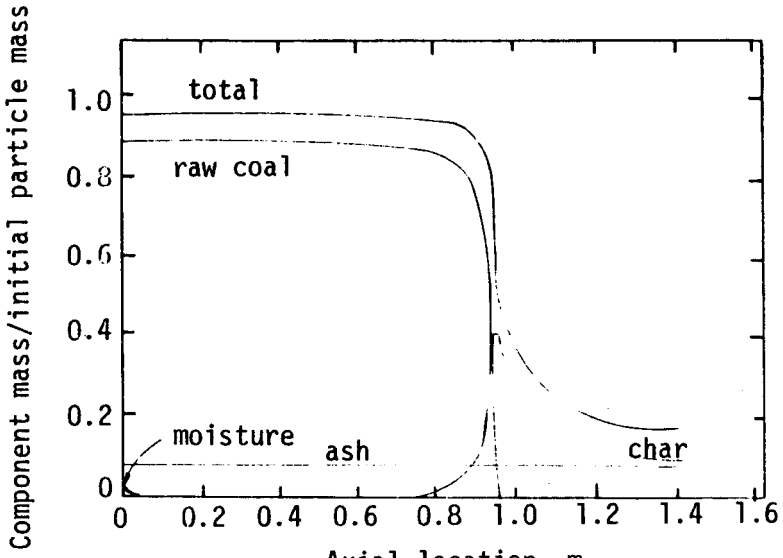

(b) Coal particle burnout

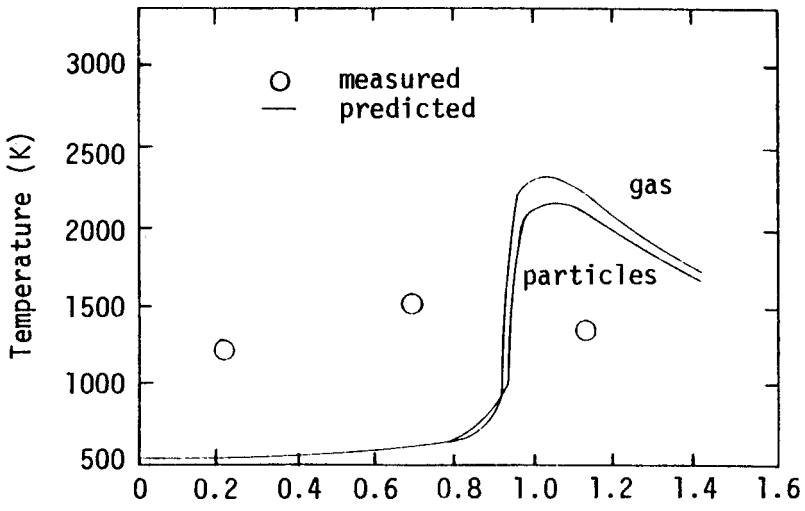

(c) Gas and particle temperature histories

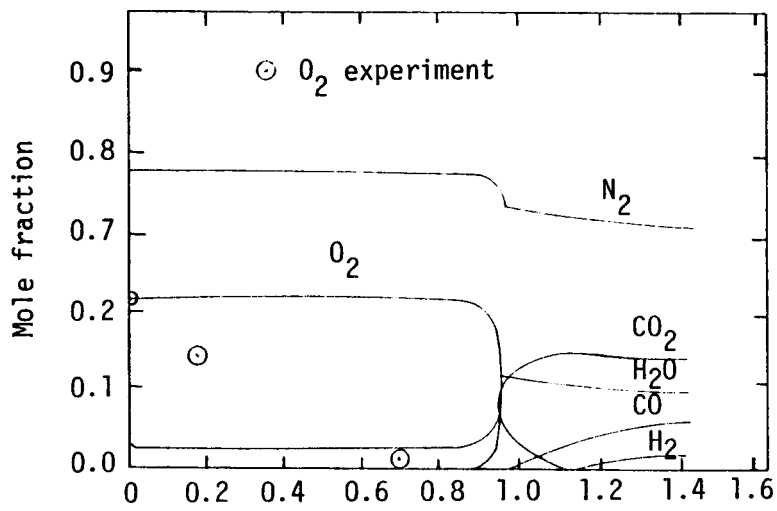

(d) Gas composition

Figure 80. Prediction of coal burnout, gas composition and temperature for Babcock and Wilcox combustor.

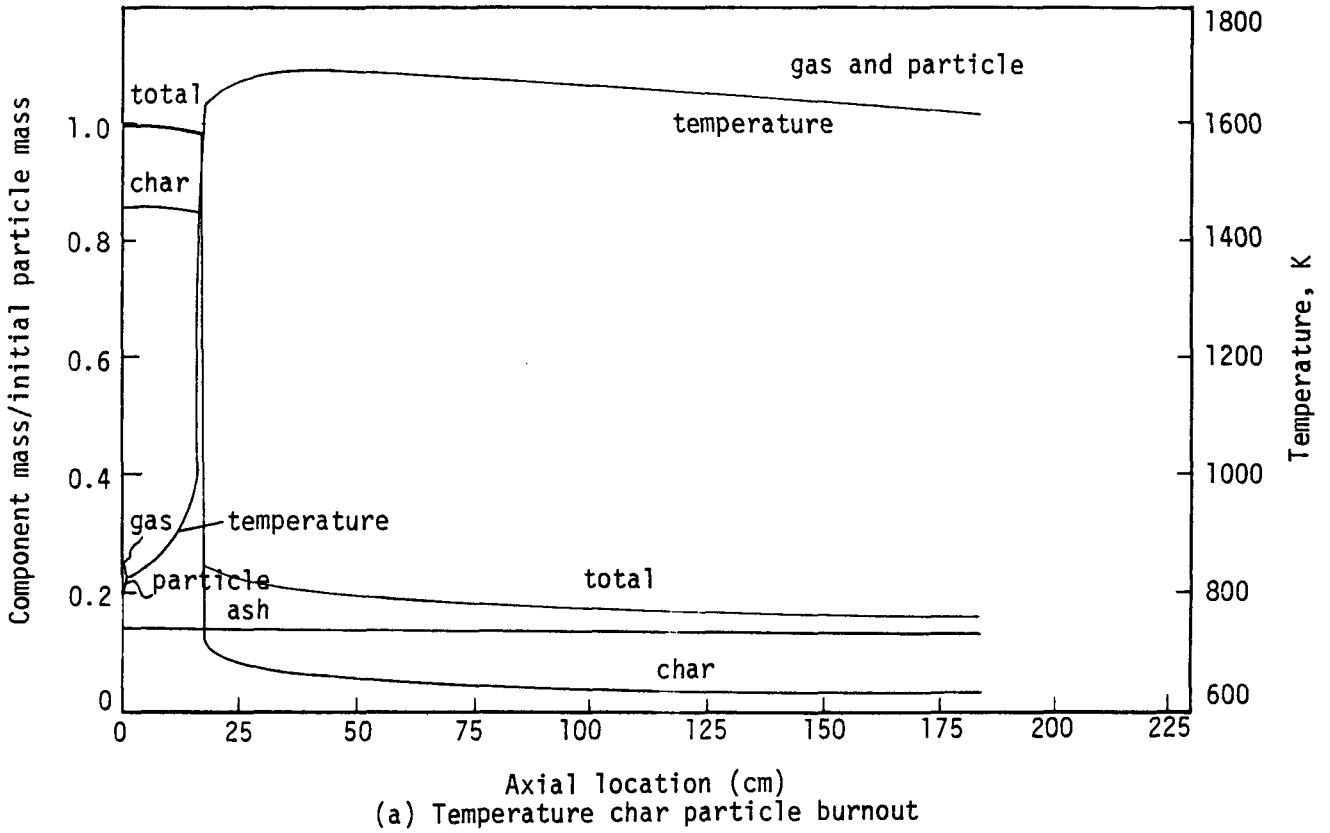

(a) Temperature char particle burnout

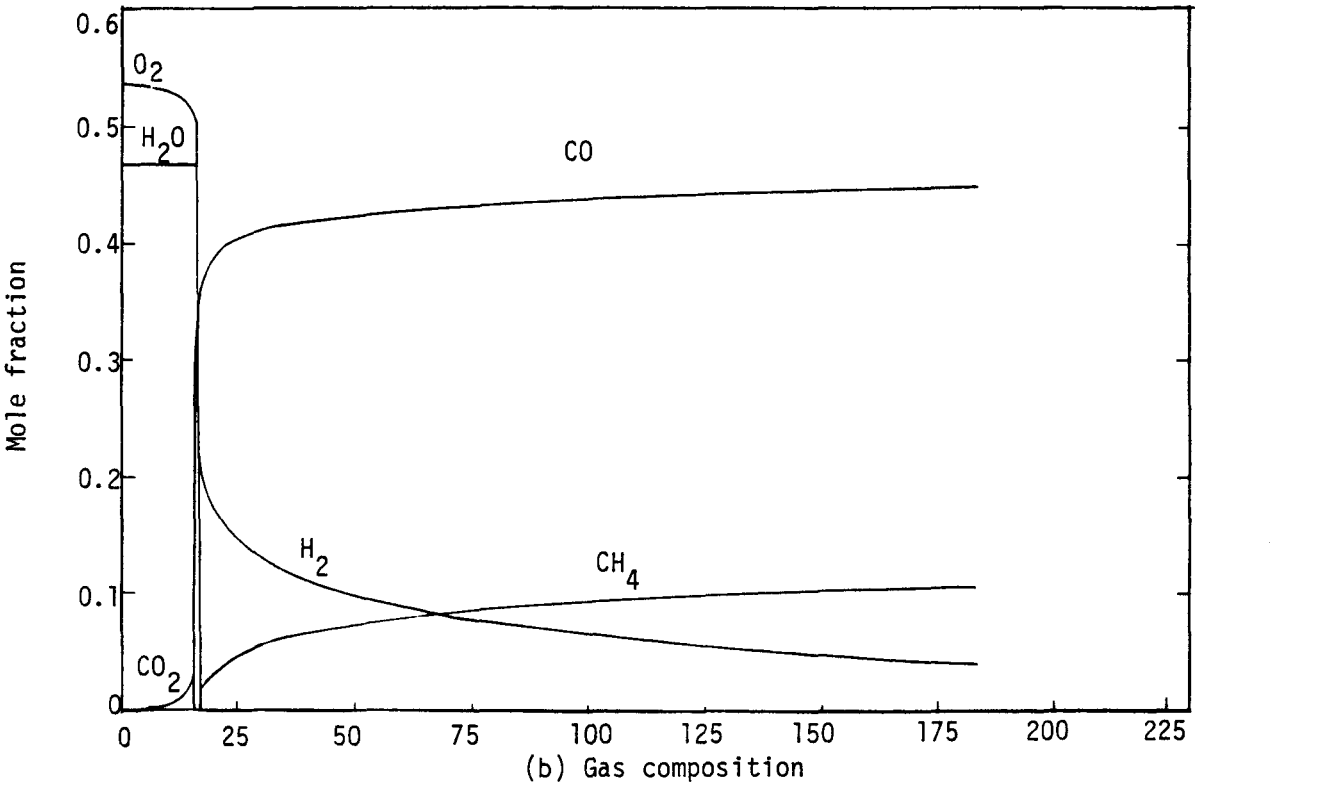

(b) Gas composition

Figure 81. Prediction of coal particle burnout and gas composition for BI-GAS Gasifier.

and selected results are shown in Figure 82. This figure shows particle mass histories for 40 μm particles in a poly-dispersed system with each of the indicated options. The predictions were made for the BYU combustor. The differences between these two particle diameter options was small for this particular application. The reason appeared to be that even in the shrinking particle model the diameter change was less than a factor of two.

Other applications of 1-DICOG in helping to interpret experimental pollution studies are discussed by Rees (37) and are not included herein.

3. Controlling Rate Processes

The relative importance of initial particle heat-up, devolatilization, oxidizer diffusion, and heterogeneous char reaction in controlling coal burnout was examined with 1-DICOG. The rate of initial particle heat-up was an important step in the overall reaction process. The coal or char particles received or lost energy by radiation from downstream particles and from the vessel walls; they also exchanged energy by conduction to the gases which surrounded them. The rate of energy with the incoming particles determined where in the reactor, if at all, the particle ignition would occur. In parametric studies with the Foster-Wheeler gasifier, the effect of wall temperature on this process was examined. Selected results are shown in Table 28. Since no volatile particle matter was present, the heat-up could not come from particle-gas conduction. Particle-wall, and particle-particle radiation were the only initial heat-up mechanisms. With a wall temperature of 1800 K, ignition was predicted at an axial positon of 0.5 m from the burner inlet; however, with a wall temperature of 1200 K, it was predicted that the particles would not ignite in the 4.5 m length of the reactor.

The rate of devolatilization in these systems has already been discussed. As soon as devolatilization began, the process proceeded rapidly to completion. The devolatilization rate was affected only slightly by particle size. After devolatilization was initiated, the gaseous products reacted immediately in the gas phase and the gas temperature rose rapidly. The particle temperature subsequently rose due to the hot gases.

Diffusion of the oxidizer to the particle surface and surface heterogeneous char reacton are two rate processes that are tied closely together. The relative importance of each was a significant question when evaluating coal reaction models. The oxidizer must diffuse to the particle surface before reaction could take place and, conversely, the oxidizer must be depleted at the surface by char reaction before further diffusion could proceed. Pore diffusion and oxidizer adsorption were accounted for in this formulation only through the magnitudes of the experimental rate constants which were based on external spherical surface areas. Parametric predictions were made by selectively altering the diffusion rate to determine the controlling mechanism (see Table 28). Of these two processes, surface reaction is clearly dominant for this set of conditions.

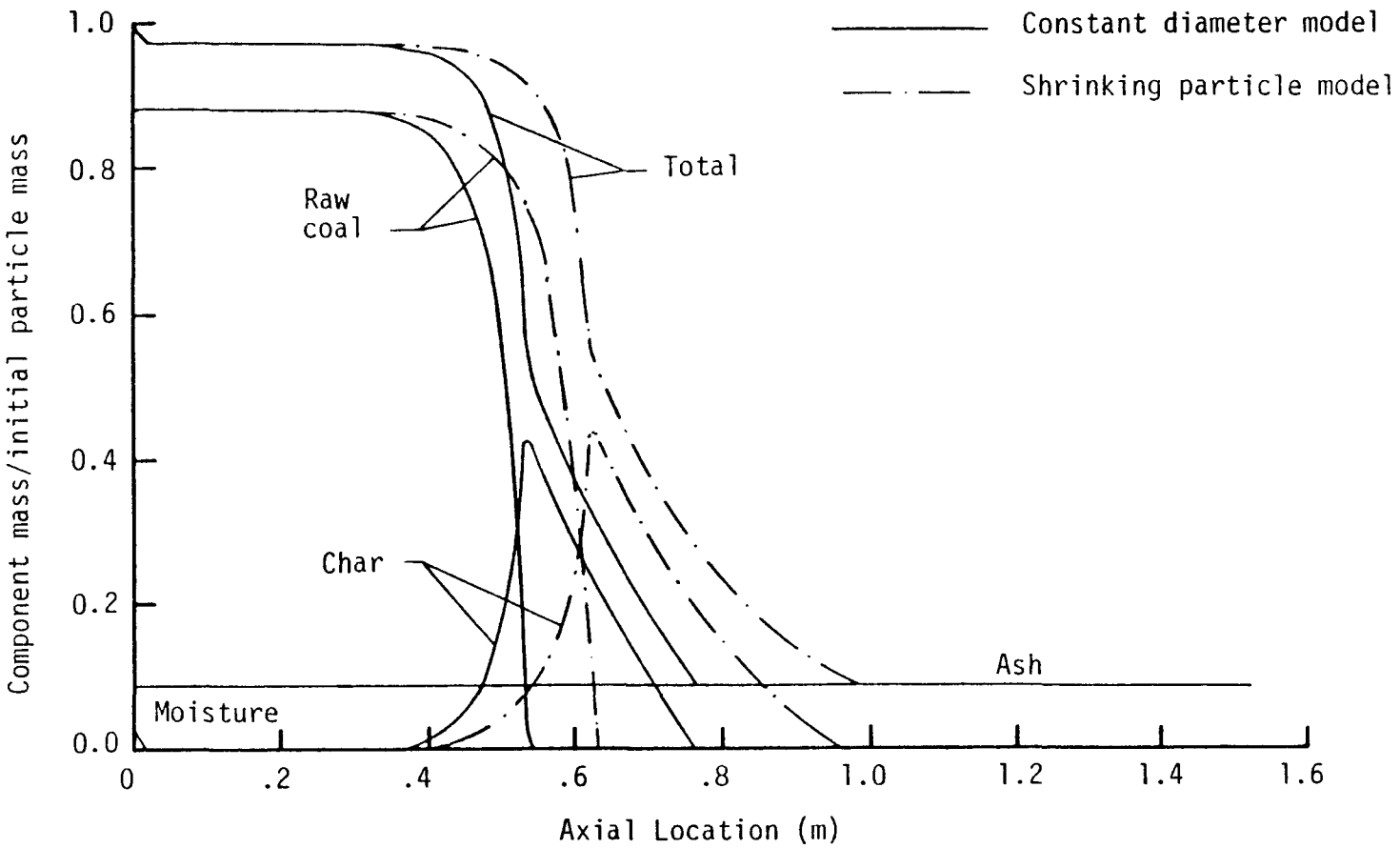

Figure 82. Predictions of 40 μm particle burnout in a poly-dispersed system for two char burnout models.

TABLE 28

SELECTED PARAMETRIC PREDICTIONS FOR EVALUATING RATE PROCESSES

Test Description	Initial Heat-up: Study Effect of Wall Temp.			Mixing Processes: Study Effect of Mixing in Laboratory Combustor			Devolatilization: Study Effect of Kinetic Parameters & Particle Size			Char Oxidation: Study Relative Importance of Oxidizer Diffusion		
Input:												
Primary: temp. (K)	761	761	761	356	356	521	521	521*	521	560	560	560
gas flow rate (gs^{-1})	1231	1231	1231	5.4	5.4	39.6	39.6	39.6	39.6	21.8	21.8	21.8
total particle flow rate	173	173	173	3.6	3.6	3.6	3.6	3.6	3.6	3.7	3.7	3.7
particle size (μm)	142	142	142	30	30	30	30	30	60	‡	‡	‡
Secondary: temp. (K)	-	-	-	589	589	-	-	-	-	-	-	-
mixing rate ($gcm^{-1}s^{-1}$)	-	-	-	(-.056x+1.96)	(-.056x+1.96)	premix	-	-	-	-	-	-
Recirculation ($g\ cm^{-1}s^{-1}$)	-	-	-	(-.058x+1.02)	0	0	-	-	-	-	-	-
Wall temperature (K)	1200	1500	1800	1200	1200	1200	1200	1200	1200	1200	1200	1200
Results:												
Onset of particle reaction (x/L)	-	0.36	0.13	0.39	0.39	0.31	0.31	0.40	0.32	0.16	0.16	0.16
Completion of devolatilization (x/L)	-	-	-	0.43	0.43	0.34	0.34	0.44	0.40	0.20	0.20	0.20
Peak particle temp. (K)	1124	2200	2205	2300	2300	2300	2300	2300	2200	2200+	2200+	2200+
Peak gas temp. (K)	1124	2400	2355	2400	2400	2400	2400	2400	2400	2400	2400	2400
Burnout at outlet (%)	0	100	100	100	100	100	100	100	100	76	70	77
Completion of char burnout (x/L)	-	0.47	0.23	0.54	0.54	0.45	0.45	0.53	0.75	-	-	-
Comments	-All predictions were for first stage of a Foster-Wheeler gasifier. -Char feedstock had no volatiles content.			-All predictions were for laboratory combustor. -Conclusions could be different different combustion chamber.			-All predictions were for laboratory combustor. -First column uses devolatilization parameters in Table 4. -Second column uses devolatilization parameters as given in footnote. -Third column same as first with different particle size.			-All predictions were for laboratory combustor. -First column is reference case. -In second column, diffusion rate changed by a factor of 0.1. -Third column diffusion rate changed by a factor of 10.0.		
Overall effect	significant			recirculation: nil secondary mixing: small			small			small		

*Devolatilization parameters: $Y_1 = 0.39$, $A_1 = 2.2 \times 10^5 s^{-1}$, $E_1 = 17.8$ kcal mol^{-1}

$Y_2 = 1.00$, $A_2 = 2.0 \times 10^{12} s^{-1}$, $E_2 = 60.0$ kcal mol^{-1}

‡Poly-dispersed particle phase of 85, 65, 50, 30, 15 μm

+50 μm particles

4. Status of 1-DICOG Development

Development of this code was completed during this contract period. The code was extensively tested and a detailed user's manual was published as Volume 2 of this final report. Instructions for obtaining this code are given in Volume 2.

Some additional one-dimensional modeling work is planned at this laboratory as part of a separate study. Tasks of particular interest include 1) extension of the code to account for particle lag effects, 2) addition of NO_x pollutant predictions, 3) revision of methods governing particle temperature, and 4) investigation of recirculation effects. The code will also be applied to additional pulverized coal combustor and gasifier measurements. Additional material regarding the formulation and application of this code was reported in an earlier EPRI report (3), and in a recently published book (38) by the principal investigator and co-workers.

C. TWO-DIMENSIONAL CODE

1. Background and Objectives

This activity was directed toward construction of a generalized coal gasification computer code in axi-symmetric coordinates for data analysis, sensitivity analysis of physical parameters, scaling, and ultimately for design and analysis of pulverized fuel gasifiers and combustors. As a first step, the description of a diffusion-limited, gas-phase combustion model (BURN) was formulated and coded. The model described the mean field values of the local velocity, reactor temperature, density, species mole fractions, and properties of the local turbulence field.

The description which follows applies to two-dimensional axi-symmetric geometries in cylindrical coordinates and is time steady. The formulation was for general recirculating flows described by elliptical, partial differential equations. The mean properties were calculated through a probability density function (P.D.F.) approach. This subsection describes the details of the model. It was particularly intended that BURN apply to gasification and combustor measurements made at this laboratory (2-4 and this study). The basis of BURN is presented, including a description of model equations and required assumptions. The solution technique used is briefly reviewed, including unique features. The predictions made for this study are then presented and experimental measurements are shown for model evaluaton. Important mechanisms illucidated by model predictions are presented. Finally, extensions to coal dust are discussed.

Because of the complexity of modeling reacting, recirculating, particle-laden systems, it was not possible to present all of the details of BURN in this final report. Partly for this reason, the principal investigator and several associates published a book (38) which presents the foundations of this modeling approach in great detail. What follows is based in large measure, on the material in that book. In addition,

Smith (39) presents the specific technical details for the basis of this code.

2. Fluid Mechanics Model

The fluid mechanics submodel consists of the momentum and continuity equations for compressible turbulent flow. The usual technique for resolving the time dependent turbulent fluctuations was to average the equations of change over a short time interval. In this way the properties of the flow were expressed in time mean and time fluctuating components. The resulting equations described the time-smoothed velocity and pressure distributions but caused cross correlations involving the fluctuating velocities and densities.

Differential Equations. The general equations of motion and continuity are presented in Refs. 38 and 40. With the following simplifications: 1) polar cylindrical coordinates, 2) axi-symmetric geometry, 3) negligible body forces, 4) time steady, 5) Newtonian fluid, 6) neglect dilitation effects, the equations to be solved before time-averaging are:

equation of continuity

$$\frac{\partial}{\partial x}(r\rho u) + \frac{\partial}{\partial r}(r\rho v) = 0 \tag{8}$$

x-component of motion

$$\frac{\partial}{\partial x}(r\rho uv) + \frac{\partial}{\partial r}(r\rho vu) - \frac{\partial}{\partial x}(\mu r\frac{\partial u}{\partial x}) - \frac{\partial}{\partial r}(\mu r\frac{\partial u}{\partial r})$$

$$= -r\frac{\partial p}{\partial x} + \frac{\partial}{\partial x}(\mu r\frac{\partial u}{\partial x}) + \frac{\partial}{\partial r}(\mu r\frac{\partial v}{\partial x}) \tag{9}$$

r-component of motion

$$\frac{\partial}{\partial x}(r\rho uv) + \frac{\partial}{\partial r}(r\rho vv) - \frac{\partial}{\partial x}(\mu r\frac{\partial v}{\partial x}) - \frac{\partial}{\partial r}(\mu r\frac{\partial v}{\partial r})$$

$$= -r\frac{\partial p}{\partial r} + \frac{\partial}{\partial x}(\mu r\frac{\partial u}{\partial r}) + \frac{\partial}{\partial r}(\mu r\frac{\partial v}{\partial r}) - \frac{2\mu v}{r} \tag{10}$$

Smith (39) discussed the limitations of these assumptions and the significance of each term in the equation set.

This equation set, along with the appropriate boundary conditions, was sufficient to solve for u, v, and p, provided that the density and viscosity were known everywhere in the field.

Turbulence Modeling. In time-averaging the transport equations for combustion systems, all of the dependent variables are fluctuating (i.e., u, v, p, ρ) and are decomposed into their time-mean and fluctuating quantities. The equations reduce to terms identical to the instantaneous form of the equation only in the time mean variables, but there are a large number of extra terms involving the fluctuating components. There are terms like $\rho u'v'$, $u\rho'v'$, etc. Historically, the terms involving

ρ' have been neglected, mainly for convenience, and the appropriate time mean density is used with the Reynolds Stresses (i.e., $\rho\ u'v'$). Favre-averaging is a viable alternative as discussed by Smith (39). This model was coded to allow options for either Reynolds or Favre averaging. The discussion which follows presents an overview of the conventional Reynolds-averaging approach.

To model the Reynolds stresses, it was assumed that (40):

$$\overline{u'v'} = -\mu_t\left(\frac{\partial \bar{u}}{\partial r} + \frac{\partial \bar{v}}{\partial x}\right) \tag{11}$$

where μ_t is the kinematic eddy viscosity. The fluctuating correlations are thus expressed in terms of the mean field variables. The problem of turbulent modeling was thus reduced to finding appropriate values for the eddy or turbulent viscosity, μ_t which is not a unique property of the fluid, but will vary from point to point. The turbulent field was modeled with a mean turbulent energy closure (MTE), where the eddy viscosity is related to the turbulent kinetic energy (k) and its rate of dissipation (ε) (41):

$$\mu_t = C_\mu \rho \bar{k}^2/\bar{\varepsilon} \tag{12}$$

where

$$k = 1/2(\overline{u'^2} + \overline{v'^2}) \tag{13}$$

The problem was, thus, to find appropriate expressions for k and ε in terms of time-average field variables.

Of the existing turbulence models, the k-ε model of Spalding and co-workers (41) seemed to be the furthest advanced and the most promising. It was particularly attractive for reacting flows of the form required for BURN. Equation 12 was utilized for the eddy viscosity and the model equations for the turbulent kinetic energy and the dissipation rate of turbulent kinetic energy were given by Launder and Spalding (41) as follows:

$$\frac{\partial}{\partial x}(r\bar{\rho}\bar{u}\bar{k}) + \frac{\partial(r\bar{\rho}\bar{v}\bar{k})}{\partial r} - \frac{\partial}{\partial x}\left(r\frac{\mu_e}{\sigma_k}\frac{\partial \bar{k}}{\partial x}\right) - \frac{\partial}{\partial r}\left(\frac{r\mu_e}{\sigma_k}\frac{\partial \bar{k}}{\partial r}\right)$$

$$= \mu_e r\{2[(\frac{\partial \bar{u}}{\partial x})^2 + (\frac{\partial \bar{v}}{\partial r})^2 + (\frac{\bar{v}}{r})^2] + (\frac{\partial \bar{u}}{\partial r} + \frac{\partial \bar{v}}{\partial x})^2 - \bar{\rho}\bar{\varepsilon}r \tag{14}$$

$$\frac{\partial}{\partial x}(r\bar{\rho}\bar{u}\bar{\varepsilon}) + \frac{\partial}{\partial r}(r\bar{\rho}\bar{v}\bar{\varepsilon}) - \frac{\partial}{\partial x}\left(\frac{r\mu_e}{\sigma_\varepsilon}\frac{\partial\bar{\varepsilon}}{\partial x}\right) + \frac{\partial}{\partial r}\left(\frac{r\mu_e}{\sigma_\varepsilon}\frac{\partial\bar{\varepsilon}}{\partial r}\right)$$

$$= \frac{r\varepsilon C_1}{k}\{2[(\frac{\partial\bar{u}}{\partial x})^2 + (\frac{\partial\bar{v}}{\partial r})^2 + (\frac{\bar{v}}{r})^2] + (\frac{\partial\bar{u}}{\partial r} + \frac{\partial\bar{v}}{\partial x})^2\} - \frac{\bar{\varepsilon}^2 C_2 \rho r}{\bar{k}} \qquad (15)$$

where

$$\mu_e = \mu_\ell + \mu_t \qquad (16)$$

This model is semi-empirical in its form and relies on dimensional analysis in the representation of some terms. A discussion of these modeled terms is given by Launder and Spalding (41). The model is still evolving and more work remains to be done. The constants C_μ, C_1, C_2, are the so called "universal" constants and may be estimated from such considerations as the known limiting cases of turbulence behind a grid and near the wall turbulence. They have been optimized by application to several isothermal and reacting flow cases (41). The values of Table 29 were recommended by Gosman and Lockwood (42) and differ somewhat with earlier values recommended by Launder and Spalding (41).

Although the k-ε model is a vast improvement over the mixing length models, for elliptic flows, there remain several difficulties (43). The model still assumes that the turbulence is able to adjust itself instantly to local changes in the mean flow field because of the assumed relationship between the Reynolds stresses and the mean strain rates. Real systems suggest that history and action-at-a-distance play important roles in local turbulence. The present k-ε model has serious problems when the local Reynolds number of turbulence is less than unity. This so called laminarization problem has been investigated to some extent (44) but the question remains yet unresolved. In addition, body forces may have a great influence on the generation, damping and transport of turbulent quantities. These have been neglected thus far. Also, the question of combustion generated turbulence is an important issue which is not considered in the present model (45).

3. Combustion Model

Turbulent Fluctuations and Mixing. Approaches for including combustion in multidimensional systems have been identified and reviewed by Smith (39). The approach outlined in this section has been hypothesized previously (45, 46) but this represents the first known formulation and application. The main thrust was to predict the complete species profiles in a gaseous-fired axi-symmetric reactor.

TABLE 29

TURBULENCE MODEL CONSTANTS (From 42)

Constant	Value
C_μ	0.09
C_1	1.44
C_2	1.92
σ_k	0.9
σ_ε	$k^2/[(C_2-C_1)C_\mu^{\frac{1}{2}}]$
κ	.4187

TABLE 30

TURBULENT COMBUSTION MODEL CONSTANTS

Constant	Value
Cg_1	2.8
Cg_2	1.92
σ_f	0.9
σ_g	0.9
σ_{ht}	0.9
σ_h^*	0.8
E*	9.793

*These constants arise from boundary conditions

The importance of properly accounting for the turbulent interactions with the combustion chemistry in diffusion flames cannot be overemphasized (46). In writing conservation equations for individual species in turbulent reacting systems, time-averaging is required. The instantaneous form of these equations can be found in several sources (38). All of these species conservation equations contain reaction rate terms of the form:

$$r_i = m_i m_j \rho^2 A \exp(-E/RT) \tag{17}$$

Proper time-averaging of such nonlinear terms was accomplished by decomposing the instantaneous variables into their main and fluctuating components, giving rise to highly complex terms of a form reported by Pratt (38). Presently, no reasonable means exist for solving such terms. Thus, no attempt was been made to incorporate full, turbulent kinetic schemes into this code.

To model combustion process for BURN, it was recognized that the fuel and oxidizer initially exist as different streams which must be intimately mixed on a molecular level before reaction could occur. The assumption was made that this micromixing process was rate-limiting and that the gaseous kinetic reactions were infinitely fast. This allowed the chemistry to be computed from equilibrium considerations and only one differential equation was required to describe the degree of "mixedness" or "unmixedness" at a point.

For cases where there are two identifiable streams or states that have uniform properties, the mixture fraction is:

$$f = m_p/(m_p + m_s) = \text{mass fraction of fluid originating in primary stream} \tag{18}$$

In turbulent flow, the mixture fraction fluctuates in time, and may be represented statistically by a probability density function (PDF). These fluctuations generally follow a Gaussian distribution except where intermittency is important. Elogobashi and Pun (47) and Pratt (48) have suggested a triangular or saw-tooth wave form for the fluctuations with a resulting uniform or top hat PDF (38, 49). This is the approach taken in BURN.

The differential equation for the mixture fraction in its Reynolds Averaged form is (39):

$$\frac{\partial}{\partial x}(r\bar{\rho}\bar{u}\tilde{f}) + \frac{\partial}{\partial r}(r\bar{\rho}\bar{v}\tilde{f}) - \frac{\partial}{\partial x}\left(\frac{r\mu_e}{\sigma_f}\frac{\partial \tilde{f}}{\partial x}\right) - \frac{\partial}{\partial r}\left(\frac{r\mu_e}{\sigma_f}\frac{\partial \tilde{f}}{\partial r}\right) = 0 \tag{19}$$

The solution of this equation, together with the fluid mechanics model, will prescribe the mean fluid values for the flow and the mixing provided the appropriate mean density is available.

The instantaneous distribution of the mixture fraction at a point is not completely defined, since the mean square fluctuation of the mixture fraction (g) must also be identified, where g is defined as:

$$g = \overline{(f - \bar{f})^2} = \frac{1}{T} \int_0^T [f(t) - \bar{f}]\, dt \tag{20}$$

where time T is large as compared to the time scale of the local turbulence. Launder and Spalding (41) show how a transport equation for g can be derived and appropriate terms modeled in a manner analagous to, and consistent with the other two equations in the k-ε turbulence model. The resulting equation is:

$$\frac{\partial}{\partial x}(r\bar{\rho}\bar{u}\bar{g}) + \frac{\partial}{\partial r}(r\bar{\rho}\bar{v}\bar{g}) - \frac{\partial}{\partial x}\left(\frac{r\mu_e}{\sigma_g}\frac{\partial g}{\partial x}\right) - \frac{\partial}{\partial r}\left(\frac{r\mu_e}{\sigma_g}\frac{\partial g}{\partial r}\right)$$
$$= c_{g1}\mu_e\left[\left(\frac{\partial \bar{f}}{\partial x}\right)^2 + \left(\frac{\partial \bar{f}}{\partial r}\right)^2\right] - c_{g2}\frac{\bar{\rho}\bar{\varepsilon}g}{\bar{k}} \tag{21}$$

With f, g and an assumed shape for the PDF, the maximum and minimum values of f (f_{max}, f_{min}) and the intermittency of primary and secondary streams (a_p, a_s) are uniquely defined (38, 49). The additional "universal" constants introduced by Equation 21 are summarized in Table 30.

Chemical Equilibrium. This section describes the techniques used in BURN to identify the local Reynolds-averaged chemical properties (i.e., species mole fractions, density, temperature, etc.).

For adiabatic operation of the reactor, the instantaneous local enthalpy (h) and element fractions may be calculated directly from f:

$$h = fh_p + (1 - f)\, h_s \tag{22}$$

$$b_k = fb_{kp} + (1 - f)b_{ks} \tag{23}$$

These equations are not dependent on the assumption of chemical equilibrium but only on the additional assumption of equality of species turbulent diffusivities. As discussed in Volume 2, the only required information for determining the local equilibrium properties was the energy level, the elemental composition and the pressure. However, the equilibrium properties are a function of f alone for a given pressure. For example:

$$T = T(b_k, h) = T[b_k(f), h(f)] = T(f) \tag{24}$$

This approach is valid only when reactor heat losses are negligible. Smith (39) discusses modifications to the approach when Equation 22 is not valid. BURN is coded to handle both the adiabatic and non-adiabatic operation.

4. Boundary Conditions

This section discusses the boundary conditions for the variables u, v, k, ε, f, g, and h. Symmetry conditions are imposed on the axis. Thus, the boundary conditions at the axis of symmetry are identical for every variable with zero radial gradients ($\partial d/\partial r = 0$). The solid-wall boundary, inlet and outlet conditions must also be specified and conditions for two inlet streams, the primary and secondary, must be specified completely. First a uniform distribution of all variables was specified at the inlet plane. The flow was assumed to have parallel injection ($v_p = v_s = 0$) with specified flow rate, from which u was calculated directly. The turbulent intensity was specified, from which the turbulent kinetic energy was calculated. For example, for the primary stream:

$$I_p = (\bar{u}_p'^2)^{1/2}/\bar{u}_p = (2\bar{k}_p)^{1/2}/u_p \tag{25}$$

The dissipation level at the inlet streams was generally unknown and must be estimated by calculation from a mixing length formulation as follows:

$$\ell_\varepsilon \equiv \frac{c_\mu^{3/4}\bar{k}^{3/2}}{\bar{\varepsilon}} = \frac{D_e}{4} \tag{26}$$

The mixture fraction at the inlet stream was known by definition (f_B = 1, f_S = 0), and thus the fluctuations in f were by definition zero everywhere at the inlet plane. The enthalpy of the inlet streams must also be specified.

The exit boundary condition for the reactor outlet was applied by using a quadratic extrapolation of the upstream conditions for all variables except the two velocity components. The radial component of velocity (v) was set equal to zero. The axial velocity component (u) was set equal to the upstream value, then adjusted to satisfy overall continuity. This last refinement simply helped the numerical procedure.

The wall boundary conditions were of special interest. It was possible to solve parabolic boundary layer equations at the wall; however, to reduce computer storage and run times, it was convenient to bridge over the semi-laminar region. The approach selected uses the Van Driest hypothesis on turbulent flow near a wall and derived wall functions which were consistent with the logarithmic law of the wall. Launder and Spalding (41) outline this derivation and Patankar and Spalding (50) give more details. In this way, the dependent variables at the wall were linked to those in the logarithmic region (also see Khalil et al., 51). When convective wall heat losses were considered, the wall function for enthalpy was found in an analogous fashion from a universal temperature profile. The turbulent kinetic energy was generated at the wall and calculated from logarithmic law of the wall considerations. Since very inadequate knowledge was known about the rate of dissipation near the wall regions, ε was calculated adjacent to the wall from length scale considerations. The wall boundary conditions on f and g are zero normal derivatives (e.g., $\partial f/\partial r = 0$, or $\partial f/\partial x = 0$). All of the boundary conditions are summarized in Table 31. Their incorporation into the numerical scheme is briefly discussed in the Solution Technique section.

5. Favre Averaging

In the Fluid Mechanics Modeling section, Reynolds averaging was introduced. Specifically, the problem arose in variable density flows with terms such as $u\,\rho'v'$ and $f\,\rho'v'$ being neglected. Some measurements cited by Bilger (45) indicate that these terms can be of the same order and sometimes greater than the momentum and mixture fraction fluxes $\rho\,\overline{u'v'}$ and $\rho\,\overline{v'f'}$. Favre averaging eliminated this problem. In Favre averaging, quantities were weighted by the instantaneous density before averaging:

$$\tilde{\phi} \equiv \frac{\overline{\rho\phi}}{\bar{\rho}} \tag{27}$$

where the tilde identifies the Favre-averaged variable. This approach eliminated double correlations involving density fluctuations from the turbulent fluxes. The resulting partial differential equations were identical in form to the uniform density flow equations except Favre-averaged variables replaced the Reynolds-averaged values. The density remaining in the equations was the time-mean density. When the equations

TABLE 31

"BURN" BOUNDARY CONDITIONS

	$\bar{u}$	$\bar{v}$	$\bar{k}$	$\bar{\varepsilon}$	g	$\bar{h}$	$\bar{f}$
primary jet	uniform at u_p	0	from primary turbulent intensity	from length scale	0	uniform at h_p	1.0
secondary jet	uniform at u_s	uniform at v_s	from secondary turbulent intensity	from length scale	0	uniform at h_s	0
symmetry	$\bar{u}_{i,1} = \bar{u}_{i,2}$	0	$\bar{k}_{i,1} = \bar{k}_{i,2}$	$\bar{\varepsilon}_{i,1} = \bar{\varepsilon}_{i,2}$	$g_{i,1} = g_{i,2}$	$\bar{h}_{i,1} = \bar{h}_{i,2}$	$\bar{f}_{i,1} = \bar{f}_{i,2}$
top wall	τ_w from wall function	0	near the wall value from wall function	near the wall values from length scale	$g_{i,j} = g_{i,j-1}$	q_w from wall	$\bar{f}_{i,j} = \bar{f}_{i,j-1}$
side wall	0	τ_w from wall function	near the wall value from wall function	near the wall values from length scale	$g_{1,j} = g_{2,j}$	q_w from wall function	$\bar{f}_{1,j} = \bar{f}_{2,j}$
outlet	$\bar{u}_{i,j} = \bar{u}_{i-1,j}$ and adjusted for continuity	0	quadratic extrapolation	quadratic extrapolation	quadratic extrapolation	quadratic extrapolation	quadratic extrapolation

Note: Saying $\phi_{i,1} = \phi_{i,2}$, etc. is the differencing scheme for $\partial\phi/\phi_n = 0$

were written in Reynolds-average form and the fluctuating density terms were neglected, effectively, the Favre-averaged equations were being used. The same modeling terms may be used for the Favre-averaged equations as was introduced previously for the Reynolds-averaged turbulent model (45, 52).

BURN was coded to handle Favre-averaged computations as well. A top hat shape for the Favre-averaged PDF was assumed and otherwise, the procedure is analogous to Reynolds-averaging. A comparison of predictions from the two techniques is given in Smith (39).

It was only logical to ask what form of the variables should be used, the Favre-averaged or the Reynolds-averaged values? An appropriate answer would be whichever form was measured. Bilger (52) shows how probe measurements might measure the Favre-averaged mole fractions if the probe samples at constant velocity. However, if the probe samples at a constant mass flow rate, then the Reynolds-mean is measured. Smith (39) provides additional discussion of this issue.

6. Solution Technique

The steady-state, second order, non-linear, elliptical partial differential equations to be solved were written in one common form. The form of this equation for a general variable and the associated variables and source terms are summarized in Table 32. The convenience of one form for all the equations meant that only one solution technique needed to be used.

Roache (53) presents an excellent review of computational techniques available for solving fluid dynamics problems. The particular fluid flow problem of interest to this dissertation, that of a recirculating flow field, has been examined extensively over a number of years by researchers at Imperial College. The solution of the flow equations in the primitive variables incorporated in TEACH (54) was used in BURN. It is an iterative, steady-state, finite-difference approach.

Each of the differential equations must be cast in to finite difference form and solved over some appropriate grid spacing. A series of grid lines, running orthogonally to the coordinate directions, define node points at their intersection, where the values of the dependent variables are usually identified. Roache (53) has reviewed application of the flow equations to various possible mesh systems and shows that in the (u, v, p) formulation, the variables u and v are most conveniently and accurately evaluated with node points lying on the boundary with p and ρ being placed at one-half grid spacing off the boundary. This staggered mesh system is used in the TEACH algorithm and it is shown in Figure 83 as it is applied in BURN. The grid spacing is not equal but concentrated in areas of largest gradients to help convergence speed. The present version of BURN uses arithmetic averaging to obtain property values at mesh boundaries between node points so the distance between nodes should not change by more than a factor of 1.1. Wormeck (55) gives an excellent detailed description of the grid used by TEACH. The details of the numerical procedure employed are discussed further

TABLE 32

BURN DIFFERENTIAL EQUATION SET

General Equation

$$\frac{1}{r}\frac{\partial}{\partial x}(r\bar{\rho}\,\bar{u}\,\bar{\phi}) + \frac{1}{r}\frac{\partial}{\partial r}(r\bar{\rho}\,\bar{v}\,\bar{\phi}) - \frac{1}{r}\frac{\partial}{\partial x}(r\Gamma_\phi\frac{\partial\bar{\phi}}{\partial x}) - \frac{1}{r}\frac{\partial}{\partial r}(r\Gamma_\phi\frac{\partial\bar{\phi}}{\partial r}) = S_\phi$$

Specific Variable ($\bar{\phi}$)	Coefficient (Γ_ϕ)	Source Term (S_ϕ)
$\bar{u}$	μ_e	$-\frac{\partial\bar{p}}{\partial x} + \frac{1}{r}[\frac{\partial}{\partial x}(r\mu_e\frac{\partial\bar{u}}{\partial x}) + \frac{\partial}{\partial r}(r\mu_e\frac{\partial\bar{v}}{\partial x})]$
$\bar{v}$	μ_e	$-\frac{\partial\bar{p}}{\partial r} + \frac{1}{r}[\frac{\partial}{\partial x}(r\mu_e\frac{\partial\bar{u}}{\partial r} + \frac{\partial}{\partial r}(r\mu_e\frac{\partial\bar{v}}{\partial r})] - \frac{2\mu_e\bar{v}}{r^2}$
$\bar{k}$	$\frac{\mu_e}{\sigma_k}$	$\Phi - \bar{\rho}\,\bar{\varepsilon}$
$\bar{\varepsilon}$	$\frac{\mu_e}{\sigma_e}$	$\frac{\bar{\varepsilon}}{\bar{k}}[C_1\Phi - C_2\bar{\rho}\,\bar{\varepsilon}]$
$\bar{g}$	$\frac{\mu_e}{\sigma_g}$	$C_{g1}\mu_e[(\frac{\partial\bar{f}}{\partial x})^2 + (\frac{\partial\bar{f}}{\partial f})^2] - \frac{C_{g2}\bar{\rho}\,\bar{\varepsilon}}{\bar{k}}$
$\bar{f}$	$\frac{\mu_e}{\sigma_f}$	0
$\bar{h}$	$\frac{\mu_e}{\sigma_h}$	0

where $\Phi = \mu_e\left\{2[(\frac{\partial\bar{u}}{\partial x})^2 + (\frac{\partial\bar{v}}{\partial r})^2 + (\frac{\bar{v}}{r})^2] + (\frac{\partial\bar{u}}{\partial r} + \frac{\partial\bar{v}}{\partial x})^2\right\}$

$\mu_e = \mu_t + \mu_\ell$

$\mu_t = C_{\mu\rho}\bar{k}^2/\bar{\varepsilon}$

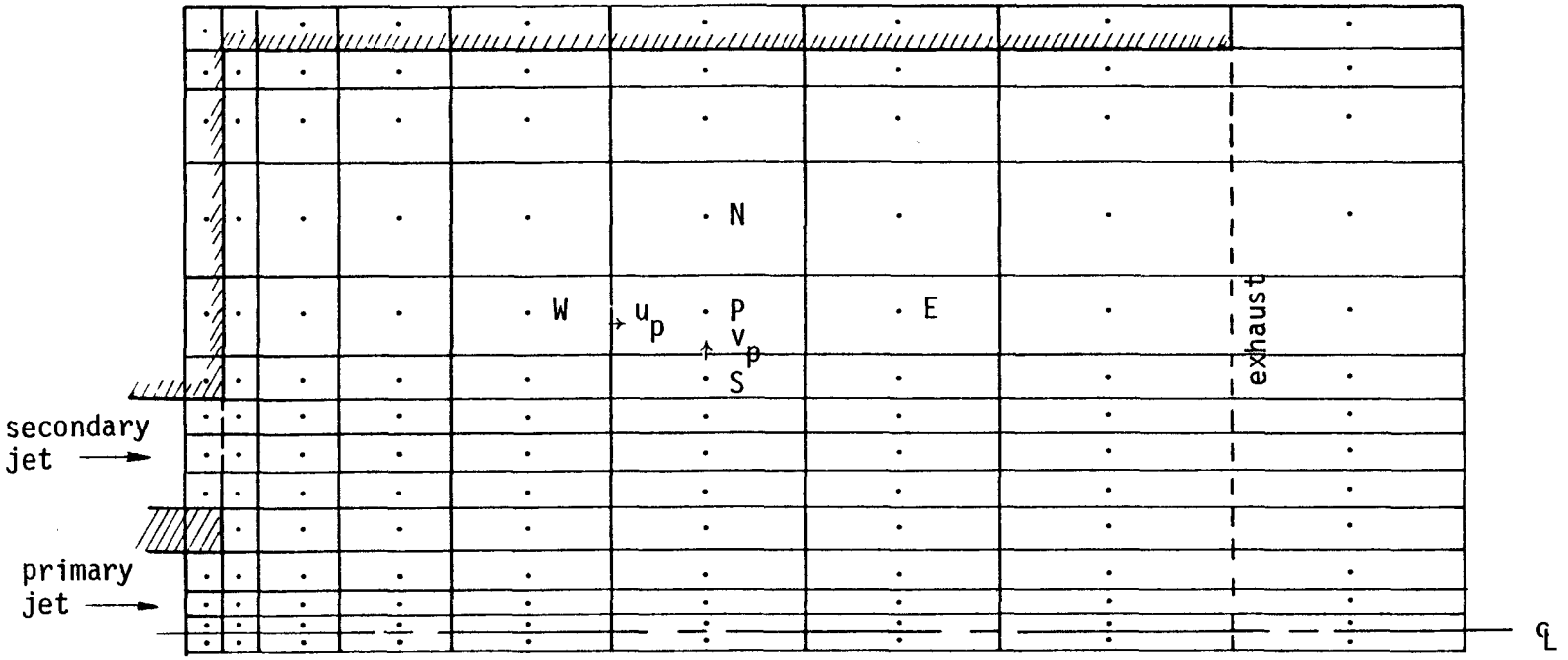

Figure 83. Sample grid pattern for BURN.

by Smith (39) including the finite difference scheme for the partial differential equations as well as the Gaussian quadrature used for the PDF.

7. Model Predictions and Verification

BURN was applied to predict the characteristics of several non-reacting (cold flow) turbulent mixing tests as well as reacting (hot-flow) gaseous, turbulent diffusion flames. Both cases were cylindrical, confined jets. The primary objective of this particular code development was not to verify in detail each of the code modules but to form a basis with reasonable verification for the future incorporation of pulverized coal. Many other investigators have studied the individual components such as the turbulent model, the numerical method, etc., as reviewed by Smith (39).

A summary of all final converged predictions made with BURN is shown in Table 33. This does not include any of the computations required for model development or debug, nor does it show any of the unsuccessful computer runs. A total of fifty-three converged, final-data computations were made.

The discussion of model predictions and verification which follows starts by addressing some numerical problems. Grid size resolution is discussed first. Inlet turbulent intensities are required as boundary conditions on the turbulence variables. Since measured values are presently unavailable, the effect of assumed conditions is studied next. Then a short discussion is given of the sensitivity of the "universal" turbulence constants. Although this study centers on reacting flow systems, some time was spent verifying and studying portions of the code by performing cold-flow validation computations. A summary of these predictions and observations is presented. Finally, the reacting flow predictions are presented, together with comparison to experimental measurements, when available.

Grid Size Resolution. Smith (39) addressed the question of numerical error, as well as identifying other authors who have also considered these issues for the same numerical technique. The variable grid spacing used in BURN was discussed previously. In this section the size of the grid used is identified as IXJ, where I represents the number of main nodes in the axial direction, and J represents the number in the radial direction. To test the sensitivity of the grid size to the predicted results it was thought that a rigorous test lies in the centerline mixing. The extent and rate of mixing is strongly affected by both the fluid mechanics (through u, v, k, ε) and the combustion (through p). A log-log plot of the centerline mixture fraction versus a dimensionless axial distance (z/r_1) is particularly useful method for displaying variations in mixing rates (5-9).

TABLE 33

SUMMARY OF "BURN" PREDICTIONS

Reactor	Number of Predictions	Comments
BYU combustor	27	o Studied effects of grid size (∿7), effect of inlet turbulent intensities (∿8), effect of fuel pyrolysis (∿4), effect of secondary temperature (∿3). o Comparisons made between Favre and Reynolds averaging. o Comparisons made between experiment and theory.
BYU cold flow facility	18	o Predictions made for conditions of Sharp, Tice and Memmott. o Studied effects of grid size (∿3), inlet turbulent intensities (∿7), effect of turbulence constants (∿3). o Comparison made between experiment and theory.
British combustor	2	o Comparison of BURN with other combustion models. o Comparison of measurement and theory.
British cold flow facility	2	o Check out of turbulence model, comparison with other cold flow mixing models, inclusion of end plate at outlet.
AEDC cold flow facility	4	o Study of effect of inlet turbulent intensities, effect of laminarization.
Total	53	

The reacting and non-reacting flow predictions for evaluating grid-size effects were performed for the laboratory combustor and cold-flow facility (3). The reacting test series of Lewis (56) wherein the combustor was fired with natural gas and the non-reacting tests of Sharp (9) were used. The experimental conditions of these combustor and cold-flow tests are summarized in Table 34.

Figure 84 shows reacting-flow axial decay graphs for several different symmetric and asymmetric grid sizes. It is apparent that grid size has a significant impact on the calculations, particularly with this configuration and conditions. The experimental centerline mixture fraction data of Lewis (56) are also shown. Figure 84 also shows axial decay graphs for the cold flow tests. The two lines for two different grid sizes show virtually no deviation. For the cold-flow tests, numerical error, due to grid resolution was eliminated with a grid size of 20 x 20; whereas, for the reacting flow case, a grid size of at least 31 x 31 is required. The main difference between the two results seemed to be in the size of the mixing chamber relative to the primary or secondary tubes. The less drastic the increase in mixing chamber, the more coarse the grid could be.

Effect of Inlet Turbulent Intensities. Equation 25 showed the turbulent intensity to be a requirement for the inlet boundary condition for the turbulent kinetic energy (k). However, the turbulent intensities of the primary and secondary streams are not generally available. Gosman, et al. (57) have used a turbulent intensity of 10%, claiming that inevitably some uncertainty is introduced, but at least a bias is not made simply to procure better agreement.

Figure 85 shows some selected examples of the effect of the inlet turbulent intensities on the centerline mixture fraction decay in a reacting flow computation for the BYU Combustor with natural gas. All computations were performed with a constant grid size of 20 x 30. A strong effect of initial turbulent intensity on the apparent core length and the decay slope was observed. This dependence of the near field to the initial conditions has also been noted by Husain and Hussain (58).

Turbulence Constants. Tables 29 and 30 summarized the turbulent constants used in BURN. While it was beyond the scope of this research project to verify the validity of these constants, selected computations were performed to test the sensitivity of model predictions to these constants.

The "universal" constants were changed one at a time by about 10%. The predictions were all performed for the reacting flow conditions of Table 34. Changing the value of one of these constants was the only change made from one prediction to the next. In all cases, the effect of these changes was minimal. The effect of changing the turbulent Schmidt and Prandtl Numbers was also examined. The effect of changing the inlet turbulent intensities by 40% was much more dramatic than changing the turbulent Schmidt Number by 40%; thus, the effect of the uncertainty in turbulent Schmidt Number was concluded to also be minimal (39).

TABLE 34

INPUT CONDITIONS FOR"BURN"COMPUTATIONS

	A. Combustor	B. Cold Flow		
		A	B	C
Primary Gas				
Temperature, K	286	284	283	283
Mass Flow Rate, g/s	3.1	24.3	22.1	22.1
Velocity, m/s	21.7	35.0	31.8	31.8
Composition: CH_4 (molar %)	85.8			
C_2H_6	6.1			
Ar	5.5	28	70	70
Air		72	30	30
N_2	2.3			
Secondary Gas				
Temperature, K	589	284	283	283
Mass Flow Rate, g/s	36.2	45.7	54.0	54.0
Velocity, m/s	34.7	35.1	41.3	41.3
Composition: N_2 (molar %)	78.3			
O_2	20.8			
Ar	0.9			
Air		100	100	100
Mixing Chamber Geometry				
Primary Diameter, cm	1.6	2.5	2.5	2.5
Secondary Diameter, cm	5.4	12.7	12.7	12.7
Chamber Diameter, cm	20.3	26.0	20.6	34.3
Parallel Injection Pressure, kPa	93.4	87.6	87.6	87.6
Wall Temperature, K	1200			

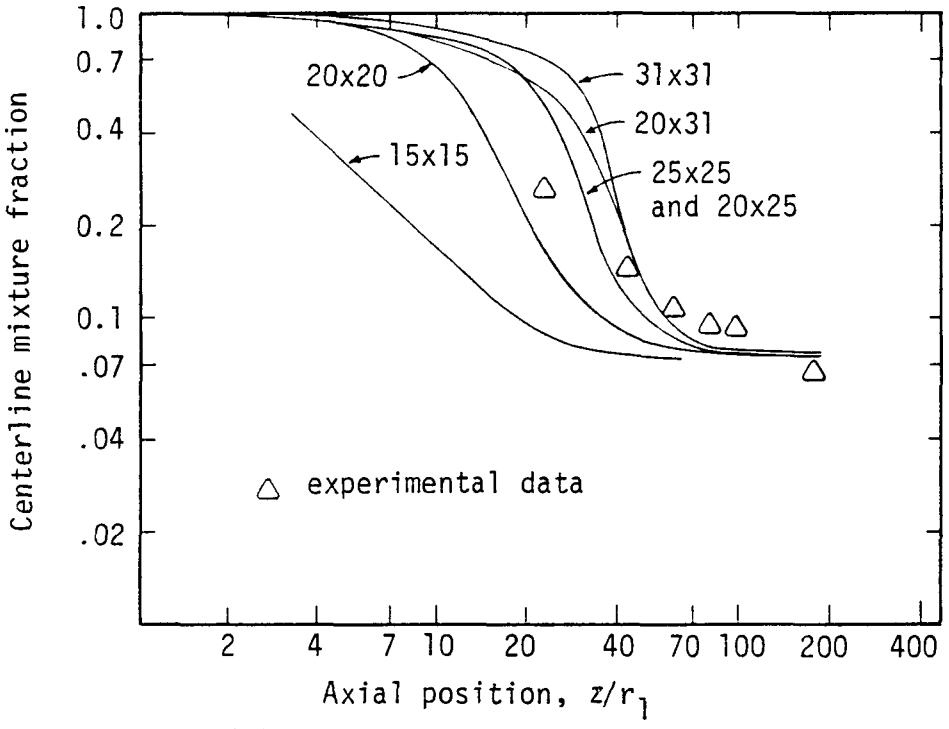

(a) Combustor tests with natural gas

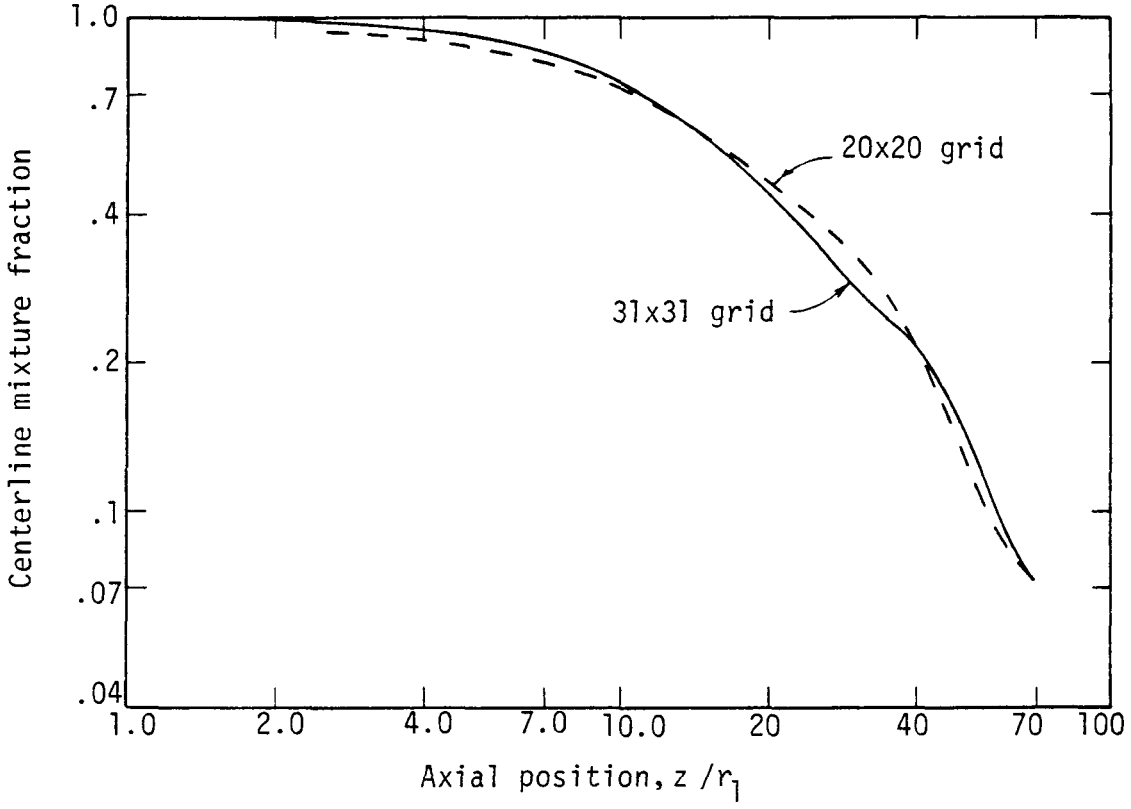

(b) Cold flow tests

Figure 84. Effect of grid size on centerline mixture fraction decay.

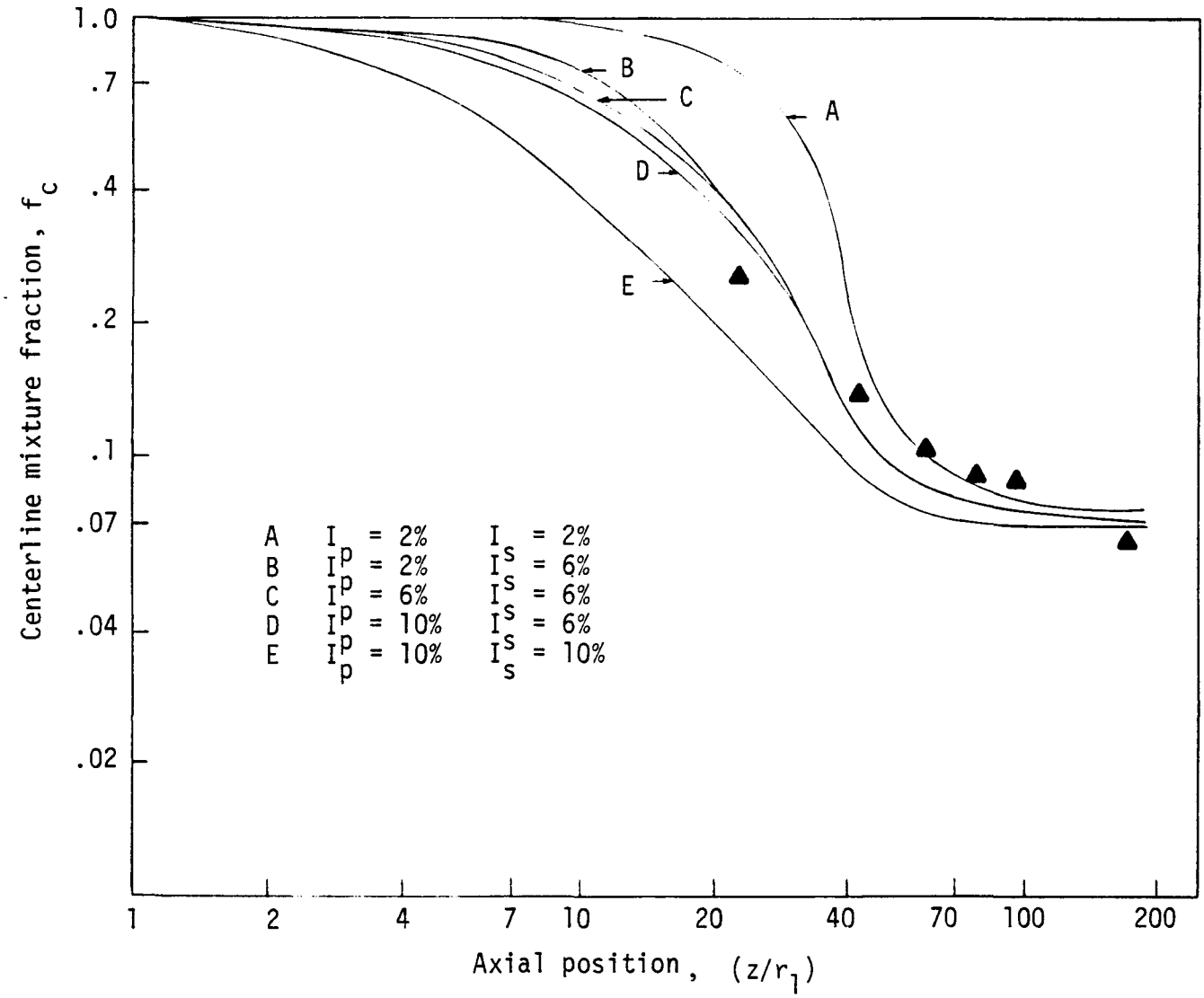

Figure 85. Effect of initial turbulent intensities on BURN predictions.

Comparison with Cold Flow Data. The cold flow facility which is discussed in Section 2 has been described in detail previously (2-12). Of interest to this study are the measurements of Tice and Smoot (8) in a recirculating mixing chamber. Two configurations and conditions were used for comparison, and are labeled conditions B and C in Table 34(b). Figure 86 shows the axial decay plots for cold flow conditions C and B respectively. The behavior predicted by BURN is shown together with the experimental data reported by Tice and Smoot (8). Predictions with different assumptions for the initial turbulent intensities are also shown. None of the lines pass through the data points very well; however, for all predictions the stream is well-mixed at (z/r_1) near 80. This location is about the same regardless of the assumed inlet turbulent intensity, geometry, or conditions. It also appears to be about the same for reacting or non-reacting systems (see Figures 84 to 86). In addition, this point seems to be verified by the data. Smith (39) discussed these observations; however, for these cold flow comparisons, uncertainties in initial turbulent intensity prevent rigorous evaluation of the code predictions.

BURN was also used to make theoretical comparisons with the independent isothermal flow measurements of Baker, et al. (59). Kahlil, et al. (51) have also compared this version of the k-ε turbulence model to the same data. This computation allowed comparison to both independent data and another code. Before the computation could be performed, BURN had to be altered to include a partial end plate blocking part of the exhaust. The exit boundary conditions had to be changed accordingly, including wall functions where required. Comparisons were made for both the mean axial velocity and the mean turbulent energy. Agreement with data is good and there was essentially no difference between the two codes for this case. Smith (39) discussed additional aspects of the code when applied to cold flow cases, including the limitations of the k-ε model for low turbulence, highly accelerating flows.

Comparison with Reacting Flow Data. Lewis (56) has conducted a series of reacting, natural gas/air tests in order to provide a consistent, detailed set of gaseous combustion data primarily for validation of this two-dimensional code. The test conditions employed are summarized in Table 34. Predictions with BURN have been made and are compared with experimental data in this subsection. To give a better visualization of the combustion system, and to present the general characteristics of the prediction, two-dimensional contour graphs have been constructed for the axial velocity, mixture fraction, temperature and O_2 concentration. These are shown in Figure 87. The recirculation zone and early mixing and combustion are evident.

During the comparison of model predictions with experimental data of Lewis (56), the equilibrium assumption was questioned. Predictions of the conditions in Table 34 showed values of some minor species (particularly H_2 and to some extent CO) to be far in excess of measured values in certain regions of the reactor. In particular, the code indicated that the fuel was pyrolyzing in hot, fuel-rich regions. The theory shows H_2 mole fractions in excess of 15%, whereas the measurements show less than 0.1% (56). Two possible reasons for this discrepency were: 1) perhaps H_2 measurements were in error because the H_2 was reacting

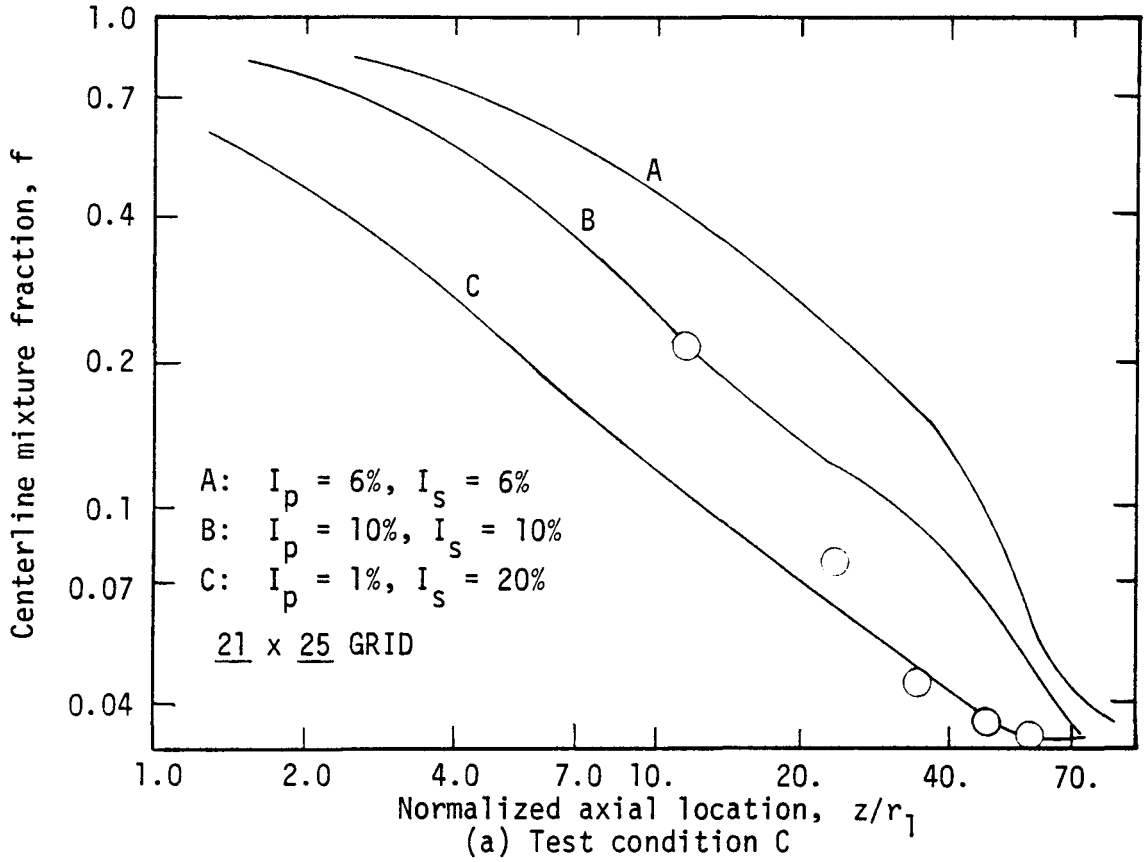

(a) Test condition C

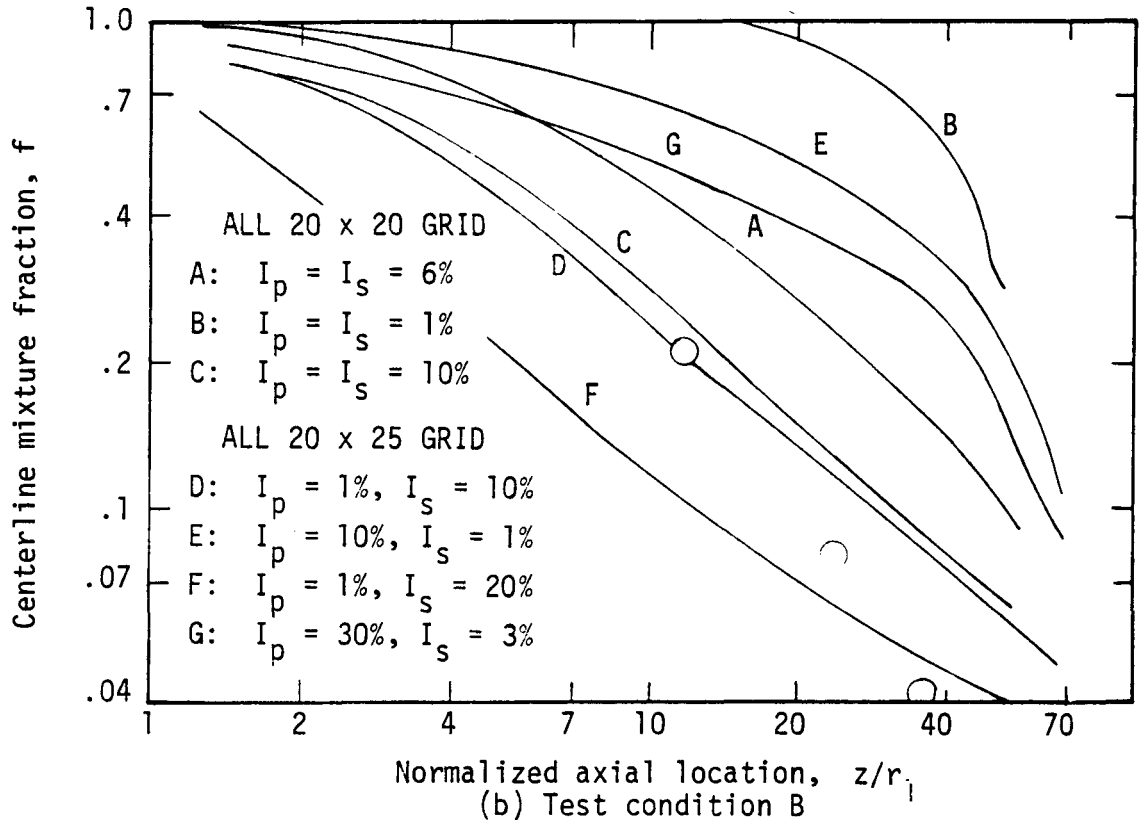

(b) Test condition B

Figure 86. Effect of inlet turbulent intensities on centerline mixture fraction decay for cold-flow mixing experiments.

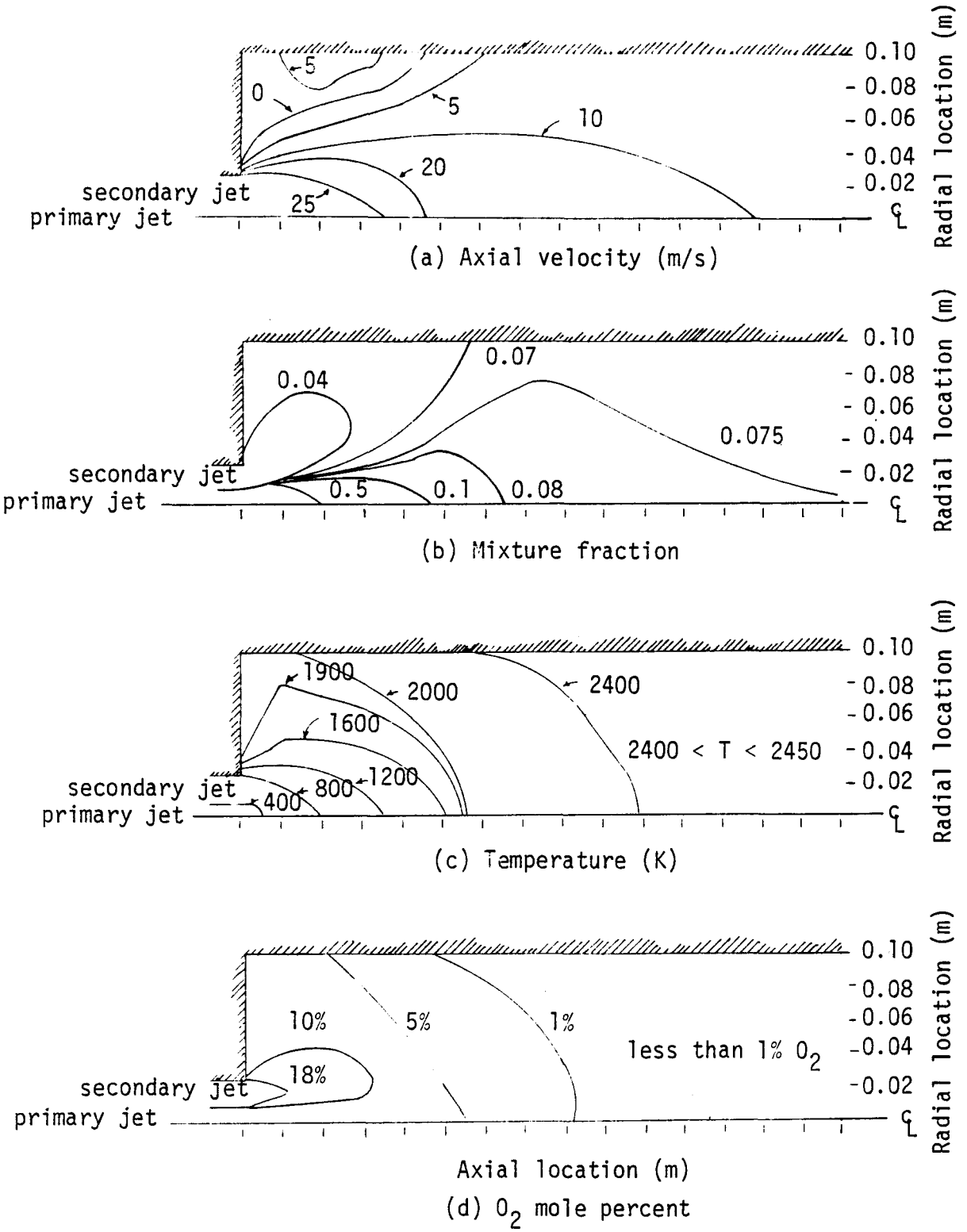

Figure 87. Predicted reactor contours for axial velocity, mixture fraction, temperature, and oxygen for gaseous combustion .

with available O_2 in the probe, 2) perhaps H_2 formation is reaction rate-limited and does not form in equilibrium amounts.

The first reason was tested by performing an oxygen balance inside the probe. If all the predicted H_2 were reacted in the probe, it would also require consumption of O_2; however, measurements indicated substantial O_2 mole fractions (on the order of predicted amounts). It was concluded that H_2 was not reacting in the probe. The second suggestion indicates that pyolysis of the fuel to H_2 is limited by kinetics and not by mixing. An estimate of the kinetic limitations was made with a detailed laminar flame propagation model (60). The computed characteristic reaction time was ten times larger than the estimated eddy life time. While other major species (CO_2, H_2O, O_2, CH_4) had reached their equilibrium values, the computed H_2 level was well below the equilibrium value. The only other noticable deviant from equilibrium was CO. Thus, equilibrium amounts of H_2 and CO might not be expected. In light of the small measured quantities of these species, the most apparent improvement to the model was to simply restrict the equilibrium calculation from considering any possible formation of CO or H_2. This may not be the only explanation for the discrepencies between measured and predicted H_2 and CO levels. For example, the chosen shape of the probability density function may be distorting the mean values of the H_2 and CO concentrations.

Figure 88 presents some of the predicted results for the gaseous combustion conditions of Lewis (56). Based on the preceding discussion, H_2 and CO were not allowed in the computation. This figure also presents measured data for the concentration profiles. Agreement between theory and measurement is poorest in the early regions of the reactor near the centerline. Lewis (56) indicates that measurements in this region of very steep gradients is less reliable for a number of reasons. The agreement in the recirculation zone is reasonable. In the aft-regions of the reactor, the CO_2 and CH_4 agreement is not as good as might be expected. This is due to the model restriction on H_2 and CO formation. Experimental measurements show about 2% H_2 and 2% CO, which could account for the discrepencies. It appears that in these aft-regions, the reactor the time scale is larger and equilibrium is more closely approached, even for H_2 and CO. Model predictions at the axial position of 137.5 cm, when CO and H_2 are included in the calculation, show much better agreement with data (Smith, 39). An interesting observation from these data and predictions is the overlap of fuel and oxidizer in all the regions of the reactor. This phenomenon resulting from unmixedness is observed both theoretically and experimentally and was discussed in detail by Smith (39). All of these predictions used the conventional Reynolds averaging and ignored the density fluctuations. Smith discusses predictions based on Favre-averaging (39).

8. Extension to Coal Dust

Extension of BURN to pulverized coal systems requires the following additional components: 1) a dispersed particle flow submodel, 2) a coal reaction submodel, 3) a model to account for mean turbulent gas phase properties that originate from the coal, and 4) a coal dust radiation submodel. Conservation equations for particle flow have been considered in a Lagrangian framework; that is, following the motion

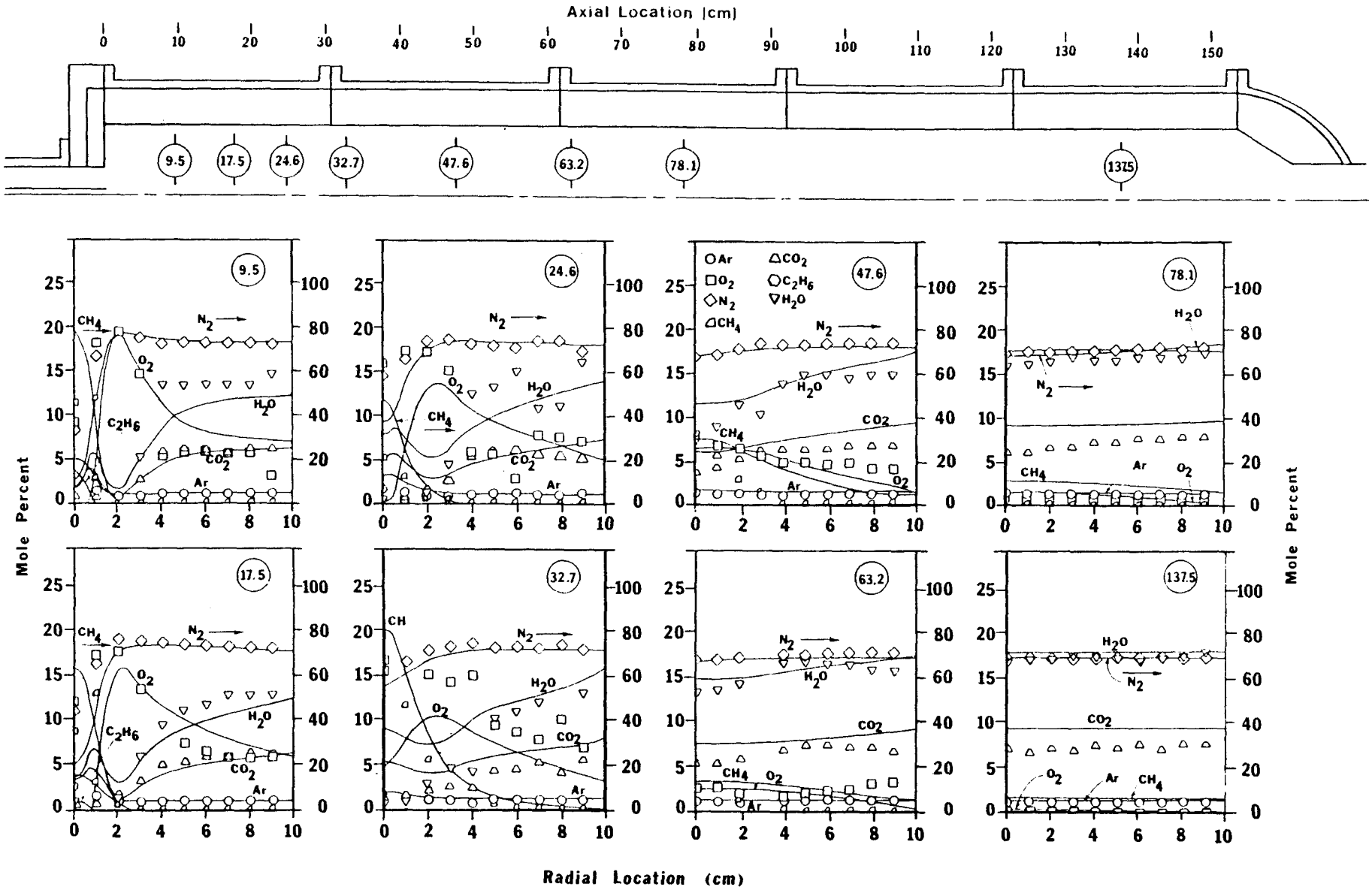

Figure 88. Two-dimensional gaseous fuel predictions and experimental radial location, cm measurements for local species composition.

of individual particles. Changes in coal properties are calculated by integration along particle pathlines, and the resulting fluxes of mass, momentum, and energy are calculated in each computational cell intersected by the particle trajectories, and are stored in (Eulerian) gas-phase source terms S_p, to be considered at a later iteration for solution of the gas-phase equations. The coal submodel follows directly from 1-DICOG. A statistical PDF method has been devised to account for the fluctuations in the coal off-gas. The formulation of the radiation submodel is based on a flux method for emitting absorbing and scattering radiation in a particle-laden system. The description of the model is documented in Smoot and Pratt (38).

This Lagrangian technique for tracking particle trajectories has been discussed in detail by Crowe (38). The most serious shortcoming of the technique is the difficulty in incorporation of turbulent diffusion of the particles. Eulerian approaches are more easily able to incorporate turbulent diffusion by a gradient approximation; however, they lack the ability to include the important history effects of the reacting particles. A Lagrangian method has been devised to handle this complexity and is being evaluated. Development, integration and evaluation of these components for extending BURN to coal dust systems is continuing at this laboratory.

C. ACCOMPLISHMENTS

1. One-Dimensional Model (1-DICOG) Accomplishments

Accomplishments for the one-dimensional model include:

- Application of the code to predict the characteristics of several laboratory and industrial combustors and gasifiers. These further applications include the BYU Rate Resolution gasifier, Foster-Wheeler gasifier, Coates' gasifier, a Babcock and Wilcox staged furnace and the BYU Rate Resolution combustor.

- Improvement in the computational efficiency of the numerical model by including such options as the pseudo-steady-state approximation for stiff differential equations, and by treating radiation as a diffusion process when calculating optically dense systems.

- Verification of the code by comparison of predicted and measured properties of the laboratory combustor for poly-dispersed particles and for different particle distributions.

- Complete documentation of the numerical model and compilation of the detailed user's manual. The one-dimensional model was a deliverable product of this research effort.

2. Two-Dimensional Model Accomplishments

Accomplishments include the following:

- Formulation, coding, and completion of a two-dimensional, axi-symmetric, turbulent gaseous combustion model. The model includes the effects of turbulent fluctuations on the composition and other properties of the reacting flow field by means of a probability density functon approach.

- Application of the gaseous combustion code to several combustion systems including cold flow mixing and reacting combustors.

- Evaluation of the code by comparison of predictions to measured properties. The experimental data base included measurements from this laboratory as well as from other laboratories.

- Comparison of model predictions with the results of other combustion models being developed at other laboratories.

- Formulation of a technique to include reacting coal particles in the turbulent combustion code. This formulation includes the interactions of the turbulent gas field with the motion of the particles as well as the effect of the turbulent fluctuations on the gas phase chemical field.

3. Observations and Conclusions for One-Dimensional Model

- The mathematical model of one-dimensional coal combustion and gasification agrees with experimental evidence for combustion within the limitations of its assumptions, of which one of the most limiting is its one-dimensional nature. Limited comparisons with gasification data were not as good.

- Predictor-corrector numerical techniques are sufficiently stable to handle transfer processes. The steady state assumption for avoiding numerical stiffness enhances computational efficiency after particle burnout.

- Secondary mixing and recirculation submodels in the one-dimensional code are not satisfactory for many systems. When these mixing processes are important, a more complex, multi-dimensional model is required.

4. Observations and Conclusions for Two-Dimensional Model

- The probability density function approach to combusting systems is a viable method for incorporation of the fluctuations

caused by turbulence; however, further investigations and determinations of the shape of the PDF are required.

- The ability to model turbulent gaseous combustion is far enough advanced to permit incorporation of reacting coal particles.

V. REPORTS AND TECHNICAL CONTACTS

A. CONTRACT REPORTS

Contract reports published during this study were:

1. Smoot, L. Douglas, Hanks, Richard W. and Hedman, Paul O., "Mixing and Gasification of Coal in Entrained Flow Systems," QPR No. 1, U. S. DOE Contract EF-77-S-01-2666, Combustion Laboratory, Brigham Young University, Provo, Utah, 15 July 1977.

2. Smoot, L. Douglas, Hanks, Richard W. and Hedman, Paul O., "Mixing and Gasification of Coal in Entrained Flow Systems," QPR No. 2, U. S. DOE Contract EF-77-S-01-2666, Combustion Laboratory, Brigham Young University, Provo, Utah, 15 October 1977.

3. Smoot, L. Douglas, Hanks, Richard W. and Hedman, Paul O., "Mixing and Gasification of Coal in Entrained Flow Systems," QPR No. 3, U. S. DOE Contract EF-77-S-01-2666, Combustion Laboratory, Brigham Young University, Provo, Utah, 15 January 1978.

4. Smoot, L. Douglas, Hanks, Richard W. and Hedman, Paul O., "Mixing and Gasification of Coal in Entrained Flow Systems," QPR No. 4, U. S. DOE Contract EF-77-S-01-2666, TID-28504 Combustion Laboratory, Brigham Young University, Provo, Utah, 15 April 1978.

5. Smoot, L. Douglas, Hanks, Richard W. and Hedman, Paul O., "Mixing and Gasification of Coal in Entrained Flow Systems," QPR No. 5, U. S. DOE Contract No. EF-77-S-01-2666, Combustion Laboratory, Brigham Young University, Provo, Utah, 15 July 1978.

6. Smoot, L. Douglas, Hanks, Richard W. and Hedman, Paul O., "Mixing and Gasification of Coal in Entrained Flow Systems," QPR No. 6, U. S. DOE Contract Combustion Laboratory, Brigham Young University, Provo, Utah, 15 October 1978.

7. Smoot, L. Douglas and Hedman, Paul O., "Mixing and Gasification of Coal in Entrained Flow Systems," QPR No. 7, U. S. DOE Contract EF-77-S-01-2666, Combustion Laboratory, Brigham Young University, Provo, Utah, 15 January 1979.

8. Smoot, L. Douglas and Hedman, Paul O., "Mixing and Gasification of Coal in Entrained Flow Systems," QPR No. 8, U. S. DOE

Contract EF-77-S-01-2666, Combustion Laboratory, Brigham Young University, Provo, Utah, 15 April 1979.

9. Smoot, L. Douglas and Hedman, Paul O., "Mixing and Gasification of Coal in Entrained Flow Systems," QPR No. 9, U. S. DOE Contract EF-77-S-01-2666, Combustion Laboratory, Brigham Young University, Provo, Utah, 15 July 1979.

B. TECHNICAL PUBLICATIONS

The following journal publications based on this research study were published or accepted for publication during this contract:

1. Memmott, Vincent J. and Smoot, L. Douglas, "Cold Flow Mixing Rate Data for Pulverized Coal Reactors," AIChE J, 24, 466 (1978).

2. Tice, Christopher L. and Smoot, L. Douglas, "Cold Flow Mixing Rates with Recirculation for Pulverized Coal Reactors," AIChE J, 24, 1029 (1978).

3. Smith, Philip J. and Smoot, L. Douglas, "One-Dimensional Models for Pulverized Coal Combustion and Gasification," accepted for publication, Comb. Sci. Tech., 1980.

In addition, papers were submitted for publication in Combustion and Flame by Smith and Smoot (two-dimensional gaseous code) and by Skinner, Price, Hedman and Smoot (ASME).

During this contract period, the book:

Smoot, L. Douglas and Pratt, David T. (Eds). Pulverized Coal Combustion and Gasification - Theory and Applications for Continous Flow Processes, Plenum Press, New York, March 1979 (333 pg. book).

was published. This book provides a detailed technical foundation for the modeling approach used in this study.

C. TECHNICAL PRESENTATIONS

The following technical presentations were made during the contract period.

1. Smith, Philip J. and Smoot, L. Douglas, "One-dimensional Model for Pulverized Coal Combustion and Gasification," 1979 Spring Meeting, Western States Section, Combustion Institute, Provo, Utah, April 23, 1979 (Preprint 79-2).

2. Hedman, Paul O. and Smoot, L. Douglas, "Coal Combustion and Gasification Research at BYU," Fourth Rocky Mountain Fuel Symposium, Salt Lake City, Utah, Feb. 9-10, 1979.

3. Smith, Philip J. and Smoot, L. Douglas, "Pulverized Coal Combustion or Gasification Model," Third Rocky Mountain Fuel Symposium, Albuquerque, New Mexico, Feb. 10-11, 1978.

4. Hedman, Paul O., Smoot, L. Douglas, Hanks, Richard W., Thurgood, J.R., and Skinner, F.D., "The BYU Rate Resolution Coal Furnace and Goal Gasifier," Third Rocky Mountain Fuel Symposium, Albuquerque, New Mexico, Feb. 10-11, 1978.

5. Smoot, L. Douglas, "Coal Gasification Processes," ERDA-NSF-EPRI Contractors Conference, Pittsburgh, Pa., August 1977.

6. Hedman, Paul O., "Coal Gasification Mixing and Kinetics," DOE Contractors Review, Lexington, Ky., August 1978.

7. Hedman, Paul O., "Coal Gasification Modeling," EPRI Modeling Conference, Palo Alto, Ca., June 1978.

Technical presentations were planned for the 5th Rocky Mountain Fuel Symposium (Feb., 1980) and the Annual ASME Meeting, Chicago, Nov., 1980. In addition, the principal investigator gave invited technical seminars on pulverized coal mixing, combustion and gasification at the University of Utah (Salt Lake City, Utah), Phillips Petroleum Co. (Bartlesville, Oklahoma), Los Alamos Scientific Laboratory (Los Alamos, New Mexico), Combustion Engineering (Windsor, Conn.), Arizona State University (Arizona), Northwestern University (Illinois), and Stone and Webster (New York).

D. THESES AND DISSERTATIONS

The following disertations and theses related to this contract study were completed during the contract period:

1. Tice, Christopher L., "Particle and Gas Mixing Rates in Confined Coaxial Jets with Recirculation," Master of Science Thesis, Chemical Engineering Department, Brigham young University, Provo, Utah, August 1977.

2. Smith, Philip J., "Theoretical Modeling of Coal or Gas-fired Turbulent Combustion or Gasification," PhD Dissertation, Chemical Engineering Department, Brigham Young University, Provo, Utah, August 1979.

In addition, theses by Sharp (cold flow mixing with recirculation), Leavitt (cold flow mixing with swirl), and Price (gasifier pollutants) were in preparation, as was the dissertation by Skinner (coal gasification).

E. TECHNICAL VISITORS AND VISITS

Contract officers for this contract from University Programs, the U.S. Department of Energy, visited this laboratory during this contract study. On Monday, December 3, 1979, Dr. Robert Wellek, DOE-Washington, D.C., and Dr. Bernard Blaustein, Pittsburgh Energy Development Center visited this laboratory and reviewed technical accomplishments on this project.

The principal investigator visited ERDA (DOE) in August of 1977 with Paul O. Hedman and November 1977, and reported technical progress on this study. In addition, laboratory personnel conducted technical visits relating to pulverized coal combustion and gasification to the following during the contract period: Electric Power Research Institute, KVB, Inc., Systems, Science and Software, Jaycor Corp., Babcock and Wilcox, Foster-Wheeler, Combustion Engineering, the U.S. Bureau of Mines, and General Motors. The principal investigator presented technical seminars at Combustion Engineering, Babcock and Wilcox, and Foster-Wheeler Corp. during the contract period. Technical results of this research work were presented in detail and discussed.

Also, during the contract period, technical visitors from Babcock and Wilcox (Ohio), Stal-Lavel (Sweden), National Research Institute (Japan), Institute of Mines (Poland), Environmental Protection Agency (North Carolina), Technical Institute (Denmark), University of Stütgardt (West Germany), University of Utah (Utah), Energy and Environmental Research Corp. (Los Angeles), U.S. Bureau of Mines (Pennsylvania), Eyring Research Institute (Utah), U.S. Department of Energy (Washington, D.C.), Aerotherm Corp. (California), University of California, Berkeley (Calif.), Texaco (Beacon, New York), Jaycor Corp. (California), General Motors (Michigan) Utah Power and Light Co. (Utah), Systems, Science and Software (California), Los Alamos Scientific Research Laboratory (New Mexico), Air Products and Chemicals (Pennsylvania), National Scientific Research Center (France), Koppers Corp. (Pennsylvania), Stone and Webster (New York), and Phillips Petroleum Co. (Oklahoma) to discuss coal combustion and gasification research. Also, on April 23-24, 1979, the Combustion Laboratory at Brigham Young University, served as host for the 1979 Spring Meeting of the Western States Section of the Combustion Institute. Eighty-five registrants participated in the conference, where the central theme was pulverized coal combustion and gasification.

F. INDUSTRIAL ADVISORY BOARD

The Industrial Advisory Board was expanded from four to six members with new representatives from GPU Services in New Jersey and Babcock and Wilcox in Alliance, Ohio added this past year. The six members were from two boiler manufacturing companies, two public utilities, one furnace research company, and a company emphasizing coal gasification. Members of this advisory board are summarized in Table 35.

A technical review meeting of this advisory board was held at the BYU Combustion Laboratory on October 19, 1978. Research work of this project was summarized in detail and facilities were inspected. Technical aspects of this program were discussed in detail. Each of the board members prepared a short letter report of this meeting. These reports are summarized in Table 35.

TABLE 35

SUMMARY OF INDUSTRIAL ADVISORY COMMITTEE RESPONSES

BOARD PARTICIPANT	COMPANY/LOCATION	SELECTED COMMENTS	KEY RECOMMENDATIONS
1. Steven A. Johnson Chemical Engineer	Babcock and Wilcox Alliance Research Ctr. Alliance, Ohio		1. Model flow fields in staged systems 2. Study effects of wall temp. 3. Obtain pollutant data with swirl 4. Use model to help scale test results 5. Add pollutant predictions to code
2. Reginald Wintrell Director, Energy Systems (Formerly of McKee Iron and Steel)	Billings Energy Corp. Provo, Utah (Formerly of Koppers Corp., Pittsburgh)		1. Maintain duel approach of modeling and measurement 2. Study chemistry of ash/slag
3. Robert J. Zoschak Technical Director Applied Thermo-dynamics Research	Foster Wheeler Development Corp. Livingston, New Jersey	1. Observed good agreement in model predictions and measurements 2. Models are of potential use to industry in furnace design	1. Conduct tests with swirl 2. Conduct tests with other coals 3. Investigate ash characteristics of the coals 4. Consider larger scale work for model validation
4. W. A. Crandall Consulting Engineer	GPU Services Corp. Parsippany, New Jersey	1. Use made of NO_x data by GPU	1. Investigate effects of coal properties on combustion and product formation 2. Investigate properties of ash produced during combustion
5. Charles E. Blakeslee Engineer	KVB, Inc. Tustin, California	1. 1-D model of interest when user's manual is available	1. Maintain present experimental and modeling emphasis 2. Test a variety of coal types
6. Val A. Finlayson Director, Research	Utah Power and Light Company Salt Lake City, Utah	1. Modeling work may have application to UPL interest in transient modeling of power plants	1. Study coal chemistry-slagging and corrosion 2. Study formation of pollutants and effects of additives

REFERENCES

1. Zahradnik, R. L., and Grace R. K., "Chemistry and Physics of Entrained Coal Gasification ," ACS 165th National Meeting, Vol. 18, No. 1, 203, Dallas, Texas (April 1973).

2. Smoot, L. D., and Hanks, R. W., "Mixing and Gasification of Coal in Entrained Flow System" ERDA Report No. FE-1767-F, ERDA Contract No. E(49-18)-1767, Brigham Young University, Provo, Utah (May 15, 1977).

3. Smoot, L. D., and Hedman, P. O., "Mixing and Kinetic Processes in Pulverized Coal Combustors," EPRI Report No. FP-806 Project No. 364-1, Brigham Young University, Provo, Utah (August, 1978).

4. Smoot, L. D., Hedman, P. O., and Smith, P. J., "Mixing and Kinetic Processes in Pulverized Coal Combustors," EPRI Final Report, Research Project 364-1-3, Brigham Young Uiversity, Provo, Utah, (August, 1979).

5. Memmott, V. J., "Rates of Mixing of Particles and Gases in Confined Jets," M. S. Thesis, Brigham Young University, Provo, Utah (April, 1977).

6. Memmott, V. J., and Smoot, L. D., "Cold Flow Mixing Rate Data for Pulverized Coal Reactors," AiChE Journal. 24, pp. 466-475, (May, 1978).

7. Tice, C. L., "Particle and Gas Mixing Rates in Confined, Coaxial Jets with Recirculation," M. S. Thesis, Brigham Young University, Provo, Utah (August, 1977).

8. Tice, C. L., and Smoot, L. D., "Cold Flow Mixing Rates with Recirculation for Pulverized Coal Reactors," AIChE Journal, 24, pp. 1029-1036, (Nov. 1978).

9. Sharp, J. L., "Particle and Gas Mixing in Confined, Recirculating Coaxial Jets with Angular Injection," Master of Science Thesis, Chemical Engineering Department, Brigham Young University, Provo, Utah (in preparation, 1980).

10. Leavitt, D. O., " " Master of Science Thesis, Chemical Engineering Department, Brigham Young University, Provo, Utah (in preparation, 1980).

11. Hedman P. O., and Smoot, L. D., "Particle-Gas Dispersion Effects in Confined Coaxial Jets," AIChE Journal, 21, pp. 372-380, (1975).

12. Allred, L. D. and Smoot, L. D., "Particle Gas Mixing Effects in Confined Nonparallel Coaxial Jets," AIAA J., 13, p. 721 (1975).

13. Beer, J. M. and Chigier N. A., "Combustion Aerodynamics," London: Applied Science Publishers, Ltd. (1972).

14. Lowry, H.H., editor, Chemistry of Coal Utilization, John Wiley and Sons, Inc., (1945).

15. Lowry, H. H., editor, Chemistry of Coal Utilization, Supplementary Volume, John Wiley and Sons, Inc. (1963).

16. Bissett, L. A., "An Engineering Assessment of Entrainment Gasification," MERC/RI-78/2, Morgantown Energy Research Center (DOE), Morgantown, West Virginia (April, 1978).

17. Skinner, F. D., "Mixing and Gasification of Pulverized Coal", Ph.D Dissertation, Chemical Engineering Department, Brigham Young University, Provo, Utah, (in preparation, 1980).

18. Price, T., "Pollutant Measurements in an Entrained Coal Gasifier" M. S. Thesis, Chemical Engineering Department, Brigham Young University, Provo, Utah, (in preparation 1980).

19. O'Keefe, A. E., "Recent and Future Advances in Air Pollution Instrumentation, Water, Air and Soil Pollution, 3, p. 447, (1974).

20. Culmo, R. F., "A Review of the Performance of the Perkin-Elmer Model 240 in the Elemental Analysis of Chemical Compounds, Elemental Analysis Application Study No. 1." Perkin-Elmer Corporation, Connecticut, (January 1974).

21. 1974 Annual Book of ASTM Standards, part 26, "Gaseous Fuels: Coal and Coke; Atmospheric Analysis," ASTM, 1926 Race Street, Philadelphia, PA, (1974).

22. Luthy, R. G., and Pochan, M. J., "Determination of Cyanide Levels in Hygas Wastewater," DOE Report FR-2496-36, DOE Contract No. EX-76-S-01-2496, Carnegie-Mellon University, Pittsburgh, PA.

23. Luthy, R. G., Bruce, S. G., Jr., Walters, R. W., and Nakles, D. V., "Identifications and Reactions of Cyanide and Thiocyanate in Coal Gasification Wastewaters," DOE Report FE-2496-23, DOE contract No. EX-76-S-01-2496, Carnegie-Mellon University, Pttsburgh, Pennsylvania.

24. Nakles, D. V., "Characterization of Hydrogen Cyanide in Production in Coal Gasification," FE-2496-29, DOE Contract EX-76-S-01-2496 Environmental Studies Institute, Carnegie-Mellon University, Pittsburgh, Pennslvania, (Dec. 1978).

25. Luthy, R. G., and Bruce, S. G., Jr., "Kinetics of Reactions of Cyanide to Form Thiocyanate," DOE Report FE-2496-32, DOE contract No. EX-76-S-01-2496, Carnegie-Mellon University, Pittsburgh, Pennsylvania.

26. Smoot, L. D. and Purcell, W. E., "Model for Mixing of a Compressible Free Jet with a Moving Environment," AIAA Journal, 5, No. 11 (Nov. 1967).

27. Strimbeck, G. R., Cordiner, J. B., Jr., Taylor, H. G., Plants, K. D., and Schmidt, L. D., "Progress Report on Operation of Pressure-Gasification Pilot Plant Utilizing Pulverized Coal and Oxygen: Bureau of Mines Rept. of Investigations 4971," p. 27, (1953).

28. Holden, J. H., Strimbeck, G. R., McGee, J. P., Willmott, L. F., and Hirst, L. L., "Operation of Pressure-Gasification Pilot Plant Utilizing Pulverized Coal and Oxygen, a Progress Report: Bureau of Mines Rept. of Investigations 5573," p. 56, (1960).

29. Selph, C., "Generalized Thermochemical Program for Complex Mixtures," Rocket Propulsion Laboratory, Edwards AFB, CA (1965).

30. von Fredersdorff, C. G., and Elliott, M. A., "Coal Gasification," in Lowry H. H., ed., Chemistry of Coal Utilization, Suppl. Vol., John Wiley and Sons, Inc., New York, (1963).

31. Strimbeck, G. R., Holden, J. H., Bonar, F., Plants, K. D., Plars, C. D., and Hirst, L. L., U. S. Bureau of Mines Rept. Investibation No. 5559, (1960).

32. Thurgood, J. R., "Mixing and Combustion of Pulverized Coal," Ph.D. Dissertation, Brigham Young University, Provo, Utah, (1979).

33. Hubbard, E. H., "The First Performance Trial and First Combustion Mechanism Trial with Pulverized Coal," J. Inst. Fuel, (1960).

34. Coates, R. L., "Experimental and Process Design Study of a Fast Pyrolytic Gasification Process," Report ERDA contract 14-32-009-548, Eyring Research Institute, Provo, Utah (October, 1977).

35. Johnson, S. A., Personal communication with Babcock and Wilcox Company, (March 30, 1978).

36. Farnsworth, J. F., and Glenn, R. A., "Status and Design Characteristics of B R/OCR BI-GAS Pilot Plant," Vol 15, No. 3., 162nd National Meeting of Am. Chem. Soc. Washington D. C., (1971).

37. Rees, D., "Pollutant Formation During Pulverized Coal Combustion," Ph.D. Dissertation, Brigham Young University, Provo, Utah, (in preparation, 1979).

38. Smoot, L. D., and Pratt, D. R., (eds.), Pulverized Coal Combustion and Gasification, Plenum, New York, (1979).

39. Smith, P. J., "Theoretical Modeling of Coal or Gas Fired Turbulent Combustion or Gasification," Ph.D. Dissertation, Brigham Young University, Provo, Utah (August, 1979).

40. Boussinesq, J., "Theoreie de l ecoulement tourbillant,: Mem. Pre. par. div. Sav., 23. Paris, (1877).

41. Lander, B. E. and Spalding, D. B., Mathematical Models of Turbulence, London, Academic Press, (1972).

42. Gosman, A. D., and Lockwood, F. C., Personal communication, Imperial College, London, (April 19-28, 1978),

43. Spalding, D. B., "Turbulence Modeling: Solved and Unsolved Problems," Turbulent Mixing in Nonreactive and Reactive Flows, edited by S. N. B. Murthy, Plenum, New York (1975).

44. Jones, W. P. and Launder, B. E., "The Prediction of Laminarization with a Two-Equation Model of Turbulence," Int. J. Heat Mass Transfer, 15, (1972).

45. Bilger, R. W., "Turbulent Jet Diffusion Flames," Prog. Energy Combust, Sci., 1, pp. 87-109, (1976).

46. Becker, H. A., "Effects of Concentration Fluctuations in Turbulent Diffusion Flames,: 15th Symposium (International) on Combustion, The Combustion Institute, Pittsburgh, PA (1974).

47. Elghobashi, S. E., and Pun W. M., "A Theoretical and Experimental Study of Turbulent Diffusion Flames in Cylindrical Furnaces," 15th Symposium (Internationa) on Combustion, The Combustion Institute Pittsburgh, PA, (1974).

48. Pratt, D. R., "Mixing and Chemical Reaction in Continuous Combustion," Prog. Energy Comb. Sci 1, Pemagon Press, pp. 73-86, (1976).

49. Tamanini, F., "On the Numerical Prediction of Turbulent Diffusion Flames," Paper presented at the joint meeting of the Central and Western States Sections of the Combustion Institute, San Antonio, Texas, (April 21-22, 1975).

50. Patankar, S. V., and Spalding, D. B., Heat and Mass Transfer in Boundary Layers,, Second Edition, Intertext Books, London, (1970).

51. Khalil, E. E., Spalding D. B., and Whitelaw, J. H., "The Calculation of Local Flow Properties in Two-Dimensional Furnaces,: Int. J. Heat Mass Transfer, 18, pp. 775-791. (1975).

52. Bilger, R. W., "Probe Measurements in Turbulent Combustion," Progress in Astronautics and Aeronautics, 53, (1977).

53. Roache, P. J., Computational Fluid Dynamics, Albuquerque, New Mexico, Hermosa Publisher, (1976).

54. Gosman, A. D., and Pun W. M., "Lecture Notes for Course Entitled 'Calculation of Recirculating Flow'," Imperial College, London, (December, 1973).

55. Wormeck, J. J., "Computer Modeling of Turbulent Combustion in a Longwell Jet-Stirred Reactor," Ph.D. Dissertation, Wasington State University, (1976).

56. Lewis M. E., "Local Measurement in Turbulent Natural Gas Combustion," M. S. Thesis, Brigham Young University, Provo, Utah (August, 1979).

57. Gosman, A. D., Lockwood, ,F. C., Salooja, A. P., "The Prediction of Cylindrical Furnaces Gaeous Fueled with Premixed and Diffusion Burners,: 17th Symposium (International) on Combustion, The Combustion Institute, (1978),

58. Husain, A. D., and Hussain, A. K. N. F., "Axisymmetric Mixing Layers: Influence of the Initial and Boundary Conditions," AIAA Journal, 17, (1979).

59. Baker, R. J., Hutchinson, P., Khail, E. E., and Whitelaw, J. H., "Measurements of Three Velocity Components in a Model Furnace with and without Combustion," 15th Symposium (International) on Combustion, The Combustion Institute, Pittsburgh, PA, (1974).

60. Hecker, W. C., "A Theoretical Study of the Kinetics, Propagation and Suppression of Methane-Air Flames,: M. S. Thesis, Brigham Young University, Provo, Utah, (April, 1975).

GOVERNMENT PRINTING OFFICE: 1980-640-258/29